Bromo and thio maleimides for functionalisation and fluorescent labelling of polymers and polymer nanoparticles

Mathew Philip Robin

Submitted for the degree of

Doctor of Philosophy

Department of Chemistry

THE UNIVERSITY OF WARWICK

March 2014

For Emma

Table of contents

Acknowledgements

First I would like to thank my supervisor Rachel for her constant guidance, support, and encouragement during my PhD. It has been an honour and a privilege to be a member of the O'Reilly group. I would also like to thank EPSRC for funding my studies, and all the technical and support staff at the University of Warwick who have provided me with help and assistance.

A huge thank-you must also go to all members of the O'Reilly group, past and present. You not only freely shared with me your time, knowledge, and ideas, but you also made the last three and a half years incredibly good fun. I could fill many pages describing my gratitude to each of you individually, but in the interest of brevity I will reserve that fate to just three of you. Firstly Nikos; for helping me become a PhD student, Joe; who was always happy and interested to discuss my work or his, and Anne; whose keen instinct helped transform this project.

I thank Olivier Colombani and Christophe Chassenieux at Université du Maine for inviting me to work in their laboratory, and providing unceasing guidance ever since. I also thank Jeff Raymond for his energy, enthusiasm and expertise during our collaboration. In particular I thank Jeff and Liz for their incredibly warm and friendly hospitality during my visit to Texas.

I must thank my family and friends for their unwavering support and encouragement, particularly my parents. Finally I thank my wife Emma for everything you do. You turn bad days into good days, and good days into better days. Without your constant love, encouragement and support I could not have completed this thesis.

Declaration of authorship

This thesis is submitted to the University of Warwick in support of my application for the degree of Doctor of Philosophy. It has been composed by myself and has not been submitted in any previous application for any degree.

The work presented (including data generated and data analysis) was carried out by the author except in the cases which are outlined below, and clearly labelled in the corresponding text.

- Poly(*D*,*L*-lactide) **3xiv** (Chapter 3) was synthesised by Anne Mabire (University of Warwick).
- Salmon calcitonin (sCT) conjugation experiments in Chapter 3 were performed by Dr Paul Wilson (University of Warwick).
- Quantum yield, molar emission, molar anisotropy, and TCSPC measurements for **3i** and **5i** (Chapter 5) were performed and analysed by Dr Jeffery Raymond (Texas A&M University, USA).
- *In vitro* FLIM studies (Chapter 5) were performed by Dr Jeffery Raymond, Dr Joanne Damborsky, Elizabeth Thom, and Prof. Ursula Winzer-Serhan (Texas A&M University, USA).
- The TEM images in Chapter 5 were acquired by Dr Anaïs Pitto-Barry and Yan Kang (University of Warwick).

Parts of this thesis have been published by the author (see list of publications).

List of publications

1. Dibromomaleimide End Functional Polymers by RAFT Polymerization Without the Need of Protecting Groups

   M. P. Robin, M. W. Jones, D. M. Haddleton, and R. K. O'Reilly, *ACS Macro Lett.*, 2012, **1**, 222–226. (Chapter 2 & 3)

2. Conjugation-Induced Fluorescent Labeling of Proteins and Polymers Using Dithiomaleimides

   M. P. Robin, P. Wilson, A. B. Mabire, J. K. Kiviaho, J. E. Raymond, D. M. Haddleton, and R. K. O'Reilly, *J. Am. Chem. Soc.*, 2013, **135**, 2875–8. (Chapter 3)

3. Hollow Block Copolymer Nanoparticles through a Spontaneous One-step Structural Reorganization

   N. Petzetakis, **M. P. Robin**, J. P. Patterson, E. G. Kelley, P. Cotanda, P. H. H. Bomans, N. A. J. M. Sommerdijk, A. P. Dove, T. H. Epps, III, and R. K. O'Reilly, *ACS Nano*, 2013, **7**, 1120–8.

4. New Functional Handle for Use as a Self-Reporting Contrast and Delivery Agent in Nanomedicine

   M. P. Robin, A. B. Mabire, J. C. Damborsky, E. S. Thom, U. H. Winzer-Serhan, J. E. Raymond, and R. K. O'Reilly, *J. Am. Chem. Soc.*, 2013, **135**, 9518–24. (Chapter 5)

5. Structural Characterization of Amphiphilic Homopolymer Micelles Using Light Scattering, SANS, and Cryo-TEM

   J. P. Patterson, E. G. Kelley, R. P. Murphy, A. O. Moughton, **M. P. Robin**, A. Lu, O. Colombani, C. Chassenieux, D. Cheung, M. O. Sullivan, T. H. Epps, III, and R. K. O'Reilly, *Macromolecules*, 2013, **46**, 6319–6325.

6. The analysis of solution self-assembled polymeric nanomaterials

   J. P. Patterson, **M. P. Robin**, C. Chassenieux, O. Colombani, and R. K. O'Reilly, *Chem. Soc. Rev.*, 2014, **43**, 2412-2425

7. Fluorescent and chemico-fluorescent responsive polymers from dithiomaleimide and dibromomaleimide functional monomers

   M. P. Robin and R. K. O'Reilly, *Chem. Sci.*, 2014, **5**, 2717-2723 (Chapter 4)

List of symbols and abbreviations

a – Mark-Houwink parameter

A – Amplitude

A *or* Abs – Absorption

A_2 – Second virial coefficient

$A(\tau)$ – Distribution of relaxation times

AIBN – 2,2′-Azobis(2-methylpropionitrile)

ATRP – Atom transfer radical polymerisation

BCP – Block copolymer

BINOL – 1,1'-Bi-2-naphthol

BME – β-Mercaptoethanol

Boc – *Tert*-butyloxycarbonyl

BPO – Benzoyl peroxide

br – Broad peak in ^{1}H NMR spectrum

BSA – Bovine serum albumin

c – Concentration

ca. – Circa

CDSA – Crystallisation driven self-assembly

CLD – Crosslinking density

CLMs – Core-labelled micelles

CMC – Critical micelle concentration

CMS – 4-chloromethyl styrene

CP – Conjugated polymer

Cryo – Cryogenic

CTA – Chain transfer agent

CuAAC – Copper-catalysed azide-alkyne cycloaddition

Cys – Cysteine

D – Detector

D – Diffusion coefficient

d – Binomial doublet in ^{1}H NMR spectrum

D,L-LA – Racemic mixture of *D*-lactide and *L*-lactide

D_{app} – Apparent diffusion coefficient

DBM – Dibromomaleimide

DBMA – Dibromomaleimide acrylate

DBMM – 2,3-Dibromo-*N*-methylmaleimide

DBMMA – Dibromomaleimide methacrylate

DCM – Dichloromethane

DCTB – Trans-2-[3-(4-*tert*-butylphenyl)-2-methyl-2-propylidene] malonitrile

DIAD – Diisopropyl azodicarboxylate

DLS – Dynamic light scattering

$Đ_M$ – Molar mass dispersity (M_w/M_n)

DMAP – 4-Dimethylaminopyridine

DMF – Dimethylformamide

DMSO – Dimethyl sulfoxide

dn/dc – Refractive index increment

DNA – Deoxyribonucleic acid

DoF – Degree of functionalisation

DOX – Doxorubicin

DP – Number average degree of polymerisation

DRI – Differential refractive index

DTM – Dithiomaleimide

DTMA – Dithiomaleimide acrylate

DTMM – *N*-dithio-*N*-methylmaleimide

DTMMA – Dithiomaleimide methacrylate

η – Intrinsic viscosity

EDCI – 1-Ethyl-3-(3-dimethylaminopropyl)carbodiimide

EGDMA – Ethyleneglycol dimethacrylate

em – Emission

eq. – Equivalents

ET – Electron tomography *or* energy transfer

ex – Excitation

f – Free radical initiator efficiency *or* function *or* weight fraction

FAM – Carboxyfluorescein

f_C – Core block weight fraction

FLIM – Fluorescence lifetime imaging

FRET – Förster resonance energy transfer

FRP – Free radical polymerisation

FTIR – Fourier transform infra-red spectroscopy

FWHM – Full width half maximum

Γ – Rate constant for fluorescence emission

G – Instrument efficiency factor

$g_1(q,t)$ – Electric field autocorrelation function

$g_2(q,t)$ – Intensity autocorrelation function

GO – Graphene oxide

GSH – Glutathione

Hb – Hyperbranched

HeLa – Immortal cervical cancer cell line derived from Henrietta Lacks

HPLC – High-performance liquid chromatography

HR-MS – High resolution mass spectrometry

I *or* I-I – Radical initiator

$I(x)$ – Intensity as a function of x

ILMs – Interface-labelled micelles

IONP – Iron oxide nanoparticle

IRF – Instrument response function

IUPAC – International Union of Pure and Applied Chemistry

J – NMR coupling constant (refers to $^3J_{\text{H-H}}$ unless otherwise stated)

K – Collection of constants in the Zimm equation

$k_{\text{add,-add,addP,-addP,β,-β}}$ – Rate constants in the RAFT equilibria

k_D – Dynamic second virial coefficient

$k_{\text{d,i,p,s,t}}$ – Rate constant for initiator decomposition, initiation, propagation, chain transfer and termination respectively in a radical polymerisation

k_{nr} – Rate constant of non-radiative decay

k_q – Rate constant of fluorescence quenching

λ – Wavelength

L – Chain length

L-LA – L-lactide

LCST – Lower critical solution temperature

Lig. – Ligand

LPO – Lauroyl peroxide

M – Monomer *or* monochromator

M – Molar mass

m – Multiplet peak in ^{1}H NMR spectrum

m/z – Mass to charge ratio

MA – Methyl acrylate

MALDI-TOF – Matrix-assisted laser desorption/ionization time of flight

MBM – Monobromomaleimide

MI – Maleimide

MMA – Methyl methacrylate

M_{n} – Number average molecular weight

$M_{\mathrm{n,th}}$ – Theorectical M_{n} calculated from monomer loading and conversion

MS – Mass spectrometry

MW – Molecular weight

M_{w} – Weight average molecular weight

MWCO – Molecular weight cut-off

MWNT – Multi-walled carbon nanotubes

ν – Frequency

n – Refractive index *or* number of excited molecules

N_{A} – Avogadro's number

NAD(P)H – Reduced nicotinamide adenine dinucleotide (phosphate)

N_{agg} – Aggregation number

NG – Nanogel

NIPAM – *N*-isopropylacrylamide

NIR – Near infra-red

NLMs – Non-labelled micelles

ν_{max} – Vibration maxima in FTIR spectrum

NMR – Nuclear magnetic resonance

NMM – *N*-Methylmorpholine

NMP – Nitroxide mediated polymerisation

ω – Degree of stretching of coronal chains

OEGMA – Oligoethyleneglycol monomethylether methacrylate

p – Monomer conversion

PDA – Photodiode array

PEG – Poly(ethylene glycol)/poly(ethylene oxide)

Pet. – Petroleum

PFP – Pentafluorophenol

PLGA – Poly(lactic-*co*-glycolic acid)

P_n – Polymer with $DP = n$

$P_n^{\bullet}$ – Polymeric radical with $DP = n$

PRE – Persistent radical effect

Q – Quantum yield

q – Scattering vector

quin. – Binomial quintet in ^{1}H NMR spectrum

ρ – Bulk density

R – Radius

r – Fluorescence anisotropy

RAFT – Reversible addition-fragmentation chain transfer

RC – Reference cell

RDRP – Reversible-deactivation radical polymerisation

ref. – Reference

REPES – Regularized Positive Exponential Sum

R_g – Radius of gyration

RGB – Red green blue

R_h – Hydrodynamic radius

RI – Refractive index

RNA – Ribonucleic acid

ROMP – Ring-opening metathesis polymerisation

ROP – Ring-opening polymerisation

R_p – Rate of polymerisation

R_θ – Rayleigh ratio

RT – Retention time

rt – Room temperature

S – Chain transfer agent *or* light source

SC – Sample cell

sCT – Salmon calcitonin

SDS – Sodium dodecylsulfate

SEC – Size exclusion chromatography

SET-LRP – Single electron transfer living radical polymerisation

sex. – Binomial sextet in ^{1}H NMR spectrum

SLMs – Shell-labelled micelles

SLS – Static light scattering

Sty – Styrene

τ – Fluorescence lifetime *or* relaxation time

θ – Angle *or* rotational correlation time

T – Temperature

t – Time

t – Binomial triplet in ^{1}H NMR spectrum

$\tau_{\mathrm{Av,A}}$ – Amplitude average fluorescence lifetime

$\tau_{\mathrm{Av,I}}$ – Intensity average fluorescence lifetime

$^{\mathrm{t}}$BA – *Tert*-butyl acrylate

TBAI – Tetrabutylammonium iodide

T_{c} – Cloud point temperature

TCEP – Tris(2-carboxyethyl)phosphine

TCSPC – Time-correlated single photon counting

TEA – Triethylamine

TEGA – Triethyleneglycol monomethylether acrlyate

TEM – Transmission electron microscopy

TFA – Trifluoroacetic acid

T_{g} – Glass transition temperature

THF – Tetrahydrofuran

TMS – Trimethylsilane group *or* tetramethylsilane NMR standard

τ_{n} – Intrinsic fluorescence lifetime

TU – Thiourea

UV – Ultraviolet

V *or* v – Volume

V-65 – 2,2'-Azobis-2,4-dimethyl valeronitrile

VBDBM – Vinylbenzyl dibromomaleimide

VBDTM – Vinylbenzyl dithiomaleimide

vis – Visible

w – Weight

X – Quencher

Thesis Summary

This thesis explores the use of bromo and thio maleimide functional groups in polymer chemistry. The reactivity of bromomaleimide groups towards thiols is exploited as a new and efficient post-polymerisation modification reaction, while the fluorescence of the dithiomaleimide (DTM) products is utilised for labelling of polymers and polymer nanoparticles.

Chapter 1 gives an introduction to ways in which control over free radical polymerisation can be achieved using reversible-deactivation mechanisms. The incorporation of functionality into polymers, and the synthesis of polymer nanoparticles is also discussed, leading to a review of the different strategies for fabrication of fluorescent polymer nanoparticles.

In **Chapter 2** novel reversible addition-fragmentation chain transfer (RAFT) agents are developed with the aim of introducing monobromomaleimide (MBM) or dibromomaleimide (DBM) as a polymer end-group *via* RAFT.

In **Chapter 3** the fluorescent properties of the DTM group are first explored, then a novel RAFT agent/ring-opening polymerisation initiator is used for site-specific introduction of DTM fluorophores into linear polymers. Site-specific introduction of DTM groups by post-polymerisation functionalisation reaction of DBM-terminated polymers (synthesised in Chapter 2) with thiols is also developed.

In **Chapter 4** novel DTM and DBM-functional vinyl monomers are synthesised, and their RAFT polymerisation with non-functional comonomers is used to incorporate DTM and DBM functionality along polymer backbones. Post-polymerisation functionalisation of these DBM-functional polymers with thiols is also demonstrated.

In **Chapter 5** fluorescently-labelled polymer nanoparticles containing DTM fluorophores are synthesised, using the DTM-functional RAFT agent developed in Chapter 3, and DTM-functional monomers developed in Chapter 4. Nanoparticles are fabricated by block copolymer self-assembly and emulsion polymerisation. These fluorescent nanoparticles are analysed by steady-state and time-resolved fluorescence spectroscopy to assess their utility as contrast agents.

Chapter 6 summarises RAFT polymerisation data from Chapters 2, 3 and 4 to assess the extent to which the DBM and DTM groups interfere in RAFT polymerisation, and the mechanism by which this may occur.

1. Introduction

1.1. Controlling polymerisation

The essence of synthetic chemistry is the desire to control chemical reactions. When synthesising polymers, there are three elements of the product over which control can be imparted; composition (comprising sequence, tacticity and molecular weight), architecture, and functionality (Figure 1.1).[1]

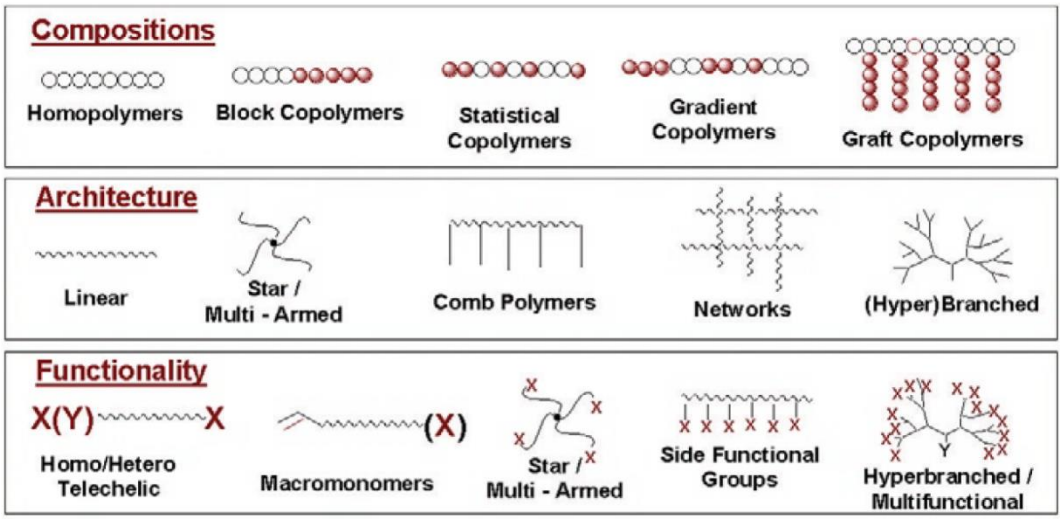

Figure 1.1. The three elements of a polymer that can be controlled by synthetic chemists. Figure adapted from ref.[1]

The key to controlling these three features of a polymer is the mechanism of the polymerisation reaction by which it is formed. Although the current state-of-the-art for sequence control in synthetic polymers relies on the use of templates or iterative synthesis,[2] control over the other features of a polymer can be achieved by living polymerisation and reversible-deactivation radical polymerisation (RDRP) mechanisms.

1.1.1. Living polymerisation

A chain-growth polymerisation in which chain transfer and termination (see Figure 1.2) are absent is termed a living polymerisation.[3] During a living polymerisation the number average degree of polymerisation (DP) is a linear function of conversion, with the final DP controlled by the stoichiometry of initiator to monomer. As such control over the molecular weight distribution is obtained, with the molar-mass dispersity ($Đ_M$, defined as the ratio of weight and number average molecular weights M_w/M_n) obeying the rule $Đ_M = 1+(1/DP)$.[4] Composition is controlled by the order and ratio in which monomers

are added to the growing polymer, while architecture and functionality can be controlled by selection of (multi)functional initiators and monomers.

However, the requirement for a complete absence of termination and chain transfer imposes stringent requirements on reaction conditions. Living ionic polymerisation of vinyl monomers requires a complete absence of water and oxygen, and precludes the use of monomers with acidic or basic functional groups.[4] Under certain conditions the living polymerisation of cyclic olefin monomers is possible, by the ring-opening metathesis polymerisation (ROMP) mechanism. When catalyst design and reaction conditions are optimised ROMP can proceed without an appreciable amount of chain transfer or termination, while showing a high tolerance toward moisture, air and common functional groups.[5]

Free radical polymerisation (FRP) is compatible with a wide range of vinyl monomers and reaction conditions, due to its tolerance towards unprotected functional groups (alcohol, amine, acid, amide *etc.*).[6] These factors account for the prevalence of FRP in industrial polymer synthesis.[7] A high degree of control can be obtained in FRP by minimising chain transfer and termination. This is achieved by using a reversible-deactivation radical polymerisation (RDRP) mechanism.[8]

1.1.2. Reversible-deactivation radical polymerisation (RDRP)

The steps that occur in a free radical polymerisation are shown in Figure 1.2.[9] A free radical is formed by homolysis of an initiator (I-I) during initiation, with the free radical ($I^{\bullet}$) then reacting with a monomer (M). Free radicals and monomer continue to propagate until the polymer chain ceases to grow, either due to a radical-radical reaction (termination), or due to chain-transfer.

Under the steady-state approximation (constant free radical concentration) rates of initiation and termination are equal with both being much slower (*ca.* 1000 times) than propagation. This means that the average lifetime of a propagating chain is *ca.* 1 s.[10] Under this approximation the rate of polymerisation (R_p) can be expressed according to equation (1.1), where f is the initiator efficiency (the fraction of radicals $I^{\bullet}$ that leave the solvent cage unreacted after decomposition of I-I).[11]

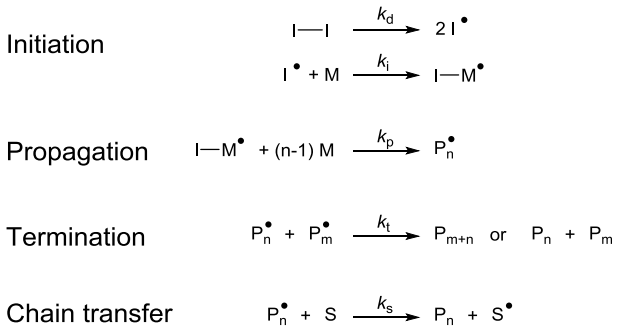

Figure 1.2. The steps (and their associated rate constants) involved in FRP. I-I is the radical initiator, M is the vinyl monomer, P_n is a polymer with $DP = n$, and S is a chain transfer agent.

$$R_p = k_p \left(f \frac{k_d}{k_t} \right)^{0.5} [M][I]^{0.5} \qquad (1.1)$$

Conceptually, termination and chain transfer cannot be eliminated, but can be reduced to a level at which they are undetectable, through use of reversible-deactivation radical polymerisation.[8] In these mechanisms a dynamic equilibrium between propagating radicals, and a dormant species is established. This has the effect of both reducing the concentration of radicals (thereby reducing the rate of termination) whilst drastically increasing the lifetime of propagating radicals, in analogy with living polymerisation.[10] This dynamic equilibrium has been achieved either by the persistent radical effect, or by a degenerative transfer process.

1.1.2.1. The persistent radical effect (PRE)

Both atom transfer radical polymerisation (ATRP)[12] and nitroxide mediated polymerisation (NMP)[13] rely on the persistent radical effect (PRE). Persistent radicals are species that cannot terminate with one another, and are only able to cross-couple with the propagating (polymeric) radicals. In ATRP the persistent radicals are transition metal complexes (X-Mt^{m+1}/L in Figure 1.3 a), which are formed by transfer of a halide atom (X) between an initiating/macromolecular species and a transition metal complex in a lower oxidation state (Mt^m/L). In NMP the persistent radical is a stable nitroxide, with activation-deactivation under thermal control (Figure 1.3 b). Radical-radical termination leads to a build up of persistent radicals, resulting in a low propagating radical concentration and therefore decreased termination. A fast activation-deactivation process

is required to give propagating radicals equal opertunity to react with monomer, in turn leading to control over molecular weight.[10]

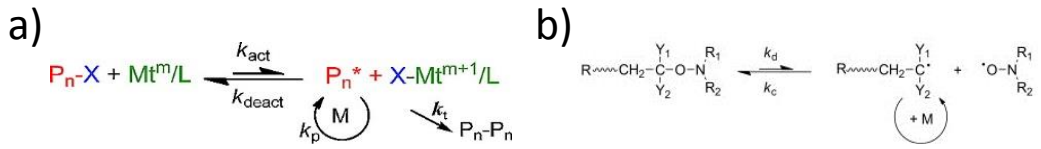

Figure 1.3. Activation-deactivation equilibria for a) ATRP and b) NMP. Figure adapted from refs.[12, 13]

As with living polymerisation, architecture and functionality can be controlled through the use of (multi)functional alkyl halide ATRP initiators or alkoxyamine NMP initiators. Furthermore if termination events are minimised, the majority of product polymer chains will retain the transferable group (halide/nitroxide), allowing them to be used as macro-initiators for block copolymer synthesis.

1.1.2.2. Degenerative transfer

An alternative strategy for molecular weight control in radical polymerisation is the use of a degenerative transfer mechanism, such as that employed in reversible-addition fragmentation chain transfer (RAFT) polymerisation.[14] In addition to the reactions associated with FRP (Figure 1.2), the presence of a RAFT agent (the thiocarbonylthio compound **1i**) results in the establishment of the RAFT equilibria (Figure 1.4). These equilibria neither create nor destroy radicals, so that under ideal conditions addition of a RAFT agent has no effect on the kinetics of FRP.

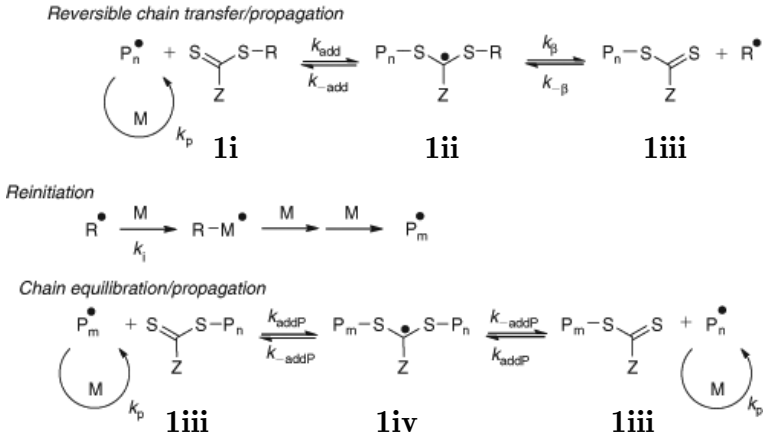

Figure 1.4. The RAFT mechanism. Figure adapted from ref.[14]

The key aspect of the RAFT mechanism is that the rapid equilibrium between dormant macro-RAFT agents (**1iii**) and propagating radicals ($P_m^{\bullet}$ and $P_n^{\bullet}$) *via* the intermediate (**1iv**) provides equal probability for all chains to grow. This leads to molecular weight control, with *DP* at complete monomer conversion dictated by [RAFT agent]:[Monomer] stoichiometry. Termination and chain transfer reactions are minimised by keeping initiator (and therefore radical) concentration low, in which case the majority of polymers will retain the thiocarbonylthio end-group (**1iii**) allowing the synthesis of block copolymers. Perrier and co-workers have recently demonstrated that by using very low initiator concentrations (< 1 mol% w.r.t. RAFT agent) termination can be almost completely eliminated, enabling the synthesis of decablock copolymers with end-group fidelity of 97% and $Đ_M = 1.15$.[15]

RAFT agent design is important for two reasons. Firstly an appropriate choice of R and Z groups is required to establish the chain equilibration (Figure 1.4). The Z group determines the electron density on the thiocarbonylthio group and therefore its reactivity toward propagating radicals. Z is chosen such that the RAFT agent is at least 10 (and preferably > 100) times more reactive towards propagating radicals than the monomer.[16] R is chosen to be a good leaving group from the intermediate radical **1ii** ($k_\beta/(k_{-add}+k_\beta) > 0.5$) and to undergo efficient re-initiation with monomer. An empirical guide to Z and R group selection has been established by Moad *et al.*, as shown in Figure 1.5.[17] The so-called 'less activated' monomers: vinyl acetate (VAc), *N*-vinylcarbazole (NVC), and *N*-vinyl-pyrrolidone (NVP) are poor homolytic leaving groups from the intermediate radicals **1ii** and **1iv**. Therefore, a less active RAFT agent (with a strongly electron donating Z group such as O or N) is required to prevent inhibition due to build-up of **1ii** and **1iv**. For this reason the 'less-activated' monomers also require an R group which is a good homolytic leaving group (such as a tertiary radical), which can also undergo efficicient re-initiation. 'More activated monomers' such as methyl methacrylate (MMA), styrene (Sty), methyl acrylate (MA), acrylamide (AM), and acrylonitrile (AN) require more active RAFT agents. These have electron withdrawing, or more weakly electron donating Z groups (C, Ph or S) which make the thiocarbonylthio more electrophilic to ensure sufficient rate of addition for the propagating radicals. Again, an R

group which is a good homolytic leaving group relative to the propagating radical is necessary.

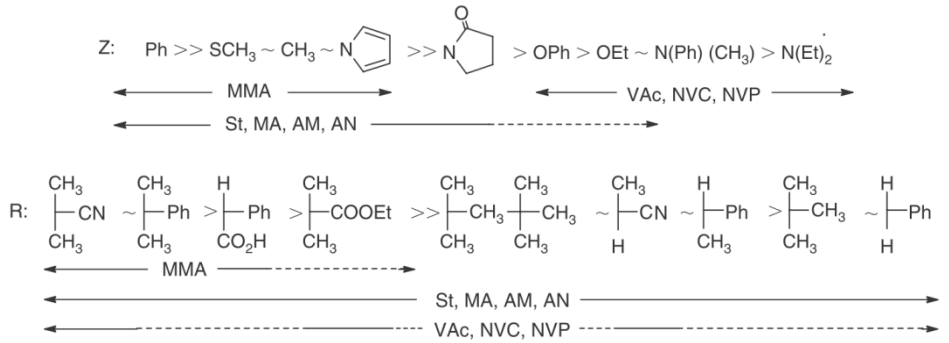

Figure 1.5. Empirical guide to RAFT agent selection. For Z, addition rates decrease and fragmentation rates increase from left to right. For R, fragmentation rates decrease from left to right. A dashed line indicates partial control. Figure and caption reproduced from ref.[17]

The second important aspect to RAFT agent design is the ability to control polymer functionality (see below) and architecture by using functional Z and R groups. For example, Stenzel and colleagues employed RAFT agents **1v-1viii** with multifunctional R and Z groups for the synthesis of 3 and 4-arm star polymers (Figure 1.6).[18]

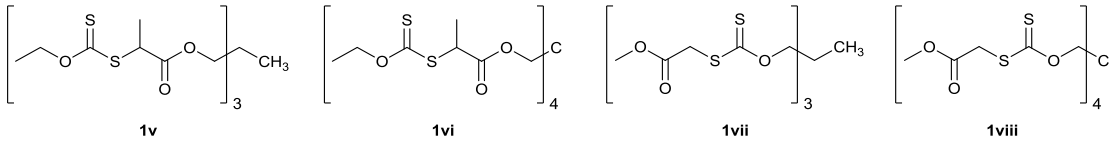

Figure 1.6. Multi-functional RAFT agents (**1v-1viii**) used in the synthesis of 3 and 4-arm star polymers.[18]

1.2. Polymer nanoparticle formation

One of the motivations for exercising control over polymer synthesis is the desire to fabricate solution state polymer particles on the nanometre scale. Control over polymer synthesis is necessary because particle formation often requires specific polymer functionality or architecture (e.g. block copolymers – see below), or because particle size depends on polymer molecular weight. Interest in polymer nanoparticles originates from the aspiration to mimic the structures and functions exhibited by nature's nanomaterials, using synthetic materials.[19] Polymer nanoparticles that demonstrate compartmentalisation,[20] catalytic activity,[21] act as transportation and delivery vehicles,[22] show stimulus responsive behaviour,[23] and exhibit luminescence,[24] have all received significant attention.

There are many classes of colloidal polymer nanoparticles, which are prepared by a variety of different routes. Three important methods for polymer nanoparticle preparation are single-chain collapse, nanoprecipitation, and dendrimer synthesis. These techniques are not utilised in this thesis, so only a brief summary of each is given in the following paragraph.

Single-chain polymer nanoparticles are prepared by the controlled folding or collapse of single polymer chains to produce particles that have diameters of < 15 nm.[25] Folding/collapse occurs *via* the reaction or association of functional groups along the polymer backbone (see Section 1.3) to form cross-links within the polymer random coil (Figure 1.7 a). Nanoprecipitation provides a very simple method for the fabrication of polymer nanoparticles.[26] The polymer is dissolved in a good solvent and this solution is exposed to an excess of non-solvent which is miscible with the solvent, either by dialysis of the solution against the non-solvent, or by dropwise addition of the solution to the non-solvent (Figure 1.7 b).[27] Nanoparticles form instantly and typically have narrow size distributions with diameters of *ca.* 200 nm. Dendrimers are branched (tree-like) macromolecules with precise structure and topology. Consisting of several generations of radially homocentric layers emanating from a central core, dendrimers have a high density and well-defined surface functionality (Figure 1.7 c).[28] Typically they are synthesised by step-wise condensation of multifunctional AB_x monomers, with attachment to a

multifunctional core (B_x) occurring as the first (divergent synthesis) or last (convergent synthesis) step. Size is determined directly from the number of generations synthesised, and unlike other polymer nanoparticles, dendrimer ensembles consist of a uniform and precise single molecular species, which is advantageous to the pharmacokinetic aspects of clinical trials.[29]

The methods given above have found many applications, however the most commonly exploited methods for polymer nanoparticle synthesis are the solution state self-assembly of block copolymers (BCPs), and micro/nanogelation. These two routes for nanoparticle preparation are utilised in Chapter 5 of this thesis, and are discussed in detail below.

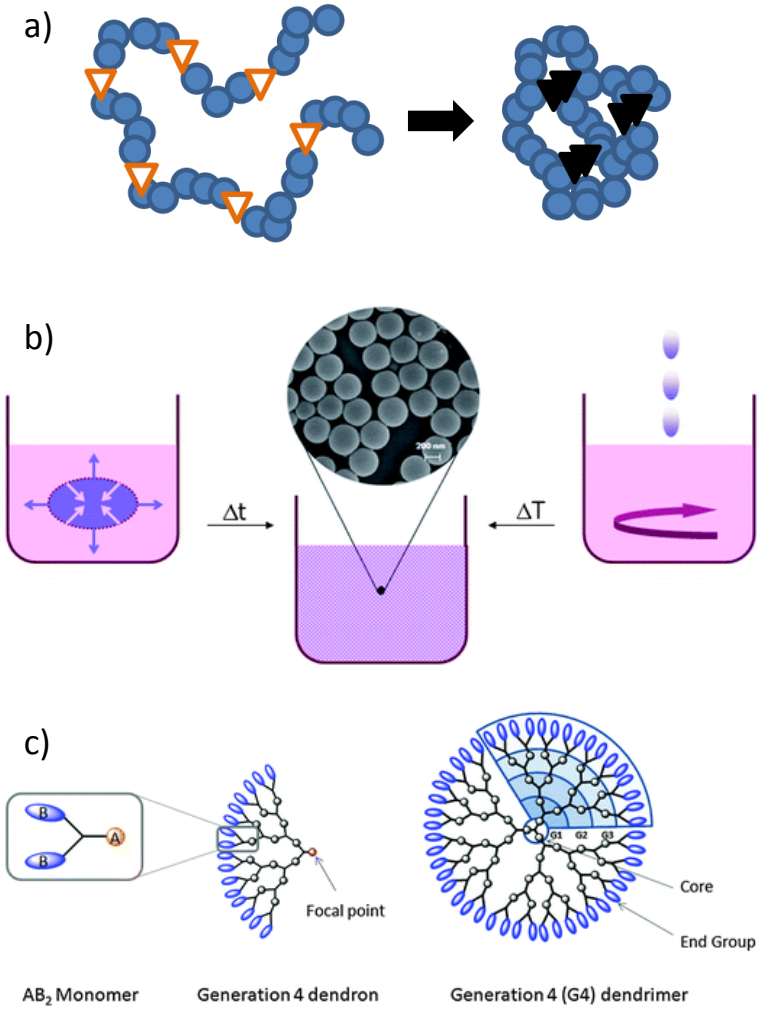

Figure 1.7 Fabrication of polymer nanoparticles. a) Single-chain collapse,[25] b) Nanoprecipitation by dialysis (left) or dropping (right),[27] c) Dendrimer synthesis.[28] Figure adapted from refs.

1.2.1. Block copolymer (BCP) self-assembly

Self-assembly of block copolymer amphiphiles occurs in selective solvents – solvents in which (at least) one block is soluble and (at least) one block is insoluble. This self-assembly is driven by the solvophobic attraction between associating blocks, which is counterbalanced by steric repulsions between solvophilic blocks (and electrostatic repulsions where these solvophilic blocks are ionised).[30] A number of different solution state self-assembled microdomain morphologies have been observed, including spherical micelles, vesicles (polymersomes), cylinders/rods, lamellae, bicontinuous structures, hexagonally packed hollow hoops (HHHs), large compound micelles (LCMs) and disc-like micelles (Figure 1.8).[31]

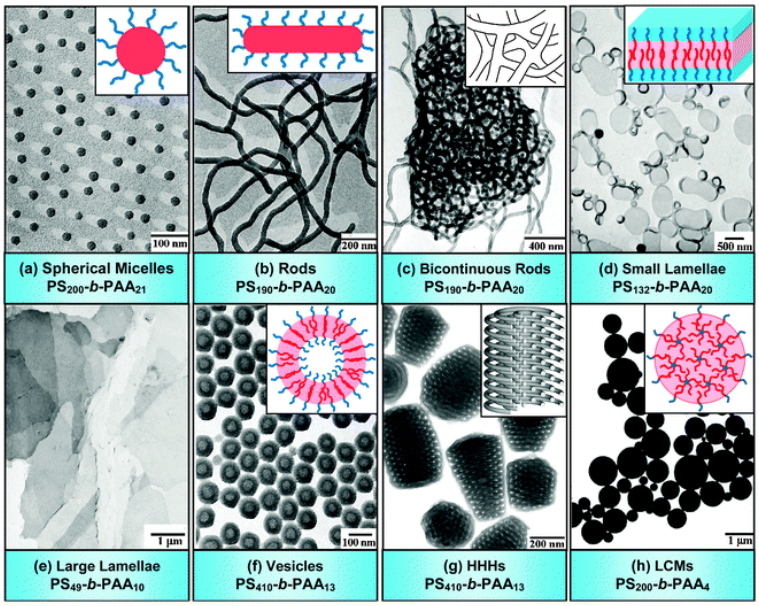

Figure 1.8. Transmission electron microscopy (TEM) images (with schematic diagrams) for various morphologies formed from amphiphilic poly(Sty)-*b*-poly(acrylic acid) block copolymers in water. Figure reproduced from ref.[31]

The relative weight fractions (f) of solvophobic and solvophilic blocks dictate the curvature obtainable by the assembled chains (Figure 1.9), with empirical rules to determine the final equilibrium morphology expected for dynamic aggregates.[32, 33] However, as illustrated in Figure 1.8, multiple morphologies can be prepared by self-assembly of BCPs with the same two blocks, having the same (or very similar) block weight fractions. This is due to the propensity for formation of kinetically trapped ('frozen') structures,[34, 35] with morphology therefore dependent on the preparation pathway.

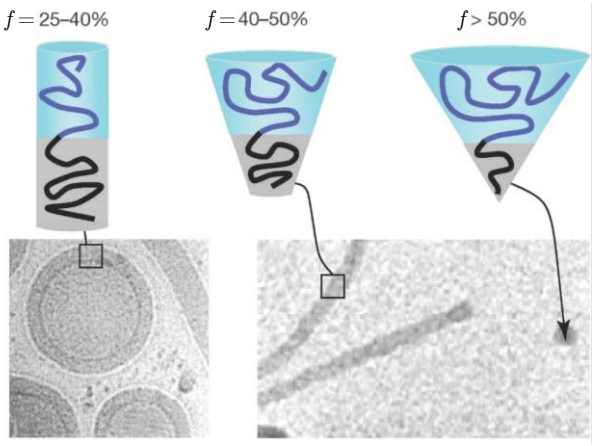

Figure 1.9. Schematics representations and cryo-TEM images of BCP assemblies with varying solvophilic (light blue block) weight-fractions (f), which form (left-to-right) vesicles, worms, and spherical micelles. Figure adapted from ref.[33]

The self-assembly of BCPs provides several benefits as a method of synthesising polymer nanoparticles. For example, the use of stimuli-responsive polymers as one or more of the constituent blocks allows the fabrication of nanoparticles whose assembly can be controlled by such stimuli. By using a core block polymer that can transition between solvophobic and solvophilic states depending on the temperature, its degree of protonation, wavelength of light irradiation *etc.*, leads to polymer micelles whose assembly depends on these stimuli.[23] An additional benefit is the ease with which further functionality can be incorporated into the micelle core or corona. Using either functional initiators or functional monomers, functionalisation reactions can be performed either pre-polymerisation, post-polymerisation or post self-assembly. This concept is discussed further in Section 1.3 and 1.4.

1.2.2. Nanogels

IUPAC defines a nanogel as being a "particle of gel of any shape with equivalent diameter of approximately 1-100 nm".[36] Nanogels can be synthesised by a variety of top-down and bottom-up approaches, however the simplest and most popular method is free radical crosslinking copolymerisation.[37] In order to obtain colloidal gels, rather than macroscopic gels, heterogeneous polymerisation is employed. For example, aqueous nanogel solutions can be prepared by an oil-in-water emulsion polymerisation which comprises monomer (including crosslinking agent), water, surfactant (above its critical micelle concentration), and a water soluble initiator.[38] The emulsion polymerisation proceeds through three

intervals, as shown in Figure 1.10. Initially (interval I), most of the monomer is located in surfactant stabilised monomer droplets (*ca.* 1-10 μm in diameter), with only a small proportion dissolved in the aqueous phase or present in surfactant micelles (*ca.* 5-10 nm diameter). Initiator radicals formed in the aqueous phase first polymerise dissolved monomer, before the increase in hydrophobicity causes these oligomers to enter the monomer micelles (nucleation). During interval II monomer consumed by propagation in the micelles is replaced by monomer from the droplets. Interval III corresponds to disappearance of the monomer droplets, followed by consumption of all monomer in the micelles.

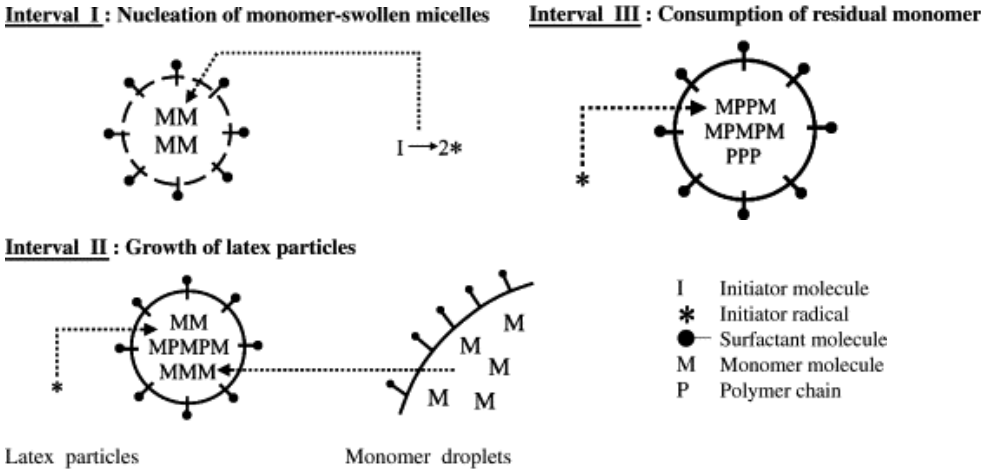

Figure 1.10. The micelle nucleation model of emulsion polymerisation. Figure adapted from ref.[38]

Because emulsion polymerisations proceed to *ca.* 100% monomer conversion, the size of the resultant nanogel particles is dependent on the concentration of latex particles which nucleate during interval I. Smith–Ewart theory predicts that this concentration is proportional to surfactant concentration, and to a lesser extent the initiator concentration. Therefore the size of the resultant nanoparticles can be controlled by the amount of surfactant used in the emulsion polymerisation; with increasing amounts of surfactant leading to an increase in nucleated particles, and therefore smaller nanogels.

The main advantage of nanogels over other classes of polymer nanoparticle is the ease with which they can be synthesised, with solutions of nanogels being produced in a single step from monomer starting materials. This fact, coupled to the wide spread usage of emulsion polymerisation for microparticle synthesis on an industrial scale, means nanogel synthesis is a scalable and potentially industrially relevant route to polymer nanoparticles.

1.3. Efficient synthesis of functional polymers

As mentioned above, control over the mechanism of polymerisation enables control over the incorporation of desirable functionality into polymers. Control over both the location of functional groups within the polymer (spatial control) and over the step in which the desired functionality is introduced (temporal control) can be exercised. This premise is illustrated in Figure 1.11.

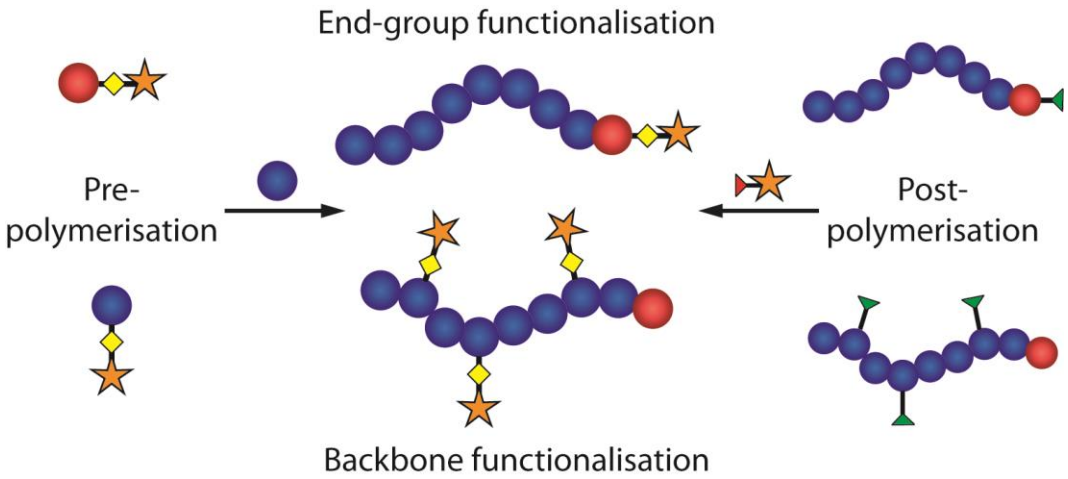

Figure 1.11. Spatial and temporal control over the introduction of polymer functionality.

Site-specific introduction of functionality can be achieved through the use of functional initiators (e.g. in ionic polymerisation, ATRP, NMP *etc.*) or functional RAFT agents. Either the functional group of interest is incorporated into the initiator/RAFT agent (pre-polymerisation), or it is inserted into preformed polymer by a post-polymerisation modification of the initiator-derived end-group. Backbone functionality can also be achieved either pre-polymerisation, using a functional monomer, or by a post-polymerisation modification. A summary of these four approaches, with the main advantage of each approach, is shown in Table 1.1. Also listed are the Chapters of this thesis in which each approach is utilised.

Table 1.1. Spatial and temporal control over the introduction of polymer functionality.

	Pre-polymerisation	**Post-polymerisation**	**Main Advantage**
Site specific	Functional initiator Chapter 2 & 3	End-group modification Chapter 3	Precise location of functional group is known
Backbone	Functional monomer Chapter 4	Pendent-group modification Chapter 4	Higher density of functional groups possible
Main Advantage	Does not require efficient chemistry as small molecules are easier to purify.	Functional group does not need to be tolerant to polymerisation conditions	

The self-assembly of functional BCPs provides a convenient route for the fabrication of polymer nanoparticles containing functional groups. In the following sections, examples of the four routes to functional polymers are given. Applications for these functional polymers are also discussed, which includes the synthesis of functional polymer micelles. Consideration of fluorescent functional group incorporation is reserved until Section 1.4, which discusses the formation of fluorescently-labelled nanoparticles using all four of these strategies.

1.3.1. Functional initiators

Functional initiators can be used to locate specific groups at precise locations on a polymer chain. Both α- and ω-chain ends can be targeted, while the use of a symmetric initiator can also allow the mid-point of a polymer chain to be functionalised. Functional initiators have been utilised in ionic polymerisation, ROMP, ATRP, NMP, and RAFT polymerisation. A wide range of functional groups have been incorporated in this way, leading to a diverse range of applications for the polymers produced. The efficiency of functional group incorporation in the final product is dependent on end-group retention (which can be almost perfect in living polymerisations and those with living characteristics) rather than the reactivity of the functional group. Rather than attempting

an exhaustive review of this topic, selected examples of functional initiators (Figure 1.12) are given below, in an attempt to highlight the scope and utility of this approach.

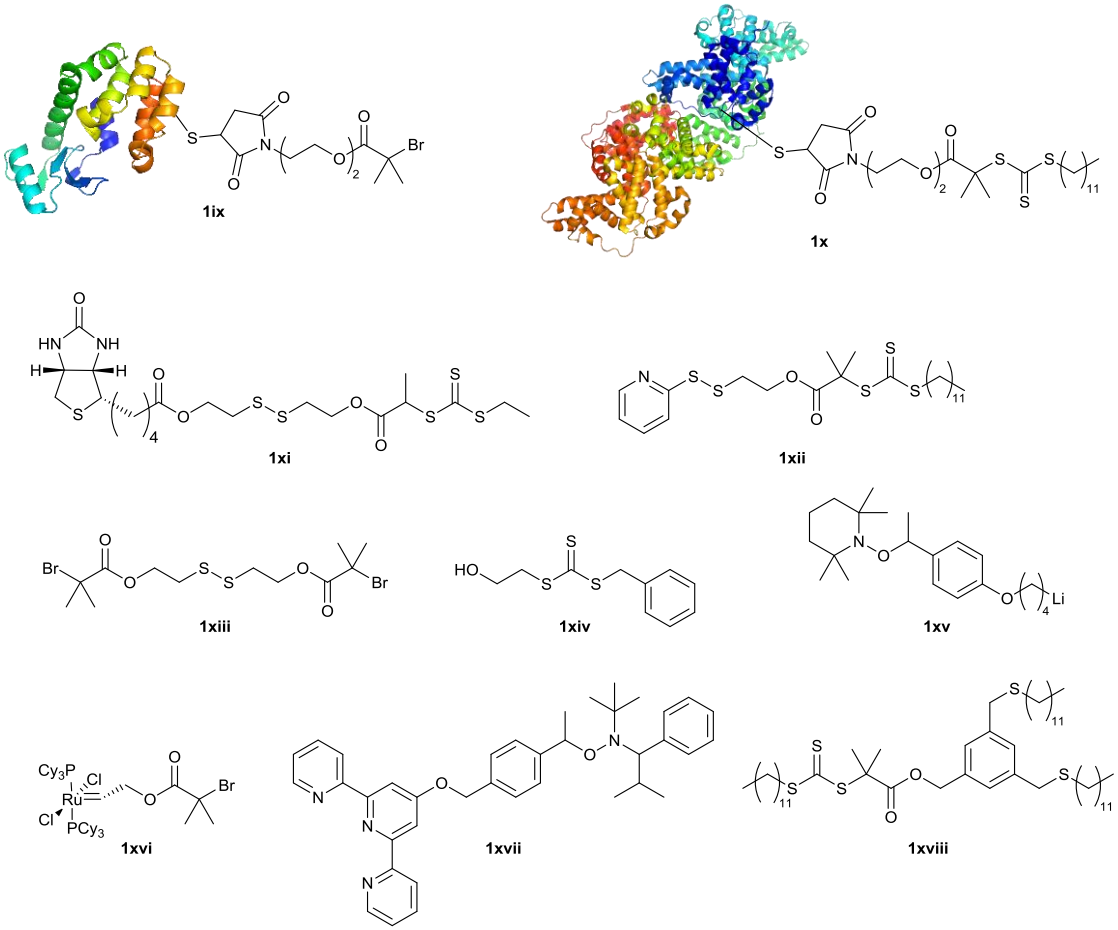

Figure 1.12. Functional initiators/RAFT agents. T4 lysozyme (2LZM) and bovine serum albumin (4F5S) structures obtained from the Protein Data Bank (PDB).

Polymer-protein conjugation is of significant interest, due to the reduced immunogenicity, improved physical stability, and improved thermal stability of the conjugates.[39] To this end protein-functional macro-initiators for ATRP and RAFT have been utilised for 'grafting-from' conjugate synthesis. For example, Maynard *et al.* attached an alkyl halide ATRP initiator to a lysozyme mutant at its engineered cysteine residue. This lysozyme-functional ATRP initiator (**1ix**) was used to polymerise *N*-isopropylacrylamide (NIPAM), resulting in a polymer-enzyme conjugate that retained its full bioactivity.[40] Sumerlin and co-workers also demonstrated 'grafting-from' polymerisation of NIPAM using a RAFT agent functionalised with bovine serum albumin (BSA) *via* a native free cysteine residue (**1x**). The thermoresponsive nature of poly(NIPAM) allowed regulation of BSA activity, with activity decreased above the poly(NIPAM) lower critical solution temperature (LCST) relative to native BSA.[41] In an alternative approach to polymer-protein

conjugation Maynard and colleagues used a RAFT agent functionalised with biotin (**1xi**) for the synthesis of poly(NIPAM) that could be immobilised on a streptavidin surface.[42]

Where an initiator/RAFT agent contains two functional groups telechelic polymers can be obtained. This was demonstrated by Phillips and Gibson, who used RAFT agent **1xii** to produce telechelic polymers with complementary reactive α- and ω-chain ends. In the presence of a base catalyst the pyridyl disulfide and trithiocarbonate chain ends reacted (with liberation of pyridine thione) to form poly(disulfide) condensation polymers. Further disulfide exchange in the form of reduction by glutathione (GSH) facilitated poly(disulfide) degradation (Figure 1.13). This degradation occurred selectively at high (intracellular) concentrations of GSH (mM), with the poly(disulfides) being stable at low (extracellular) GSH concentrations (μM).[43] Thiol degradable polymers were also produced by Oh and co-workers. They used the symmetric ATRP initiator **1xiii** to site-specifically locate disulfide bonds at the midpoint of a P(OEGMA)-*b*-P(AP)-*b*-P(OEGMA)[i] amphiphilic triblock copolymer. After self-assembly in water to form polymer micelles, cleavage of the disulfide bonds by dithiothreitol produced P(AP)-*b*-P(OEGMA) diblock copolymers, leading to a change in micelle morphology.[44]

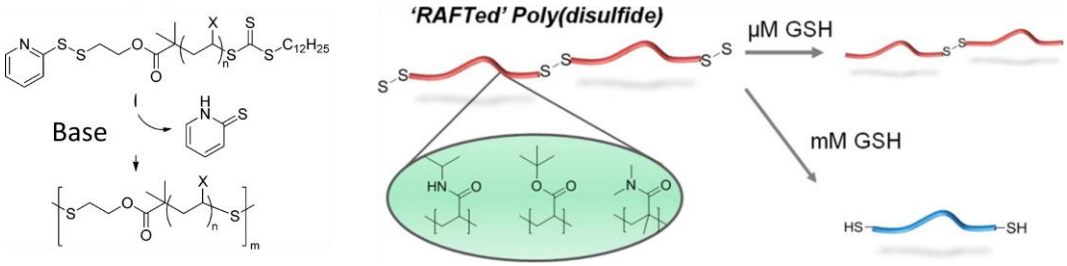

Figure 1.13. Synthesis and selective degradation of poly(disulfides) derived from the pyridyl disulfide-functional trithiocarbonate RAFT agent **1xii**.

There are many reports where the functionality that is desired in a polymer produced by one mechanism is the initiating group for a second polymerisation mechanism. These dual initiators have been utilised where diblock copolymers of two monomers that require different polymerisation techniques are desired. For example Wooley and colleagues used dual initiator **1xiv** to produce P(NAS-*co*-NAM)-*b*-P(L-LA)[ii] by sequential organocatalytic

[i] Poly[(oligo ethyleneglycol methacrylate)-*b*-(oligo propylene oxide monononylphenyl ether acrylate)-*b*-(oligo ethyleneglycol methacrylate)]
[ii] Poly[(*N*-acryloyloxy succinimide-*co*-*N*-acryloylmorpholine)-*b*-(L-lactide)]

ring-opening and RAFT polymerisation.[45] This route afforded an amphiphilic BCP that could self-assemble into polymer micelles which contained an enzymatically degradable polyester core. Miura *et al.* used dual initiator **1xv** to synthesise poly(dimethylsiloxane)-*b*-poly(Sty) by sequential anionic ring-opening polymerisation (ROP) and NMP,[46] while Grubbs and colleagues demonstrated the tandem ROMP of 1,5-cyclooctadiene and ATRP of methyl methacrylate initiated from and catalysed by dual initiator **1xvi**.[47]

Functional groups that act as ligands for metal atoms have also been of interest. For example, O'Reilly and co-workers used the terpyridine-functional NMP initiator **1xvii** to synthesise poly(acrylic acid) and poly(Sty). Complexation with ruthenium afforded an amphiphilic metallo-block copolymer which self-assembled into polymer micelles. After crosslinking of the poly(acrylic acid) shell, addition of a competitive binder for Ru broke the linkage between the blocks allowing hollow particle formation by removal of the poly(Sty) core.[48] The same group also used an SCS pincer-functional RAFT agent (**1xviii**) for the synthesis of poly(acrylic acid) amphiphilic homopolymers which could self-assemble into spherical and cylindrical micelles in water. Complexation of the SCS pincer ligand with palladium gave catalytic nanoreactors, whose activity was drastically improved over a small molecule SCS-Pd complex.[49]

1.3.2. Functional monomers

Functional monomers are used to provide polymers with large number of functional groups per chain. Homopolymerisation of functional monomers provides the highest density of the desired groups, while co-polymerisation can be used to obtain polymers with intermediate properties (such as solubility) between homopolymers of the functional and non-functional monomer. The use of living polymerisation techniques, or those with the features of living polymerisation (such as RDRP processes) allow control of *DP* and copolymer composition, therefore allowing specific densities of functionality to be targeted. The efficiency of functional monomer incorporation into the final product depends on the efficiency with which the functional monomer is polymerised. Functional groups with large steric constraints can prohibit homopolymerisation, however judicious monomer design (for example modification of a well characterised monomer) will often facilitate highly efficient polymerisation. As with the functional initiators described above, a wide range of

functional groups have been incorporated by the monomer approach. Once again, a select group of examples (rather than a comprehensive review) are given below (Figure 1.14), highlighting the scope of this approach and the range of applications to which it has been applied.

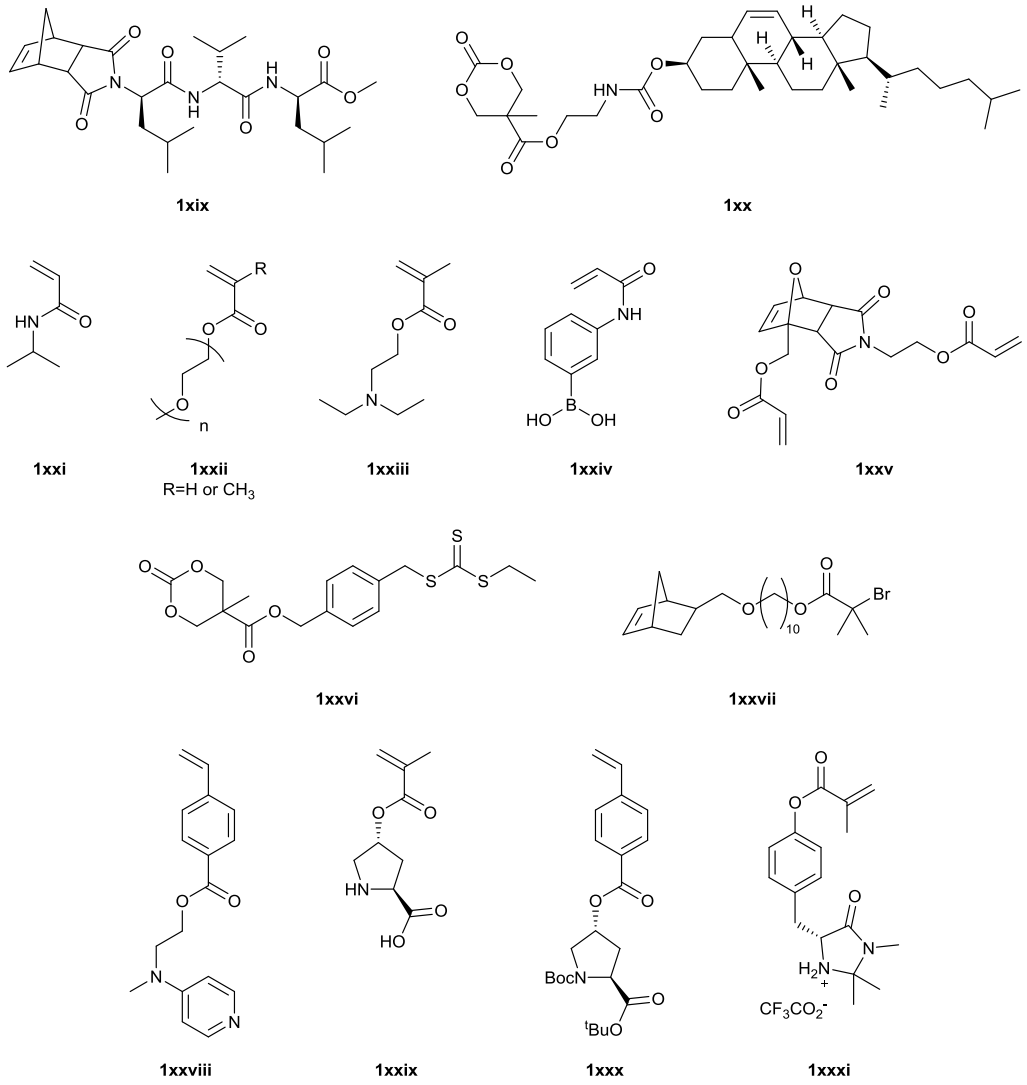

Figure 1.14. Funtional monomers

Biagini and colleagues used ROMP to produce amphiphilic BCPs containing the peptide norbornene monomers **1xix** as the hydrophobic block. These peptide units directed the aqueous self-assembly of these BCPs leading to the unprecedented formation of bicontinuous structures (Figure 1.15 a&b).[50] Cholesterol was also incorporated into the hydrophobic block of an amphiphilic BCP prepared by organocatalytic ROP using cyclic carbonate monomer **1xx**. Yang *et al.* demonstrated the templating ability of this cholesterol functionality with aqueous self-assembly of these BCPs affording stacks of disc-

like micelles, due to cholesterols propensity for rotative face-on-face stacking (Figure 1.15 c).[51]

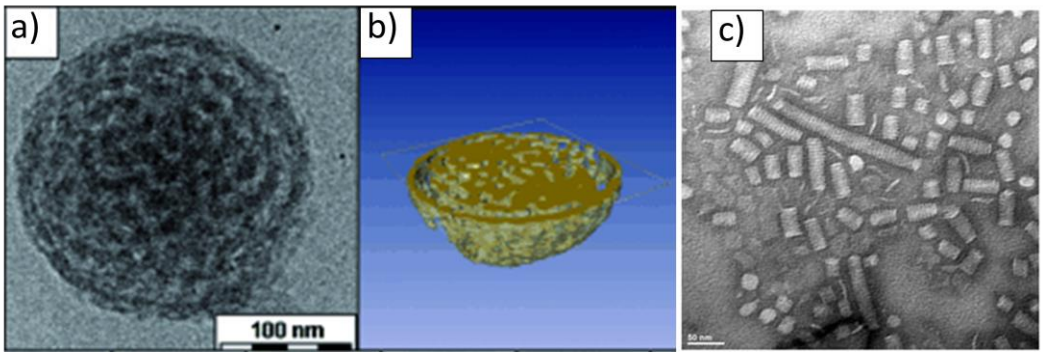

Figure 1.15. a) Cryo-TEM image and b) cryo-ET reconstruction of self-assembled poly(**1xix**)-containing BCPs.[50] c) Negatively stained TEM image of self-assembled poly(**1xx**)-containing BCPs.[51] Figure adapted from refs.

Functional groups that are responsive to stimuli are routinely incorporated into polymers through the use of functional monomers. Common examples include NIPAM (**1xxi**) and oligoethylene glycol (meth)acrylates (**1xxii**), which show an LCST in water.[52, 53] Copolymerisation of these monomers with non-responsive monomers allows LCSTs to be tuned over a *ca.* 100 °C temperature range. Response to pH is another commonly desired functionality, which is provided by monomers such as *N*,*N*,-(diethylamino)ethyl methacrylate (**1xxiii**).[54] More exotic stimuli have also been investigated, for example Sumerlin and co-workers performed the RAFT polymerisation of the boronic acid monomer **1xxiv**, which undergoes a reversible reaction with diols. The use of multifunctional diols allowed cross-linked networks of poly(**1xxiv**) homopolymers to be formed, while reaction with poly(dimethylacrylamide-*b*-**1xxiv**) amphiphilic BCPs afforded star polymers. These stars were shown to be dynamic in solution, with a reversible star-to-unimer transition afforded by alternation between monofunctional and multifunctional diols.[55] The maleimide-furan Diels-Alder adduct can also be utilised as a dynamic cross-linker. Haddleton and colleagues used ATRP to chain extend poly(methyl methacrylate) with the diacrylate monomer **1xxv**, affording star polymers which could be cleaved by the retro Diels-Alder reaction at high temperature.[56]

Monomers containing initiator functionality have been utilised in the synthesis of graft/brush copolymers. Where this initiator functionality provides an orthogonal

polymerisation mechanism a 'grafting-from' strategy is pursued. For example Dove and co-workers performed organocatalytic ring-opening homo- or copolymerisation of the cyclic carbonate monomer (**1xxvi**), with subsequent RAFT polymerisation affording a range of degradable graft copolymers.[57] A one-pot, two-step 'grafting-from' approach was pursued by Wooley and colleagues, using monomer (**1xxvii**). First ROMP of **1xxvii**, then ATRP of MMA were performed using the Grubbs catalyst, to give graft copolymers with a poly(norbornene) backbone and PMMA brushes.[58]

Monomers containing catalytically active functional groups are also of interest, for the fabrication of polymeric 'nanoreactors' which improve catalyst recyclability and enhance reactivity *via* the 'concentrator effect'.[59] For example O'Reilly *et al.* have introduced 4-(*N*,*N*-dimethylamino)pyridine (**1xxviii**),[60, 61] L-proline (**1xxix** and **1xxx**),[62-64] and the MacMillan catalyst (**1xxxi**)[65] into RAFT copolymers, RAFT BCPs for micellar self-assembly, and into polymer nanogels by radical cross-linking polymerisation.

1.3.3. Post-polymerisation modification using highly efficient reactions

Post-polymerisation modification provides a means of incorporating functionality that is intolerant to polymerisation reaction conditions. This approach is also appropriate for producing libraries of functional polymers based on a single polymeric backbone. However, highly efficient reactions which reach *ca.* 100% conversion are required as it can be very difficult (or even impossible) to purify polymers that differ in functionality, rather than molecular weight.[66] For this reason 'click' reactions are commonly applied to post-polymerisation modification of polymers.[67] In addition to the original 'click' criteria proposed by Sharpless,[68] further requirements for reactions where one or more reagents are a polymer were made by Barner-Kowollik *et al.* (Figure 1.16).[69]

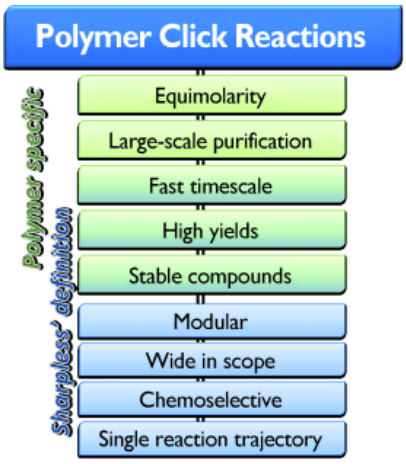

Figure 1.16. Requirements for click reactions involving one or more polymeric reagents (blue: originally defined by Sharpless; green and blue–green: adapted requirement related to synthetic polymer chemistry). Figure and caption reproduced from ref.[69]

The condition for equimolarity specifically applies to polymer-polymer conjugation 'click' reactions, with Barner-Kowollik *et al.* conceding that if simple purification (such as selective precipitation) can be used to remove a component, it is reasonable to use this reagent in excess to shorten the reaction time.

1.3.3.1. The 'click' reactions

'Click' reactions, and those reactions that might subsequently have been downgraded to 'highly efficient', applied in the synthesis of functionalised polymers have been reviewed by Schubert and colleagues (Figure 1.17).[66] Including 'clickable' functional groups into the polymer structure allows the introduction of a huge variety of functionality, e.g. biological substrates, responsive group *etc.* that might not have been accessible by the functional initiator and monomer approaches detailed above.

To highlight the scope of this approach several examples of the 'clickable' initiators and monomers that have been utilised by polymers chemists, along with the functional groups incorporated using this strategy, are detailed below.

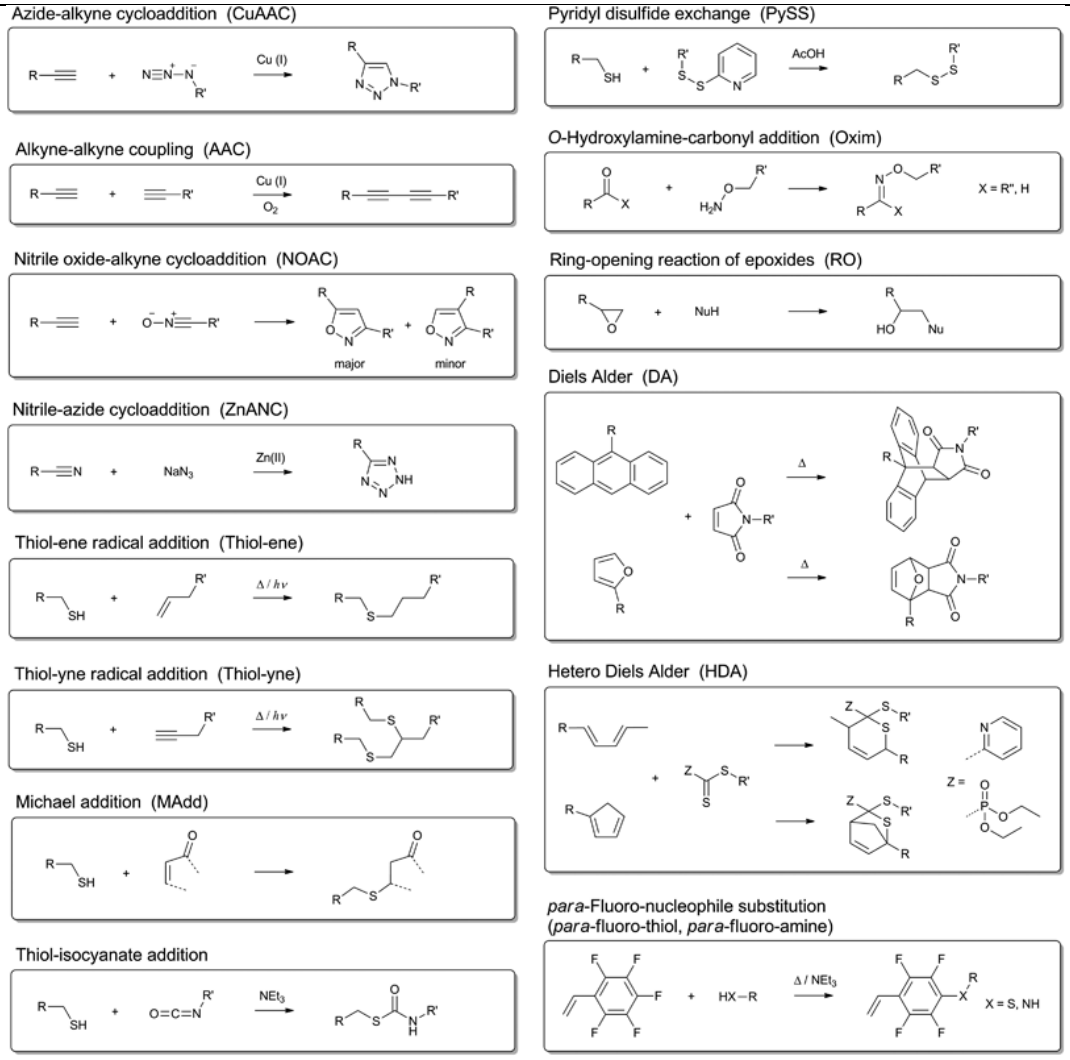

Figure 1.17. Highly efficient reactions used in post-polymerisation modification. Figure reproduced from ref.[66]

1.3.3.2. Clickable initiators

As the original polymer 'click' chemistry, the copper-catalysed azide-alkyne cycloaddition (CuAAC) reaction has been widely utilised.[70] For example, carbohydrate-functionalised hyperbranched polymers have been prepared by Whittaker and co-workers using CuAAC. Copolymerisation of 2-(dimethylamino)ethyl acrylate and 2,2,2-trifluoroethyl acrylate, with ethyleneglycol dimethacrylate as a crosslinking agent was mediated by RAFT agent **1xxxii** (Figure 1.18). The result was hyperbranched polymers that could be modified with an azide-functional mannose, by CuAAC reaction with the alkyne groups introduced by **1xxxii**. These hyperbranched polymers demonstrated applications as ^{19}F magnetic resonance imaging (MRI) agents, which could show affinity to mannose-binding lectins.[71] The CuAAC reaction was also used by O'Reilly and colleagues for the fabrication of DNA-polymer conjugates *via* a post-polymerisation modification. Using RAFT agent

1xxxiii, poly(NIPAM) was synthesised with a pentafluorophenyl ester α-chain end. Reaction with 3-azido-1-aminopropane produced azide-terminated poly(NIPAM), which underwent CuAAC with alkyne-functional single-stranded (ss) DNA. Poly(NIPAM) and poly(Sty) synthesised using RAFT agent **1xxxiv** were functionalised with azide modified ssDNA by CuAAC, with these nucleic acid-functional polymers acting as 'giant surfactant' in aqueous solution state self-assembly.[72] Synthetic polymers have also been functionalised with double-stranded short interfering (si) RNA using a post-polymerisation functionalisation by Maynard and co-workers. Using a pyridyl disulfide-functional ATRP initiator (**1xxxv**) glycopolymers were synthesised from a D-glucosamine methacrylate monomer. A disulfide exchange reaction between polymer chain ends and thiol-functional siRNA afforded nucleic acid-functional glycopolymers. This conjugation was shown to be reversible, with the addition of dithiothreitol leading to cleavage of the adduct.[73]

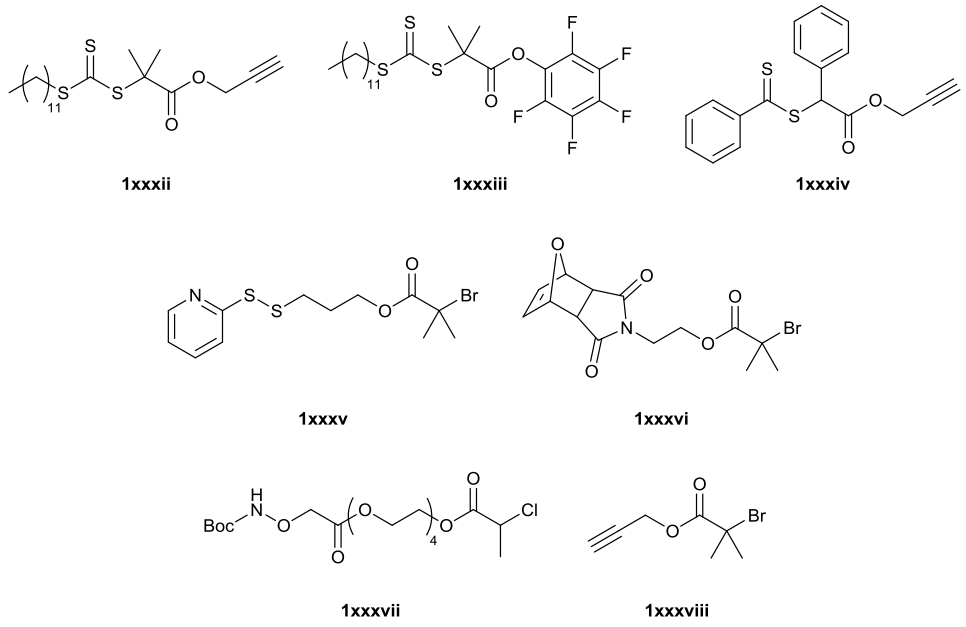

Figure 1.18. Initiators/RAFT agents for post-polymerisation functionalisation *via* 'click' reactions.

In addition to nucleic acid macromolecules, polymers prepared by RDRP processes have also been functionalised with peptide macromolecules by post-polymerisation modification reactions. Haddleton and co-workers demonstrated that Michael addition between thiol and maleimide groups could be used for the synthesis of protein-polymer conjugations. Maleimide-furan terminated polymers were produced using ATRP initiator **1xxxvi**, with subsequent retro Diels-Alder reaction revealing the maleimide group. Reaction with the

free cysteine residue of BSA produced protein-functionalised poly(OEGMA) and poly(glycerol methacrylate).[74] Oxime-ligation has also been utilised for post-polymerisation functionalisation of polymers with proteins. Maynard and colleagues used ATRP initiator **1xxxvii** for the synthesis of poly(NIPAM) with Boc-protected aminooxy α-chain ends. Reaction with ketone-functional BSA (prepared by lysine conjugation to an *N*-hydroxy succinimidyl levulinate) afforded the thermoresponsive protein-functional polymer.[75]

A post-polymerisation functionalisation strategy for conjugation of multi-walled carbon nanotubes (MWNTs) with polymers has also been achieved using a 'clickable' initiator. Gao and co-workers used the commercially available ATRP initiator **1xxxviii** to synthesise alkyne-terminated poly(Sty). The MWNTs were first grafted with a layer of azide-functional polymer, allowing subsequent CuAAC to produce carbon nanotubes functionalised with poly(Sty).[76] A similar approach was taken for the functionalisation of RDRP polymers with silica nanoparticles. Ranjan and Brittain used RAFT agent **1xxxii** for the synthesis of alkyne-terminated poly(acrylamide) and poly(Sty), the latter also being synthesised by ATRP using initiator **1xxxviii**. Functionalisation with azide modified silica nanoparticles afforded the desired core-shell particles.[77]

1.3.3.3. Clickable monomers

The polymerisation of reactive monomers (Figure 1.19) gives polymers with pendent groups along the backbone, which can undergo highly efficient/'click' post-polymerisation functionalisation reactions. As opposed to end-group functionalisation which imparts only one or two reactive groups to the final polymer, the use of clickable monomers allows a higher degree of polymer modification to be achieved. The exact degree of functionalisation can also be controlled independently of polymer molecular weight, by copolymerisation of the functional monomer with a non-functional monomer at specific monomer feed ratios. The reactive nature of the clickable groups often means reaction times, monomer conversions, and loadings must be kept low, due to side reactions during RDRP processes.[66]

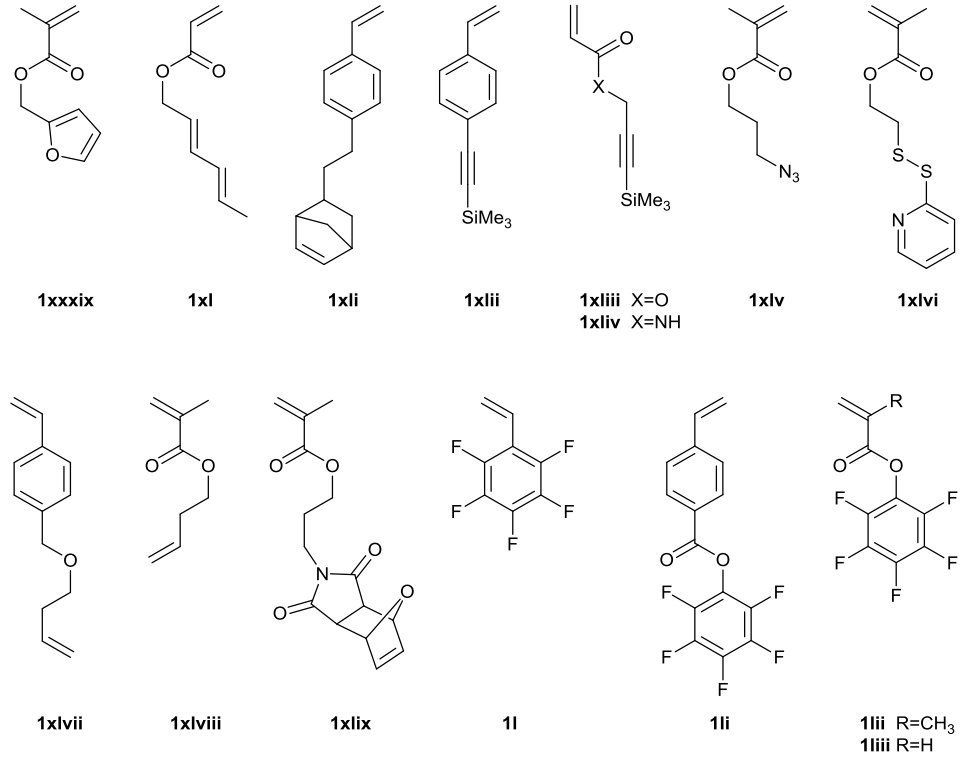

Figure 1.19. Vinyl monomers with reactive functional groups used for post polymerisation functionalisation.

There are many examples of reactive vinyl monomers based on the most popular click reactions. For example, Kavitha and Singha used ATRP to copolymerise the commercially available furan-functional methacrylate monomer **1xxxix** with MMA. The resultant copolymers could then be thermo-reversibly cross-linked by the Diels-Alder reaction with a bismaleimide.[78] Monomers that undergo hetero Diels-Alder reactions have also been polymerised, such as the diene-functional acrylate **1xl**, and the norbornyl styrene **1xli**. Both monomers were copolymerised with Sty *via* RAFT polymerisation. Subsequent reaction of poly(Sty-*co*-**1xl**) with pyridin-2-yldithioformate-terminated polymers gave combs,[79] while the reaction of dipyridyl tetrazine was used for functionalisation of micelles with poly(Sty-*co*-**1xli**) cores.[80]

The CuAAC click reaction has also been widely employed. For example Hawker *et al.* used the alkyne monomers **1xlii**, **1xliii** and **1xliv** in NMP (with the TMS protecting group required to prevent side reactions of radicals with the alkyne group), to give a range of polymers that could undergo functionalisation with small molecule azides.[81] This was used as part of a cascade strategy where esterification/amidation was used alongside CuAAC for simultaneous orthogonal functionalisation. Because the azides also contained alcohol or

amine groups they acted as 'linkers', with activated esters (*N*-hydroxy succinimide or anhydride) acting as the terminal groups (Figure 1.20). Azide-functional monomers have also been used; for example Matyjaszewski and co-workers used ATRP to produce homopolymers of **1xlv**, which were shown to undergo highly efficient CuAAC reactions with model small molecule alkynes.[82]

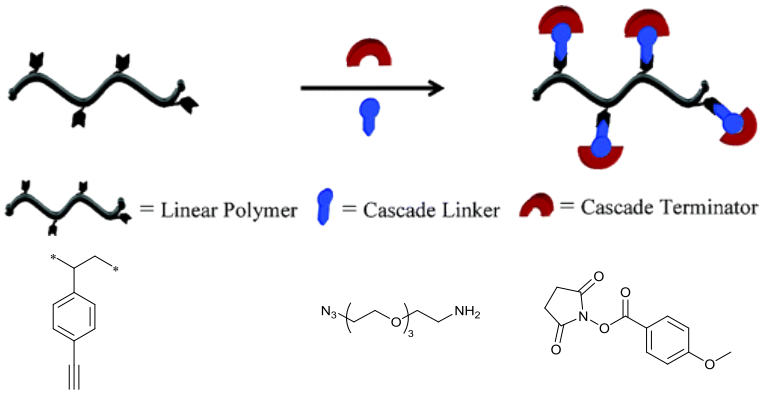

Figure 1.20. Simultaneous orthogonal functionalisation *via* a cascade reaction, with example structures for the three components. Figure adapted from ref.[81]

Thiol-reactive monomers have also proved popular, with three highly efficient reactions possible. Bulmas *et al.* showed that the pyridyl disulfide-containing monomer **1xlvi** could be polymerised by RAFT, and that the resultant homopolymers undergo disulfide exchange reactions with thiols including the tripeptide glutathione.[83] Hawker and colleagues copolymerised the alkene-functional monomers **1xlvii** and **1xlviii** by RAFT and ATRP respectively, observing no cross-linking (*i.e.* no polymerisation of the pendent alkene).[84] Radical thiol-ene reactions were demonstrated with a range of model thiols, with a photochemical radical initiator giving a more efficient reaction than a thermal initiator. Thiol-Michael addition reactions have also been used to functionalise polymer hydrogels of OEGMA and **1xlix** synthesised by FRP. The reactive maleimide C=C double bond was unmasked post-polymerisation by the retro Diels-Alder reaction.[85] By using a biotin-functional thiol, streptavidin could be immobilised into the hydrogel structure. These hydrogels showed a high degree of specificity due to the effective anti-biofouling OEGMA scaffold which prevented non-specific protein interactions.

Fluorinated monomers also enable efficient post-polymerisation modification. Schubert *et al.* demonstrated that NMP polymers of **1l** can be modified by both amines and thiols *via*

a para-fluoro-nucleophilic substitution, for the synthesis of graft copolymers and glycopolymers respectively.[86, 87] Alternatively, pentafluorophenol (PFP) has been used as an activated ester group by Theato *et al.* Interestingly, they showed that copolymers of **1li** and **1lii** synthesised by RAFT polymerisation could be sequentially functionalised, as aromatic amines were only reactive toward the more reactive vinylbenzyl PFP-ester, allowing for the construction of highly functionalised block copolymers.[88] Moore and O'Reilly demonstrated the post-polymerisation functionalisation of **1liii** homopolymers with the amino acid L-tryptophan. These chiral pendent groups were demonstrated to discriminate between enantiomers of 1,1'-bi-2-naphthol (BINOL), with poly(L-tryptophan) showing stronger interaction with *S*-BINOL.[89]

1.4. Strategies for preparing fluorescently-labelled nanoparticles

One class of functional groups that are frequently incorporated into polymer materials are fluorophores. Both pre- and post-polymerisation modification of initiators and monomers have been used for this purpose. These topics are discussed in Chapter 3 and Chapter 4 respectively, where the application of dibromomaleimide and dithiomaleimide chemistry to fluorescent labelling is developed.

Fluorescence spectroscopy and microscopy is a widely used technique for the detection and visualisation of compounds containing fluorophores. Fluorescently-labelled nanoparticles possess several features that make them more valuable for this purpose than classical fluorescent organic dyes.[90] Organic dyes often have low absorption coefficients, which reduces detection sensitivity, and are susceptible to photobleaching, thus limiting their use to short-term measurements. Furthermore, organic fluorophores often have short emission lifetimes, which can prohibit use in time-resolved measurements, while the toxicity of many organic fluorophores impedes their application to *in vitro* and *in vivo* analysis.[91] On the contrary, polymer nanoparticles with fluorescent functionality often contain multiple fluorophores leading to brighter emission, while the encapsulation of fluorophores in a macromolecular structure improves dye stability, and can impart biocompatibility to the fluorescently-labelled agent.[91] Covalent attachment of the dye molecules to the polymer nanoparticles is more efficient and stoichiometrically precise than physical absorption of the fluorophore, and also reduces leaching of the dye from the nanoparticle.[90]

What follows is a short demonstration of the ways in which fluorescently-labelled polymer nanoparticles can be prepared. Depending on the labelling strategy used, the location of the fluorophore within the polymer nanoparticle can be varied, while additional particle properties can be selected based on the synthetic particle formation strategy employed.

1.4.1. Block copolymer (BCP) micelles

The polymerisation of monomers containing fluorescent functional groups has been utilised to produce amphiphilic BCPs that can self-assemble to form fluorescent micelles. For example Liu and co-workers used two different fluorescent monomers, whose fluorophores

comprised a Förster resonance energy transfer (FRET) pair. In FRET a pair of fluorophores (the donor and acceptor) are coupled by a dipole–dipole interaction, so that excitation of the donor is followed by energy transfer to the acceptor, resulting in acceptor emission.[92] Using these FRET pair monomers Liu and co-workers prepared BCP micelles of poly(Sty)-*b*-poly(NIPAM) labelled with an oxadiazole FRET donor in the Sty core and rhodamine FRET acceptor in the NIPAM corona (Figure 1.21).[93] Initially the rhodamine was in the non-emissive spirolactam form, so oxadiazole (green) emission was observed. However, an increase of pH to > 6, or the presence of Hg^{2+} ions lead to formation of the acyclic emissive rhodamine, leading to FRET and therefore rhodamine emission. Subsequent increase of the temperature above the poly(NIPAM) LCST caused dehydration of the coronal chains, causing them to collapse onto the core, which decreased the donor-acceptor distance leading to a FRET enhancement.

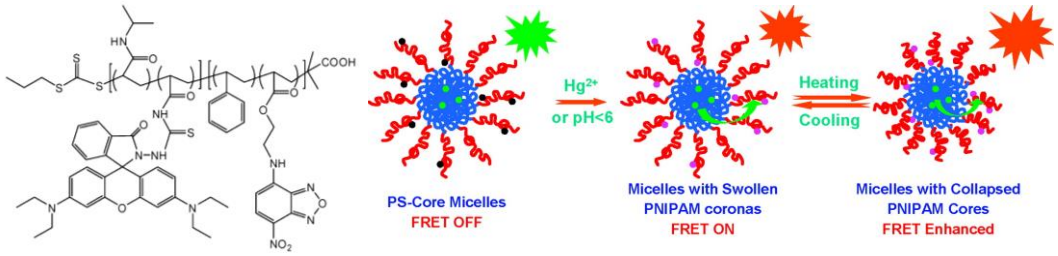

Figure 1.21. Synthesis of pH, temperature and Hg^{2+} responsive core/corona dye-labelled micelles using oxadiazole and rhodamine monomers. Figure adapted from ref.[93]

Clickable monomers have also been used to produce fluorescent amphiphilic BCPs for the self-assembly of fluorescent micelles. An incredible example of this is the recent work of Manners and colleagues. Poly(ferrocenyl dimethylsilane)-*b*-poly(dimethylsiloxane-*co*-methylvinylsiloxane) BCPs were synthesised by anionic ring opening polymerisation. The vinyl groups of the methylvinylsiloxane units were subsequently functionalised by the thiol-ene 'click' reaction to produce three different BCPs containing BODIPY dyes with either red, green or blue emission (Figure 1.22 a). Crystallisation driven self-assembly (CDSA)[94] led to the formation of cylindrical micelles with uniform contour lengths of *ca.* 2 μm whose emission wavelength could be tuned based on the ratio of red: green: blue BCPs in the CDSA reaction mixture. A full spectrum of emission was achieved, including white light, with emission visualised in solution and by confocal microscopy (Figure 1.22 b). Both symmetric (Figure 1.22 c) and asymmetric (Figure 1.22 d) multi-block

cylindrical micelles could be fabricated by sequential BCP addition due to the living nature of CDSA, leading to the formation of "nanoscale RGB pixels".[95]

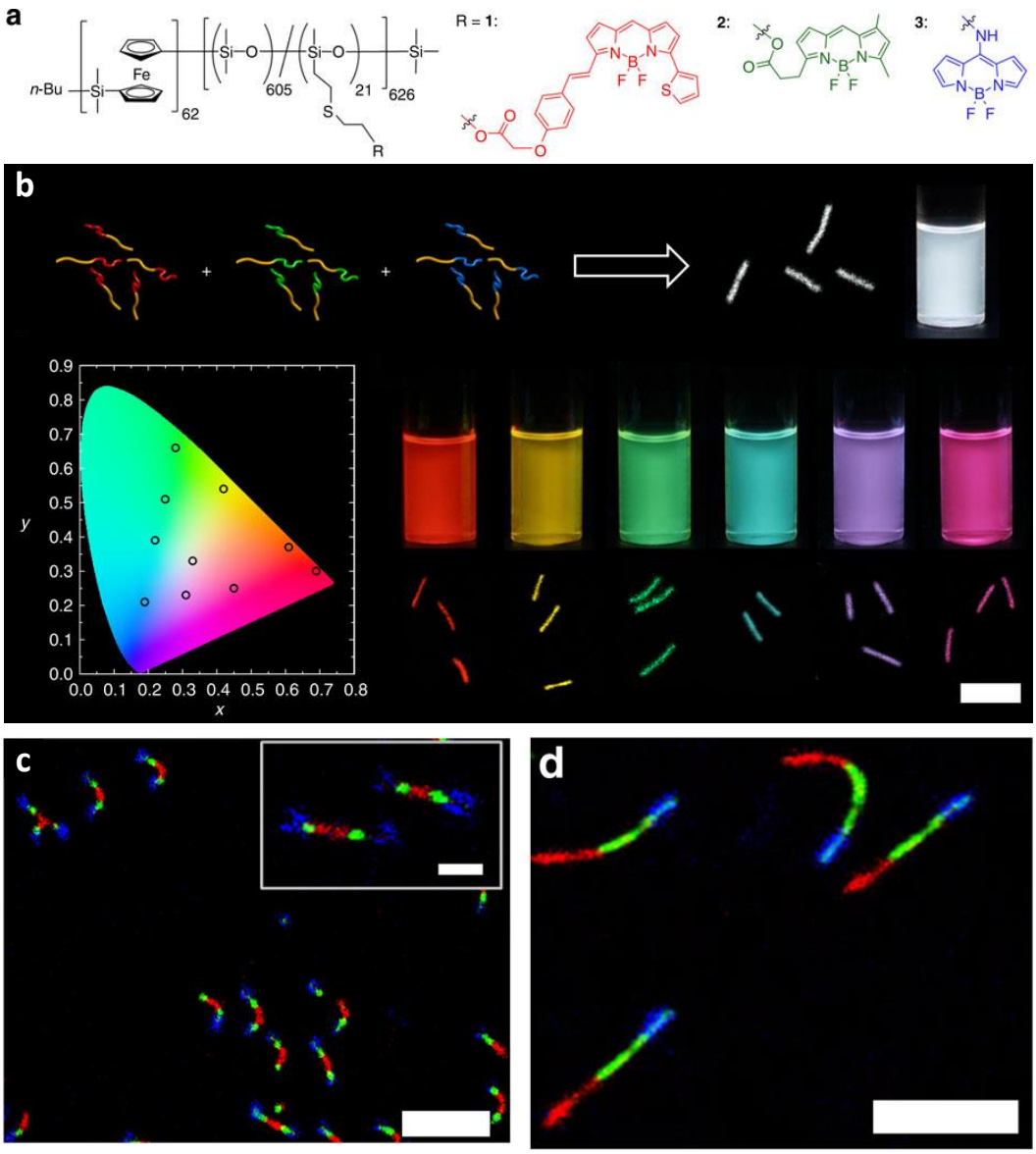

Figure 1.22 a) Synthesis of red, green and blue emissive BODIPY-labelled BCPs. b) CDSA of mixtures of these BCPs into cylindrical micelles with tuneable emission wavelength (3 μm scale bar). c) Symmetric (5 μm scale bar, 1 μm inset scale bar) and d) Asymmetric (5 μm scale bar) multiblock micelles. Figure adapted from ref.[95]

Fluorescent micelles have been formed by the self-assembly of site-specifically labelled BCPs. For example Farinha *et al.* utilised a phenanthrene-functional RAFT agent in the synthesis of poly(*N*-decylacrylamide)-*b*-poly(*N*,*N*-diethylacrylamide) amphiphilic BCPs. By using an R-group labelled RAFT agent, and polymerising the hydrophobic poly(*N*-decylacrylamide) block first, micelles with the phenanthrene fluorophore in their core were formed upon aqueous solution state self-assembly. By loading the micelles with anthracene

and studying the effect of FRET with anthracene on micelle emission lifetime, the authors were able to calculate micelle core radii from the measured Förster critical radius.[96] A site-specific post-polymerisation functionalisation of BCP end-groups with a fluorophore has also been employed in fluorescent micelle fabrication. Kataoka and co-workers synthesised a PEG-*b*-P(D,L-LA) diblock copolymer by successive anionic ring opening polymerisation, and subsequently attached pyrene to the hydroxyl chain end of the P(D,L-LA) block *via* an esterification reaction. The high sensitivity of fluorescence detection was then utilised in the study of micelle/unimer exchange dynamics (by measuring exchange between labelled and non-labelled micelles), which demonstrated that micelles where dynamic at 40 °C (above the core block T_g) and frozen at 25 °C (below the core block T_g).[97]

Post-polymerisation modifications for the introduction of fluorescent labels have also been performed on assembled BCP micelles. For example the use of monomers with reactive (or latently reactive) functional groups in BCP synthesis can afford micelles with reactive functional groups in the core and corona. This was demonstrated by Wooley and colleagues who produced poly(acrylic acid)-*b*-poly(Sty) and poly(acrylic acid)-*b*-poly(Sty-*co*-vinylbenzyl chloride) BCPs by NMP. Self-assembly afforded spherical micelles which were shell cross-linked using a bisamine. The poly(acrylic acid) shells were further functionalised with alkyne and azide groups by amidation with propargylamine or azidopropylamine respectively, allowing CuAAC reaction with azide- or alkyne-functional hydrophilic fluorescein dye. Azide groups were introduced into the core by reaction of vinylbenzyl chloride units with sodium azide. Attempts to label the core with the hydrophilic alkyne-fluorescein in aqueous media were unsuccessful, suggesting poor access to the core. Instead, by swelling the core with an organic solvent reaction with a hydrophobic alkynyl-dansyl dye was successfully demonstrated.[98] The same group also demonstrated the potential to fluorescently label a BCP micelle at the interface between core and corona by self-assembly and subsequent functionalisation of a triblock copolymer with a reactive midblock. A PEG-functional RAFT agent was used in the synthesis of poly(ethylene glycol)-*b*-poly(*N*-acryloxysuccinimide)-*b*-poly(Sty) BCPs with aqueous self-assembly affording spherical micelles (Figure 1.23). The midblock was labelled *via* amidation reaction of the activated ester groups with amine-functional near infra-red (NIR) carbocyanine fluorophores. The subsequent reaction of residual succinimide groups

with bisamine, or hydrolysis by water afforded a cross-linked poly(acrylic acid) midblock.[99]

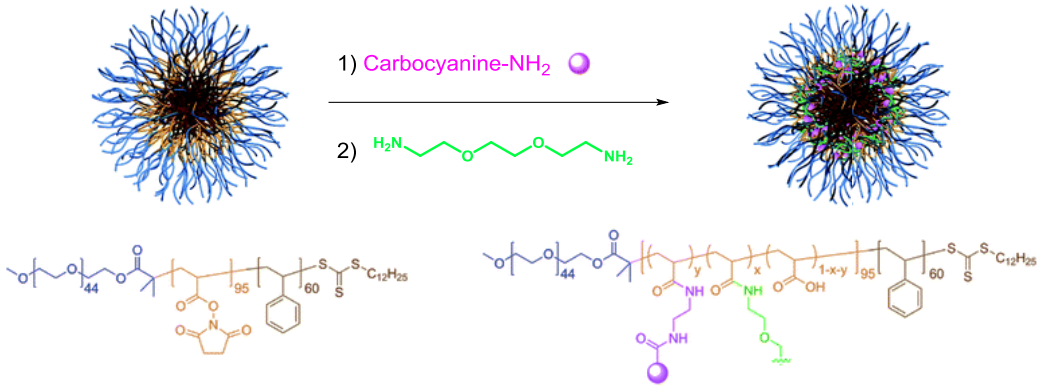

Figure 1.23. Post self-assembly functionalisation of triblock copolymer micelles with NIR fluorescent dyes. Figure adapted from ref.[99]

Post self-assembly fluorescent labelling has also been achieved where an initiator with reactive functionality was used for BCP synthesis. Using a symmetric bifunctional RAFT agent, Davis and co-workers synthesised poly(PEG acrylate)-*b*-poly(Sty)-*b*-poly(PEG acrylate) triblock copolymers with a pyridyl disulfide group at the α- and ω-chain ends. Addition of rhodamine-thiol to self-assembled micelles resulted in a disulfide exchange reaction to give a rhodamine-functionalised corona. The authors calculated that *ca.* 80% of the pyridyl dilsulfide units were available for dye conjugation (by comparison with the reaction of the non-assembled polymer in organic solvent), suggesting that the remaining *ca.* 20% were embedded in the poly(Sty) core.

1.4.2. Nanogels

Nanogel particles synthesised by emulsion or mini-emulsion polymerisation can be fluorescently-labelled by several different routes. In contrast to the encapsulation of dye molecules during the (mini)emulsion polymerisation,[100] the use of functional monomers allows for the covalent attachment of fluorophores. For example Zeng and colleagues performed a miniemulsion copolymerisation of methyl methacrylate with two fluorescent monomers that formed a FRET donor-acceptor pair; a naphthalimide donor and a merocyanine acceptor. The photo-response of merocyanine (which forms a non-emissive spiropyran upon irradiation with UV light and reverts to the emissive merocyanine form under visible light) was used as a trigger for FRET emission.[101]

Post synthesis functionalisation of nanogel particles using 'click' chemistry has also been demonstrated. Nanogels were synthesised by performing the CuAAC reaction between azide-functional dextran and alkyne-functional dextran in an inverse emulsion. The use of a 3-fold excess of azide-dextran resulted in residual N_3 groups, allowing particle modification with an alkyne-functional cyanine dye (Alexa Fluor 647). Fluorescent labelling allowed the bio-distribution of these dextran nanogels after injection into mice to be analysed by confocal microscopy.[102]

1.4.3. Conjugated polymer nanoparticles

Another strategy for the synthesis of fluorescent polymer nanoparticles is to form the particles from fluorescent π-conjugated polymers. This can be achieved by performing the step-growth polymerisation in dispersion, as demonstrated by Mecking and co-workers. They employed a miniemulsion Glaser coupling polymerisation to produce poly(arylene diethynylene) particles with diameters of 20-30 nm. Introducing perylene-diimide or fluorenone units through copolymerisation allowed the emission maxima of the nanoparticles to be adjusted (Figure 1.24).[103]

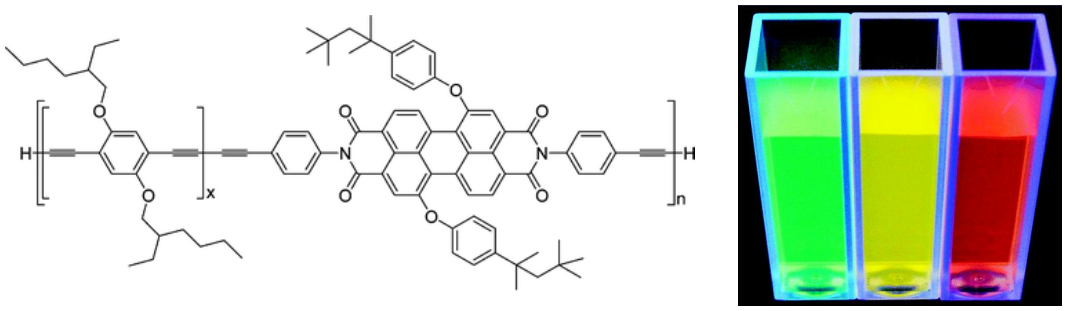

Figure 1.24. Arylene diethynylene/perylene-diimide copolymers formed by step-growth miniemulsion polymerisation (left) and solutions of the resultant conjugated nanoparticle dispersions (under 366 nm light) for different monomer loadings (right). Figure adapted from ref.[103]

In addition to their fabrication by dispersion polymerisation, highly emissive conjugated polymer nanoparticles can also be prepared by one of three post-polymerisation routes (Figure 1.25).[104] By separating polymer and particle formation into two steps, these post-polymerisation methods eliminate the difficulties of conducting step-growth metal-catalysed polymerisations in dispersion.[105] Nanoparticles can be prepared from conjugated polymers (CPs) by nanoprecipitation, where the CP is dissolved in a good solvent and rapidly added to an excess of a poor solvent under ultrasonic dispersion. Alternatively, in

the miniemulsion method the CP is dissolved in a good solvent (e.g. dichloromethane) and then dispersed in an immiscible solvent (e.g. water) by ultrasonication. In the self-assembly method positively and negatively charged CPs are separately dissolved or dispersed, then these solutions/dispersions are blended together, causing aggregation of the oppositely charged CPs. Landfester *et al.* demonstrated conjugated polymer nanoparticle formation by the miniemulsion approach using poly(*p*-phenylene), poly(fluorene), or poly(cyclopentadithiophene). Chloroform solutions of the pre-synthesised polymers were miniemulsified in water using sodium dodecylsulfate (SDS) as surfactant, with the resultant fluorescent particles having diameters between 75-250 nm.[106]

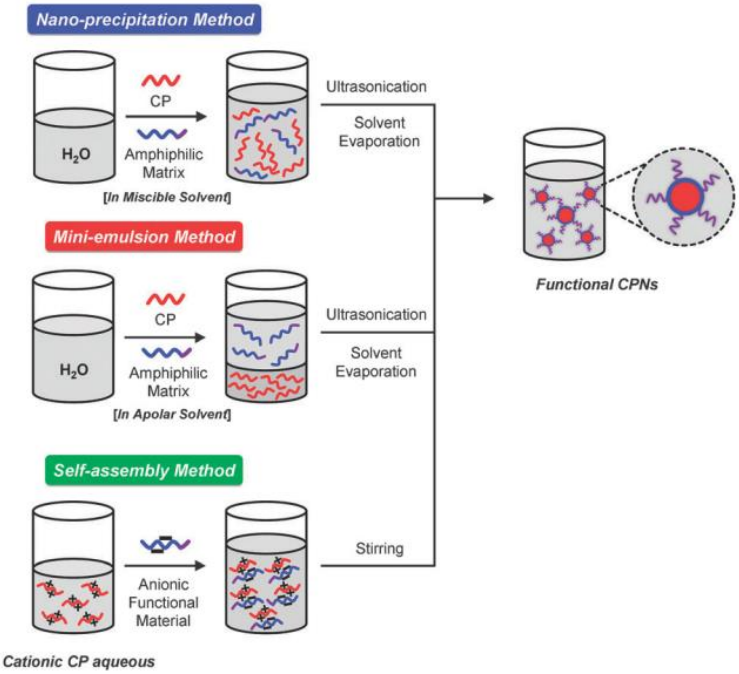

Figure 1.25. The three post-polymerisation routes for conjugated polymer nanoparticle preparation. Figure adapted from ref.[104]

1.4.4. Single chain polymer nanoparticles

Although a relatively new field in nanoparticle design, there have been several reports of fluorescent particle synthesis using single chain polymer collapse. For example, Hamilton and Harth demonstrated a post-synthesis modification of poly(acrylic acid) single chain nanoparticles (Figure 1.26 a). Chain collapse was achieved by copolymerisation of a vinylbenzosulfone, which will dimerise at high temperature to form dibenzocyclooctadiene cross-links.[107] Amine groups were introduced into the poly(acrylic acid) particles by amidation with, and subsequent deprotection of *N*-trifluoroacetyl-ethylenediamine. These

amine groups could then react with an *N*-hydroxysuccinimide-functional fluorophore (Alexa Fluor 568), to produce fluorescently-labelled particles. Further conjugation to a peptide and a dendron produced molecular dendritic transporter nanoparticle vectors whose cellular uptake could be monitored by confocal microscopy.[108]

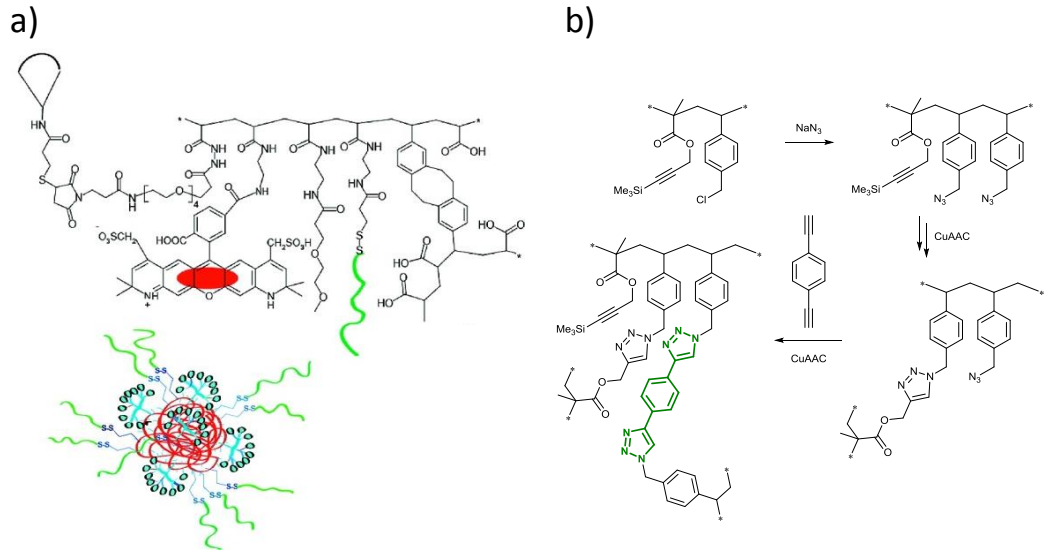

Figure 1.26. Fluorescently-labelled single chain polymer nanoparticles prepared by a) Hamilton and Harth (figure adapted from ref.)[108] and b) Pomposo and co-workers.[109]

A more simple strategy for the synthesis of fluorescently-labelled single chain polymer nanoparticles was pursued by Pomposo and co-workers (Figure 1.26). Copolymers of a TMS protected alkyne-functional methacrylate with an excess of 4-chloromethyl styrene (CMS) were synthesised by RAFT polymerisation. The CMS units were converted to azides using NaN_3, with the CuAAC 'click' reaction leading to chain collapse. Residual azide groups were cross-linked using 1,4-diethynylbenzene, leading to the formation of the triazole-benzene-triazole fluorophore which has an emission maxima of *ca.* 400 nm.[109]

1.4.5. Alternative strategies

Aside from the principle methods used for the synthesis of fluorescent polymer nanoparticles detailed above, there are two other strategies that merit mentioning. Nanoprecipitation of linear polymers provides a simple route to polymer nanoparticles, and therefore the use of fluorescent polymers can give the resultant nanoparticles emissive properties. This was demonstrated by Horisawa *et al.*, who modified a commercially available lactide/glycolide copolymer (PLGA) by amidation of the acid chain ends with

fluoresceinamine. Nanoprecipitation of the modified PLGA from methanol/acetone gave fluorescent polymer particles with diameters of *ca.* 250 nm.[110]

As mentioned in Section 1.2, dendrimers can be considered as polymer nanoparticles with a precise molecular structure. The high density of surface functionality provides an ideal target for fluorophore incorporation. This is demonstrated in work from Schlüter and colleagues who functionalised a first generation poly(amidoamine) variant dendrimer (**1liv**, Figure 1.27). Three peripheral amine groups were conjugated to a dansyl dye, with the remaining three amines used as points of attachment for an enzymatically cleavable oligopeptide spacer. Cellular uptake and distribution in human HeLa cells was investigated by confocal microscopy, with the peptide spacer offering the potential for attachment of active agents (e.g. a drug) which could be released by the action of an intracellular protease.[111]

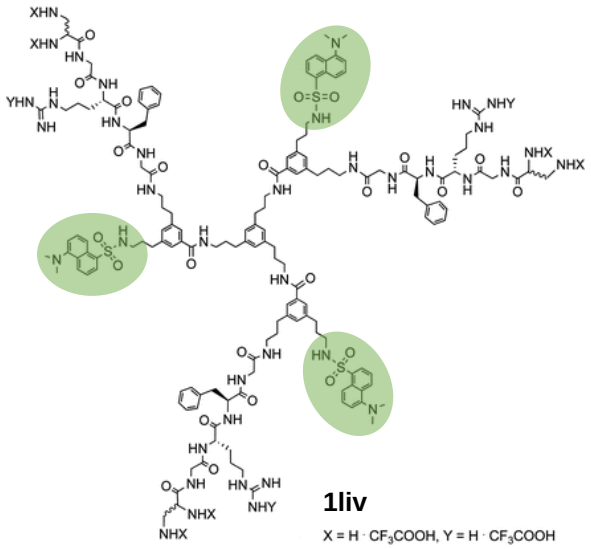

Figure 1.27. Poly(amidoamine) type dendrimer **1liv**, with fluorescent dansyl functionality (highlighted in green). Figure adapted from ref.[111]

1.5. Summary

The theme of this introduction has been the control over polymer structure that is possible using the tools of modern synthetic chemistry. Control can be imparted over the nature of single macromolecules, as well as the fabrication of colloidal polymer nanoparticles.

One way in which control over single polymer molecules manifests is the functional groups that can be incorporated. This can be achieved either before polymerisation through the use of functional initiators and monomers, or after polymerisation through the use of efficient post-polymerisation modification reactions. This subject is explored in the next three chapters of this thesis, where novel functional initiators and monomers are developed for the incorporation of dibromomaleimide and dithiomaleimide groups *via* pre- and post-polymerisation functionalisation. The chemistry of the dibromomaleimide and dithiomaleimide groups is discussed in the introduction to Chapter 2.

An often encountered motive for functional group incorporation is the desire to fluorescently label polymers and polymer nanoparticles. This is first explored in Chapter 3 of this thesis, following the serendipitous discovery of a novel class of fluorophores. The desire to control both polymer functionality and the synthesis of polymer nanoparticles culminates in Chapter 5, with the development of fluorescently-labelled nanogels and BCP micelles.

1.6. References

1. K. Matyjaszewski and J. Spanswick, *Mater. Today*, 2005, **8**, 26-33.

2. J.-F. Lutz, M. Ouchi, D. R. Liu and M. Sawamoto, *Science*, 2013, **341**, 1238149.

3. M. Szwarc, *Nature*, 1956, **178**, 1168-1169.

4. P. C. Hiemenz and T. P. Lodge, *Polymer Chemistry*, 2nd edn., CRC Press, Boca Raton, 2007.

5. C. W. Bielawski and R. H. Grubbs, *Prog. Polym. Sci.*, 2007, **32**, 1-29.

6. G. Moad, E. Rizzardo and S. H. Thang, *Acc. Chem. Res.*, 2008, **41**, 1133-1142.

7. M. F. Cunningham and R. Hutchinson, in *Handbook of Radical Polymerization*, eds. K. Matyjaszewski and T. P. Davis, John Wiley & Sons, Inc., New York, 2002, pp. 333-360.

8. A. D. Jenkins, R. G. Jones and G. Moad, *Pure Appl. Chem.*, 2010, **82**, 483-491.

9. A. Ravve, *Principles of Polymer Chemistry*, Plenum Press, New York:, 1995.

10. W. A. Braunecker and K. Matyjaszewski, *Prog. Polym. Sci.*, 2007, **32**, 93-146.

11. C. Barner-Kowollik, P. Vana and T. P. Davis, in *Handbook of Radical Polymerization*, eds. K. Matyjaszewski and T. P. Davis, John Wiley & Sons, Inc., 2002, pp. 187-261.

12. K. Matyjaszewski, *Macromolecules*, 2012, **45**, 4015-4039.

13. J. Nicolas, Y. Guillaneuf, C. Lefay, D. Bertin, D. Gigmes and B. Charleux, *Prog. Polym. Sci.*, 2013, **38**, 63-235.

14. G. Moad, E. Rizzardo and S. H. Thang, *Aust. J. Chem.*, 2012, **65**, 985-1076.

15. G. Gody, T. Maschmeyer, P. B. Zetterlund and S. Perrier, *Macromolecules*, 2014, **47**, 639–649.

16. D. J. Keddie, G. Moad, E. Rizzardo and S. H. Thang, *Macromolecules*, 2012, **45**, 5321–5342.

17. G. Moad, E. Rizzardo and S. H. Thang, *Aust. J. Chem.*, 2009, **62**, 1402-1472.

18. J. Bernard, A. Favier, L. Zhang, A. Nilasaroya, T. P. Davis, C. Barner-Kowollik and M. H. Stenzel, *Macromolecules*, 2005, **38**, 5475-5484.

19. G. Pasparakis, N. Krasnogor, L. Cronin, B. G. Davis and C. Alexander, *Chem. Soc. Rev.*, 2010, **39**, 286-300.

20. X. Huang and B. Voit, *Polym. Chem.*, 2013, **4**, 435-443.

21. P. Cotanda, N. Petzetakis and R. K. O'Reilly, *MRS Communications*, 2012, **2**, 119-126.

22. Y. Lu and K. Park, *Int. J. Pharm.*, 2013, **453**, 198-214.

23. E. G. Kelley, J. N. L. Albert, M. O. Sullivan and T. H. Epps, III, *Chem. Soc. Rev.*, 2013, **42**, 7057-7071.

24. S. M. Janib, A. S. Moses and J. A. MacKay, *Adv. Drug Deliv. Rev.*, 2010, **62**, 1052-1063.

25. A. Sanchez-Sanchez, I. Pérez-Baena and J. Pomposo, *Molecules*, 2013, **18**, 3339-3355.

26. C. Vauthier and K. Bouchemal, *Pharm. Res.*, 2009, **26**, 1025-1058.

27. S. Schubert, J. J. T. Delaney and U. S. Schubert, *Soft Matter*, 2011, **7**, 1581-1588.

28. M. V. Walter and M. Malkoch, *Chem. Soc. Rev.*, 2012, **41**, 4593-4609.

29. Y. Cheng, L. Zhao, Y. Li and T. Xu, *Chem. Soc. Rev.*, 2011, **40**, 2673-2703.

30. O. V. Borisov, E. B. Zhulina, F. A. M. Leermakers and A. H. E. Müller, in *Self Organized Nanostructures of Amphiphilic Block Copolymers I*, eds. A. H. E. Müller and O. V. Borisov, Springer Berlin Heidelberg, 2011, vol. 241, pp. 57-129.

31. Y. Mai and A. Eisenberg, *Chem. Soc. Rev.*, 2012, **41**, 5969-5985.

32. D. E. Discher and A. Eisenberg, *Science*, 2002, **297**, 967-973.

33. D. E. Discher and F. Ahmed, *Annu. Rev. Biomed. Eng.*, 2006, **8**, 323-341.

34. R. C. Hayward and D. J. Pochan, *Macromolecules*, 2010, **43**, 3577-3584.

35. T. Nicolai, O. Colombani and C. Chassenieux, *Soft Matter*, 2010, **6**, 3111-3118.

36. R. G. Jones, C. K. Ober, P. Hodge, P. Kratochvíl, G. Moad and M. Vert, *Pure Appl. Chem.*, 2013, **85**, 463-492.

37. N. Sanson and J. Rieger, *Polym. Chem.*, 2010, **1**, 965-977.

38. C. S. Chern, *Prog. Polym. Sci.*, 2006, **31**, 443-486.

39. R. M. Broyer, G. N. Grover and H. D. Maynard, *Chem. Commun.*, 2011, **47**, 2212-2226.

40. K. L. Heredia, D. Bontempo, T. Ly, J. T. Byers, S. Halstenberg and H. D. Maynard, *J. Am. Chem. Soc.*, 2005, **127**, 16955-16960.

41. P. De, M. Li, S. R. Gondi and B. S. Sumerlin, *J. Am. Chem. Soc.*, 2008, **130**, 11288-11289.

42. K. L. Heredia, L. Tao, G. N. Grover and H. D. Maynard, *Polym. Chem.*, 2010, **1**, 168-170.

43. D. J. Phillips and M. I. Gibson, *Biomacromolecules*, 2012, **13**, 3200–3208.

44. B. K. Sourkohi, R. Schmidt and J. K. Oh, *Macromol. Rapid Commun.*, 2011, **32**, 1652-1657.

45. S. Samarajeewa, R. Shrestha, Y. Li and K. L. Wooley, *J. Am. Chem. Soc.*, 2012, **134**, 1235–1242.

46. Y. Miura, Y. Sakai and I. Taniguchi, *Polymer*, 2003, **44**, 603-611.

47. C. W. Bielawski, J. Louie and R. H. Grubbs, *J. Am. Chem. Soc.*, 2000, **122**, 12872-12873.

48. A. D. Ievins, A. O. Moughton and R. K. O'Reilly, *Macromolecules*, 2008, **41**, 3571-3578.

49. J. P. Patterson, P. Cotanda, E. G. Kelley, A. O. Moughton, A. Lu, T. H. Epps, III and R. K. O'Reilly, *Polym. Chem.*, 2013, **4**, 2033-2039.

50. A. L. Parry, P. H. H. Bomans, S. J. Holder, N. A. J. M. Sommerdijk and S. C. G. Biagini, *Angew. Chem., Int. Ed.*, 2008, **47**, 8859-8862.

51. S. Venkataraman, A. L. Lee, H. T. Maune, J. L. Hedrick, V. M. Prabhu and Y. Y. Yang, *Macromolecules*, 2013, **46**, 4839-4846.

52. S. Hocine and M.-H. Li, *Soft Matter*, 2013, **9**, 5839-5861.

53. J.-F. Lutz, *J. Polym. Sci., Part A: Polym. Chem.*, 2008, **46**, 3459-3470.

54. S. Dai, P. Ravi and K. C. Tam, *Soft Matter*, 2008, **4**, 435-449.

55. A. P. Bapat, D. Roy, J. G. Ray, D. A. Savin and B. S. Sumerlin, *J. Am. Chem. Soc.*, 2011, **133**, 19832-19838.

56. J. A. Syrett, G. Mantovani, W. R. S. Barton, D. Price and D. M. Haddleton, *Polym. Chem.*, 2010, **1**, 102-106.

57. R. J. Williams, R. K. O'Reilly and A. P. Dove, *Polym. Chem.*, 2012, **3**, 2156-2164.

58. C. Cheng, E. Khoshdel and K. L. Wooley, *Nano Lett.*, 2006, **6**, 1741-1746.

59. A. Lu and R. K. O'Reilly, *Curr. Opin. Biotechnol.*, 2013, **24**, 639-645.

60. P. Cotanda and R. K. O'Reilly, *Chem. Commun.*, 2012, **48**, 10280-10282.

61. P. Cotanda, A. Lu, J. P. Patterson, N. Petzetakis and R. K. O'Reilly, *Macromolecules*, 2012, **45**, 2377-2384.

62. A. Lu, T. P. Smart, T. H. Epps, III, D. A. Longbottom and R. K. O'Reilly, *Macromolecules*, 2011, **44**, 7233-7241.

63. A. Lu, P. Cotanda, J. P. Patterson, D. A. Longbottom and R. K. O'Reilly, *Chem. Commun.*, 2012, **48**, 9699-9701.

64. A. Lu, D. Moatsou, D. A. Longbottom and R. K. O'Reilly, *Chem. Sci.*, 2013, **4**, 965-969.

65. B. L. Moore, A. Lu, D. A. Longbottom and R. K. O'Reilly, *Polym. Chem.*, 2013, **4**, 2304-2312.

66. U. Mansfeld, C. Pietsch, R. Hoogenboom, C. R. Becer and U. S. Schubert, *Polym. Chem.*, 2010, **1**, 1560-1598.

67. C. J. Hawker, V. V. Fokin, M. Finn and K. B. Sharpless, *Aust. J. Chem.*, 2007, **60**, 381-383.

68. H. C. Kolb, M. Finn and K. B. Sharpless, *Angew. Chem., Int. Ed.*, 2001, **40**, 2004-2021.

69. C. Barner-Kowollik, F. E. Du Prez, P. Espeel, C. J. Hawker, T. Junkers, H. Schlaad and W. Van Camp, *Angew. Chem., Int. Ed.*, 2011, **50**, 60-62.

70. K. A. Günay, P. Theato and H.-A. Klok, *J. Polym. Sci., Part A: Polym. Chem.*, 2013, **51**, 1-28.

71. K. J. Thurecht, I. Blakey, H. Peng, O. Squires, S. Hsu, C. Alexander and A. K. Whittaker, *J. Am. Chem. Soc.*, 2010, **132**, 5336-5337.

72. T. R. Wilks, J. Bath, J. W. de Vries, J. E. Raymond, A. Herrmann, A. J. Turberfield and R. K. O'Reilly, *ACS Nano*, 2013, **7**, 8561-8572.

73. V. Vázquez-Dorbatt, Z. P. Tolstyka, C.-W. Chang and H. D. Maynard, *Biomacromolecules*, 2009, **10**, 2207-2212.

74. G. Mantovani, F. Lecolley, L. Tao, D. M. Haddleton, J. Clerx, J. J. L. M. Cornelissen and K. Velonia, *J. Am. Chem. Soc.*, 2005, **127**, 2966-2973.

75. K. L. Heredia, Z. P. Tolstyka and H. D. Maynard, *Macromolecules*, 2007, **40**, 4772-4779.

76. Y. Zhang, H. He, C. Gao and J. Wu, *Langmuir*, 2009, **25**, 5814-5824.

77. R. Ranjan and W. J. Brittain, *Macromolecules*, 2007, **40**, 6217-6223.

78. A. A. Kavitha and N. K. Singha, *Macromol. Chem. Phys.*, 2007, **208**, 2569-2577.

79. A. Bousquet, C. Barner-Kowollik and M. H. Stenzel, *J. Polym. Sci., Part A: Polym. Chem.*, 2010, **48**, 1773-1781.

80. C. F. Hansell and R. K. O'Reilly, *ACS Macro Lett.*, 2012, **1**, 896-901.

81. M. Malkoch, R. J. Thibault, E. Drockenmuller, M. Messerschmidt, B. Voit, T. P. Russell and C. J. Hawker, *J. Am. Chem. Soc.*, 2005, **127**, 14942-14949.

82. B. S. Sumerlin, N. V. Tsarevsky, G. Louche, R. Y. Lee and K. Matyjaszewski, *Macromolecules*, 2005, **38**, 7540-7545.

83. L. Wong, C. Boyer, Z. Jia, H. M. Zareie, T. P. Davis and V. Bulmus, *Biomacromolecules*, 2008, **9**, 1934-1944.

84. L. M. Campos, K. L. Killops, R. Sakai, J. M. J. Paulusse, D. Damiron, E. Drockenmuller, B. W. Messmore and C. J. Hawker, *Macromolecules*, 2008, **41**, 7063-7070.

85. I. Kosif, E.-J. Park, R. Sanyal and A. Sanyal, *Macromolecules*, 2010, **43**, 4140-4148.

86. C. Ott, R. Hoogenboom and U. S. Schubert, *Chem. Commun.*, 2008, 3516-3518.

87. C. R. Becer, K. Babiuch, D. Pilz, S. Hornig, T. Heinze, M. Gottschaldt and U. S. Schubert, *Macromolecules*, 2009, **42**, 2387-2394.

88. K. Nilles and P. Theato, *J. Polym. Sci., Part A: Polym. Chem.*, 2010, **48**, 3683-3692.

89. B. L. Moore and R. K. O'Reilly, *J. Polym. Sci., Part A: Polym. Chem.*, 2012, **50**, 3567-3574.

90. V. Sokolova and M. Epple, *Nanoscale*, 2011, **3**, 1957-1962.

91. M. J. Ruedas-Rama, J. D. Walters, A. Orte and E. A. H. Hall, *Anal. Chim. Acta*, 2012, **751**, 1-23.

92. J. R. Lakowicz, *Principles of Fluorescence Spectroscopy*, Springer, 2009.

93. J. Hu, L. Dai and S. Liu, *Macromolecules*, 2011, **44**, 4699-4710.

94. X. Wang, G. Guerin, H. Wang, Y. Wang, I. Manners and M. A. Winnik, *Science*, 2007, **317**, 644-647.

95. Z. M. Hudson, D. J. Lunn, M. A. Winnik and I. Manners, *Nat. Commun.*, 2014, **5**, 3372.

96. G. Marcelo, T. J. V. Prazeres, M.-T. Charreyre, J. M. G. Martinho and J. P. S. Farinha, *Macromolecules*, 2009, **43**, 501-510.

97. Y. Yamamoto, K. Yasugi, A. Harada, Y. Nagasaki and K. Kataoka, *J. Control. Release*, 2002, **82**, 359-371.

98. R. K. O'Reilly, M. J. Joralemon, K. L. Wooley and C. J. Hawker, *Chem. Mater.*, 2005, **17**, 5976-5988.

99. G. Sun, M. Y. Berezin, J. Fan, H. Lee, J. Ma, K. Zhang, K. L. Wooley and S. Achilefu, *Nanoscale*, 2010, **2**, 548-558.

100. K. Landfester, *Angew. Chem., Int. Ed.*, 2009, **48**, 4488-4507.

101. J. Chen, P. Zhang, G. Fang, P. Yi, X. Yu, X. Li, F. Zeng and S. Wu, *J. Phys. Chem. B*, 2011, **115**, 3354-3362.

102. D. A. Heller, Y. Levi, J. M. Pelet, J. C. Doloff, J. Wallas, G. W. Pratt, S. Jiang, G. Sahay, A. Schroeder, J. E. Schroeder, Y. Chyan, C. Zurenko, W. Querbes, M. Manzano, D. S. Kohane, R. Langer and D. G. Anderson, *Adv. Mater.*, 2013, **25**, 1449-1454.

103. M. C. Baier, J. Huber and S. Mecking, *J. Am. Chem. Soc.*, 2009, **131**, 14267-14273.

104. L. Feng, C. Zhu, H. Yuan, L. Liu, F. Lv and S. Wang, *Chem. Soc. Rev.*, 2013, **42**, 6620-6633.

105. C. Wu and D. T. Chiu, *Angew. Chem., Int. Ed.*, 2013, **52**, 3086-3109.

106. K. Landfester, R. Montenegro, U. Scherf, R. Güntner, U. Asawapirom, S. Patil, D. Neher and T. Kietzke, *Adv. Mater.*, 2002, **14**, 651-655.

107. T. A. Croce, S. K. Hamilton, M. L. Chen, H. Muchalski and E. Harth, *Macromolecules*, 2007, **40**, 6028-6031.

108. S. K. Hamilton and E. Harth, *ACS Nano*, 2009, **3**, 402-410.

109. L. Oria, R. Aguado, J. A. Pomposo and J. Colmenero, *Adv. Mater.*, 2010, **22**, 3038-3041.

110. E. Horisawa, K. Kubota, I. Tuboi, K. Sato, H. Yamamoto, H. Takeuchi and Y. Kawashima, *Pharm. Res.*, 2002, **19**, 132-139.

111. S. Fuchs, H. Otto, S. Jehle, P. Henklein and A. D. Schluter, *Chem. Commun.*, 2005, 1830-1832.

2. Bromomaleimide-terminated RAFT polymers

2.1. Abstract

In this chapter novel RAFT agents are synthesised, having R groups functionalised with either the dibromomaleimide (DBM) or monobromomaleimide (MBM) group (**2i** and **2ii** respectively, Figure 2.1). RAFT polymerisations of a range of monomers (*tert*-butyl acrylate, methyl acrylate, triethylene glycol monomethylether acrylate, styrene, and *N*-isopropyl acrylamide) are investigated. The DBM-functional RAFT agent is found to afford good control over acrylate polymerisations, to give DBM-terminated poly(acrylates), without the requirement of a protecting group for the DBM C=C double bond. Polymerisation of styrene and NIPAM with the DBM CTA is found to be severely retarded. In the case of the MBM CTA, all monomers are found to copolymerise with the MBM C=C double bond, resulting in the formation of hyperbranched polymers.

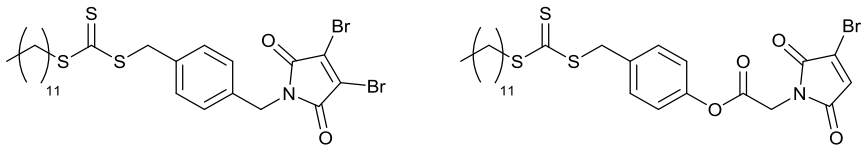

Figure 2.1. Novel dibromomaleimide (**2i**) and monobromomaleimide (**2ii**) functional RAFT agents developed in this Chapter.

2.2. Introduction

2.2.1. Maleimide-terminated polymers

It is highly desirable to be able to control polymer chain end functionality, as the chain ends serve as distinct attachment points for conjugation of the polymer to other polymers, small molecules, or biomacromolecules such as polypeptides or polynucleotides. For polymers synthesised by living polymerisation or RDRP, chain end functionality is introduced using a functional initiator/chain transfer agent.[1,2] A wide range of functional groups have been introduced to polymer chain ends in this way, and particularly significant amongst these are groups that undergo highly efficient (or 'click') reactions.[3,4] It is necessary that post-polymerisation reactions be highly efficient due to the difficulty in the purification of polymer chains that vary only in the nature of their end-groups. For this reason, polymer end-groups that undergo cycloadditions (Diels-Alder,[5] hetero-Diels-Alder,[6] azide-alkyne[7]), thiol-ene and thiol-yne reactions,[8,9] pyridyl-disulfide exchanges,[10] as well as end-groups containing activated esters,[11] have all been widely exploited.

Maleimide groups are particularly versatile as polymer chain ends, as maleimide undergoes two highly efficient functionalisation reactions.[12] Maleimide groups react with thiols *via* a Michael addition, and undergo Diels-Alder cycloadditions with dieneophiles such as furan or anthracene (Scheme 2.1). The thiol Michael addition has proved popular for polymer-protein conjugation, reacting maleimide-terminated polymers with the thiol group of reduced cysteine residues.[13-17] The maleimide-anthracene Diels-Alder cycloaddition has been widely exploited by the groups of Tunca and Sanyal to build a variety of polymer architectures;[18] diblock copolymers,[5] 3-arm stars,[19] multi-arm star block copolymers,[20,21] cyclic homo- and block-copolymers,[22] and graft copolymers.[23] The thermally reversible nature of the maleimide-furan Diels-Alder adduct has also been exploited, with maleimide and furan-terminated polymers reacting to form cross-linked polymer networks with a thermo-reversible sol-gel transition.[24]

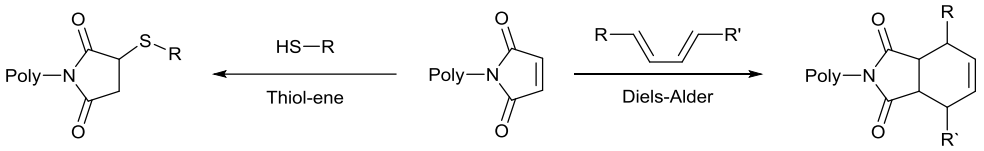

Scheme 2.1. Thiol-ene and Diels-Alder reaction of polymers with a maleimide chain end.

Maleimide groups have been incorporated into polymer chain ends using a variety of maleimide-functionalised initiators and RAFT agents. In the living ring-opening polymerisation of cyclic esters, maleimide-functional alcohol initiators were used to give α-chain end functional polylactides and polycaprolactones.[25,26] Initiators containing maleimide-furan Diels-Alder adducts were also used, with the maleimide functionality revealed by the retro Diels-Alder reaction, either *in situ* under the high temperature conditions of a Sn-catalysed ROP reaction,[27] or in a subsequent step following organocatalytic ROP.[28,29] Polystyrene with maleimide α-chain ends has also recently been synthesised by living polymerisation, utilizing a maleimide-functionalised benzyl chloride as the initiator for cationic polymerisation.[30]

The C=C double bond of the maleimide group is highly reactive toward radical polymerisation; for example *N*-functional maleimides and styrene are a well-known donor/acceptor pair that have a strong tendency to form alternating copolymers (Scheme 2.2).[31] This fact which has been exploited for the synthesis of graft copolymers,[30] star polymers,[32] and for sequence control in radical polymerisations.[33] For this reason it has usually been necessary to protect the C=C double bond of maleimide-containing initiators or chain transfer agents when performing RDRP such as ATRP or RAFT. These maleimides have been protected as Diels-Alder adducts, for example with furan or dimethylfulvene,[15,17,23,34-37] with deprotection occurring *via* the retro Diels-Alder reaction at elevated temperatures. This approach successfully prevents reaction of propagating radicals with the maleimide so long as polymerisations are stopped before reaching high conversions. Post-polymerisation transformation of the thiocarbonylthio RAFT end group has also been used to introduce the maleimide functionality, either by radical cross-coupling with a maleimide-furan functional diazo compound,[13,16] or *via* aminolysis of the thiocarbonylthio to a thiol followed by reaction with an excess of bismaleimide.[14,38]

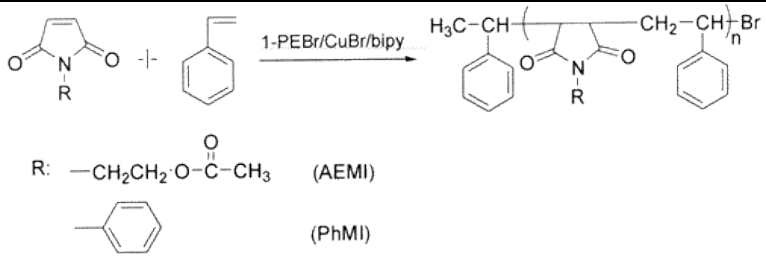

Scheme 2.2. The synthesis of alternating copolymers of styrene and the *N*-functional maleimides AEMI and PhMI by ATRP. Figure reproduced from ref.[31]

2.2.2. Bromomaleimide chemistry

Recently, the groups of Baker and Caddick have demonstrated that bromomaleimides, like maleimides, undergo highly efficient reactions with thiols. Rather than a Michael addition, this reaction proceeds *via* an addition-elimination reaction, with loss of Br anion and retention of the C=C double bond (Scheme 2.3). This double bond retention facilitates further reaction *via* addition-elimination, allowing cleavage of the thioether linkage. Initially they demonstrated that monobromomaleimide (**2A**) will react with the model thiol *N*-Boc-Cys-OMe (**2B**) to give the corresponding thiomaleimide (**2C**) in quantitative yield in < 1 min (Scheme 2.3 a).[39]

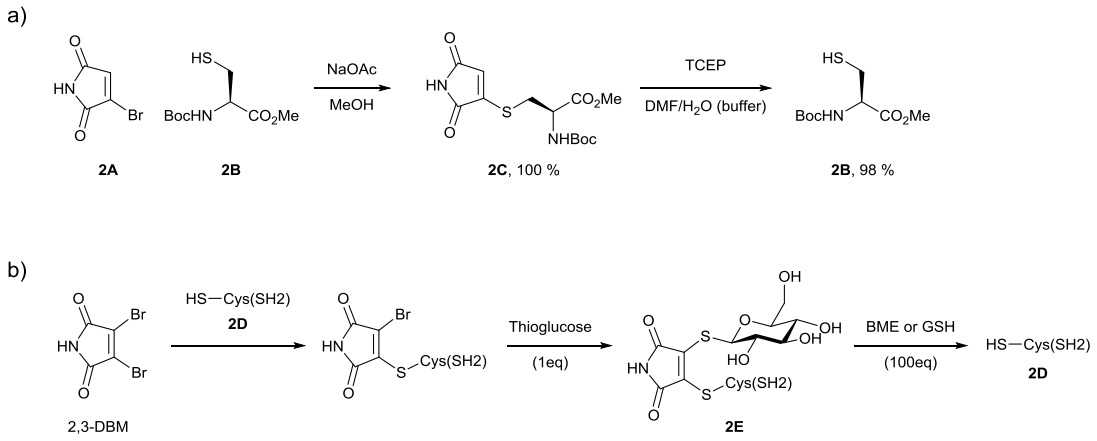

Scheme 2.3 a) Reaction of monobromomaleimide with *N*-Boc-Cys-OMe, and subsequent cleavage with TCEP.[39] b) Reaction of 2,3-dibromomaleimide with the Grb2 SH2 domain, then thioglucose, followed by cleavage with an excess of thiol (BME or GSH).[40]

They showed this reaction occurs at a greater rate than the reaction of **2B** with maleimide, and with 100% selectivity in the presence of a competing amine nucleophile.[39] They also showed that the reducing agent tris(2-carboxyethyl)phosphine (TCEP) reacted with **2C**, releasing the original thiol (**2B**). Baker and Caddick then went on to show that 2,3-dibromomaleimide (2,3-DBM) can undergo a highly efficient reaction with two thiols,

to form a dithiomaleimide (DTM, Scheme 2.3 b).[40] They reacted 2,3-DBM with a protein containing a reduced cysteine residue (the L111C mutant of the Grb2 SH2 domain, **2D**), before addition of thioglucose to form a glycoprotein (**2E**). Again, retention of the double bond allows further reaction. In this case the addition of an excess of a third thiol – either β-mercaptoethanol (BME) or glutathione (GSH) – leads to the DTM product of this third thiol, with elimination of the first two thiols (**2D** and thioglucose). Baker and Caddick also showed that 2,3-DBM reacts very rapidly with the two free thiols of a reduced disulfide bond (in the protein somatostatin) to form a DTM bridge, with the reduced protein being reformed by addition of excess BME (Scheme 2.4).[40]

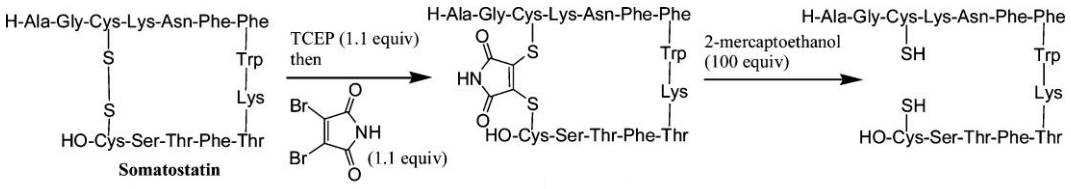

Scheme 2.4. Reversible modification of the disulfide bond of somatostatin by 2,3-DBM. Figure and caption reproduced from ref.[40]

Simple *N*-functionalisation of 2,3-DBM allowed Baker and Caddick to use this disulfide bridging for the construction of more complex protein conjugates. Using an *N*-fluorescein-DBM allowed labelling of somatostatin with this fluorophore.[40] An antibody-drug conjugate of the Fab fragment of trastuzumab with doxorubicin (DOX) was formed using an *N*-DOX-DBM.[41] Most recently a carcinoembryonic antigen specific single-chain Fv fragment was labelled with fluorescein, biotin, or nitroxide spin labels using the corresponding *N*-functionalised DBMs.[42]

Polymer-protein conjugates were also synthesised, using DBM-terminated polymers prepared by post-polymerisation functionalisation reactions. Coupling of hydroxyl-functional polyethylene glycol (PEG) to DBM *via* the Mitsunobu reaction gave a reagent for fast and efficient 'PEGylation' of somatostatin and salmon calcitonin through the disulfide bridging reaction.[43,44] PEG-methacrylates prepared by ATRP were also functionalised with a DBM group by Haddleton and co-workers using two separate approaches. Polymerisation with an azide-containing initiator, followed by CuAAC with an *N*-alkyne DBM gave the desired product, as did use of a Boc-protected amine initiator, followed by Boc group deprotection and condensation/elimination with dibromomaleimide

anhydride. Both these DBM-functional PEG-methacrylates were shown to be fast and efficient 'PEGylating' agents for salmon calcitonin.[44]

The aim of this chapter was to synthesise DBM- and MBM-terminated polymers using a functional RAFT agent, rather than by post-polymerisation functionalisation. Haddleton and co-workers had recently reported that it was not possible to use a DBM-functional initiator in ATRP, as DBM caused retardation of PEG-methacrylate polymerisation by this mechanism.[44] As a result we decided to investigate RAFT polymerisation as an alternative, due to its high tolerance towards functional groups.

2.3. Results and discussion

2.3.1. RAFT agents design and synthesis

In order to synthesise polymers with a DBM or MBM end-group by RAFT polymerisation it was necessary to design and synthesise a RAFT agent with a DBM- or MBM-functional group as part of either the R group (giving α-chain end functionality), or the Z group (giving ω-chain end functionality). According to the RAFT mechanism there is the potential for loss of both the R and Z group from the products of the polymerisation (Figure 1.4 and Figure 2.2).[45]

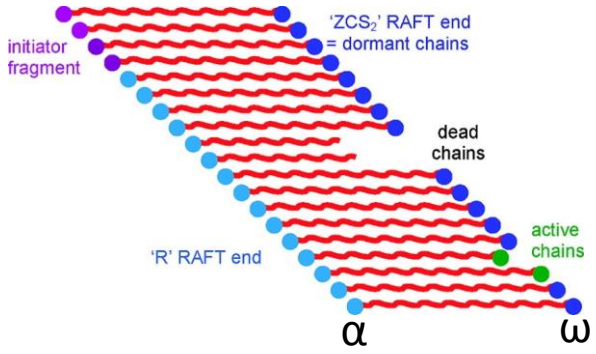

Figure 2.2. The products of a RAFT polymerisation. Figure adapted from ref.[45]

Before the chain equilibrium is established, monomer initiation occurs by attack of initiator-derived radicals, generating propagating monomer radicals. Therefore, a proportion of the final polymer chains will have initiator-derived, rather that CTA-derived α-chain ends. Any termination of the propagating radicals, for example by disproportionation or recombination with initiator-derived radicals, will result in 'dead' polymer chains that no longer have the ZCS_2 RAFT end group. Therefore complete end-group fidelity for either R or Z group is not possible in a RAFT polymerisation. However, R functionalisation was preferred, as the Z group can be lost from the final polymer product by hetero- or homolytic degradation of the reactive thiocarbonylthio group through which it is attached to the polymer chain.[46]

A dodecyltrithiocarbonate Z group, and a 1,4-substitued benzyl R group were chosen, to give a RAFT agent that could control polymerisation of styrenic, acrylate and acrylamide monomers.[1] Trithiocarbonates can be synthesised in a simple one-pot process by reaction of a thiol with carbon disulfide to form the trithiocarbonate anion, followed by alkylation

with an alkyl halide corresponding to the desired R group.[47] Due to the reactivity of DBM and MBM towards thiols, the trithiocarbonate was prepared first by reaction of 1-dodecanethiol, carbon disulfide and 4-(chloromethyl)benzyl alcohol, to give the alcohol-functional CTA **2iii** as previously reported (Scheme 2.5 a).[48]

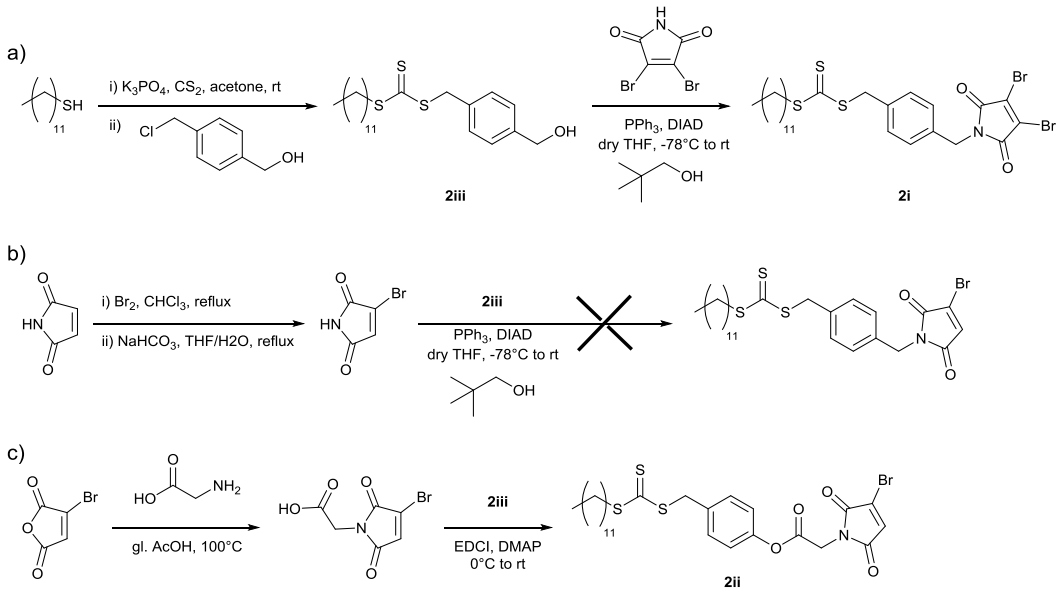

Scheme 2.5 a) Synthesis of DBM-functional RAFT agent (**2i**). b) Attempted synthesis of an MBM-functional RAFT agent. c) Successful synthesis of MBM-functional RAFT agent (**2ii**).

DBM was then introduced in the second step using a modified version of the Mitsunobu reaction.[49] Walker showed that to avoid the side reaction of maleimide with PPh_3, and inhibition of the reaction by the resultant Ph_3P-DIAD betaine, the order of addition for the reagents was crucial. In order to obtain the highest yields PPh_3 was added first, then DIAD, alcohol and finally maleimide. Furthermore, to promote formation of the dioxaphosphorane intermediate from the Ph_3P-DIAD betaine, 1.5 *eq.* of alcohol were used relative to the other reagents to give the optimum yield. This same high yield could be achieved by using 1 *eq.* of the desired alcohol, with 0.5 *eq.* of a 'dummy ligand' neopentyl alcohol thereby increasing yield relative to the alcohol of interest. Reaction of alcohol-functional CTA (**2iii**) with 2,3-dibromomaleimide (2,3-DBM) under these conditions gave the desired DBM CTA (**2i**) in an overall yield of 41%. Characterization by ^{1}H and ^{13}C NMR spectroscopy confirmed the structure (Figure 2.3), with the characteristic resonances of the dibromomaleimide group identified by ^{13}C NMR spectroscopy at 163.6 and

129.5 ppm (C13 and C12 respectively) along with the diagnostic resonance attributable to the trithiocarbonate group (C5) at 223.5 ppm.[50]

An attempt to synthesise a MBM-functional RAFT agent *via* the Mitsunobu reaction of the alcohol-functional CTA **2iii** with monobromomaleimide was unsuccessful (Scheme 2.5 b). The product isolated appeared to be a dimer of **2iii**, suggesting that the NH proton of MBM is not acidic enough to be deprotonated by the zwitterionic acid. Instead, a carboxylic acid-functional MBM was synthesised according to Monneret *et al.*,[51] and coupled to the alcohol-functional CTA (**2iii**) using an EDCI/DMAP esterification (Scheme 2.5 c), with an overall yield of 24%. The product was characterised by HR-MS, and by ^{1}H NMR spectroscopy which showed the characteristic MBM proton (H17) at 6.95 ppm, and ^{13}C NMR spectroscopy which showed MBM resonances at 167.8, 164.8, 132.5, and 131.9 ppm for C14, C15, C17 and C16 respectively (Figure 2.4).

2.3.2. Polymerisations with DBM RAFT agent

To confirm that the choice of R and Z groups in the DBM and MBM RAFT agents (**2i** and **2ii** respectively) was indeed appropriate for the monomers of interest, a series of polymerisations were first conducted with the precursor alcohol-functionalised CTA **2iii** (Scheme 2.6 and Table 2.1).

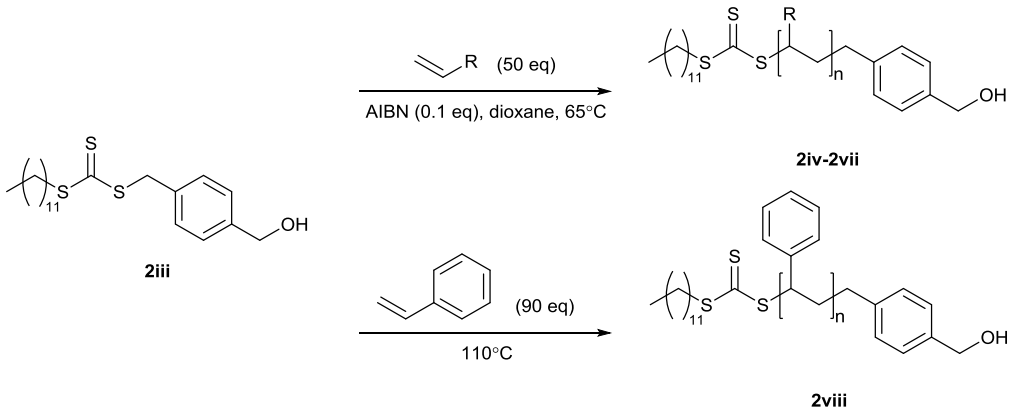

Scheme 2.6. RAFT polymerisations with **2iii** as CTA.

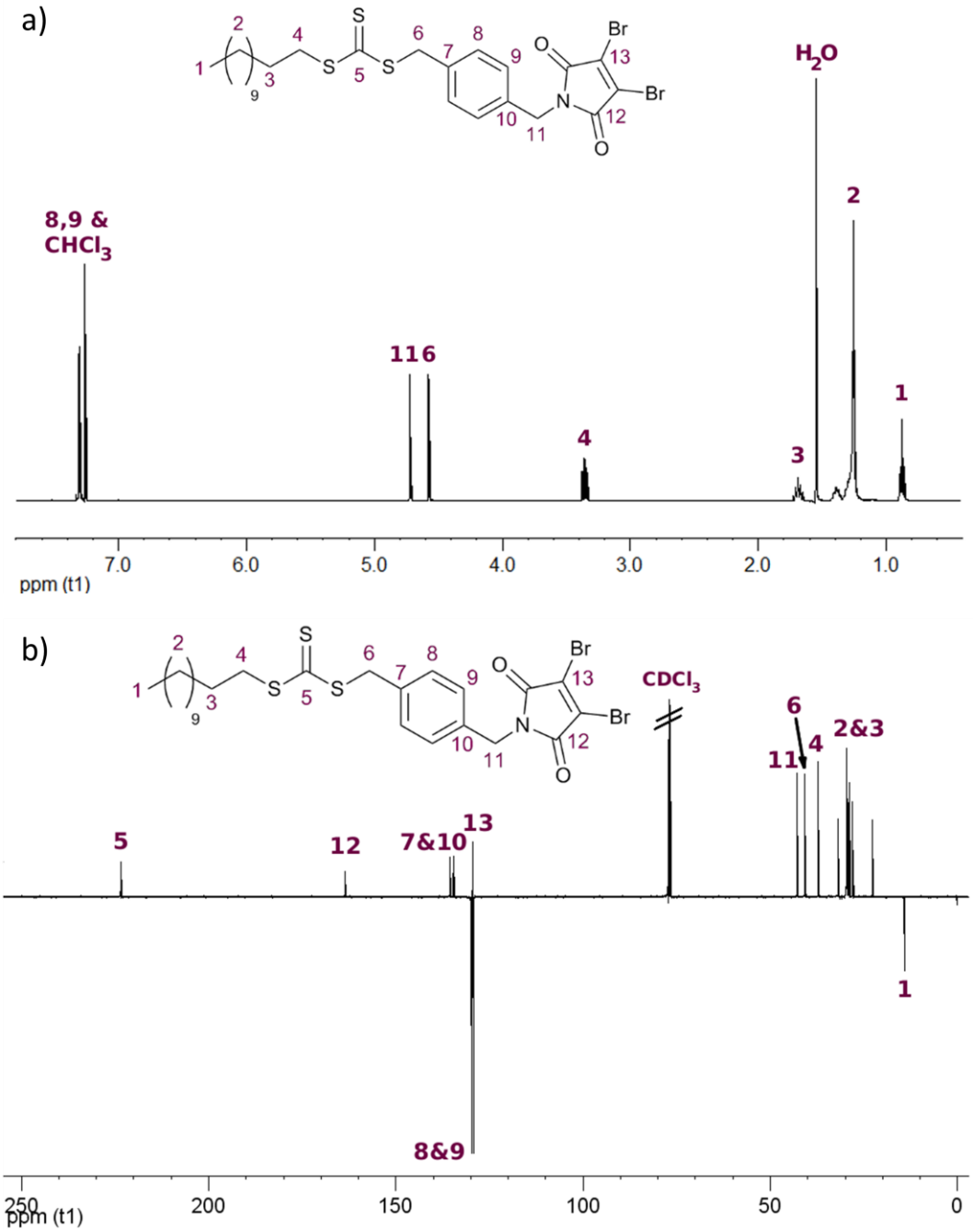

Figure 2.3 a) ^{1}H NMR spectrum (400 MHz, $CDCl_3$) and b). ^{13}C NMR spectrum (125 MHz, $CDCl_3$) of (**2i**)

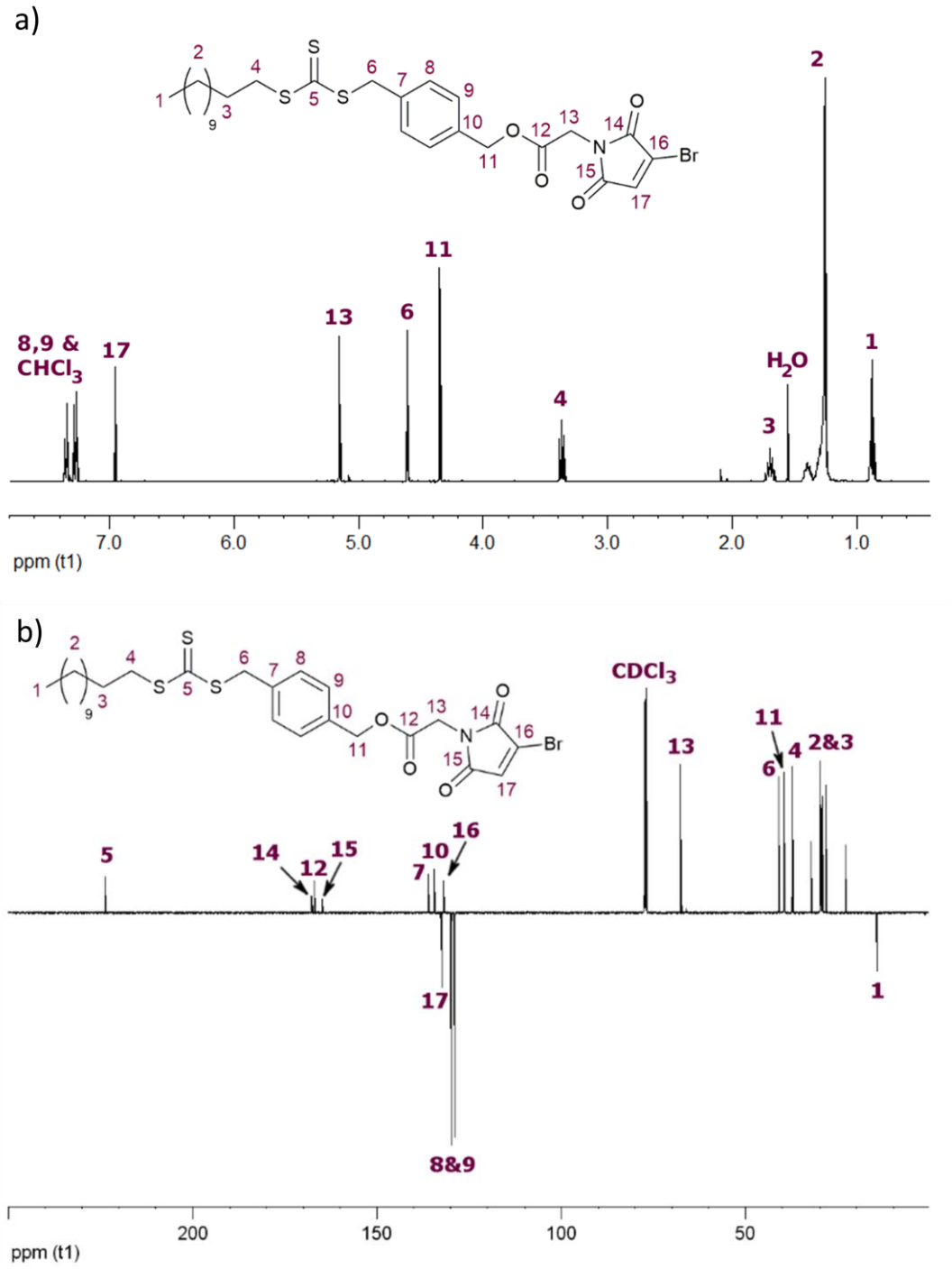

Figure 2.4 a) ^{1}H NMR spectrum (500 MHz, $CDCl_3$) and b) ^{13}C NMR spectrum (125 MHz, $CDCl_3$) of **2ii**.

Table 2.1. RAFT polymerizations conducted with CTA (**2iii**), performed at 65 °C in dioxane.

	Monomer	**[2iii:M:AIBN]**	**Time (h)**	M_n [a] **(kDa)**	$M_{n,th}$ [b] **(kDa)**	$Đ_M$ [a]	p [b] **(%)**
2iv	^{t}BA	1:50:0.1	3	6.3	6.4	1.12	93
2v	MA	1:50:0.1	16	4.7	4.4	1.15	94
2vi	TEGA	1:50:0.1	16	7.3	11.2	1.36	99
2vii	NIPAM	1:50:0.1	16	5.9	6.0	1.12	99
2viii	Sty [c]	1:90:0	16	6.2	6.4	1.23	64

[a] Molecular weight data were obtained by SEC. Samples were taken without fractionation or precipitation. [b] Monomer conversion (p) monitored by ^{1}H NMR spectroscopy. $M_{n,th}$ calculated from monomer conversion. [c] Styrene polymerisations were conducted in bulk, with thermal initiation at 110 °C.

Styrene (Sty), *N*-isopropylacrylamide (NIPAM), and a series of acrylates – *tert*-butyl (^{t}BA), methyl (MA) and triethyleneglycol monomethylether (TEGA)[52] – were studied to give a range of hydrophobic, hydrophilic and temperature responsive polymers. Polymerisations of ^{t}BA, MA, TEGA and NIPAM were conducted using the radical initiator AIBN ([2iii]:[AIBN] = 1:0.1), at 65 °C, with varying monomer/dioxane ratios of 1/1 (*v/v*), 1/1 (*v/v*), 1/2 (*v/v*), and 2/3 (*w/w*) respectively to ensure complete monomer dissolution. Sty polymerisations were conducted in bulk at 110 °C, without the addition of AIBN (thermal initiation of Sty)[53]. All polymerisations proceeded to high conversion, with a good control over molecular weight (low $Đ_M$), demonstrating that this combination of R and Z groups was indeed a suitable choice for RAFT polymerisation of these monomers.

A final control reaction was performed with **2i** in the presence of 0.1 *eq.* of AIBN in dioxane solvent at 65 °C to test for homopolymerisation of the DBM C=C double bond. After 6 h there was no evidence of polymerisation by ^{1}H NMR spectroscopy or SEC analysis, confirming that the dibromomaleimide group was stable under these model radical polymerisation conditions.

Polymerisations mediated by **2i** of a series of different monomers were then conducted, under the same conditions as those studied with CTA **2iii**, according to Scheme 2.7 and Table 2.2.

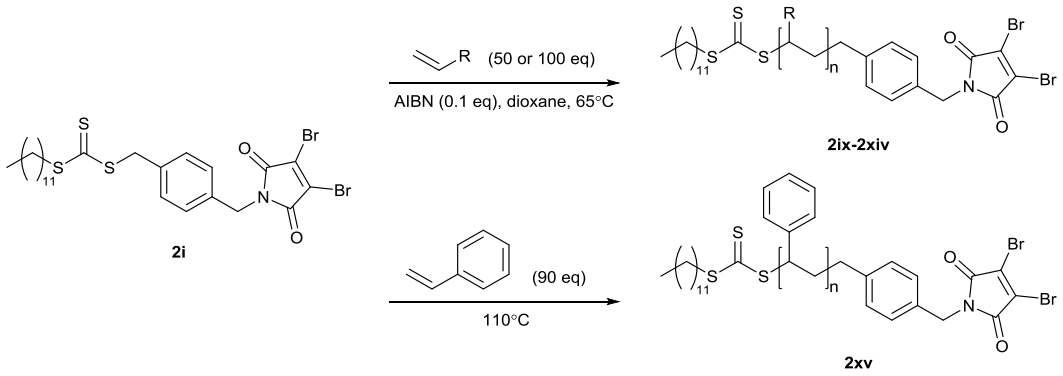

Scheme 2.7. RAFT polymerisation with **2i** as CTA.

Table 2.2. RAFT polymerizations conducted with CTA (**2i**), performed at 65 °C in dioxane.

	Monomer	**[2i:M:AIBN]**	**Time (h)**	M_n [a] **(kDa)**	$M_{n,th}$ [b] **(kDa)**	$Đ_M$ [a]	p [b] **(%)**
2ix	^{t}BA	1:50:0.1	3	2.5	3.0	1.31	37
2x	^{t}BA	1:50:0.1	6	5.7	6.0	1.15	84
2xi	^{t}BA	1:100:0.1	3	10.5	11.4	1.15	84
2xii	MA	1:50:0.1	3	4.3	4.2	1.20	54
2xiii	TEGA	1:50:0.1	16	5.5	5.9	1.27	48
2xiv	NIPAM	1:50:0.1	16	0.8	0.7	1.12	1
2xv	Sty [c]	1:90:0[d]	16	1.0	1.0	1.41	4

[a] Molecular weight data were obtained by SEC. Samples were taken without fractionation or precipitation. [b] Monomer conversion (p) monitored by ^{1}H NMR spectroscopy. $M_{n,th}$ calculated from monomer conversion. [c] Styrene polymerisations were conducted in bulk, with thermal initiation at 110 °C.

Initial polymerisation of ^{t}BA with [**2i**]:[^{t}BA]:[AIBN] 1:50:0.1 at 65 °C in dioxane (1/1 *v/v* w.r.t. ^{t}BA) was found to proceed reasonably rapidly, with 37% conversion reached after 3 h (**2ix**), and 84% conversion achieved after 6 h (**2x**) to give a well-defined polymer with $Đ_M = 1.15$, as measured by SEC. When the equivalents of ^{t}BA were doubled by halving the concentration of **2i** and AIBN, the reaction was found to proceed more rapidly, with 84% conversion reached after just 3 h (**2xi**). This is contrary to expectations, as the rate of polymerisation is proportional to the square root of initiator concentration (assuming constant radical concentration),[54] and hinted at a deviation from ideal RAFT

polymerisation kinetics. Interference of bromomaleimides in RAFT polymerisation was found to be a reoccurring feature of the work in this thesis, and a summary of all relevant data and an investigation into the cause is given in Chapter 6. Nonetheless, kinetic analysis of this ^{t}BA polymerisation confirmed a linear increase of molecular weight with conversion, with measured and theoretical values of M_n (based on conversion) in good agreement, and gave a linear first-order rate plot (Figure 2.5). An induction period of approximately 40 min was observed, which could be attributed to incomplete deoxygenation, or an initial build-up of the intermediate $CS_2Z^{\bullet}$ radical due to slow fragmentation rate of the CH_2Ph R group.[1]

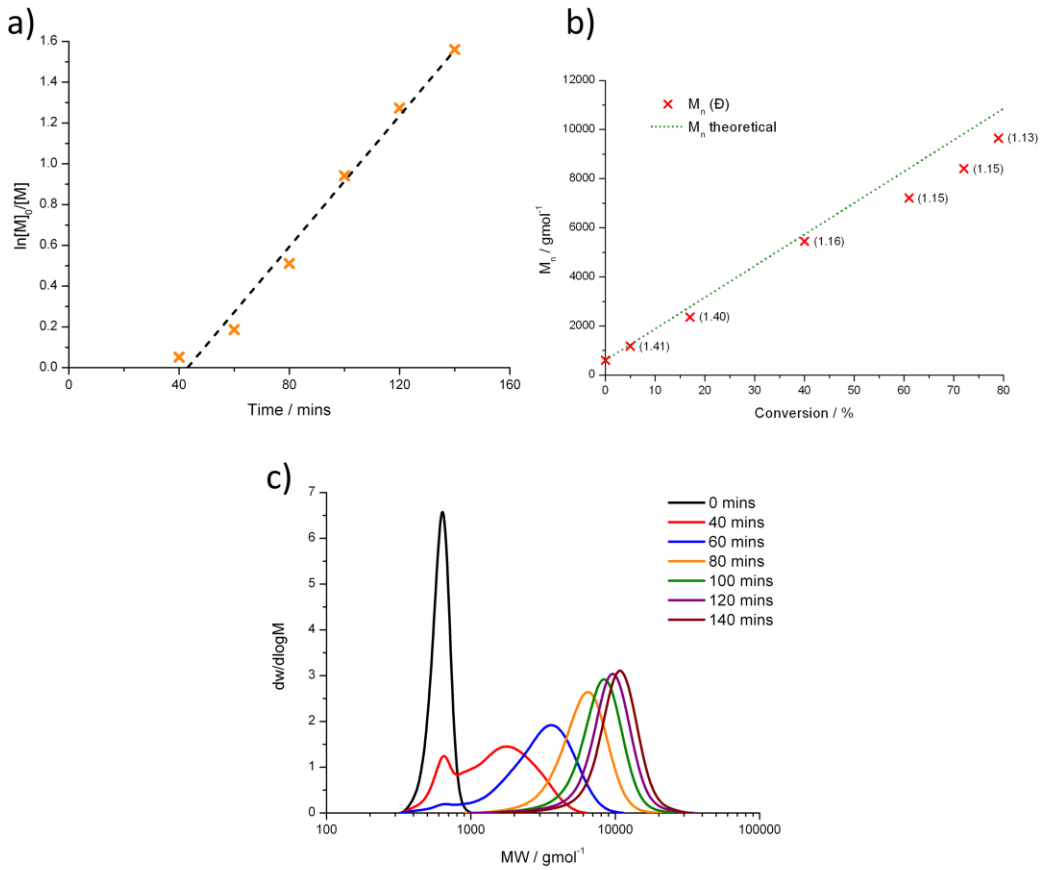

Figure 2.5. ^{t}BA RAFT polymerisation with **2i** (**2xi** in Table 2.2); a) First order kinetics of ^{t}BA consumption with linear fit; b) M_n and $Đ_M$ (as measured by SEC – THF eluent, P(Sty) standards) as a function of monomer conversion with theoretic values (line); c) Evolution of molecular weight distribution (as measured by SEC – THF eluent, P(Sty) standards) as a function of time.

The purified polymer (**2xi**) as characterized by SEC was well defined having a narrow molecular weight distribution ($Đ_M = 1.15$), while the UV-Vis spectrum of the polymer,

provided by a PDA detector fitted to the SEC, showed the characteristic trithiocarbonate absorbance (λ_{max} = 307 nm) confirming the presence of the RAFT end-group (Figure 2.6).

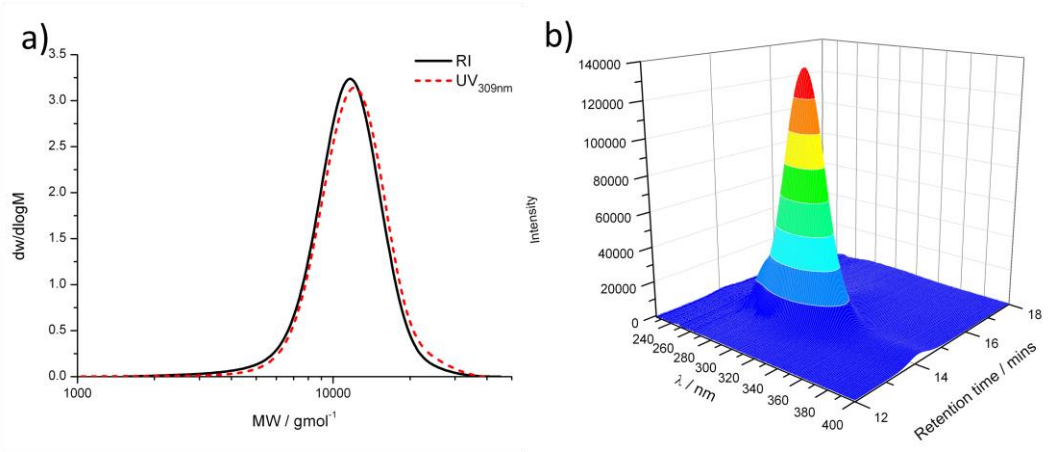

Figure 2.6. a) Molecular weight distributions of **2xi** obtained by SEC with RI and UV (309 nm) detectors, eluting with THF and calibrated against P(Sty) standards; b) Three dimensional SEC chromatogram obtained using a PDA detector

The ^{1}H NMR spectrum of **2xi** indicated retention of the trithiocarbonate end-group with resonances due to the C$\underline{H}_3$ and SC$\underline{H}_2$ protons (H1 and H4 respectively). R group retention was also observed, with resonances due to the PhC$\underline{H}_2$N protons (H14). End-group analysis indicated $DP = 84$, in accordance with conversion which also indicated $DP = 84$. By performing a ^{13}C NMR experiment with a long acquisition time, a spectrum was obtained which showed resonances at 163.6 and 129.5 ppm corresponding to N$\underline{C}$(O) and $\underline{C}$Br (C15 and C16 respectively), indicating that the DBM group had remained intact (Figure 2.7).

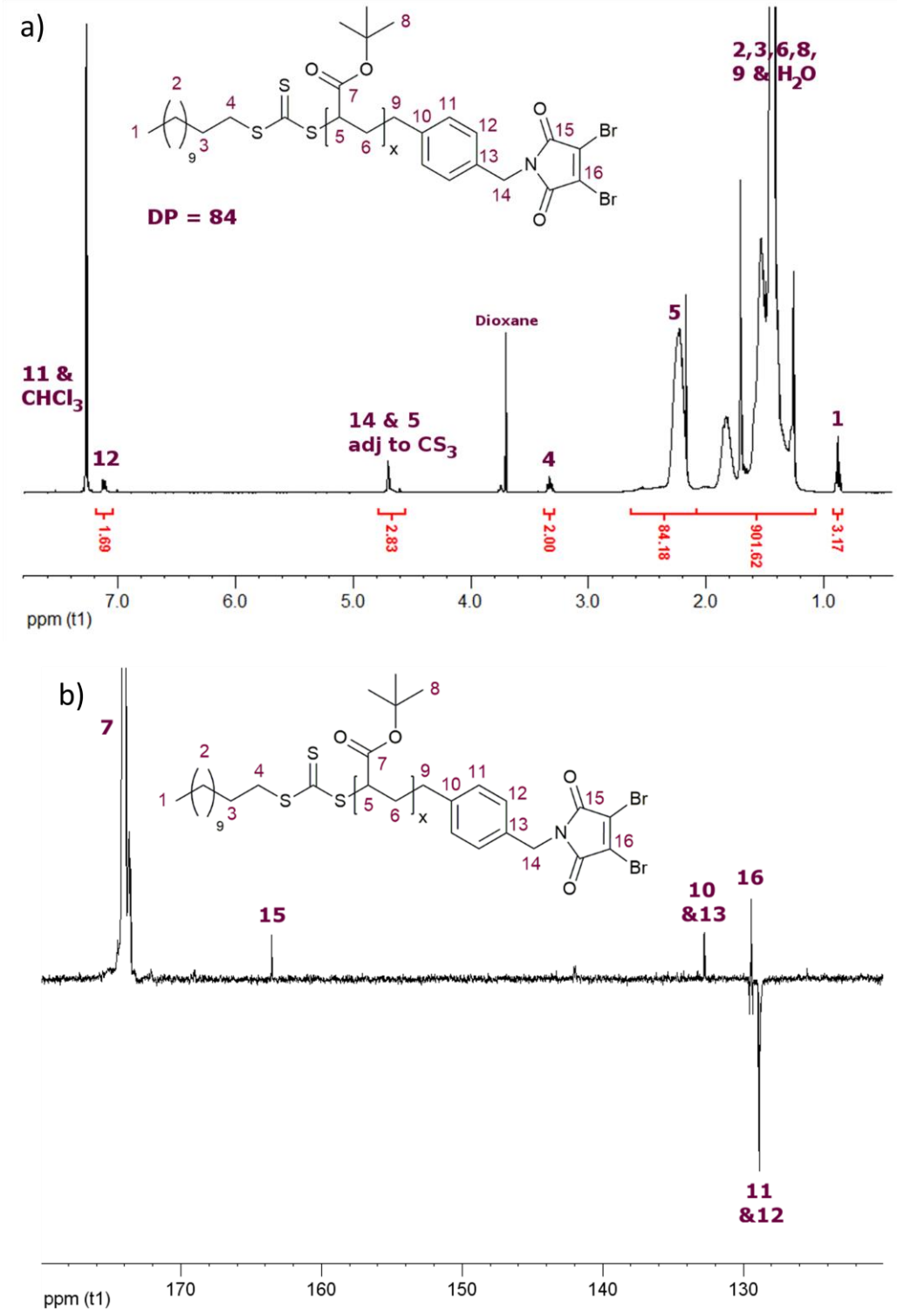

Figure 2.7. a) ^{1}H NMR spectrum (400 MHz, $CDCl_3$) and b) Partial ^{13}C NMR spectrum (125 MHz, $CDCl_3$) of **2xi**.

Further polymerisations with the acrylates MA (**2xii**) and TEGA (**2xiii**) were also found to proceed with good control over molecular weight. ^{1}H NMR spectroscopy (Figure 2.8) indicated retention of both the Z and R end-groups, with *DP* calculated by end-group analysis (26 for **2xii** and 24 for **2xiii**) in good agreement with that expected from conversion (27 for **2xii** and 24 for **2xiii**).

SEC analysis of polymers **2xii** and **2xiii** indicated narrow molecular weight distributions ($Đ_M = 1.20$ and 1.27 respectively). SEC analysis with a UV detector ($\lambda_{abs} = 309$ nm) indicated that the polymers had retained the trithiocarbonate end-group, with good overlay of UV and RI molecular weight distributions (Figure 2.9).

It had not been possible to analyse P^{t}BA (**2xi**) by MALDI-TOF mass spectrometry, as the polymer could not be ionised. However, for PMA (**2xii)** and PTEGA (**2xiii**) MALDI-TOF spectra were obtained using an alkali salt as cationisation agent.[55,56] These spectra provided further evidence for the presence of the DBM end-group with excellent agreement between observed and theoretical masses, and the isotope pattern expected for a species with two Br atoms (Figure 2.10-Figure 2.13). The presence of a single discrete molecular species in both cases suggests a high degree of end-group fidelity.

Polymerisation of NIPAM (**2xiv**) and Sty (**2xv**) were unsuccessful with CTA **2i**, with conversion reaching only 1% and 4% respectively after 16 h. This is in contrast to the polymerisation of NIPAM (**2vii**) and Sty (**2viii**) with the alcohol-functional CTA **2iii**, which reached 99% and 64% conversion respectively in the same amount of time. The cause of this polymerisation inhibition is explored further in Chapter 6, where related data from Chapter 3 and Chapter 4 is also discussed.

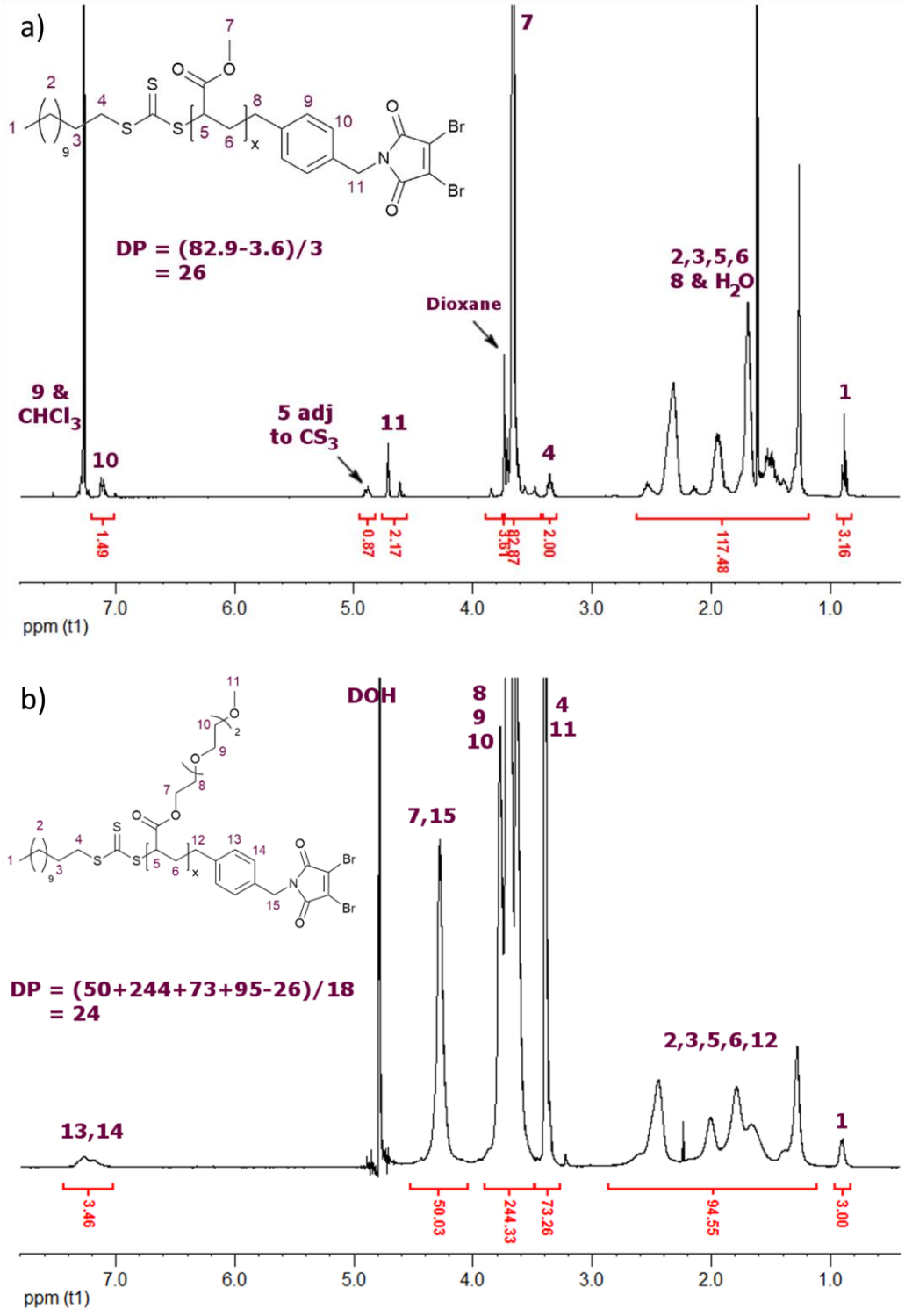

Figure 2.8. a) ^{1}H NMR spectrum (400 MHz, $CDCl_3$) of **2xii**. b) ^{1}H NMR spectrum (400 MHz, D_2O) of **2xiii**.

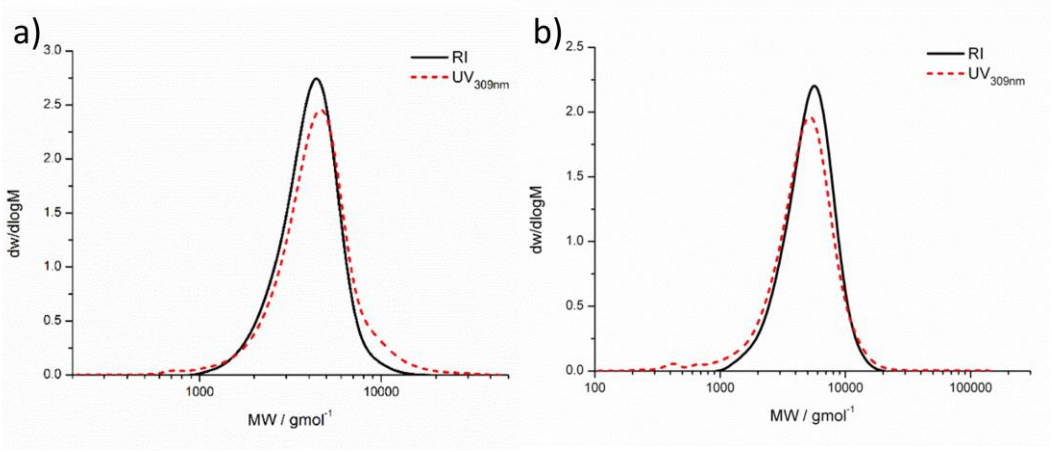

Figure 2.9. Molecular weight distributions obtained by SEC with RI and UV (309 nm) detectors, eluting with THF and calibrated against poly(styrene) standards for a) **2xii** and b) **2xiii**.

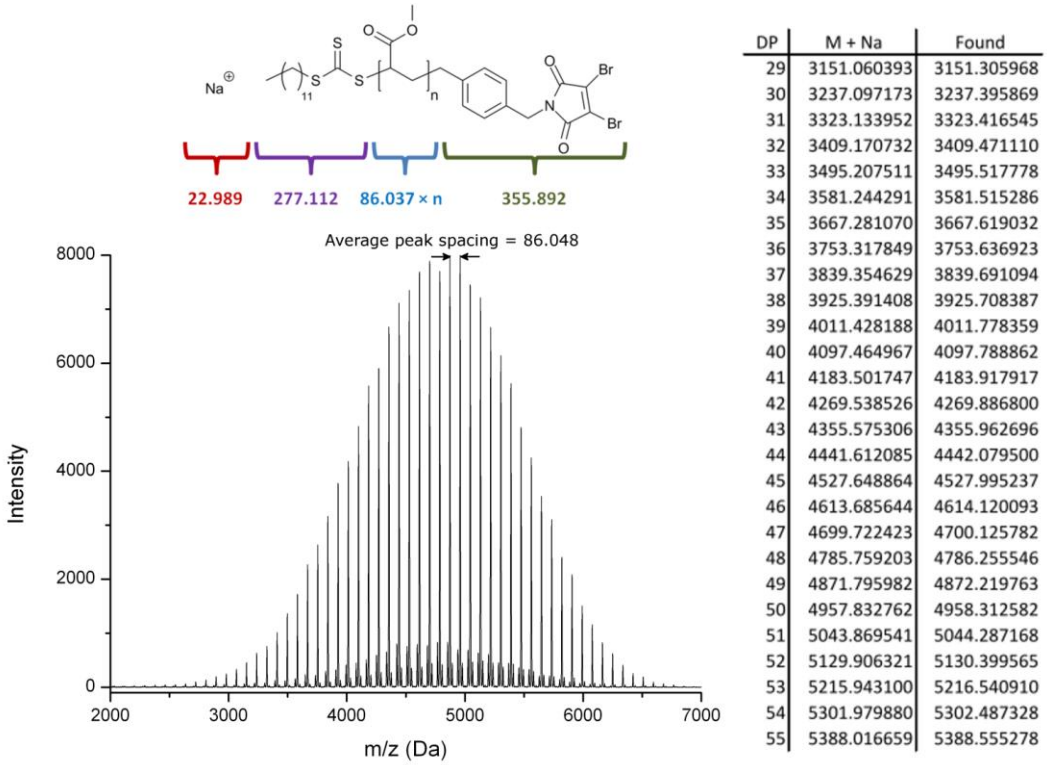

DP	M + Na	Found
29	3151.060393	3151.305968
30	3237.097173	3237.395869
31	3323.133952	3323.416545
32	3409.170732	3409.471110
33	3495.207511	3495.517778
34	3581.244291	3581.515286
35	3667.281070	3667.619032
36	3753.317849	3753.636923
37	3839.354629	3839.691094
38	3925.391408	3925.708387
39	4011.428188	4011.778359
40	4097.464967	4097.788862
41	4183.501747	4183.917917
42	4269.538526	4269.886800
43	4355.575306	4355.962696
44	4441.612085	4442.079500
45	4527.648864	4527.995237
46	4613.685644	4614.120093
47	4699.722423	4700.125782
48	4785.759203	4786.255546
49	4871.795982	4872.219763
50	4957.832762	4958.312582
51	5043.869541	5044.287168
52	5129.906321	5130.399565
53	5215.943100	5216.540910
54	5301.979880	5302.487328
55	5388.016659	5388.555278

Figure 2.10. MALDI-TOF mass spectrum of **2xii**. Spectrum collected in linear mode, with high resolution masses obtained in reflector mode. Average difference between calculated and found $m/z = 0.387080$. Minor distribution corresponds to sodium ion of the F1 fragmentation of the trithiocarbonate.[56]

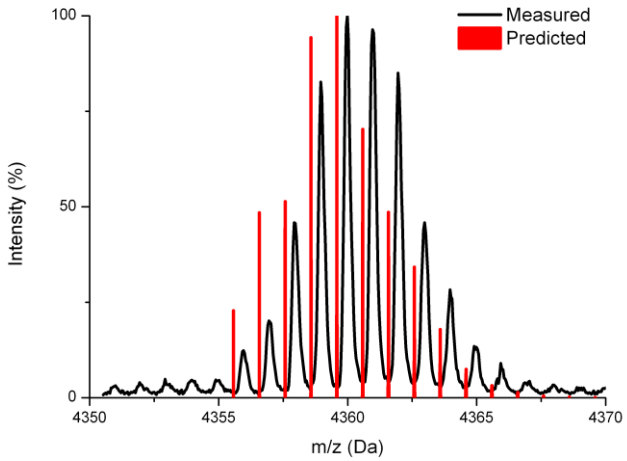

Figure 2.11. Predicted and actual isotope pattern from the MALDI-TOF mass spectrum of **2xii**.

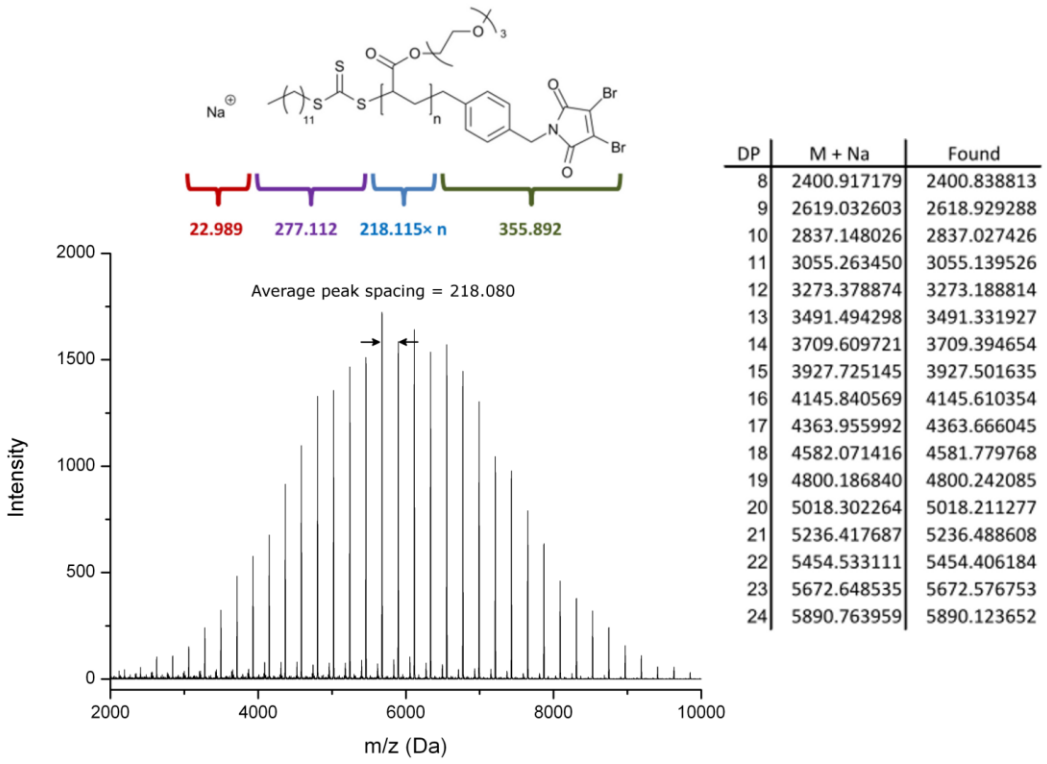

DP	M + Na	Found
8	2400.917179	2400.838813
9	2619.032603	2618.929288
10	2837.148026	2837.027426
11	3055.263450	3055.139526
12	3273.378874	3273.188814
13	3491.494298	3491.331927
14	3709.609721	3709.394654
15	3927.725145	3927.501635
16	4145.840569	4145.610354
17	4363.955992	4363.666045
18	4582.071416	4581.779768
19	4800.186840	4800.242085
20	5018.302264	5018.211277
21	5236.417687	5236.488608
22	5454.533111	5454.406184
23	5672.648535	5672.576753
24	5890.763959	5890.123652

Figure 2.12. MALDI-TOF mass spectrum of **2xiii**. Spectrum collected in linear mode, with high resolution masses obtained in reflector mode. Average difference between calculated and found $m/z = 0.181482$. Minor distribution corresponds to sodium ion of the F1 fragmentation of the trithiocarbonate.[56]

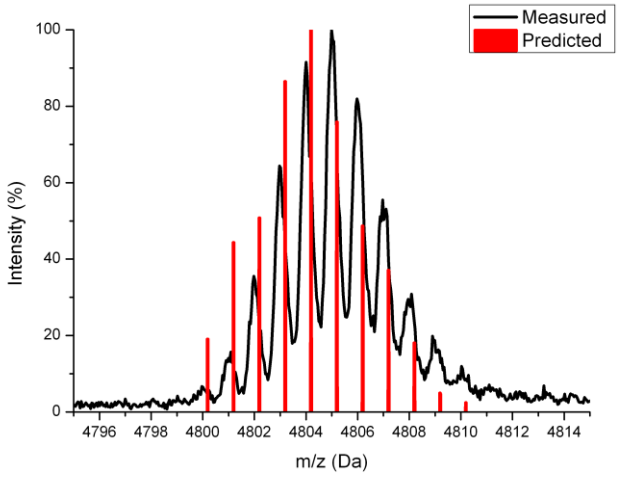

Figure 2.13. Predicted and actual isotope pattern from the MALDI-TOF mass spectrum of **2xiii**.

2.3.3. Polymerisations with MBM RAFT agent

An initial test reaction was performed to assess whether the MBM C=C double bond was susceptible to homopolymerisation. A degassed solution of **2ii** and 0.1 *eq.* of AIBN in dioxane was heated at 65 °C for 6 h. During this time there was no evidence of polymerisation by ^{1}H NMR spectroscopy with the resonance of MBM proton (indicated in Scheme 2.8) being unchanged, or SEC analysis which saw no change to the molecular weight distribution.

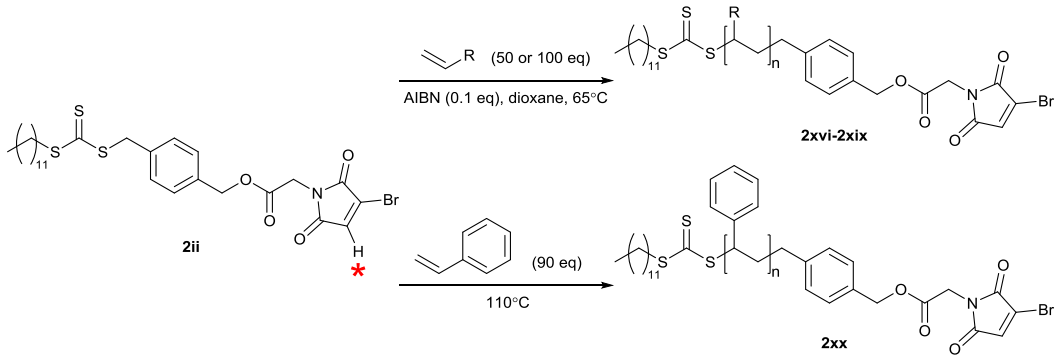

Scheme 2.8. RAFT polymerisation with **2ii** as CTA. The MBM proton of the CTA is indicated by ⋆

Polymerisations mediated by **2ii** of ^{t}BA, MA, TEGA and NIPAM were conducted with [AIBN]:[**2ii**] = 0.1:1, at 65 °C, with varying monomer/dioxane ratios of 1/1 (*v*/*v*), 1/1 (*v*/*v*), 1/2 (*v*/*v*), and 2/3 (*w*/*w*) respectively to ensure complete monomer dissolution. Sty

polymerisations were conducted in bulk at 110 °C, without the addition of AIBN (thermal initiation of Sty). Details of the reactions are given in Scheme 2.8 and Table 2.3.

Table 2.3. RAFT polymerizations conducted with CTA (**2ii**), performed at 65 °C in dioxane.

	Monomer	**[2ii:M:AIBN]**	**Time (h)**	M_n [a] **(kDa)**	$M_{n,th}$ [b] **(kDa)**	$Đ_M$ [a]	p [b] **(%)**
2xvi	^{t}BA	1:100:0.1	3	31.2	11.5	1.53	85
2xvii	MA	1:100:0.1	3	25.6	7.4	1.46	79
2xviii	TEGA	1:50:0.1	16	16.9	10.9	1.54	93
2xix	NIPAM	1:50:0.1	16	0.5	0.7	1.64	3
2xx	Sty [c]	1:90:0	16	7.2	2.4	2.42	19

[a] Molecular weight data were obtained by SEC. Samples were taken without fractionation or precipitation. [b] Monomer conversion (p) monitored by ^{1}H NMR spectroscopy. $M_{n,th}$ calculated from monomer conversion. [c] Styrene polymerizations were conducted in bulk, with thermal initiation at 110 °C.

Polymerisation of ^{t}BA (**2xvi**) proceeded rapidly, with 85% conversion reached after 3 h. However, conversion ^{1}H NMR spectra revealed that the MBM proton of the RAFT agent **2ii** was consumed at a faster rate than ^{t}BA (Figure 2.14). SEC analysis showed a significant deviation of M_n from theoretical values, with high dispersity ($Đ_M > 1.4$) throughout. Molecular weight distribution was multimodal throughout the reaction, even at 30 min when ^{t}BA and MBM conversions were very low (1% and 10% respectively).

Analysis of the purified polymer by SEC with a viscometry detector allowed the plotting of a Mark-Houwink curve ($\ln[\eta]$ vs $\ln[MW]$ where η is the intrinsic viscosity measured by the viscometry detector, and MW is the molecular weight calculated by a Universal Calibration).[57] Measuring the gradient gave $a = 0.29$ (Figure 2.15) which indicates that the polymer adopted a more compact structure in solution than a linear flexible polymer, which have $0.5 < a < 0.8$ (for example P^{t}BA **2xi** had $a = 0.62$ under the same conditions).[58]

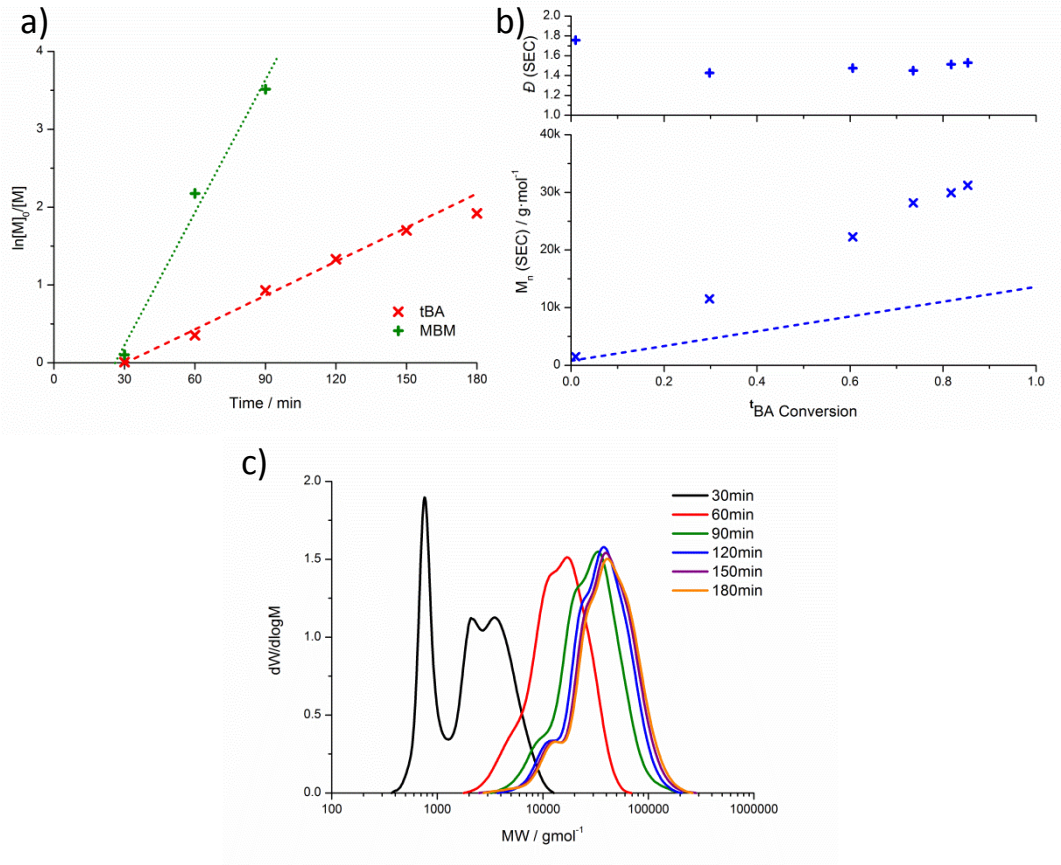

Figure 2.14. ^{t}BA RAFT polymerisation with **2ii** (**2xvi** in Table 2.3); a) First order kinetics of ^{t}BA and MBM consumption with linear fits; b) M_n and $Đ_M$ (as measured by SEC) as a function of ^{t}BA conversion with theoretic values (line); c) Evolution of molecular weight distribution (as measured by SEC) as a function of time.

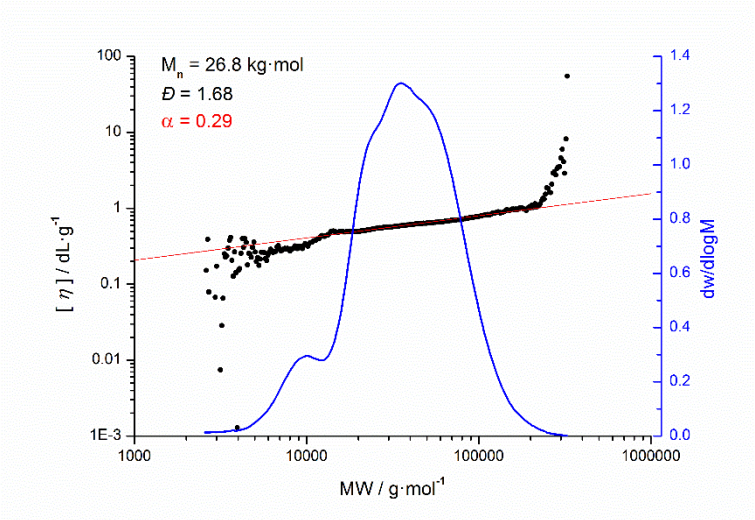

Figure 2.15. SEC molecular weight distribution and Mark-Houwink plot for **2xvi**.

This suggests that **2xvi** has a branched structure, due to copolymerisation of ^{t}BA and the MBM C=C double bond. In fact, a RAFT agent containing a polymerisable double bond would be expected to give a hyperbranched polymer, as demonstrated for example by the

groups of Zhao, Rimmer and Sumerlin.[59-61] Attack of propagating radicals at the less hindered position of the MBM C=C double bond would lead to the formation of a radical stabilised by the Br (Scheme 2.9.). This radical would then propagate with monomer, leading to the creation of a branch point. The result is a species with one C=C double bond and two trithiocarbonate groups, which can be considered as an AB_2 monomer.[62] Further polymerisation of AB_2 monomers leads to the formation of highly branched polymers without gelation.[63]

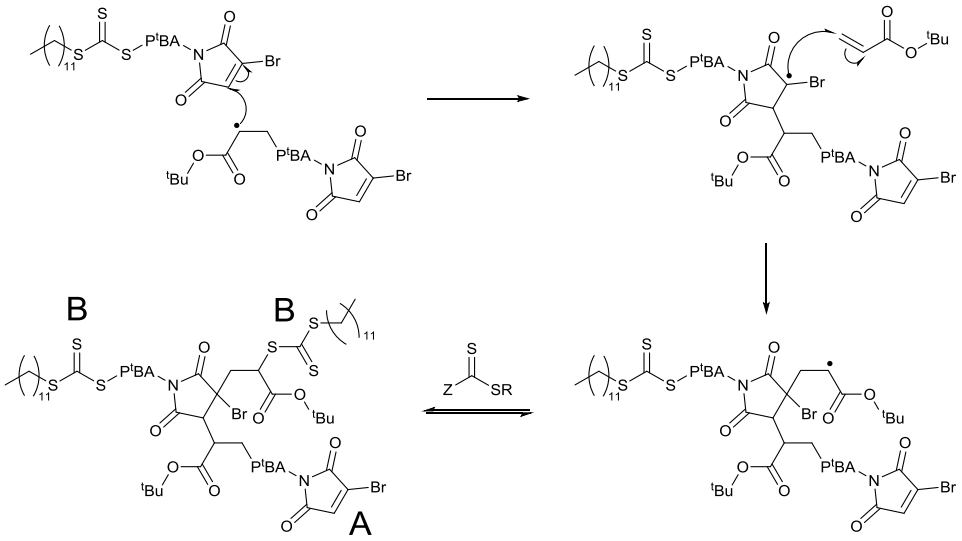

Scheme 2.9. Proposed mechanism for the formation of hyperbranched P^{t}BA in RAFT polymerisation mediated by **2ii**.

^{1}H NMR spectroscopy indicated that the ratio of trithiocarbonate end-group to P^{t}BA was 90:1 (using the C<u>H</u>(CO_2) backbone resonances), in reasonable agreement with 85% conversion of 100 eq (Figure 2.16). ^{t}BA. There was no resonance corresponding to the MBM proton (6.95 ppm), instead there was a broad resonance attributed to the poly(bromosuccinimide) unit (H8), as well as a broad resonance attributed to P^{t}BA units adjacent to these poly(bromosuccinimide) units (H9).

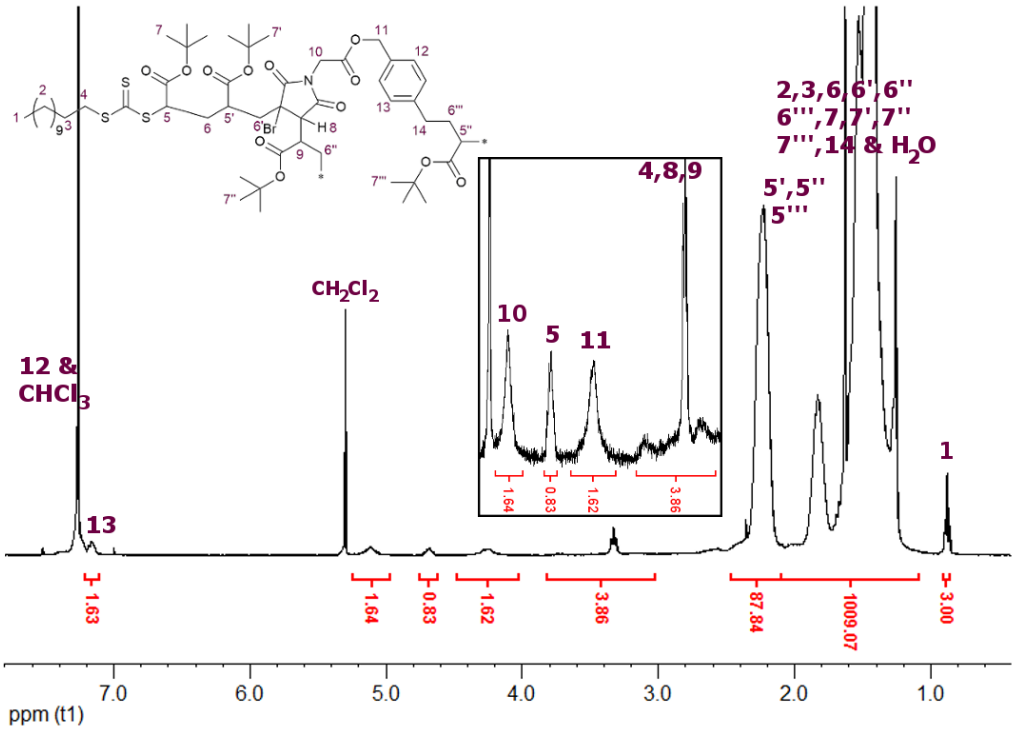

Figure 2.16. ^{1}H NMR spectrum (400 MHz, $CDCl_3$) of **2xvi**.

RAFT polymerisations of MA, TEGA and Sty (**2xvii**, **2xviii** and **2xx** respectively) showed similar results, with large deviations of M_n measured by SEC from theoretical M_n, high dispersities ($1.4 < Đ_M < 2.5$), and complete loss of the MBM proton (6.95 ppm) in conversion ^{1}H NMR spectra. Again this suggested polymerisation of the C=C double bond of the CTA, with formation of hyperbranched polymers. In the case of NIPAM (**2xix**) almost complete loss of the MBM proton (6.95 ppm) was observed by ^{1}H NMR spectroscopy (> 89%), however very little NIPAM conversion was obtained (3%) after 16 h reaction. SEC showed the appearance of a high molecular weight shoulder due to branching, leading to a large dispersity ($Đ_M = 1.64$). These results suggest that the MBM double bond was reacting during the polymerisation, but that radicals centred on the resultant succinimide carbon were not able to propagate. These findings are further discussed in Chapter 6, in relation to other data concerning polymerisations in the presence of bromo-and thiomaleimides.

In an attempt to prevent the formation of hyperbranched polymers when using CTA **2ii**, a series of ^{t}BA polymerisations were conducted with changes to various reaction conditions, as detailed in Table 2.4. The aim was to find conditions which favoured ^{t}BA propagation, and disfavoured polymerisation of the MBM group of **2ii**.

Table 2.4. Polymerisation of ^{t}BA with **2ii** in dioxane at ^{t}BA/dioxane = 1/1 (*v/v*)

	[**2ii**]:[^{t}BA]:[Initiator]	Initiator	T (°C)
2xvi	1:100:0.1	AIBN	65
2xxi	1:100:0.025	AIBN	65
2xxii	1:100:0.1	AIBN	80
2xxiii	1:100:0.1	V-65	50
2xxiv	1:1000:0.1	AIBN	65

The polymerisation was conducted with a reduced radical concentration, by using 0.025 *eq.* of AIBN (**2xxi**). A higher temperature (80 °C), which would result in a higher radical concentration, was also attempted (**2xxii**). By using the initiator 2,2'-azobis-2,4-dimethyl valeronitrile (V-65) a lower reaction temperature (50 °C) was investigated (**2xxiii**). A much lower radical and CTA concentration was also attempted, with 1000 *eq.* of ^{t}BA used (**2xxiv**). However, in all cases consumption of the MBM group of **2ii** was significantly faster than ^{t}BA conversion, leading to high $Đ_{M}$ and significant deviations of M_{n} from theoretical values as the result of branching (Figure 2.17).

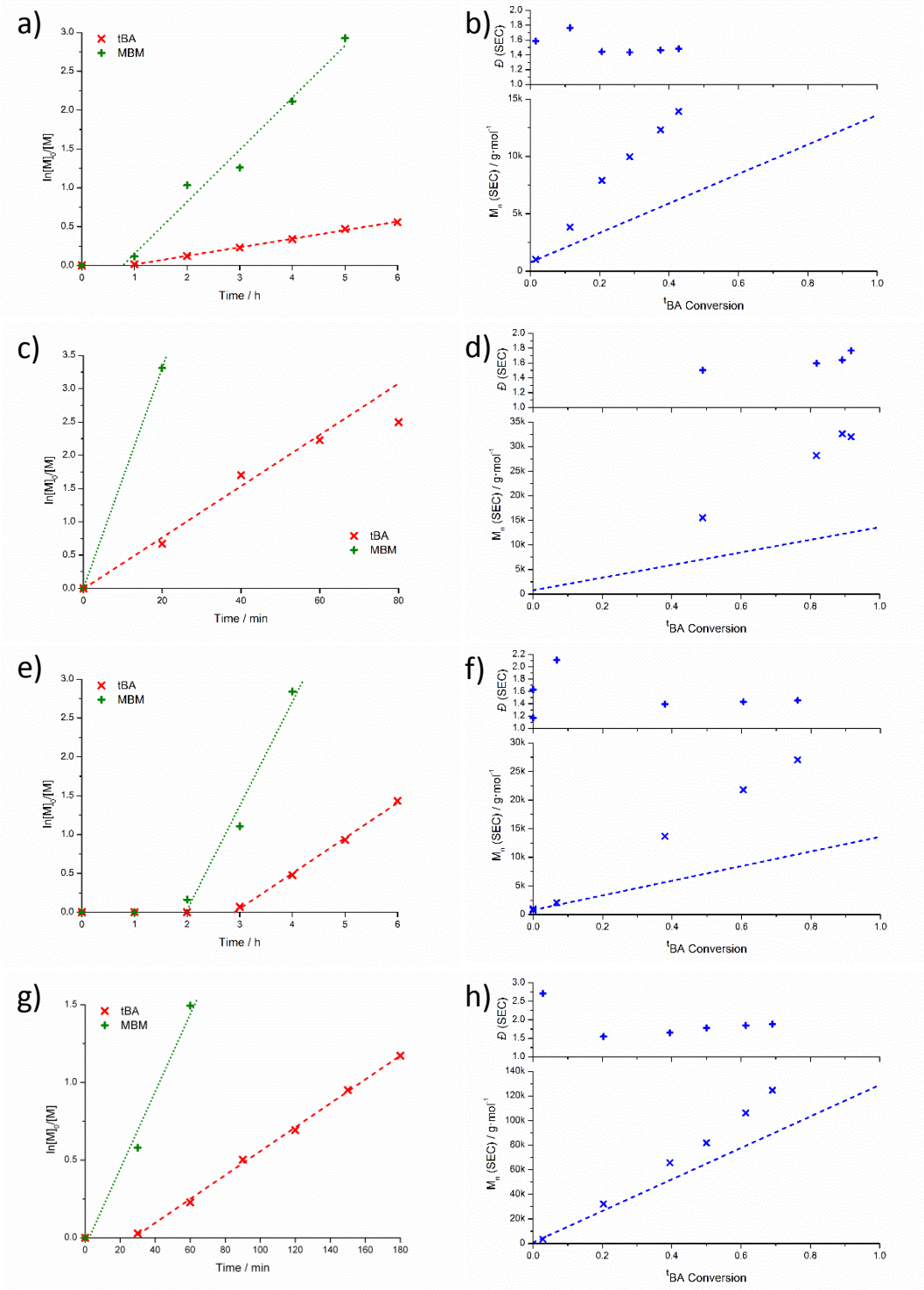

Figure 2.17. ^{t}BA RAFT polymerisations with **2ii**. First order kinetics of ^{t}BA and MBM consumption with linear fits (left), M_n and $Đ_M$ (as measured by SEC; THF eluent, PSty standards) as a function of ^{t}BA conversion with theoretic values as a line (right), for a&b) **2xxi**, c&d) **2xxii**, e&f) **2xxiii**, g&h) **2xxiv**.

2.4. Conclusions

In this chapter RAFT agents with R groups bearing either the dibromomaleimide (DBM) or monobromomaleimide (MBM) functional groups were successfully synthesised.

RAFT polymerisation of acrylates with the DBM CTA were found to proceed with good control over molecular weight, and with retention of both the DBM-functional R group and the trithiocarbonate Z group at the α– and ω-chain ends respectively. This indicates that; contrary to the maleimide functional group which requires protection during radical polymerisation to avoid reaction of its C=C double bond, the DBM group does not require protection. Polymerisation of styrene and NIPAM with this CTA were found to be significantly inhibited, with only low conversions reached.

RAFT polymerisations with the MBM CTA were found to lead to a loss of control over molecular weight, with significant deviations of M_n from theoretical values, large dispersities, and multimodal molecular weight distributions. Consumption of the MBM proton indicated the polymerisation of the MBM C=C double bond, which ^{1}H NMR spectroscopy and SEC analysis revealed to be resulting in hyperbranched polymers. Despite trying a range of polymerisation conditions, it was not possible to prevent branching occurring at a faster rate than monomer polymerisation.

The post-polymerisation functionalisation of DBM-terminated poly(acrylates) synthesised in this chapter is explored in Chapter 3. The question of the way in which bromomaleimide groups influence RAFT polymerisations arises again in Chapter 4, and this phenomenon is explored in detail in Chapter 6.

2.5. Experimental

2.5.1. Materials and apparatus

Tert-butyl acrylate (^{t}BA), methyl acrylate (MA) and styrene (Sty) were vacuum distilled over CaH_2 prior to use, and stored at 4 °C. *N*-Isopropylacrylamide (NIPAM) was recrystallised from a 9:1 mixture of hexanes: acetone and subsequently stored at 4 °C. 2,2'-azobis(2-methylpropionitrile) (AIBN) was recrystallised twice from methanol and stored at 4 °C in the dark. 1,4-Dioxane was passed through a basic alumina plug immediately before use. All other chemicals and reagents were purchased from Aldrich and used as received. Solvents were purchased from Fisher Scientific and used as received. Dry solvents were used directly from a drying and degassing solvent tower delivery system.

^{1}H and ^{13}C NMR spectra were recorded on a Bruker DPX-300, DPX-400, DRX-500, AV-600 or AV-700 spectrometer in $CDCl_3$ unless otherwise stated. Chemical shifts are given in ppm downfield from the internal standard tetramethylsilane, and coupling constants (J) correspond to $^{3}J_{H\text{-}H}$ unless otherwise stated. Size exclusion chromatography (SEC) measurements were conducted using Varian 390-LC-Multi detector suites fitted with differential refractive index (DRI), photodiode array (PDA) and viscometry detectors, equipped with a guard column (Varian Polymer Laboratories PLGel 5 µm, 50×7.5 mm) and two mixed D columns (Varian Polymer Laboratories PLGel 5 µm, 300×7.5 mm). The mobile phase was either tetrahydrofuran with 2% triethylamine, chloroform with 2% triethylamine or dimethylformamide with 5 mM NH_3BF_4 at a flow rate of 1.0 mL·min^{-1}. Data was analysed using Cirrus v3.3 with calibration curves produced using either Varian Polymer laboratories Easi-Vials linear poly(styrene) or poly(methyl methacrylate) standards. Infrared spectra were recorded (neat) on a Perkin Elmer, Spectrum 100 FT-IR Spectrometer. High Resolution Mass Spectrometry (HR-MS) was conducted on a Bruker UHR-Q-TOF MaXis with electrospray ionization. MALDI-TOF mass spectrometry was conducted using a Bruker Daltonics Ultraflex II MALDI-TOF mass spectrometer, equipped with a nitrogen laser delivering 2 ns laser pulses at 337 nm with positive ion TOF detection performed using an accelerating voltage of 25 kV. Solutions in THF (50 µl) of trans-2-[3-(4-*tert*-butylphenyl)-2-methyl-2-propylidene] malonitrile (DCTB) as a matrix (40 g·l^{-1}), sodium trifluoroacetate as cationisation agent (0.1 g·l^{-1}) and sample (1.0 g·l^{-1})

were mixed, and 0.5 μL of the mixture was applied to the target plate. Spectra were recorded in reflector mode calibrating with SpheriCal (1.2-8 kDa) standards, and linear mode calibrating with PEG-Me 2 kDa and 5 kDa standards. Elemental analysis was performed by Warwick Analytical Service; CHN analysis was performed using a CE 440 Elemental Analyser, and S analysis was obtained by combustion procedure followed by titrimetric determination.

2.5.2. Synthetic protocols

Triethylene glycol monomethylether acrylate (TEGA) was synthesised as previously reported.[52]

2-(3-bromo-2,5-dioxo-2,5-dihydro-1H-pyrrol-1-yl)acetic acid was synthesised as previously reported.[51]

Monobromomaleimide was synthesised as previously reported.[64]

(Dodecylsulfanyl)([(4-[hydroxymethyl]phenyl)methyl]sulfanyl)methanethione (**2iii**) was synthesised as previously reported.[48]

3,4-Dibromo-1-([4-([([dodecylsulfanyl]methanethioyl)sulfanyl]methyl)phenyl] methyl)-2,5-dihydro-1H-pyrrole-2,5-dione (2i)

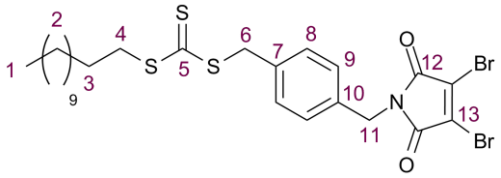

To a flame dried flask under an inert N_2 atmosphere was added triphenyl phosphine (2.40 g, 9.14 mmol) and dry THF (100 mL). The mixture was cooled to -78 °C before adding dropwise diisopropyl azodicarboxylate. (1.85 g, 9.14 mmol). The mixture was stirred for 5 min before adding **2iii** (3.64 g, 9.14 mmol), stirred a further 5 min before adding neopentylalcohol (0.40 g, 4.57 mmol), and stirred a further 5 min before adding 2,3-dibromomaleimide (2.33 g, 9.14 mmol). The reaction was allowed to warm to room temperature while stirring for 16 h. The solvent was removed *in vacuo*, and the crude mixture purified by column chromatography (SiO_2, pet. ether : DCM = 2:1) to give the product as a yellow solid (2.67 g, 46%). R_f =0.21. ^{1}H NMR (400 MHz, $CDCl_3$) δ7.34-7.28

(4H, m, H8 & H9), 4.72 (2H, s, H11), 4.58 (2H, s, H6), 3.36 (2H, t, J = 7.5 Hz, H4), 1.69 (2H, quin., J = 7.5 Hz, H3), 1.46-1.20 (18H, m, H2), 0.88 (3H, t, J = 7.0 Hz, H1); ^{13}C NMR (125 MHz, $CDCl_3$) δ223.5 (C5), 163.6 (C12), 135.6 (C7), 134.6 (C10), 129.7 (C8), 129.5 (C13), 129.1 (C9), 42.8 (C11), 40.7 (C6), 37.2 (C4), 32-22 (C2-3), 14.1 (C1); FTIR (neat) ν1781 and 1720 cm^{-1} (maleimide), 1593 and 1517 cm^{-1} (aromatic); Elemental analysis: Calculated (%) C 47.25, H 5.23, N 2.20, S 15.14; Found (%) C 47.33, H 5.25, N 2.16, S 15.13

(4-[([(dodecylsulfanyl)methanethioyl]sulfanyl)methyl]phenyl)methyl 2-(3-bromo-2,5-dioxo-2,5-dihydro-1H-pyrrol-1-yl)acetate (2ii)

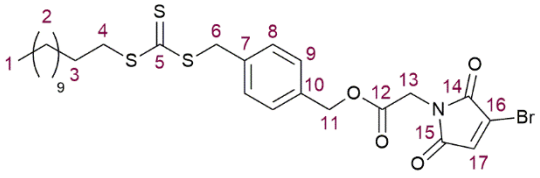

2iii (0.600 g, 1.50 mmol) 2-(3-bromo-2,5-dioxo-2,5-dihydro-1H-pyrrol-1-yl)acetic acid (0.352 g, 1.50 mmol), *N*-(3-Dimethylaminopropyl)-N'-ethylcarbodiimide hydrochloride (0.346 g, 1.81 mmol) and 4-(Dimethylamino)pyridine (36.8 mg, 0.301 mmol) were added to a flame dried round bottomed flask. The vessel was purged with N_2 gas while cooling to 0 °C before addition of dry THF (15 mL). The reaction was allowed to warm to room temperature while stirring for 16 h, at which point the solvent was removed *in vacuo*. The resultant solids were dissolved in DCM (200 mL) and washed with water (100 mL x 3), brine (100 mL) and dried over $MgSO_4$. The solvent was removed *in vacuo* and the crude product purified by column chromatography (SiO_2, pet. ether: ethyl acetate = 4:1) to give the product as a yellow solid (0.518 g, 56%). R_f =0.22. ^{1}H NMR (500 MHz, $CDCl_3$) δ7.34 (2H, d, J = 8.0 Hz, H8), 7.27 (2H, d, J = 8.0 Hz, H9), 6.95 (1H, s, H17), 5.15 (2H, s, H13), 4.60 (2H, s, H6), 4.34 (2H, s, H11), 3.34 (2H, t, J = 7.5 Hz, H4), 1.69 (2H, quin, J = 7.5 Hz, H3), 1.42-1.21 (18H, m, H2), 0.87 (3H, t, J = 6.5 Hz, H1); ^{13}C NMR (125 MHz, $CDCl_3$) δ223.7 (C5), 167.8 (C14), 166.9 (C12), 164.8 (C15), 136.1 (C7), 134.5 (C10), 132.5 (C17), 131.9 (C16), 129.7 (C8), 128.9 (C9), 67.6 (C13), 41.1 (C6), 39.7 (C11), 37.4 (C4), 32.2, 29.9-29.1, 22.9 (C2), 28.2 (C3). 14.3 (C1); FTIR (neat) ν1752 and 1718 cm^{-1} (maleimide and ester), 1587 and 1517 cm^{-1} (aromatic); HR-MS (MaXis) *m/z* found 636.0876, calc. 636.0882 ([M + Na]$^+$, 100%).

General procedure for RAFT polymerisations with 2i, 2ii or 2iii

Typically; to a polymerisation ampoule was added a solution of RAFT agent, AIBN, and monomer in dioxane. The solution was degassed by three freeze-pump-thaw cycles, the ampoule sealed under N_2 and the reaction stirred at the required temperature. Periodically samples were taken for ^{1}H NMR spectroscopy and SEC analysis. Control reactions without monomer were performed in an identical fashion.

For P^{t}BA, PMA and PSty the product was isolated by repeated precipitation into ice cold methanol/water (9:1 *v/v*) and dried over $MgSO_4$ then *in vacuo.*

For PNIPAM the product was isolated by repeated precipitation into diethyl ether and dried *in vacuo.*

For PTEGA the product was isolated by exhaustive dialysis against deionised water (MWCO 3500 Da), before the water was removed by lyophilisation.

2.6. References

1. G. Moad, E. Rizzardo and S. H. Thang, *Aust. J. Chem.*, 2012, **65**, 985-1076.

2. K. Matyjaszewski, *Macromolecules*, 2012, **45**, 4015-4039.

3. U. Mansfeld, C. Pietsch, R. Hoogenboom, C. R. Becer and U. S. Schubert, *Polym. Chem.*, 2010, **1**, 1560-1598.

4. K. Kempe, A. Krieg, C. R. Becer and U. S. Schubert, *Chem. Soc. Rev.*, 2012, **41**, 176-191.

5. H. Durmaz, B. Colakoglu, U. Tunca and G. Hizal, *J. Polym. Sci., Part A: Polym. Chem.*, 2006, **44**, 1667-1675.

6. C. F. Hansell, P. Espeel, M. M. Stamenović, I. A. Barker, A. P. Dove, F. E. Du Prez and R. K. O'Reilly, *J. Am. Chem. Soc.*, 2011, **133**, 13828-13831.

7. J. A. Opsteen and J. C. M. van Hest, *Chem. Commun.*, 2005, 57-59.

8. L. M. Campos, K. L. Killops, R. Sakai, J. M. J. Paulusse, D. Damiron, E. Drockenmuller, B. W. Messmore and C. J. Hawker, *Macromolecules*, 2008, **41**, 7063-7070.

9. D. Konkolewicz, A. Gray-Weale and S. Perrier, *J. Am. Chem. Soc.*, 2009, **131**, 18075-18077.

10. C. Boyer, J. Liu, L. Wong, M. Tippett, V. Bulmus and T. P. Davis, *J. Polym. Sci., Part A: Polym. Chem.*, 2008, **46**, 7207-7224.

11. P. J. Roth, F. D. Jochum, R. Zentel and P. Theato, *Biomacromolecules*, 2009, **11**, 238-244.

12. D. J. Hall, H. M. Van Den Berghe and A. P. Dove, *Polym. Int.*, 2011, **60**, 1149-1157.

13. K. L. Heredia, G. N. Grover, L. Tao and H. D. Maynard, *Macromolecules*, 2009, **42**, 2360-2367.

14. M. Li, P. De, H. Li and B. S. Sumerlin, *Polym. Chem.*, 2010, **1**, 854-859.

15. G. Mantovani, F. Lecolley, L. Tao, D. M. Haddleton, J. Clerx, J. J. L. M. Cornelissen and K. Velonia, *J. Am. Chem. Soc.*, 2005, **127**, 2966-2973.

16. L. Tao, C. S. Kaddis, R. R. Ogorzalek Loo, G. N. Grover, J. A. Loo and H. D. Maynard, *Chem. Commun.*, 2009, 2148-2150.

17. J. Geng, G. Mantovani, L. Tao, J. Nicolas, G. Chen, R. Wallis, D. A. Mitchell, B. R. G. Johnson, S. D. Evans and D. M. Haddleton, *J. Am. Chem. Soc.*, 2007, **129**, 15156-15163.

18. G. Hizal, U. Tunca and A. Sanyal, *J. Polym. Sci., Part A: Polym. Chem.*, 2011, **49**, 4103-4120.

19. A. Dag, H. Durmaz, G. Hizal and U. Tunca, *J. Polym. Sci., Part A: Polym. Chem.*, 2008, **46**, 302-313.

20. A. Dag, H. Durmaz, U. Tunca and G. Hizal, *J. Polym. Sci., Part A: Polym. Chem.*, 2009, **47**, 178-187.

21. H. Durmaz, A. Dag, C. Onen, O. Gok, A. Sanyal, G. Hizal and U. Tunca, *J. Polym. Sci., Part A: Polym. Chem.*, 2010, **48**, 4842-4846.

22. H. Durmaz, A. Dag, G. Hizal and U. Tunca, *J. Polym. Sci., Part A: Polym. Chem.*, 2010, **48**, 5083-5091.

23. B. Gacal, H. Durmaz, M. A. Tasdelen, G. Hizal, U. Tunca, Y. Yagci and A. L. Demirel, *Macromolecules*, 2006, **39**, 5330-5336.

24. T. Ikeda, D. Oikawa, T. Shimasaki, N. Teramoto and M. Shibata, *Polymer*, 2013, **54**, 3206-3216.

25. N. Xu, F.-S. Du and Z.-C. Li, *J. Polym. Sci., Part A: Polym. Chem.*, 2007, **45**, 1889-1898.

26. W. M. Gramlich, M. L. Robertson and M. A. Hillmyer, *Macromolecules*, 2010, **43**, 2313-2321.

27. X. Xiong and Y. Xu, *Polym. Bull.*, 2010, **65**, 455-463.

28. R. J. Pounder, M. J. Stanford, P. Brooks, S. P. Richards and A. P. Dove, *Chem. Commun.*, 2008, 5158-5160.

29. M. J. Stanford, R. L. Pflughaupt and A. P. Dove, *Macromolecules*, 2010, **43**, 6538-6541.

30. S. Kuroda and T. Hagiwara, *Polymer*, 2011, **52**, 1869 - 1873.

31. G.-Q. Chen, Z.-Q. Wu, J.-R. Wu, Z.-C. Li and F.-M. Li, *Macromolecules*, 2000, **33**, 232-234.

32. G. Deng and Y. Chen, *Macromolecules*, 2004, **37**, 18-26.

33. J.-F. Lutz, *Acc. Chem. Res.*, 2013, **46**, 2696-2705.

34. O. Gok, H. Durmaz, E. S. Ozdes, G. Hizal, U. Tunca and A. Sanyal, *J. Polym. Sci., Part A: Polym. Chem.*, 2010, **48**, 2546-2556.

35. J. A. Syrett, G. Mantovani, W. R. S. Barton, D. Price and D. M. Haddleton, *Polym. Chem.*, 2010, **1**, 102-106.

36. E. Bays, L. Tao, C.-W. Chang and H. D. Maynard, *Biomacromolecules*, 2009, **10**, 1777-1781.

37. Z. P. Tolstyka, J. T. Kopping and H. D. Maynard, *Macromolecules*, 2008, **41**, 599-606.

38. M. Li, P. De, S. R. Gondi and B. S. Sumerlin, *J. Polym. Sci., Part A: Polym. Chem.*, 2008, **46**, 5093-5100.

39. L. M. Tedaldi, M. E. B. Smith, R. I. Nathani and J. R. Baker, *Chem. Commun.*, 2009, 6583-6585.

40. M. E. B. Smith, F. F. Schumacher, C. P. Ryan, L. M. Tedaldi, D. Papaioannou, G. Waksman, S. Caddick and J. R. Baker, *J. Am. Chem. Soc.*, 2010, **132**, 1960-1965.

41. L. Castaneda, A. Maruani, F. F. Schumacher, E. Miranda, V. Chudasama, K. A. Chester, J. R. Baker, M. E. B. Smith and S. Caddick, *Chem. Commun.*, 2013, **49**, 8187-8189.

42. F. F. Schumacher, V. A. Sanchania, B. Tolner, Z. V. F. Wright, C. P. Ryan, M. E. B. Smith, J. M. Ward, S. Caddick, C. W. M. Kay, G. Aeppli, K. A. Chester and J. R. Baker, *Sci. Rep.*, 2013, **3**, 1525.

43. F. F. Schumacher, M. Nobles, C. P. Ryan, M. E. B. Smith, A. Tinker, S. Caddick and J. R. Baker, *Bioconjugate Chem.*, 2011, **22**, 132-136.

44. M. W. Jones, R. A. Strickland, F. F. Schumacher, S. Caddick, J. R. Baker, M. I. Gibson and D. M. Haddleton, *J. Am. Chem. Soc.*, 2012, **134**, 1847-1852.

45. G. Moad, E. Rizzardo and S. H. Thang, *Acc. Chem. Res.*, 2008, **41**, 1133-1142.

46. R. Guo, X. Wang, C. Guo, A. Dong and J. Zhang, *Macromol. Chem. Phys.*, 2012, **213**, 1851-1862.

47. J. Skey and R. K. O'Reilly, *Chem. Commun.*, 2008, 4183-4185.

48. N. Petzetakis, A. P. Dove and R. K. O'Reilly, *Chem. Sci.*, 2011, **2**, 955-960.

49. M. A. Walker, *J. Org. Chem.*, 1995, **60**, 5352-5355.

50. C. Copeland, R. Conway, J. Patroni and R. Stick, *Aust. J. Chem.*, 1981, **34**, 555-557.

51. C. Monneret, D. Dauzonne, J. Hickman, A. Pierre, L. Kraus-Berthier, B. Pfeiffer and P. Benard, *US Pat.,* US20060247246A1, 2006.

52. F. Hua, X. Jiang, D. Li and B. Zhao, *J. Polym. Sci., Part A: Polym. Chem.*, 2006, **44**, 2454-2467.

53. J. Chiefari, Y. K. B. Chong, F. Ercole, J. Krstina, J. Jeffery, T. P. T. Le, R. T. A. Mayadunne, G. F. Meijs, C. L. Moad, G. Moad, E. Rizzardo and S. H. Thang, *Macromolecules*, 1998, **31**, 5559-5562.

54. C. Barner-Kowollik, P. Vana and T. P. Davis, in *Handbook of Radical Polymerization*, eds. K. Matyjaszewski and T. P. Davis, John Wiley & Sons, Inc., 2002, pp. 187-261.

55. C. Ladavière, P. Lacroix-Desmazes and F. Delolme, *Macromolecules*, 2009, **42**, 70-84.

56. O. I. Strube, L. Nothdurft, M. Drache and G. Schmidt-Naake, *Macromol. Chem. Phys.*, 2011, **212**, 574-582.

57. P. C. Hiemenz and T. P. Lodge, *Polymer Chemistry*, 2nd edn., CRC Press, Boca Raton, 2007.

58. J. E. Mark, *Physical Properties of Polymers Handbook*, Springer, 2007.

59. C. Zhang, Y. Zhou, Q. Liu, S. Li, S. Perrier and Y. Zhao, *Macromolecules*, 2011, **44**, 2034-2049.

60. A. P. Vogt, S. R. Gondi and B. S. Sumerlin, *Aust. J. Chem.*, 2007, **60**, 396-399.

61. S. Carter, B. Hunt, and S. Rimmer, *Macromolecules*, 2005, **38**, 4595–4603.

62. C. J. Hawker, J. M. J. Frechet, R. B. Grubbs and J. Dao, *J. Am. Chem. Soc.*, 1995, **117**, 10763-10764.

63. B. I. Voit and A. Lederer, *Chem. Rev.*, 2009, **109**, 5924-5973.

64. R. Vanel, F. Berthiol, B. Bessières, C. Einhorn and J. Einhorn, *Synlett*, 2011, 1293-1295.

3. Fluorescent dithiomaleimides, and their utility for site-specific labelling of polymers

3.1. Abstract

In this chapter the serendipitous discovery of a novel fluorophore is reported. Dithiomaleimides (DTMs) with alkyl substituents on the N and S are found to be emissive, exhibiting a broad excitation spectrum spanning 250-400 nm, with corresponding emission between 500-550 nm. As a demonstration of the versatile nature of the DTM fluorophore, it is incorporated into a RAFT agent/ROP initiator. This RAFT agent/ROP initiator is utilised for the synthesis of fluorescently-labelled polymers *via* a pre-polymerisation functionalisation strategy. Fluorescent labelling of polymers is also demonstrated *via* a post-polymerisation functionalisation, by reaction of the dibromomaleimide-terminated polymers (synthesised in Chapter 2) with thiols.

3.2. Introduction

3.2.1. Fluorescent labelling

Fluorophore attachment is a widely utilised method for labelling chemical analytes, biomolecules, and macromolecules, due to the many desirable features of fluorescence sensing.[1] Fluorescence emission can be detected with high sensitivity using relatively inexpensive equipment, which results in rapid and low-cost sensing in a non-destructive and non-invasive fashion. The high sensitivity of emission detection can be understood through the origin of the phenomena, and the way in which it is measured.

Absorption occurs where a photon of sufficient energy ($h\nu_A$) interacts with a molecule, causing promotion of an electron from the ground state (S_0) to an excited state (for example S_1), as shown in the Jablonski diagram[2] (Figure 3.1).

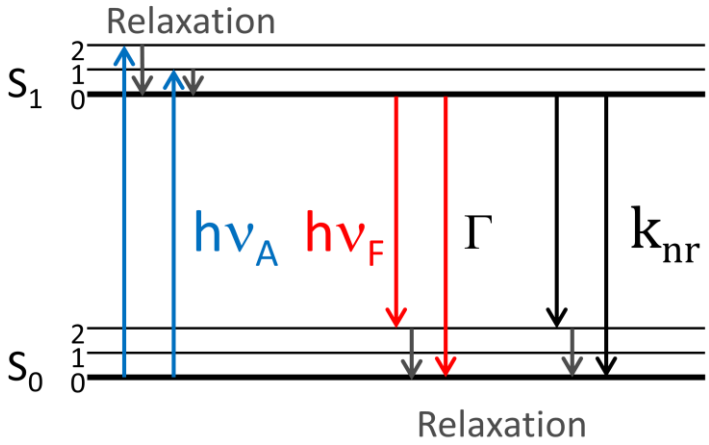

Figure 3.1. Simplified Jablonski diagram explaining the processes of absorption, emission, and non-radiative decay.

The electron is promoted to an excited vibrational state, according to the Franck-Condon principle (Figure 3.2),[2] but relaxes to the ground vibrational state (of the excited electronic state) within 10^{-12} s *via* internal conversion. Return to any vibrational energy level of the ground state (S_0) occurs either by emission of a photon with energy $h\nu_F$, or by a non-radiative process such as collision. These competing processes occur with rate Γ for fluorescence emission, and k_{nr} for non-radiative processes respectively. Thermal equilibration to the vibrational ground state (of the ground electronic state) then rapidly occurs by internal conversion (10^{-12} s). Because of internal conversion immediately

subsequent to excitation and emission, it must follow that $h\nu_A > h\nu_F$. Therefore emission occurs at a longer wavelength than excitation, with the difference between $\lambda_{max,ex}$ and $\lambda_{max,em}$ being referred to as the Stokes shift.[1]

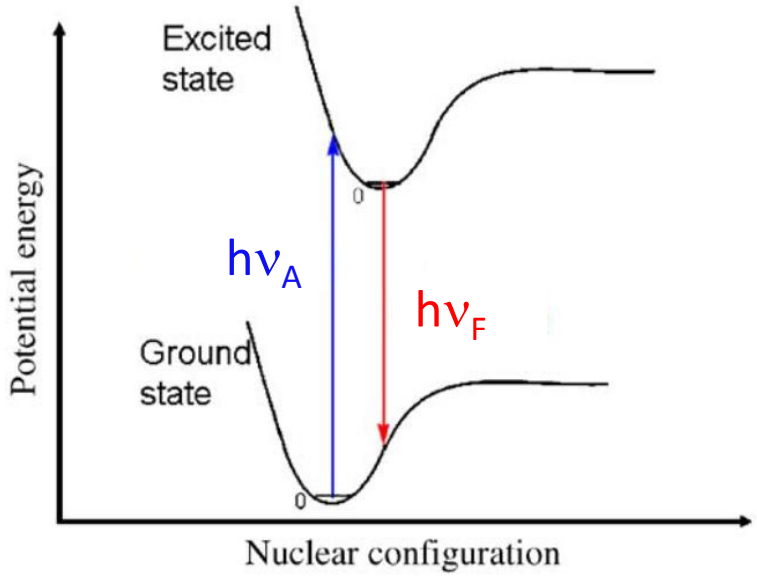

Figure 3.2. A schematic absorption and emission energies level diagram illustrating the Franck-Condon principle and the origin of the Stokes shift. Figure adapted from ref.[3]

A fluorescence lifetime (τ) can be calculated according to equation (3.1), using the rate constants for emission and non-radiative decay (Γ and k_{nr} respectively). The fluorescence lifetime (τ) corresponds to the average time the molecule spends in the excited state prior to emission. A quantum yield (Q), defined as the ratio of photons emitted to the number absorbed can also be calculated using equation (3.2).

$$\tau = \frac{1}{\Gamma + k_{nr}} \tag{3.1}$$

$$Q = \frac{\Gamma}{\Gamma + k_{nr}} \tag{3.2}$$

Fluorescence lifetimes are typically on the order of 10 ns, and quantum yield can be as high as 0.95 for commonly used fluorophores such as fluorescein and rhodamine.[4] This means that a single molecule can emit many thousands of times per second.

The way fluorescence emission is measured also results in very high sensitivity, for example compared to absorption spectroscopy, despite a very similar experimental set-up (Figure 3.3).

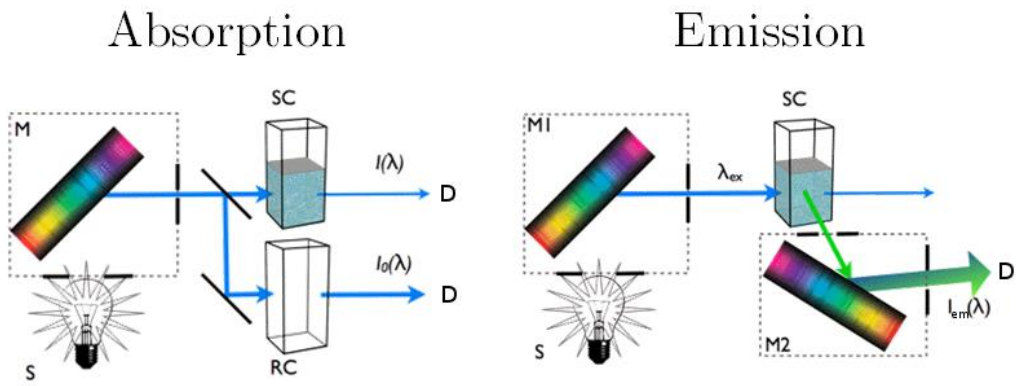

Figure 3.3. Experimental set-up for absorption and emission spectroscopy. Figure adapted from reference.[5]

In both cases a light source (S) is directed through a monochromator (M), providing the required range of wavelengths. In absorption spectroscopy the beam is then split, and directed at the sample cell (SC) as well as a reference cell (RC) which contains only solvent. The transmitted light $I(\lambda)$ and $I_0(\lambda)$ for sample and reference respectively is directed to a detector (D), and absorption ($A(\lambda)$) calculated according to equation (3.3).

$$A(\lambda) = \log \frac{I_0(\lambda)}{I(\lambda)} \tag{3.3}$$

In fluorescence spectroscopy, light with wavelength λ_{ex} is selected by the monochromator (M1) and directed at the sample cell. Emission ($I_{flu}(\lambda)$) is detected at 90°, preventing detection of transmitted λ_{ex} and limiting the contribution of scattered light. A second monochromator (M2) allows excitation spectra (I_{em} as a function of λ_{ex} with constant λ_{em}) to also be recorded. Therefore, because fluorescence is measured against a dark background it has much greater sensitivity compared to absorption, which is measured against the background of transmission through RC. Added to this, photomultiplier tubes can detect single photons, meaning that fluorescence is routinely detected at fluorophore concentrations below 10^{-10} M.

3.2.2. Site-specific fluorescent labelling of polymers

There are many applications where it is highly desirable to incorporate a fluorescent label into the structure of a polymer, to facilitate tracking and monitoring.[6] Labelling is commonly achieved either by copolymerisation with a dye-containing monomer, or by end-group functionalisation. The former approach is discussed extensively in Chapter 4.

The advantage of labelling polymers at their chain end is the site-specific nature of this approach. Labelling is achieved either before polymerisation through the use of a functional initiator, or after polymerisation through a post-polymerisation modification. One or both chain ends can be labelled in this way with excellent efficiency possible, provided end-group fidelity remains high. End-group labelling enables a precise stoichiometry of dye incorporation, with the resulting low fluorophore concentration decreasing the effect of self-quenching. As discussed in Chapter 1 functionality (such as catalytic activity, response to stimuli, initiators for grafting *etc.*) can be incorporated along a polymer backbone through the use of a functional monomer. In this situation the high density of functional group incorporation along the polymer backbone is essential to the final application. Therefore the use of dye incorporation by end-group conjugation (rather than by using a fluorescent monomer) can enable combination of backbone functionality and fluorescent labelling.[7]

For post-polymerisation functionalisation, highly efficient reactions are required. Esterifications between hydroxyl-terminated polymers and acid-functional dyes,[8] amidations between amine-containing dyes and activated ester polymer end-groups,[9] and 'click' chemistry such as the CuAAC reaction,[10] have all been widely employed. An advantage of this approach is the ease with which a library of polymers with different fluorophore end-groups could be constructed from a single scaffold. However, despite the stated efficiency of these reactions, full conversion often requires a large excess of small molecule fluorophores, necessitating their frequently difficult removal during purification.

A variety of functional initiators and chain transfer agents have been used to synthesise polymers with a fluorophore as an end-group (Figure 3.4). Dye-labelled anionic polymerisation initiators have been prepared by reaction of alkyl lithium compounds with

the ethylene-functional polycyclic aromatic hydrocarbons anthracene (**3A**) and phenanthrene (**3B**).[11, 12]

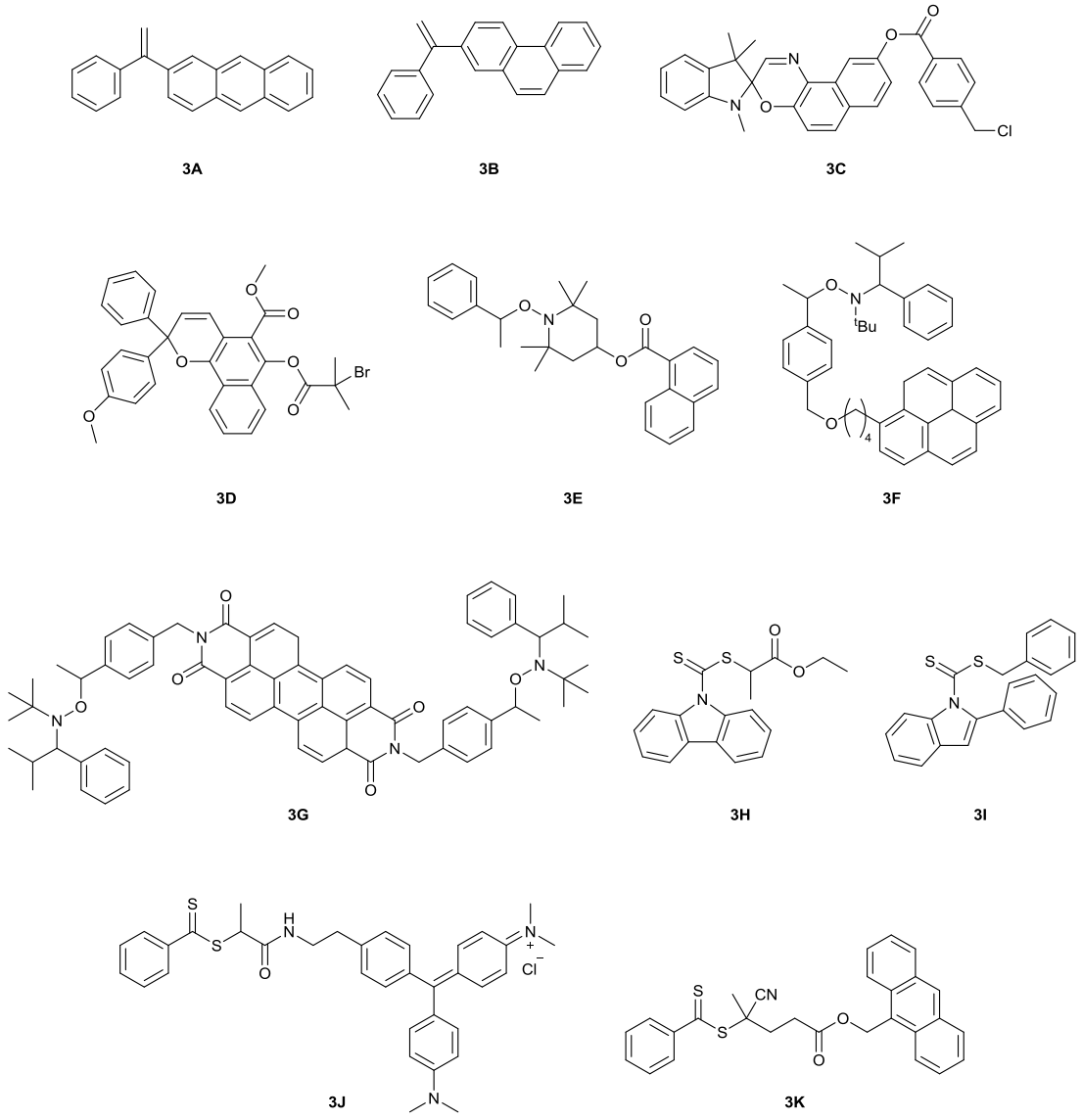

Figure 3.4. Fluorescently-labelled initiators/RAFT agents.

ATRP initiators based both on chloromethylbenzyl and bromoisobutyrl initiating groups have been conjugated to the hydroxyl-functional dyes spirooxazine (**3C**) and naphthopyran (**3D**) by esterification reactions.[13, 14] Alkoxyamine initiators for NMP with napthyl (**3E**), pyrene (**3F**), and perylene (**3G**) labels have been synthesised, with the fluorophore attached to either the mediating nitroxide fragment (**3E**), the initiating fragment (**3F**), or two initiating fragments (**3G**), allowing the synthesis of α-, ω-, and mid-chain labelled polymers.[15-17] The potential for specific labelling of α- or ω-chain ends also exists for RAFT agents, with fluorophore attachment to either the activating Z group, or

the labile R group. Z group fluorophores are often directly incorporated as part of the thiocarbonylthio group, for example as a carbazole (**3H**) or indole (**3I**) dithiocarbamate.[18] R group fluorophores have been attached using a variety of protocols, for example by amidation (**3J**) or esterification (**3K**) of a carboxy-functional RAFT agent.[19, 20]

Polymers labelled at their chain end with a fluorophore have been used in a wide range of applications, one example being their use as biological probes. Kiessling *et al.* prepared antigenic polymer ligands for cell internalisation by ROMP.[21] An alkyne-functional rhodamine was attached to the azide-terminated polymers by a CuAAC reaction, which allowed polymer uptake in live cells to be visualised by fluorescence microscopy. Membrane labelling was also accomplished by Lienkamp and co-workers who produced a synthetic mimic of antimicrobial peptide (SMAMP) by ROMP, using an activated-ester terminating agent.[22] Reaction with amino-nitrobenzoxadiazole gave labelled polymers that were found to accumulate in the membranes of *E. coli* cells, allowing imaging by confocal microscopy.

Site-specific end-group labelling has also been applied to the study of the fundamental properties of polymers and polymerisation mechanisms. Krausch and colleagues synthesised dye-labelled poly(Sty) by reaction of hydroxyl-terminated poly(Sty) with rhodamine B chloride.[23] With this material they measured the dependence of diffusion coefficient on molecular weight for solutions of polystyrene in toluene by fluorescence correlation spectroscopy. Moerner and Fuller *et al.* studied the dynamics of polymer chains in the melt by single molecule imaging. They used a perylene-functional NMP initiator to synthesise end-labelled and mid-chain labelled poly(isoprene) (PI). The tethered dye molecules acted as local environment reporters for the PI chain, demonstrating that there was no difference in chain mobility (and by extension local environment) between chain ends and chain centres.[17] The groups of Parent and Hawker used fluorescent labels to study end-group fidelity in NMP. Using fluorescently-labelled NMP initiators they used fluorescence emission to quantify the molarity of fluorophore present in the final product of polymerisation, and hence the retention of initiator-derived end-group during the reaction.[15, 16]

Site-specific attachment of a fluorophore end-group in polymers is also important when used in combination with polymerisation of a dye-labelled monomer in the construction of light-harvesting materials. For example, Ghiggino and colleagues synthesised an anthracene-functional RAFT agent with which they polymerised an acenaphthyl monomer.[20] The result was a polymer with an energy donor backbone and acceptor end-groups, which showed an excitation energy transfer efficiency of up to 70%.

3.2.3. Fluorescence of maleimide derivatives

The maleimide group is known to be an effective quencher of fluorescence. This is observed when a fluorophore is directly conjugated to the maleimide through the N (**3L**, Figure 3.5), and is due to the maleimide's low lying n,π* transition which provides a non-radiative pathway for excited state decay.[24]

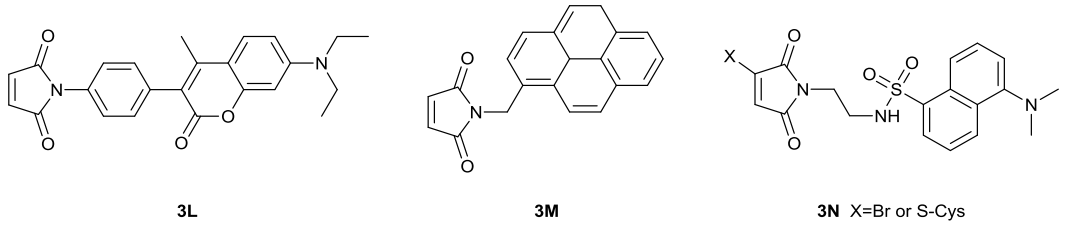

Figure 3.5. Fluorophores quenched by attachment to maleimide

When the C=C double bond of the maleimide becomes saturated, for example upon Michael addition of a thiol, quenching is eliminated and the fluorophore becomes emissive. In this way *N*-fluorophore maleimides have been used as fluorescent probes for the detection of thiols.[25-27] Quenching is also observed when fluorophores are tethered to the maleimide N without direct conjugation through use of a spacer group (**3M**, Figure 3.5). In this case quenching is caused by photoinduced electron transfer (PET) to the C=C double bond. Therefore emission can again be returned upon Michael addition of a thiol which gives a saturated thio-ether product.[28, 29] Interestingly, it has very recently been reported by the Baker and Caddick group that monothio- and monobromo-maleimides also act as emission quenchers,[30] when attached to a dansyl group by a non-conjugated linker to the maleimide N (**3N**, Figure 3.5). Upon addition of a thiol (one or two equivalents respectively for monothio- and monobromo-maleimide) a dithiosuccinimide is formed, with loss of the C=C double bond leading to loss of quenching and therefore emission.

Conversely, it is possible to produce fluorophores with the maleimide group incorporated, by direct conjugation to the maleimide C=C double bond. Although these fluorophores are not routinely used as fluorescent probes, their emission spans almost the entire visible spectrum. As many of the emissive maleimide derivatives form amorphous glass they have found applications in light-emitting diode devices.[31, 32]

The synthesis of 2-aryl and 2,3-diarylmaleimides (Ar = phenyl, napthyl, pyridyl, thienyl, indolyl, or naphthylphenylamino, for example **3O** in Figure 3.6) produces fluorophores with quantum yields of up to 1.00, emission maximum ranging from 460-680 nm, and often large Stokes shifts (>100 nm).[31-35]

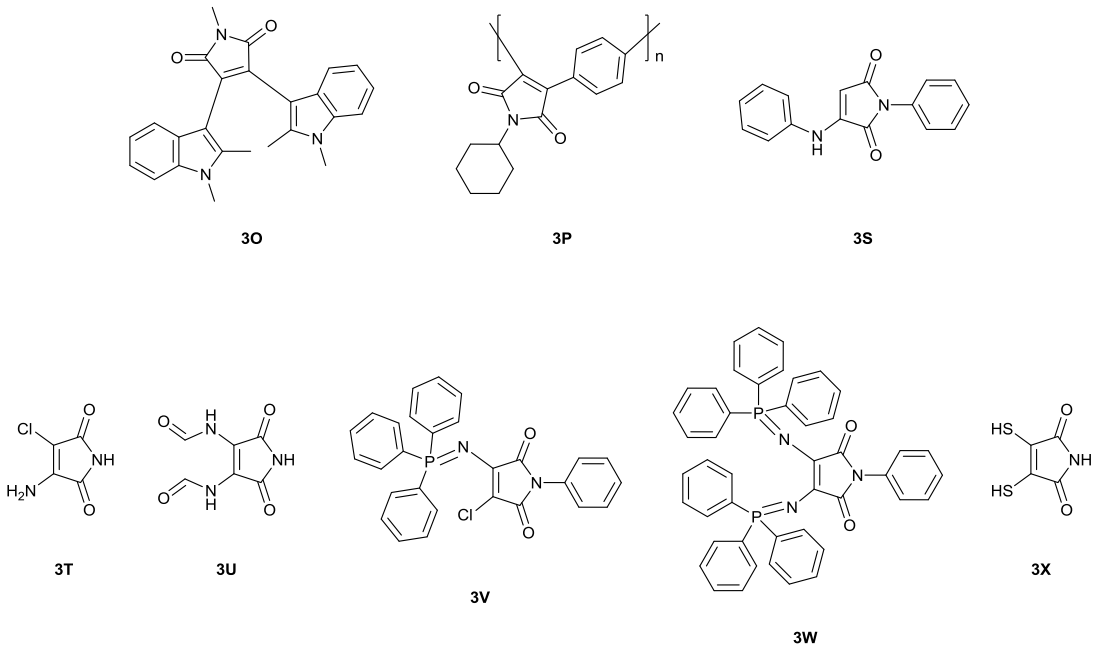

Figure 3.6. Fluorophores with the maleimide group directly incorporated into their structure.

The use of bifunctional aryl groups (1,4-phenyl or 2,5-thienyl) also allowed the synthesis of alternating and random conjugated copolymers, which had $\lambda_{max,em}$ = 520-550 nm (**3P** in Figure 3.6).[35] Substituting one maleimide H with Br, and the other with an indolyl group also yields a weakly emissive fluorophore (**3Q**, Scheme 3.1), with $Q \leq 0.02$ and $\lambda_{max,em}$ = 530-560 nm. However, upon coordination to a Lewis-acidic Zn complex this bromoindoylmaleimide sees an 80-fold increase in emissivity (**3R**, Scheme 3.1).[36]

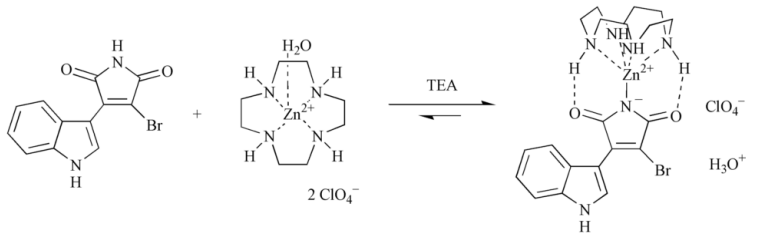

3Q **3R**

Scheme 3.1. Weakly emissive bromoindoylmaleimide **3Q**, and its reversible coordination to a Lewis-acidic Zn complex to form the 80-fold more emissive **3R**. Figure adapted from ref.[36]

There have also been a few reports of emissive maleimides with heteroatom conjugation. Kato and Naka recently reported that arylaminomaleimides (**3S** in Figure 3.6) are emissive, having $\lambda_{max,em}$ = 490-520 nm, with Stokes shifts of over 100 nm.[37] These compounds were found to have aggregation-induced emission, and also displayed pH-responsive fluorescence. Marzolph, Scharf and co-workers demonstrated that chloroamino- and diaminomaleimides (**3T** and **3U** in Figure 3.6) were emissive,[38] while Watson *et al.* reported the crystal structures of three other heteroatom substituted maleimides (**3V**, **3W** and **3X** in Figure 3.6), noting that they "fluoresce strongly".[39] Besides these few reports, very little attention has been paid to these classes of fluorescent maleimide derivatives. The only other example found in the literature was a patent that demonstrated the use of dichloro- and dibromomaleimide as stains which become fluorescent in the presence of amines and thiols. Reaction products were not characterised, but the author did speculate that nucleophilic attack by amino or thiol groups caused elimination of the halogen.[40]

3.3. Results and Discussion

3.3.1. Dithiomaleimide fluorescence

As discussed in Chapter 2, the reaction of 2,3-DBM with 2 equivalents of a thiol in the presence of a base gives a dithiomaleimide (DTM) product.[41] To verify this fact 2,3-DBM was reacted with *n*-butanethiol in diethyl ether, with triethylamine as the base catalyst (**3i** Scheme 3.2).

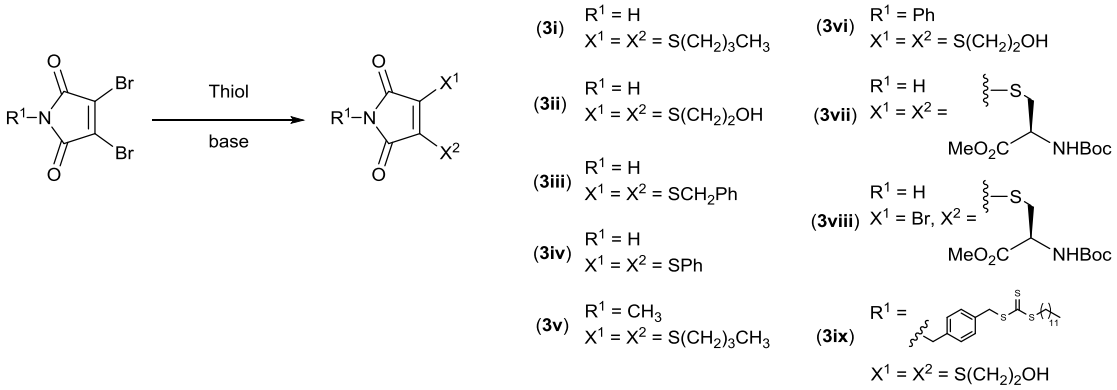

Scheme 3.2. Synthesis of thiomaleimides *via* the addition/elimination reaction of 2,3-DBM with thiols

The product was purified by flash column chromatography and characterised by ^{1}H and ^{13}C NMR spectroscopy (Figure 3.7), and high resolution mass spectroscopy.

It was observed that, when placed under the hand-held long wave UV lamp (365 nm) both the neat product (an oil) as well as solutions of **3i** were emissive. Although **3i** has been synthesised on one previous occasion, no mention of fluorescence was made.[42]

To fully characterise the emission a 2D excitation-emission spectrum of a solution of **3i** in $CHCl_3$ was performed (Figure 3.8). The spectrum shows that $\lambda_{max,em} = 520$ nm, with $\lambda_{max,ex} = 415$ nm, corresponding to a large Stokes shift of 105 nm. There is also a secondary excitation maximum centred at $\lambda_{ex} = 265$ nm, with Stokes shift 255 nm. HPLC with simultaneous absorption and emission detection confirmed that a single species was present, and that this species was the source of the fluorescence (Figure 3.9).

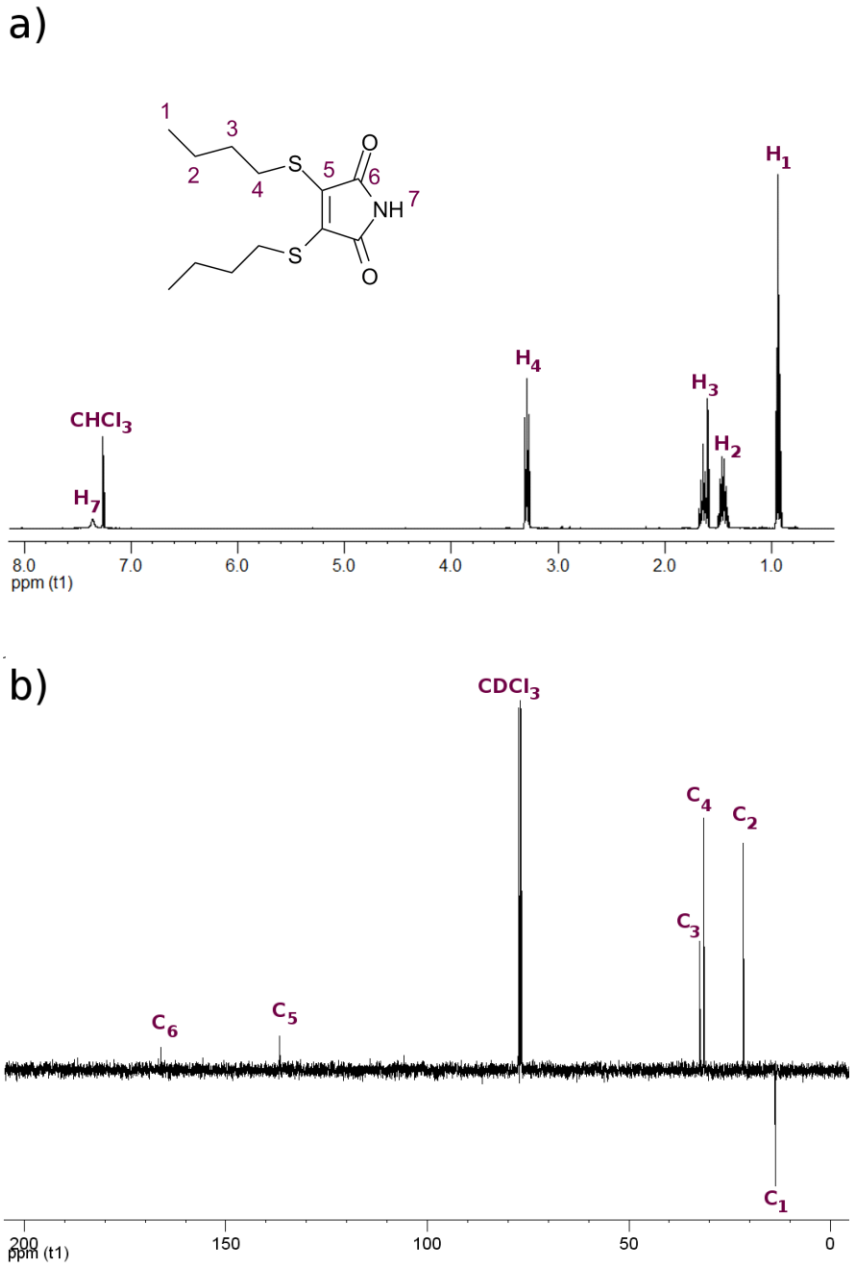

Figure 3.7 a) ^{1}H NMR (400 MHz, $CDCl_3$) spectrum and b) ^{13}C NMR (100 MHz, $CDCl_3$) spectrum for **3i**.

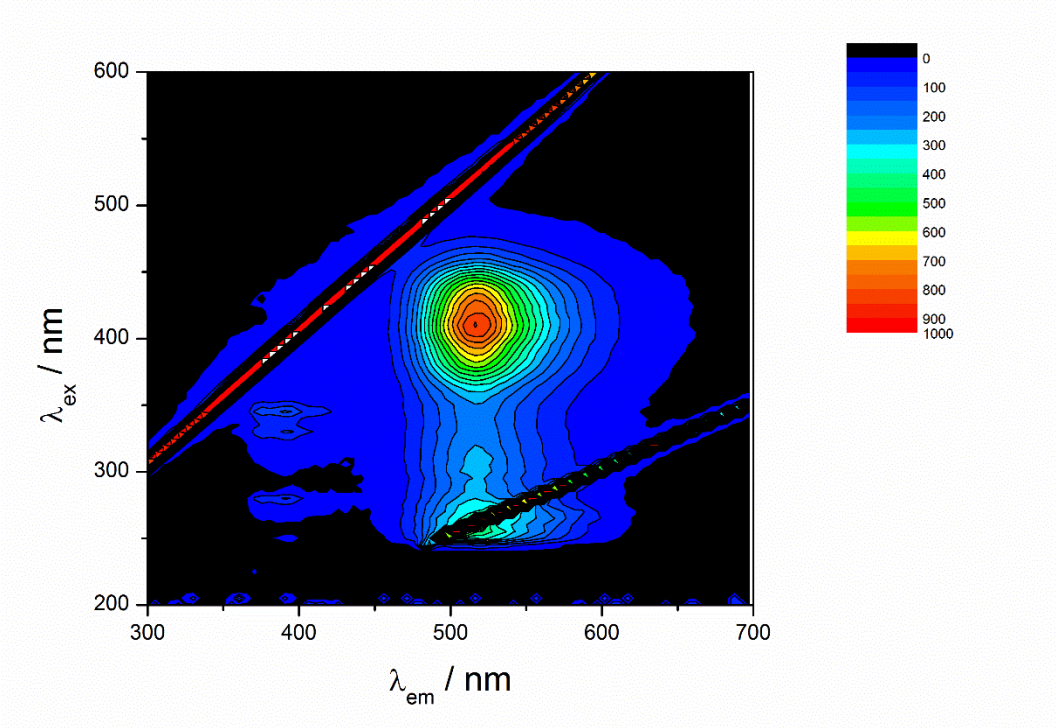

Figure 3.8. 2D excitation-emission spectrum of **3i** ($CHCl_3$ solution), with 5 nm step size

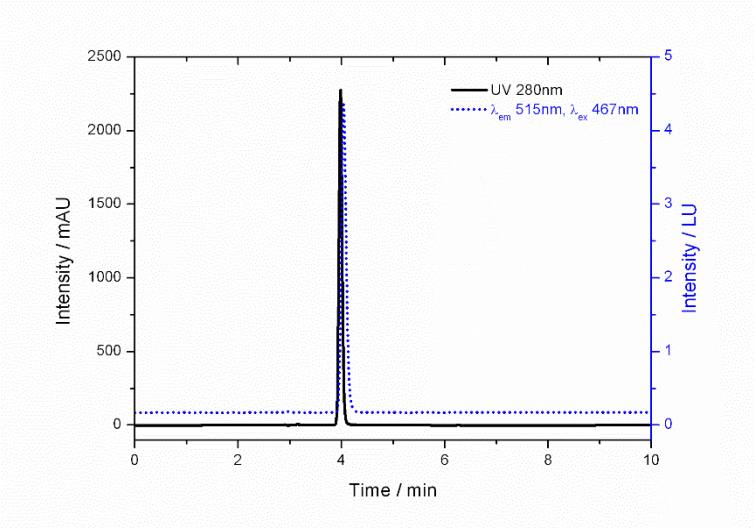

Figure 3.9. HPLC chromatogram of **3i** with simultaneous UV (λ_{abs} = 280 nm) and fluorescence (λ_{ex} = 467 nm, λ_{em} = 515 nm) detection.

In order to explore the potential use of DTMs as fluorescent probes, a range of DTMs with varying substituents at the N and S positions were explored (Scheme 3.2). The S substituent was simply altered according to the choice of thiol in the addition-elimination reaction with 2,3-DBM. The mercaptoethanol derivative (**3ii**), and the benzyl mercaptan derivative (**3iii**) showed excitation and emission spectra that were very similar to those of **3i** (Figure 3.10 and Table 3.1).

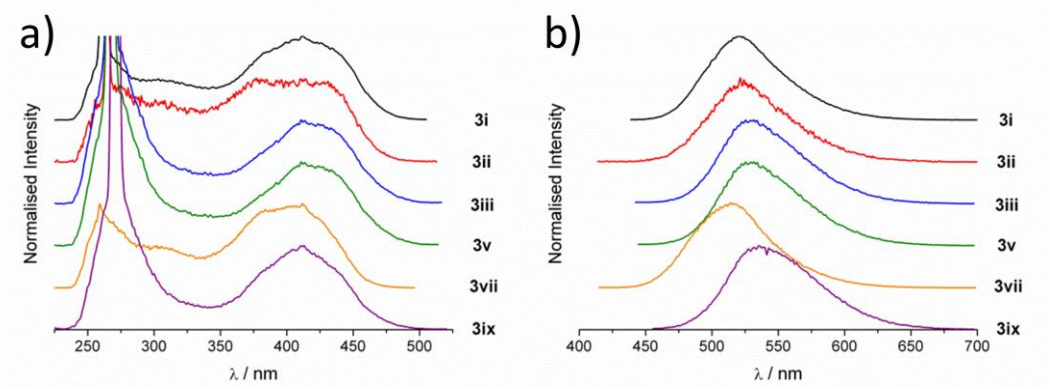

Figure 3.10 a) Excitation and b) Emission spectra of DTMs **3i-3iii**, **3v**, **3vii** and **3ix** as solutions in $CHCl_3$. Excitation and emission were measured at $\lambda_{em,max}$ and $\lambda_{ex,max}$ respectively (given in Table 3.1).

Table 3.1. Excitation and emission maxima (in $CHCl_3$) for the series of thiomaleimides **3i-3ix**.

	$\lambda_{ex,max}$ **(nm)**	$\lambda_{em,max}$ **(nm)**
3i	415	520
3ii	400	525
3iii	410	520
3iv	-	-
3v	415	530
3vi	-	-
3vii	405	515
3viii	360	465
3ix	412	538

It is significant to note that varying the thiol substituent also allowed the solubility of the DTM to be altered drastically; while **3i** and **3iii** are soluble in most organic solvents (including hexane), **3ii** is water-soluble, with solution state fluorescence retained in all solvents tested. Reaction of 2,3-DBM with thiophenol gave a DTM with Ph directly conjugated to the maleimide π-system (**3iv**), which was found to have drastically reduced emission (*vide infra*).

The N substituent of DTMs can also be varied. The simplest way to achieve this was to perform the addition-elimination reaction with commercially available 2,3-dibromo-*N*-methylmaleimide (DBMM). The reaction between DBMM and *n*-butanethiol gives DTM

3v, which again gives a fluorescent product with similar spectral characteristics to compounds **3i-3iii**. There are several reactions by which *N*-functionalisation of DTMs can be achieved. Dibromomaleimides can undergo alkylation with alkyl bromides and chlorides,[43, 44] and react with primary alcohols under Mitsunobu conditions.[43, 45] Functionalisation with primary amines is also possible, either by reaction with dibromomaleic anhydride,[41, 46] or under the recently developed milder conditions using an 'activated' *N*-methoxycarbonyl bromomaleimide.[47] *N*-phenyl DBM was synthesised by reaction of aniline and dibromomaleic anhydride according to Burke *et al.*,[48] and addition-elimination with mercaptoethanol gave the corresponding DTM **3vi**. Direct conjugation of a phenyl group to the maleimide π-system again lead to a drastic reduction in emission as had been seen with **3iv** (Figure 3.11).

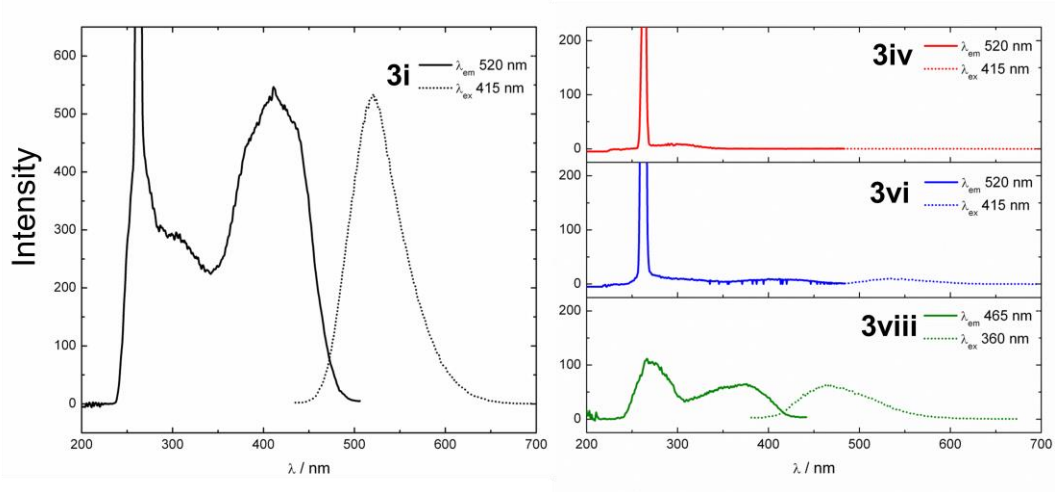

Figure 3.11. Excitation and emission spectra of 0.1 mM solutions in $CHCl_3$ for **3i**, **3iv**, **3vi** and **3viii**.

It appears that the lone pairs on the N and S atoms must be available to contribute to the resonance structure of the DTM ring, in order for significant emission to occur.

DBM has previously been shown to be able to bridge the disulfide bonds of the proteins salmon calcitonin (sCT) and somatostatin,[41, 43] with the resultant product bearing the DTM motif. It seemed that the fluorescent nature of these products may have been overlooked, so as a test reaction the addition-elimination of 2,3-DBM was performed with a protected cysteine *N*-Boc-Cys-OMe. The resultant product **3vii** had the expected excitation and emission for a DTM (Figure 3.10 and Table 3.1), suggesting that it was likely that the DTM-bridged proteins would also be fluorescent. Formation of a

thiobromomaleimide by addition of a single thiol was also investigated. By using an excess of DBM, a single equivalent of *N*-Boc-Cys-OMe was added to give **3viii**. This product was emissive, but with significantly reduced intensity when compared to the DTMs synthesised. A shift in $\lambda_{max,ex}$ and $\lambda_{max,em}$ was also observed, with values of 360 nm and 465 nm respectively (Figure 3.11 and Table 3.1). This result suggests that a conjugate of DBM with a protein *via* a single cysteine residue would also be fluorescent.

The fluorescence of protein conjugates containing a DTM bridged disulfide was subsequently established by collaborators working in the Haddleton group at University of Warwick. Native sCT was reduced using TCEP before addition of DBM, with HPLC using UV-vis and fluorescence detectors confirming the formation of a fluorescent conjugate (Figure 3.12).[iii]

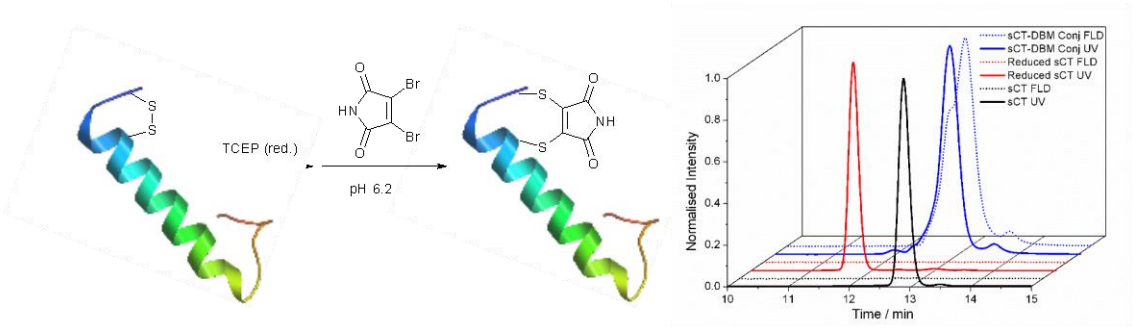

Figure 3.12. Scheme for the synthesis of sCT-DBM conjugates (left). HPLC analysis of the reaction with simultaneous UV (λ_{abs} = 280 nm) and fluorescence (λ_{ex} = 341 nm, λ_{ex} = 502 nm) detection.[49]

3.3.2. DTM labelling of polymers – Fluorescent initiator

Having established the emissive nature of small molecule DTMs, and those incorporated into proteins as disulfide bridges, it was decided to explore the utility of the DTM group for the fluorescent labelling of polymers. In Chapter 2 it was shown that the DBM group can be incorporated into a RAFT agent (**2i**), and that this CTA can be used to control the polymerisation of acrylates, giving polymers with DBM groups at their α-chain end. Therefore adopting a similar strategy with a DTM-functional CTA would allow site-specific fluorescent labelling of RAFT polymers at the α-chain end.

[iii] All experiments and analysis carried out by Paul Wilson (University of Warwick).

Reaction of **2i** with mercaptoethanol in the presence of a base resulted in the formation of the DTM-functional RAFT agent **3ix**, according to Scheme 3.2. High resolution mass spectrometry, ^{1}H and ^{13}C NMR spectroscopy (Figure 3.13) confirmed the desired structure had been obtained.

This reaction provided a simple route to a DTM-functional RAFT agent, as the precursor **2i** had already been synthesised. This approach also had the advantage that it results in an R-group labelled CTA, which is preferable to a Z-group labelled CTA, as previously discussed in Chapter 2. The fluorescence spectrum of a solution of **3ix** in chloroform was very similar to the previous DTM fluorophores, indicating that incorporation into a RAFT agent did not affect the spectral characteristics (Figure 3.10 and Table 3.1).

Haddleton *et al.* had previously shown that while the DBM group in an ATRP initiator caused retardation of the ATRP of PEG-methacrylate, when it was replaced with a DTM group the polymerisation proceeded to high conversion.[50] It was therefore anticipated that the DTM CTA **3ix** might cause less retardation of RAFT polymerisation than the DBM CTA **2i**, so that as well as acrylates, it might also be possible to polymerise styrene and NIPAM with **3ix**.

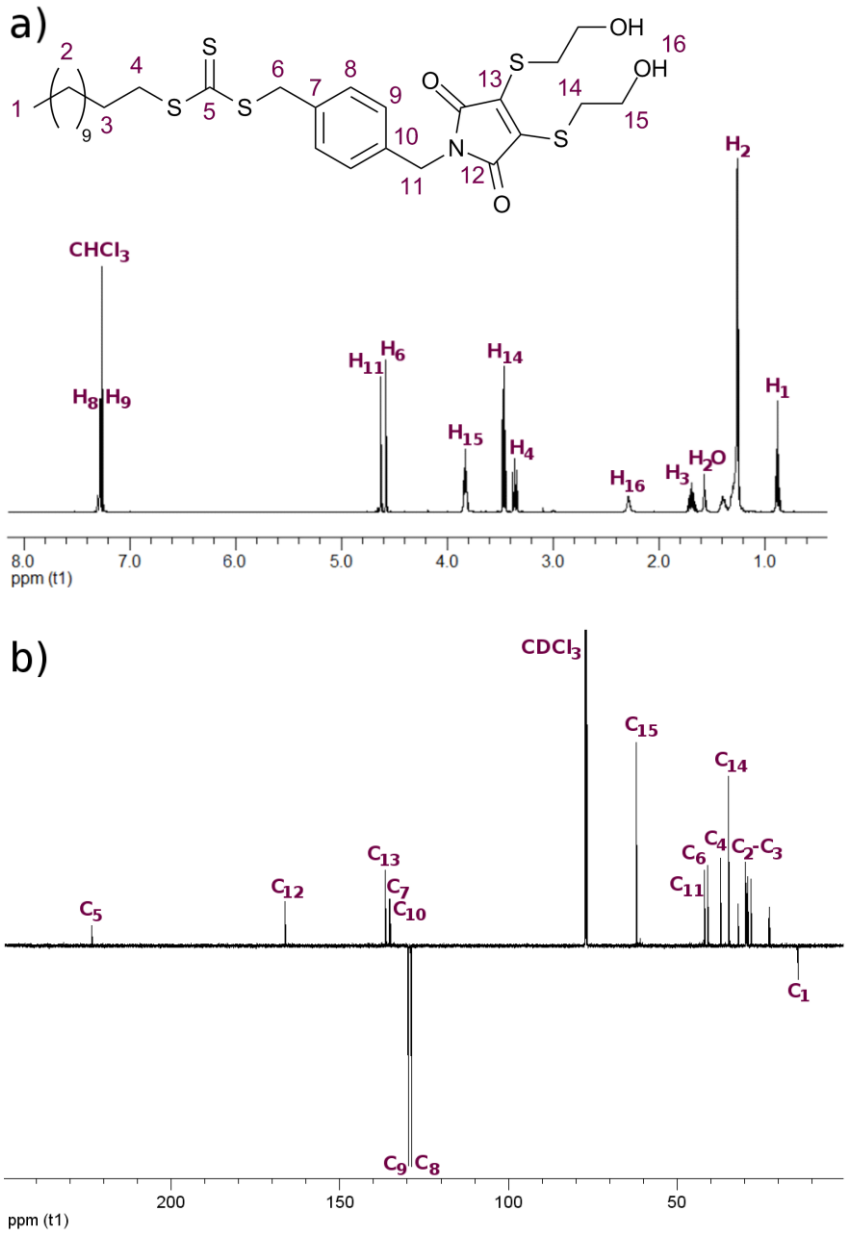

Figure 3.13 a) ^{1}H NMR (400 MHz, $CDCl_3$) spectrum and b) ^{13}C NMR (176 MHz, $CDCl_3$) spectrum for **3ix**.

The initial polymerisation of ^{t}BA in dioxane solution with AIBN as radical initiator at 65 °C (**3x**, Scheme 3.3 and Table 3.2) gave good control over molecular weight ($Đ_M$ = 1.11, Figure 3.14).

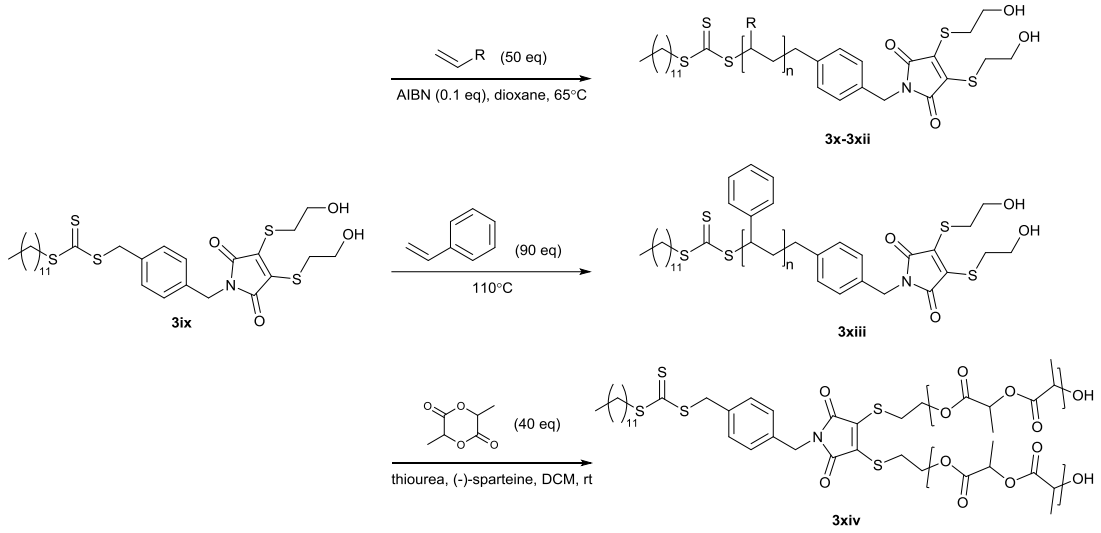

Scheme 3.3. RAFT polymerisations with **3ix** as CTA (top and middle), and ROP with **3ix** as bifunctional initiator (bottom).

Table 3.2. Fluorescent polymers synthesized by RAFT and ROP using **3ix**.

	Polymer	M_n [a] (kg·mol^{-1})	M_n [b] (kg·mol^{-1})	$Đ_M$ [b]	$\lambda_{ex,max}$ [c] (nm)	$\lambda_{em,max}$ [c] (nm)
3x	P^{t}BA	7.0	6.7	1.11	412	535
3xi	PTEGA	5.7	3.9	1.20	412	535
3xii	PNIPAM	2.7	3.3	1.16	412	530
3xiii	PSty	5.1	4.9	1.39	382	520
3xiv	P(D,L-LA)	6.7	9.8	1.09	410	520

[a] Calculated by ^{1}H NMR spectroscopy end-group analysis. [b] Measured by SEC. [c] Measured as a solution in $CHCl_3$.

The presence of both the DTM group at the α-chain end, and trithiocarbonate group at the ω-chain end was observed by ^{1}H NMR spectroscopy. Resonances for the SC$\underline{H}_2$ protons of both groups were clearly visible at 3.33 and 3.44 ppm respectively (H4 and H12, Figure 3.15).

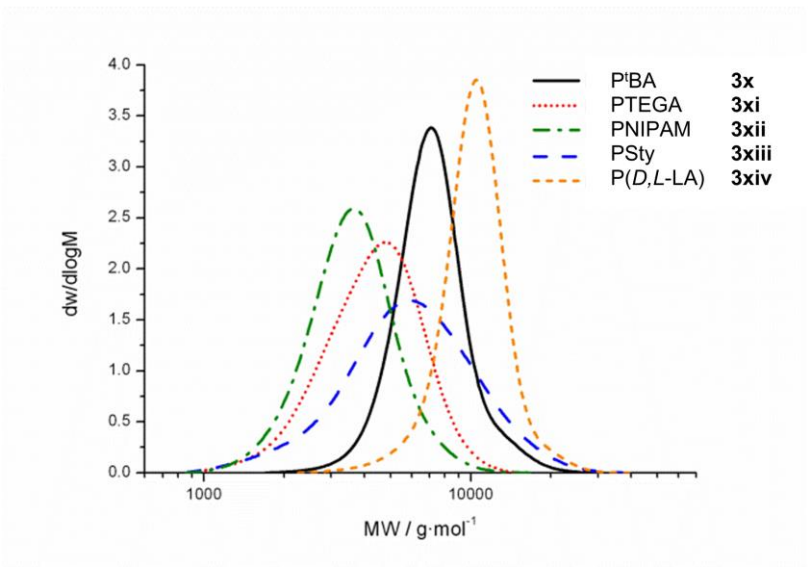

Figure 3.14. *MW* distributions for polymers **3x-3xiv** obtained by SEC.

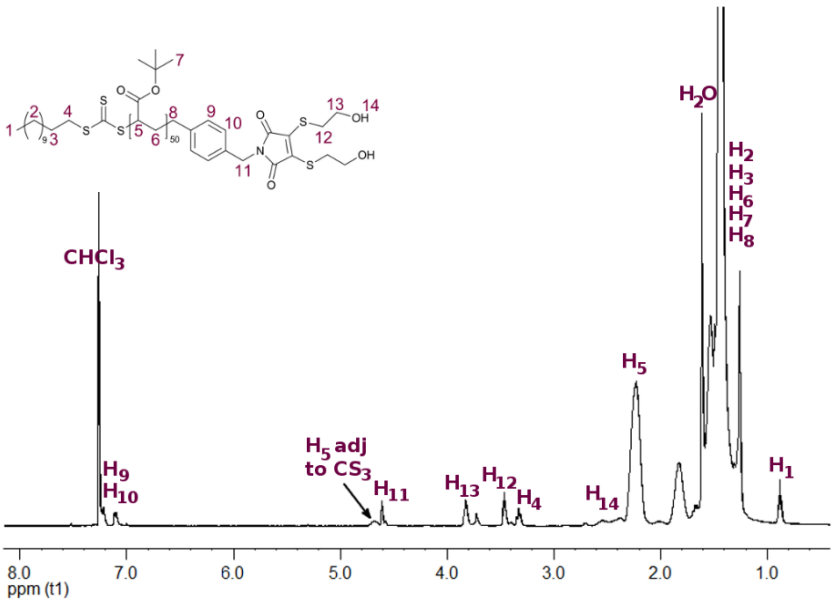

Figure 3.15. ^{1}H NMR (400 MHz, $CDCl_3$) spectrum for **3x**.

The 3D SEC spectrum of **3x** collected using a PDA detector showed that the polymer peak had a $\lambda_{max,abs} = 309$ nm corresponding to the trithiocarbonate group, with a secondary $\lambda_{max,abs} = 407$ nm corresponding to the DTM group (Figure 3.16).

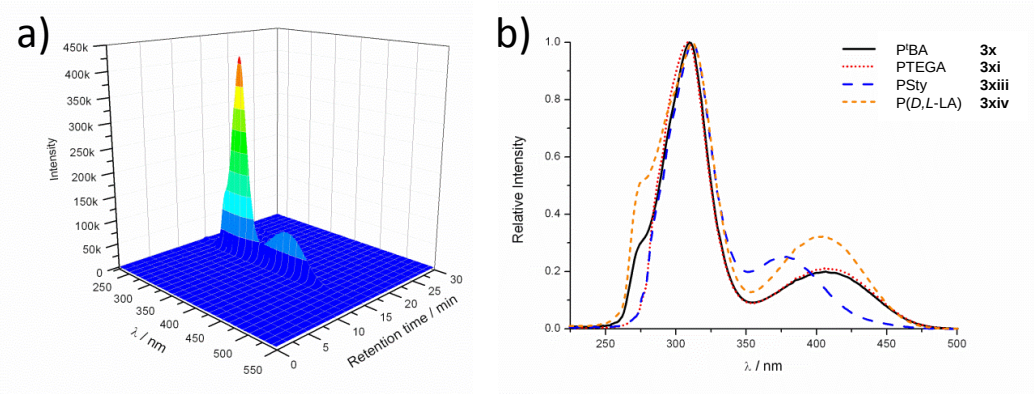

Figure 3.16 a) Three dimensional SEC chromatogram for P^{t}BA (**3x**), obtained using a PDA detector, eluting with THF. b) UV-vis spectra for polymer peaks of **3x**, **3xi**, **3xiii** and **3xiv** obtained using an SEC coupled to a PDA detector eluting with THF.

Steady state fluorescence spectroscopy indicated that **3x** was highly fluorescent, with the expected spectra (Figure 3.17) and corresponding λ_{max} for excitation and emission (Table 3.2) for a DTM fluorophore.

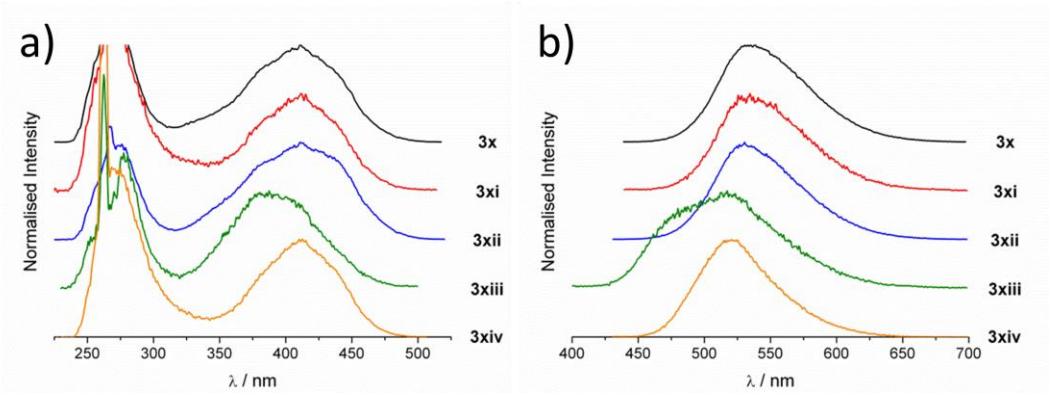

Figure 3.17 a) Excitation and b) Emission spectra of DTM-labelled polymers **3x-3xiv** as solutions in $CHCl_3$. Excitation and emission were measured at $\lambda_{em,max}$ and $\lambda_{ex,max}$ respectively (given in Table 3.2).

Integrated emission was higher for the DTM-containing polymer, compared to the small molecule dyes, which was attributed to two effects related to the local environment of the fluorophore. In the end-group labelled polymers, the ability of the DTM to form self-quenching dimers or higher aggregates is reduced due to the shielding from the polymer chain. This shielding also reduces both the frequency and amplitude of collision events with solvent molecules, which also act to decrease emission by providing a pathway for non-radiative decay of the excited state.[1]

Polymerisation of TEGA was achieved under the same conditions as ^{t}BA (Scheme 3.3), to give a water-soluble fluorescently-labelled PTEGA (**3xi**, Table 3.2). Good control over molecular weight was observed ($Đ_M$ = 1.20, Figure 3.14), and the presence of the DTM was again shown by ^{1}H NMR spectroscopy (for example H17 at 3.8 ppm, Figure 3.18) and SEC with PDA detection (polymer absorbance at *ca.* 400 nm, Figure 3.16 b).

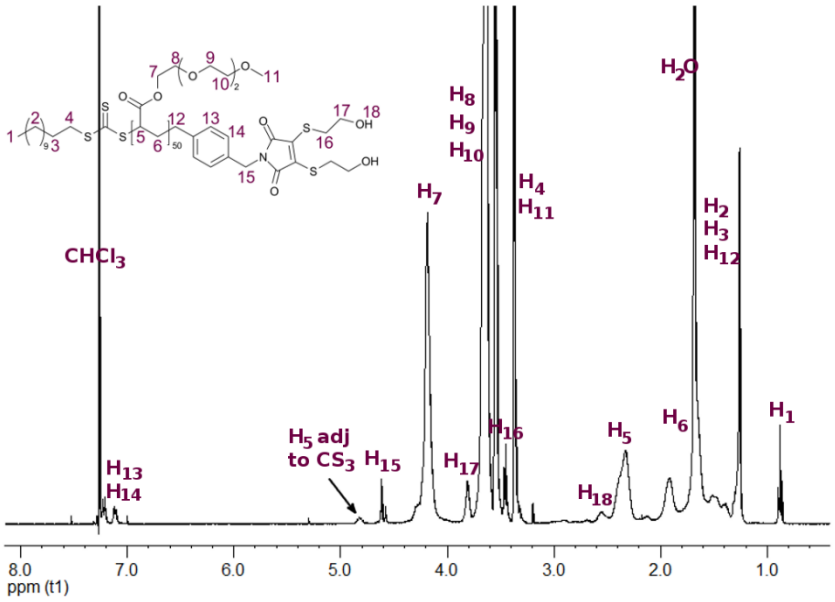

Figure 3.18. ^{1}H NMR (400 MHz, $CDCl_3$) spectrum for **3xi**.

In addition, MALDI-TOF mass spectroscopy confirmed the presence of the desired DTM end-groups, with high end-group fidelity indicated by lack of significant additional mass distributions (Figure 3.19).

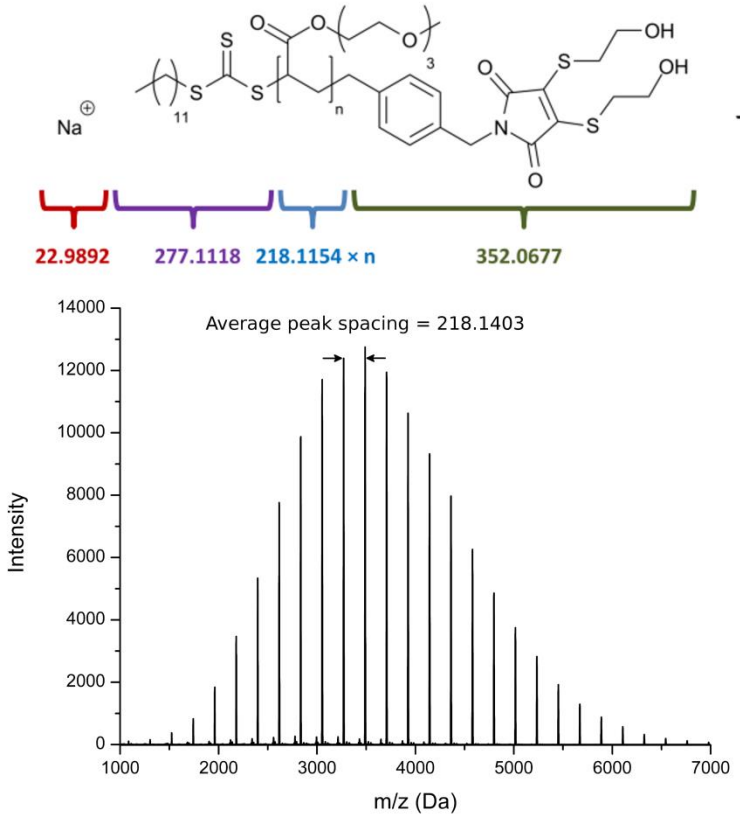

DP	$[M + Na]^+$	Found
1	870.2848	870.1041
2	1088.4002	1088.2793
3	1306.5156	1306.4370
4	1524.6310	1524.5777
5	1742.7464	1742.7113
6	1960.8619	1960.8364
7	2178.9773	2178.9535
8	2397.0927	2397.0656
9	2615.2081	2615.1792
10	2833.3236	2833.2915
11	3051.4390	3051.4084
12	3269.5544	3269.5281
13	3487.6698	3487.6510
14	3705.7853	3705.7815
15	3923.9007	3923.9120
16	4142.0161	4142.0557
17	4360.1315	4360.2045
18	4578.2470	4578.3551
19	4796.3624	4796.5306
20	5014.4778	5014.6839
21	5232.5932	5232.8964
22	5450.7087	5451.0510

Figure 3.19. MALDI-TOF mass spectra of **3xi** collected in linear mode, with high resolution masses obtained in reflector mode. Average difference between calculated and found $m/z = 0.0257$ Da.

Polymerisation of NIPAM with the DTM CTA **3ix** was attempted using the same polymerisation conditions (Scheme 3.3). Whereas the DBM CTA **2i** resulted in 1% conversion under these same conditions, the polymerisation of NIPAM mediated by **3ix** reached 28% conversion after 16 h. This is still much lower than $p > 99\%$ obtained with the alcohol-functional CTA **2iii**, but nonetheless indicates that retardation of polymerisation is not as significant for **3ix** when compared with **2i**. The resultant PNIPAM (**3xii**) had a narrow molecular weight distribution ($Đ_M = 1.16$, Table 3.2, Figure 3.14). End-groups corresponding to both trithiocarbonate and DTM chain ends were observed in the ^{1}H NMR spectrum (for example H4 and H14 at 3.33 ppm and 3.47 ppm respectively, Figure 3.20).

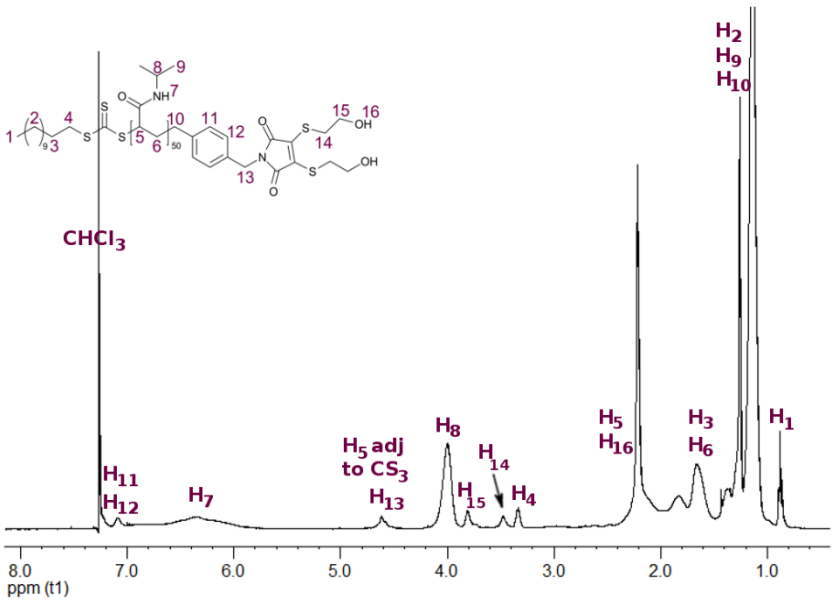

Figure 3.20. ^{1}H NMR (400 MHz, $CDCl_3$) spectrum for **3xii**.

Although **3xii** was not compatible with the THF SEC system connected to the PDA detector, analysis by DMF SEC with simultaneous detection by DRI and UV absorption (309 nm and 400 nm) indicated that the trithiocarbonate and DTM groups remained attached to the polymer (Figure 3.21).

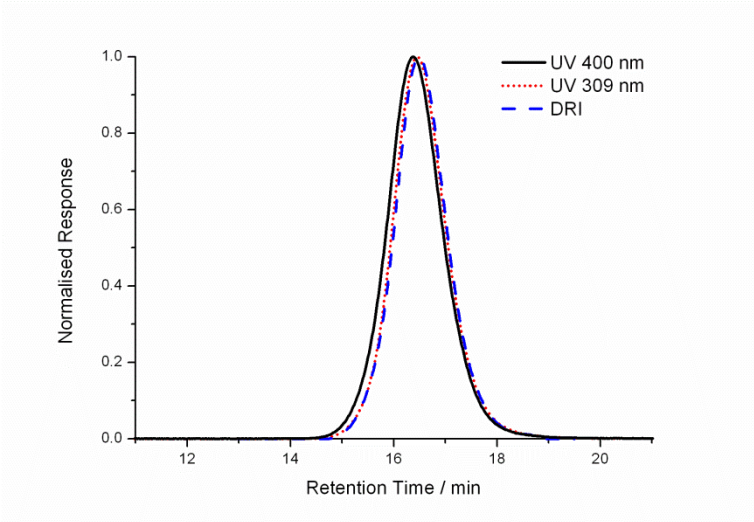

Figure 3.21. SEC chromatograms obtained for **3xii** using a UV detector set to 400 nm and 309 nm, and a DRI detector, eluting with DMF.

MALDI-TOF MS provided further confirmation of the presence of the end-groups resulting from **3ix**, with excellent agreement between predicted and measured masses (Figure 3.22).

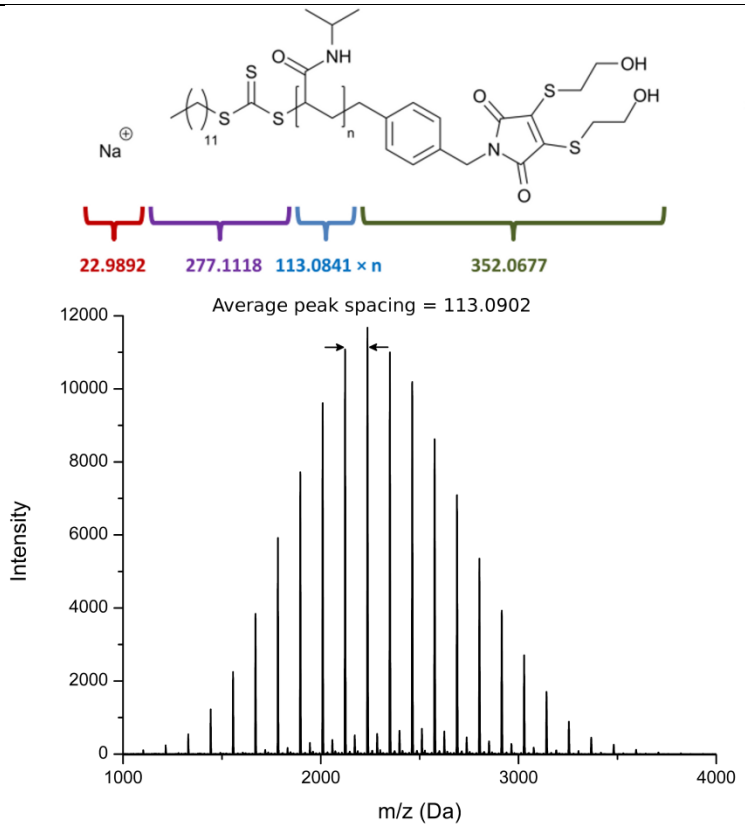

DP	$[M + Na]^+$	Found
3	991.4210	991.2912
4	1104.5050	1104.4012
5	1217.5891	1217.5083
6	1330.6732	1330.6130
7	1443.7572	1443.7126
8	1556.8413	1556.8090
9	1669.9254	1669.9023
10	1783.0094	1782.9932
11	1896.0935	1896.0819
12	2009.1776	2009.1704
13	2122.2616	2122.2564
14	2235.3457	2235.3419
15	2348.4297	2348.4261
16	2461.5138	2461.5099
17	2574.5979	2574.5961
18	2687.6819	2687.6797
19	2800.7660	2800.7648
20	2913.8501	2913.8452
21	3026.9341	3026.9355
22	3140.0182	3140.0191
23	3253.1023	3253.1062
24	3366.1863	3366.1884
25	3479.2704	3479.2740
26	3592.3544	3592.3648

Figure 3.22. MALDI-TOF mass spectra of **3xii** collected in linear mode, with high resolution masses obtained in reflector mode. Average difference between calculated and found $m/z = 0.0214$ Da.

Polymerisation of styrene with CTA **3ix** was also possible, with the reaction of 90 *eq.* Sty under thermal initiation conditions (Scheme 3.3) proceeding to $p = 55\%$ after 16 h (c.f. $p = 64\%$ with CTA **2iii**). Reasonable control over molecular weight was seen ($Đ_M = 1.39$, Figure 3.14), with trithiocarbonate and DTM end-groups identified by ^{1}H NMR spectroscopy (H4, H12, H13, Figure 3.23) and SEC (polymer absorbance at *ca.* 310 and 400 nm, Figure 3.16).

As with P^{t}BA (**3x**), fluorescence spectroscopy of PTEGA (**3xi**), PNIPAM (**3xii**), and PSty (**3xiii**) all showed the expected emission for a DTM-containing species (Figure 3.17 and Table 3.2).

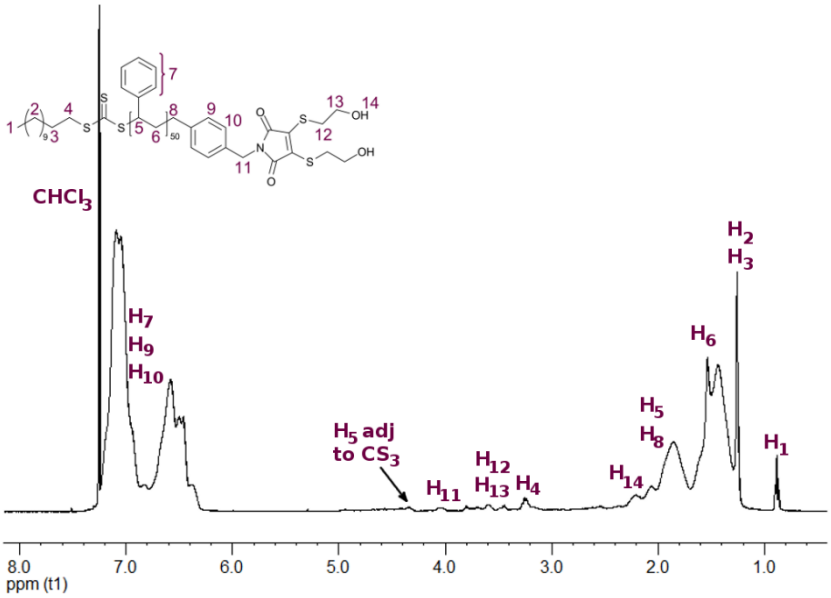

Figure 3.23. ^{1}H NMR spectrum (400 MHz, $CDCl_3$) for **3xiii**.

Because mercaptoethanol was chosen for the synthesis of the DTM group, CTA (**3ix**) contains two hydroxyl groups which can be used as initiating sites for organocatalytic ring-opening polymerisation of lactide (Scheme 3.3).[51] This would allow for site specific labelling of poly(lactide) at the middle of the block, assuming that initiation and polymerisation from both hydroxyl groups was equally as efficient. Using the thiourea/(-)-sparteine co-catalyst system of Hedrick *et al.* (Scheme 3.3),[52] poly(D,L-lactide) (**3xiv**) was synthesised with good control over molecular weight ($Đ_M = 1.09$, Figure 3.14).[iv] No adverse effects on the reaction were observed, with $p > 99\%$ obtained within 2 h. The polymer was purified by precipitation and prep. SEC (Bio-Beads) to remove the organocatalysts, with ^{1}H NMR spectroscopy (Figure 3.24) and MALDI-TOF MS of the product showing excellent end-group fidelity and very low levels of transesterification (Figure 3.25).

[iv] Poly(D,L-lactide) (**3xiv**) was synthesised by Anne Mabire (University of Warwick).

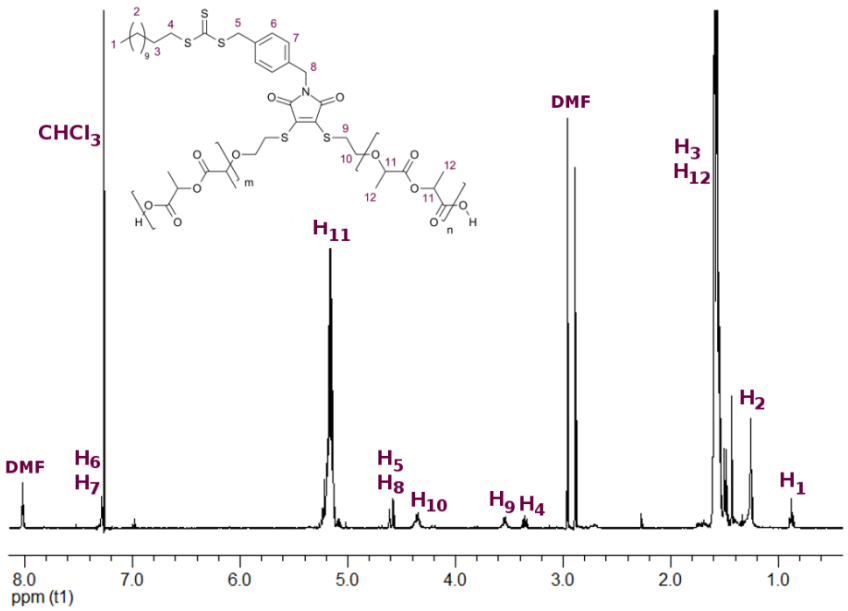

Figure 3.24. ^{1}H NMR (400 MHz, $CDCl_3$) spectrum for **3xiv**.

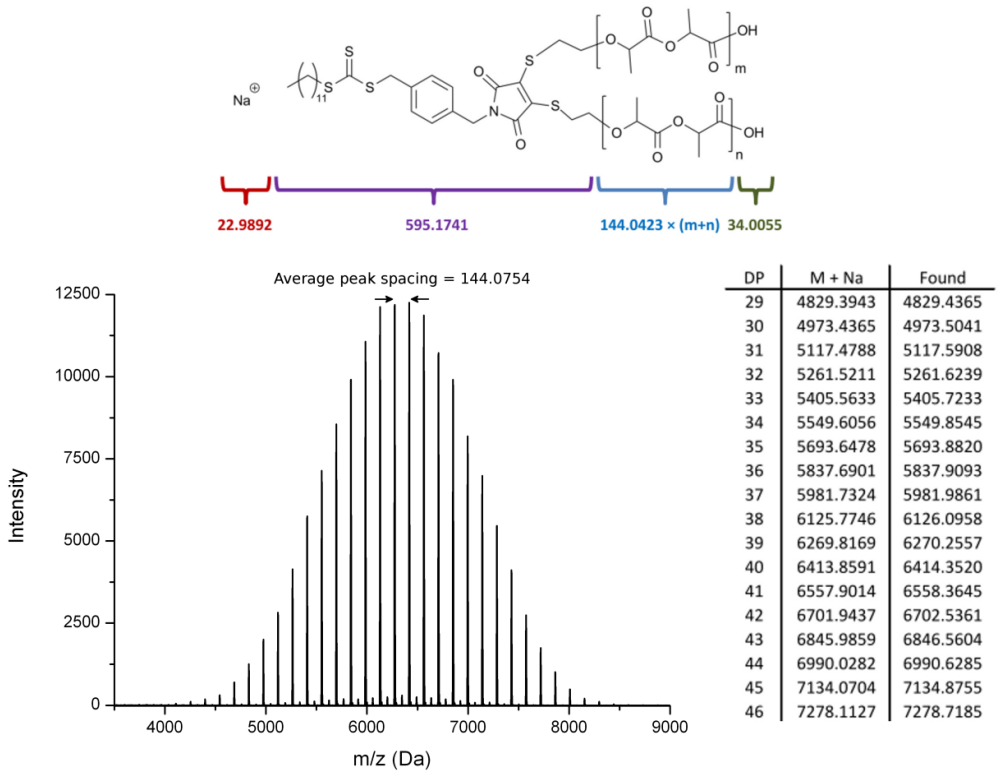

DP	M + Na	Found
29	4829.3943	4829.4365
30	4973.4365	4973.5041
31	5117.4788	5117.5908
32	5261.5211	5261.6239
33	5405.5633	5405.7233
34	5549.6056	5549.8545
35	5693.6478	5693.8820
36	5837.6901	5837.9093
37	5981.7324	5981.9861
38	6125.7746	6126.0958
39	6269.8169	6270.2557
40	6413.8591	6414.3520
41	6557.9014	6558.3645
42	6701.9437	6702.5361
43	6845.9859	6846.5604
44	6990.0282	6990.6285
45	7134.0704	7134.8755
46	7278.1127	7278.7185

Figure 3.25. MALDI-TOF mass spectra of **3xiv** collected in linear mode, with high resolution masses obtained in reflector mode. Average difference between calculated and found $m/z = 0.3519$ Da.

3.3.3. DTM labelling of polymers – Post-polymerisation functionalisation

In addition to a pre-polymerisation strategy for fluorescent labelling of polymers with the DTM fluorophore, a post-polymerisation functionalisation strategy is also possible using

the chemistry developed in Chapter 2. Rather than performing the addition-elimination reaction of DBM and thiol with the RAFT agent/ROP initiator (**3ix**), this DTM-forming reaction could instead be conducted on DBM-terminated polymers. In Chapter 2 it was shown that DBM-terminated poly(acrylates) can be synthesised using the DBM-functional RAFT agent **2i**. A summary of these two approaches is shown in Scheme 3.4.

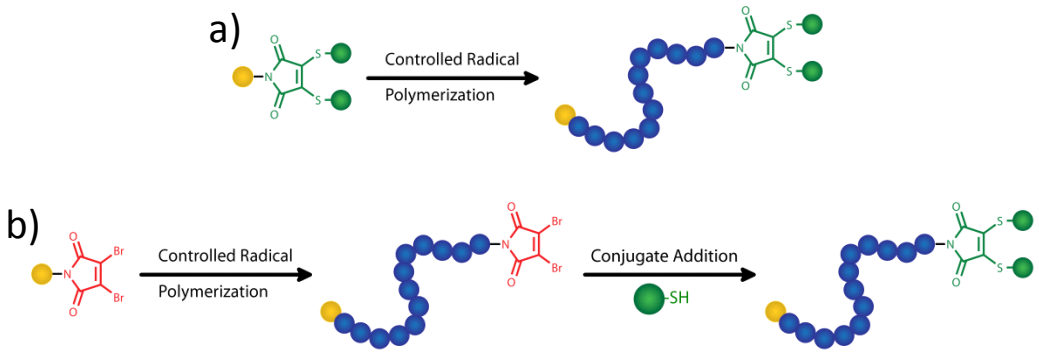

Scheme 3.4. The two routes to polymers labelled with the DTM fluorophore. a) Polymerisation with a fluorescent initiator. b) Post-polymerisation functionalisation reaction.

The reaction of 2,3-DBM and DBM-terminated poly(PEG methacrylate) with disulfide-bridge-containing proteins has been reported by the groups of Baker, Caddick and Haddleton.[41, 43] They performed the reactions in phosphate buffered saline (100 mM sodium phosphate, 150 mM NaCl) at pH 6.2-8, using DMF where required to solubilise 2,3-DBM. Therefore these conditions were chosen to investigate the reaction of DBM-terminated PTEGA (**2viii**) with the model thiol *N*-Boc-Cys-OMe (Scheme 3.5).

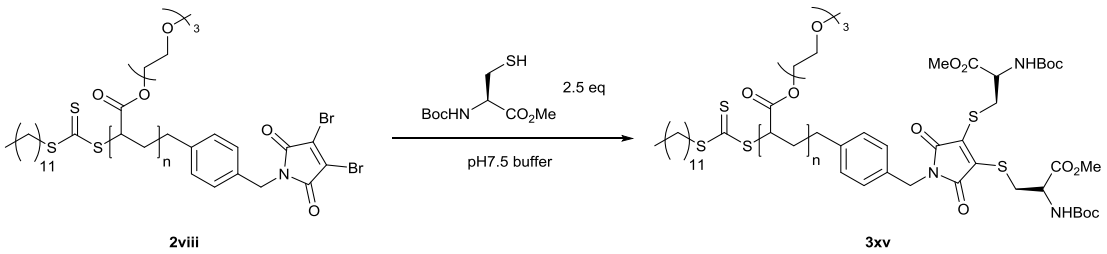

Scheme 3.5. Post-polymerisation end-group functionalisation of DBM-terminated PTEGA (**2viii**) with *N*-Boc-Cys-OMe

PTEGA was dissolved in buffer at 10 g/L, and a slight excess (2.5 *eq.*) of thiol was added as a solution in DMF (5% *v/v* w.r.t. buffer). An instant colour change was observed due to the formation of the DTM fluorophore. After 5 minutes a sample was withdrawn for analysis by MALDI-TOF MS (Figure 3.26).

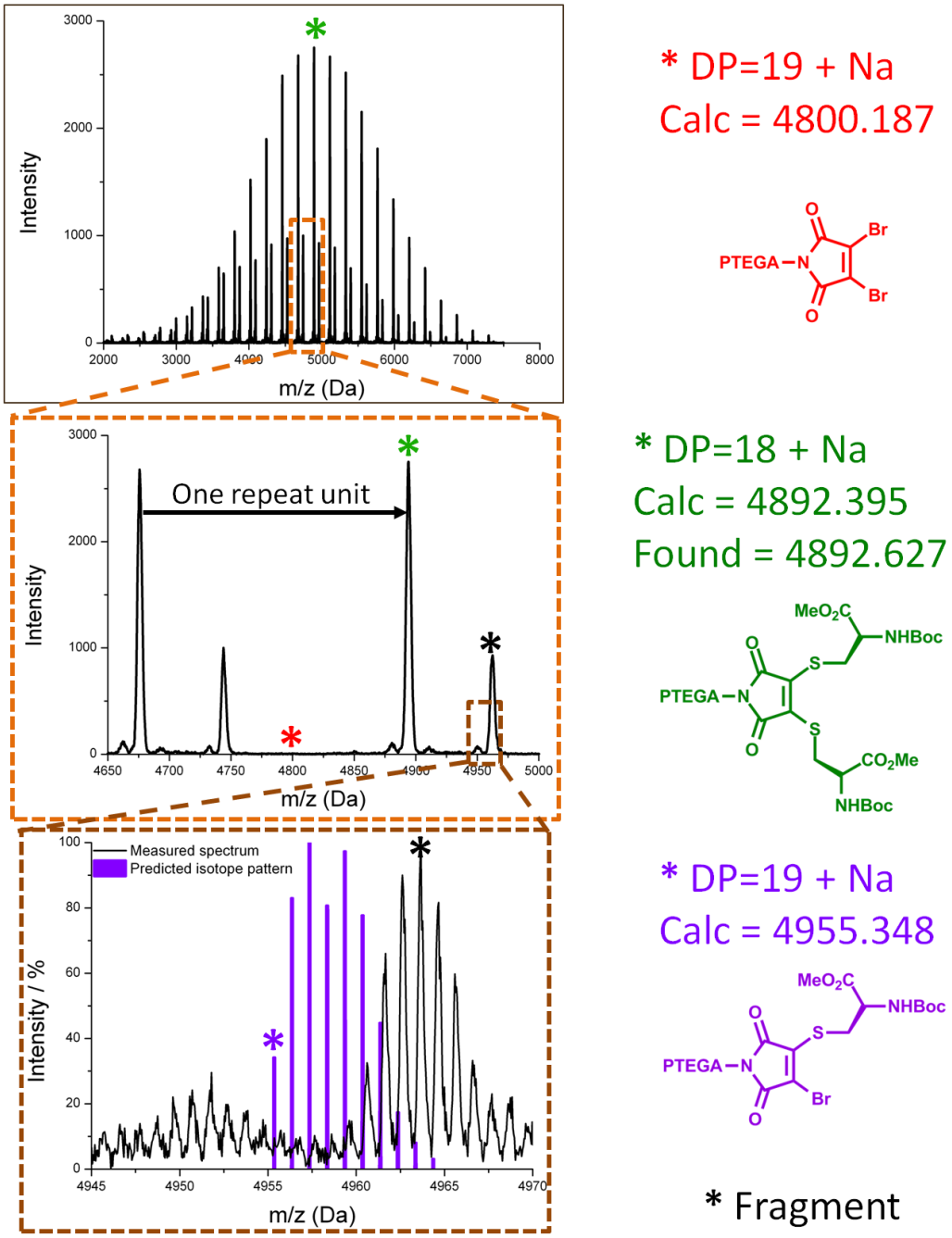

Figure 3.26. MALDI-TOF MS analysis of **3xv**. Top and middle spectra were collected in linear mode. Bottom spectrum and accurate masses obtained in reflector mode.

The major distribution corresponded to PTEGA with the DTM end-group. Complete consumption of the starting material **2viii** was also observed, with no peak corresponding to the mass of PTEGA with the DBM end-group. A second distribution of masses was observed, however this did not correspond to any assignable products. The intensity of

this peak was seen to increase with increasing laser power, and also to be increased in reflector mode, suggesting that it corresponded to a fragmentation reaction occurring during the MALDI-TOF experiment. This fragment had a mass close to that of the singly-substituted species, however careful inspection of the high resolution spectrum obtained in reflector mode showed that no singly-substituted product remained. Together this data indicates that complete conversion was reached within 5 minutes of the addition of *N*-Boc-Cys-OMe. The formation of a fluorescent product could be simply verified by viewing the reaction mixture under a long wave (365 nm) UV lamp (Figure 3.27).

An initial investigation of the end-group functionalisation reaction in organic solvent with the hydrophobic DBM-terminated PMA (**2vi**) was also conducted. Following conditions for the reaction of small molecule DBM with primary thiols in organic media,[48] thiol conjugation was attempted in THF, with imidazole as base (Scheme 3.6).

Reaction with 10 *eq.* of dodecanethiol in the presence of 10 *eq.* of imidazole (**3xvi**) at a polymer concentration of 10 g/L was observed to proceed much slower that the aqueous reaction with *N*-Boc-Cys-OMe (**3xv**). The reaction was monitored by removing samples for MALDI-TOF MS analysis, and after 1 hour consumption of the DBM-terminated polymer was observed, alongside formation of the singly-substituted product. After 6 hours reaction time a small amount of doubly-substituted product (DTM) was observed, however even at extended reaction times (96 hours) single substitution was the major product.

Dove *et al.* have previously shown that in the Michael addition of thiols to maleimide-terminated poly(lactide), reaction of dodecanethiol was slower than that of primary thiols having shorter carbon chains.[53] They also showed that the conversion obtained was dependant on the solvent used. Both effects were assigned to accessibility of the maleimide end-groups. To try and improve the conversion for the reaction of DBM-terminated PMA (**2vi**), the shorter chain thiol mercaptoethanol ($HSCH_2CH_2OH$) was investigated. Reaction of **2vi** with a slight excess (2.5 *eq.*) of mercaptoethanol in the presence of imidazole (2.5 *eq.*) was also slow (**3xvii**), and after 96 hours single substitution was again the major product.

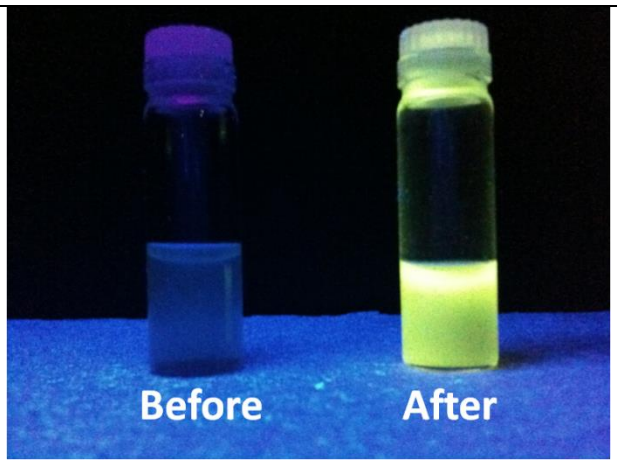

Figure 3.27. Photograph of an aqueous solution of PTEGA before (**2viii**) and after (**3xv**) end-group modification with *N*-Boc-Cys-OMe, viewed under a 365 nm lamp.

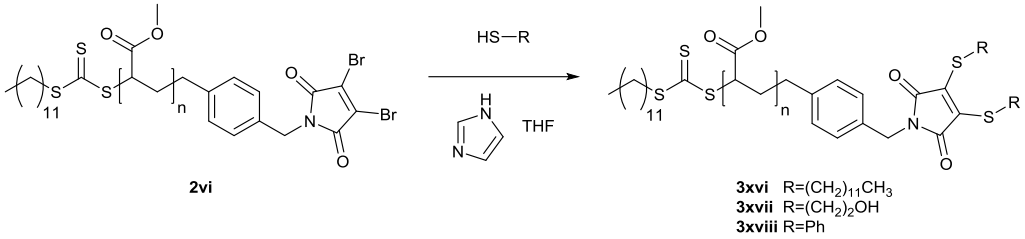

Scheme 3.6. Post-polymerisation end-group functionalisation of DBM-terminated PMA (**2vi**) with a thiol

Dove *et al.* found that the fastest reaction was obtained for the aromatic thiol HSPh. Following this approach reaction of DBM-terminated PMA with thiophenol (**3xviii**) was found to proceed rapidly, when a slight excess of thiol and imidazole (2.5 *eq.*) were used. MALDI-TOF MS analysis showed that after 15 min the major product was the DTM adduct, with complete conversion reached after 1 hour (Figure 3.28).

Analysis by SEC showed no appreciable change in the molecular weight distribution of the product **3xviii**, suggesting that the polymer was stable under these reaction conditions (Figure 3.29). The UV-vis spectrum for the polymer peak collected by the PDA detector (Figure 3.29) indicated the presence of the trithiocarbonate end-group ($\lambda_{max,abs}$ = 307 nm), as well as the DTM absorption ($\lambda_{max,abs}$ = 415 nm). As observed with the small molecule analogue **3iv**, the direct conjugation of Ph groups to the DTM gave a non-emissive product.

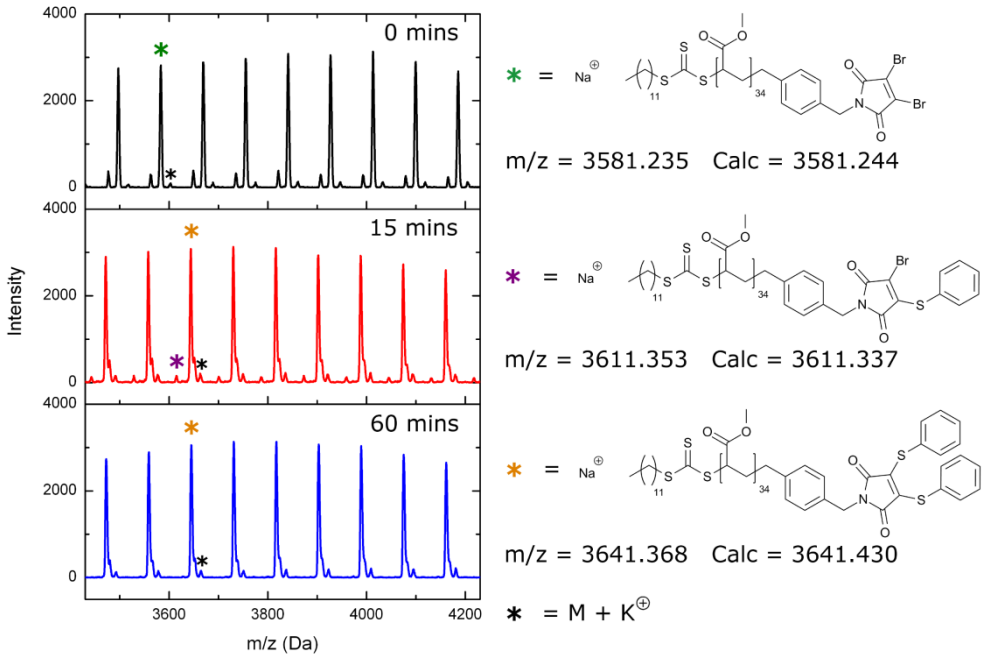

Figure 3.28. MALDI-TOF MS analysis of **3xviii**. Spectra collected in linear mode, with high resolution masses obtained in reflector mode.

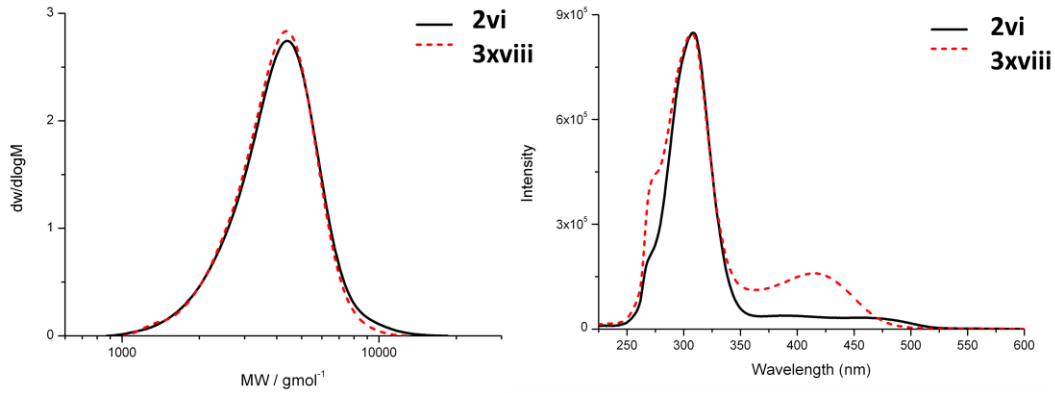

Figure 3.29. Molecular weight distribution (left) and UV-vis spectrum (right) of DBM-terminated PMA (**2vi**) and dithiophenol-maleimide-terminated PMA (**3xviii**) obtained by SEC with a DRI and PDA detector.

Further optimisation of the end-group functionalisation reaction in organic media, including variation of solvent, thiol and base was conducted by MChem student William Laye.[54] For reactions of DBM-terminated P(TEGA) a range of aromatic thiols with various electron donating or withdrawing substituents were tested. The rate of reaction was found to depend upon the pK_a of the thiol (as an indication of nucleophilicity), with electron withdrawing groups resulting in a lower pK_a and therefore a faster rate of reaction. In parallel with the observations for reaction of maleimide-terminated poly(lactide) with thiols made by Dove *et al.*, the rate of reaction for DBM-terminated

polymers was strongly influenced by the solvent. For P(TEGA) the fastest reactions were observed in polar organic solvents (DMSO, DMF), with very slow reactions in less polar solvents (DCM, THF), in contrast to the reaction of PMA with thiophenol (**3xviii**), which proceeded rapidly in THF. This implies that solubility of the P(TEGA) polymer chain was an important factor. Reactions in buffered aqueous solutions demonstrated the fastest rates of conjugation, providing both excellent solubility to the P(TEGA), as well as a base catalyst.

3.4. Conclusions

The dithiomaleimide (DTM) group has been shown to be a fluorophore which can be excited by wavelengths in the range 250-450 nm, and emits between 500-550 nm. DTMs are formed by an addition-elimination reaction between dibromomaleimide (DBM) and thiols, resulting in conjugation-induced fluorescence. Choice of thiol allows for facile variation of the substituents on the DTM, while a range of reactions for the *N*-functionalisation of the maleimide are known. The result is that DTMs are a versatile choice of dye for fluorescent labelling. This was demonstrated by incorporation of the DTM group at polymer chain ends by two approaches; either pre-polymerisation through the use of a DTM-functional CTA, or by post-polymerisation conjugation of thiols to some of the DBM-terminated polymers synthesised in Chapter 2. The potential of this DTM fluorophore for the fluorescent labelling of polymeric and self-assembled structures is further explored in the next two chapters.

Subsequent to this work, there have been two reports from Chen *et al.* where the reaction of bromomaleimide-terminated polymers with thiols has been used to construct polymer conjugates. Both miktoarm stars with DTM at the branching point, [55] and cyclic polymers with DTM at the ring closure have been formed.[56] This work further demonstrates the utility of DTM chemistry in polymer science.

3.5. Experimental

3.5.1. Materials and apparatus

Tert-butyl acrylate (^{t}BA) and styrene (Sty) were vacuum distilled over CaH_2 prior to use, and stored at 4 °C. *N*-Isopropylacrylamide (NIPAM) was recrystallised from a 9:1 mixture of hexanes: acetone and subsequently stored at 4 °C. 2,2'-azobis(2-methylpropionitrile) (AIBN) was recrystallised from methanol and stored at 4 °C in the dark. Triethylene glycol monomethylether acrylate (TEGA) was synthesised as previously reported,[57] and stored in the dark at -20 °C. 1,4-Dioxane was passed through a basic alumina plug immediately before use. D,L-lactide was donated by Purac and further purified/dried over 4 Å molecular sieves in dichloromethane before being dried under vacuum and sublimed. (-)-Sparteine was dried over CaH_2 and distilled prior to use, and 1-(3,5-bis(trifluoromethyl)phenyl)-3-cyclohexyl-thiourea (TU catalyst) was prepared and dried as previously reported.[52] All other chemicals and reagents were purchased from Aldrich and used as received. Solvents were purchased from Fisher Scientific and used as received. Dry solvents were used directly from a drying and degassing solvent tower delivery system. Lactide polymerisations were conducted in a nitrogen filled glove-box.

^{1}H and ^{13}C NMR spectra were recorded on a Bruker DPX-300, DPX-400, DRX-500, AV-600 or AV-700 spectrometer in $CDCl_3$ unless otherwise stated. Chemical shifts are given in ppm downfield from the internal standard tetramethylsilane, and coupling constants (J) correspond to $^{3}J_{H\text{-}H}$ unless otherwise stated. Size exclusion chromatography (SEC) measurements of P^{t}BA, PMA, PTEGA and PSty were conducted using an Agilent 390-MDS fitted with differential refractive index (DRI) and photodiode array (PDA) detectors equipped with a guard column (Varian Polymer Laboratories PLGel 5 µm, 50×7.5 mm) and two mixed D columns (Varian Polymer Laboratories PLGel 5 µm, 300×7.5 mm). The mobile phase was tetrahydrofuran with 2% triethylamine eluent at a flow rate of 1 mL/min. SEC measurements for PNIPAM were conducted using an Agilent 390-MDS fitted with differential refractive index (DRI) and UV-vis detector equipped with a guard column (Varian Polymer Laboratories PLGel 5 µm, 50×7.5 mm) and two mixed D columns (Varian Polymer Laboratories PLGel 5 µm, 300×7.5 mm). The mobile phase was dimethylformamide with LiBr (1 g/L) at a flow rate of 1 mL/min. SEC data was analysed

using Cirrus v3.3 with calibration curves produced using Varian Polymer laboratories Easi-Vials linear poly(styrene) standards (162-2.4×10^5 g/mol) for THF, or poly(methyl methacrylate) standards (200-4.7×10^5 g/mol) for DMF. Infrared spectra were recorded (neat) on a PerkinElmer, Spectrum 100 FT-IR Spectrometer. High Resolution Mass Spectrometry (HR-MS) was conducted on a Bruker UHR-Q-TOF MaXis with electrospray ionisation. MALDI-TOF mass spectrometry was conducted using a Bruker Daltonics Ultraflex II MALDI-TOF mass spectrometer, equipped with a nitrogen laser delivering 2 ns laser pulses at 337 nm with positive ion TOF detection performed using an accelerating voltage of 25 kV. Solutions in tetrahydrofuran (50 μl) of trans-2-[3-(4-*tert*-butylphenyl)-2-methyl-2-propylidene] malonitrile (DCTB) as a matrix (40 g/L), sodium trifluoroacetate as cationisation agent (1.0 g/L) and sample (1.0 g/L) were mixed, and 0.5 μl of the mixture was applied to the target plate. Spectra were recorded in reflector mode calibrating with SpheriCal (1200-8000 Da) standards, and linear mode calibrating with PEG-Me 2 kDa and 5 kDa standards. Fluorescence spectra were collected on a PerkinElmer LS 55 Fluorescence Spectrometer. HPLC was carried out using Phenonenex Luna 100 Å (5 μm) 250 x 4.6 mm columns. The HPLC system was an Agilent 1260 infinity series stack equipped with an Agilent 1260 binary pump, mixer and degasser. Samples were injected using an Agilent 1260 autosampler and detection was achieved using an Agilent 1260 variable wavelength detector, connected in series. UV detection was monitored at $\lambda = 280$ nm, and fluorescence excitation and emission parameters were dependent upon fluorescence spectra results. The mobile phase was MeCN (far UV) with 0.04% TFA.

3.5.2. Synthetic protocols

The synthesis of DBM-terminated PMA (**2vi**) and DBM-terminated P(TEGA) (**2viii**) was described in Chapter 2.

3,4-bis(butylsulfanyl)-2,5-dihydro-1H-pyrrole-2,5-dione (3i)

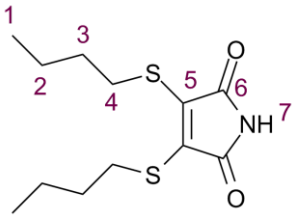

2,3-Dibromomaleimide (1.16 g, 4.55 mmol) was dissolved in diethyl ether (30 mL) and cooled to 0 °C in an ice bath. To the cooled solution, butanethiol (0.842 g, 9.33 mmol) was added and stirred for 5 minutes. Triethylamine (0.944 g, 9.33 mmol) was added dropwise to the cooled solution, whereby an immediate yellow colour was observed and a white precipitate. Upon complete addition of triethylamine, the solution was allowed to warm to room temperature and left to stir for 16 hours. Diethyl ether (70 mL) was added, and the organic solution washed with water (150 mL), brine (150 mL) and dried over anhydrous $MgSO_4$. The solution was filtered and concentrated *in vacuo*, and the crude product obtained as an orange oil. The crude mixture was purified by column chromatography (SiO_2, petroleum ether: ethyl acetate = 9:1) to yield the product as an orange oil (0.42 g, 42%). $R_f = 0.31$. ^{1}H NMR (400 MHz, $CDCl_3$) δ 7.45-7.30 (1H, br, H7), 3.29 (4H, t, J = 7.5 Hz, H4), 1.64 (4H quin, J = 7.5 Hz, H3), 1.45 (4H, sex, J = 7.5 Hz, H2), 0.93, (3H, t, J = 7.5 Hz, H1); ^{13}C NMR (100 MHz, $CDCl_3$) δ 166.1 (C6), 136.8 (C5), 32.5 (C3), 31.5 (C4), 21.7 (C2), 13.6 (C1); FTIR (neat) ν_{max} / cm^{-1} 3282 (H-N of maleimide), 1770 and 1704 (C=O of maleimide); HR-MS (MaXis) *m/z* found 274.0926, calc. 274.0930 ($[M+H]^+$, 100%); $\lambda_{ex,max}$ ($CHCl_3$) 415 nm, $\lambda_{em,max}$ ($CHCl_3$) 520 nm.

^{1}H and ^{13}C NMR spectra shown in Figure 3.7.

3,4-bis[(2-hydroxyethyl)sulfanyl]-2,5-dihydro-1H-pyrrole-2,5-dione (3ii)

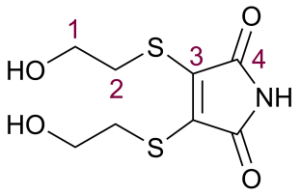

This compound was prepared using the procedure previously reported by Baker *et al.*[45]

^{1}H NMR (400 MHz, CD_3OD) δ 3.75 (4H, t, J = 6.5 Hz, H1), 3.42 (4H, t, J = 6.5 Hz, H2); ^{13}C NMR (126 MHz, CD_3OD) δ 167.5 (C4), 136.2 (C3), 61.3 (C1), 33.4 (C2); FTIR (neat) ν_{max} / cm^{-1} 3267 br (H-N maleimide and H-O alcohol), 1767 & 1696 (C=O maleimide); HR-MS (MaXis) *m/z* found 272.0022, calc. 272.0022 ($[M+Na]^+$, 100%); $\lambda_{ex,max}$ ($CHCl_3$) 400 nm, $\lambda_{em,max}$ ($CHCl_3$) 525 nm.

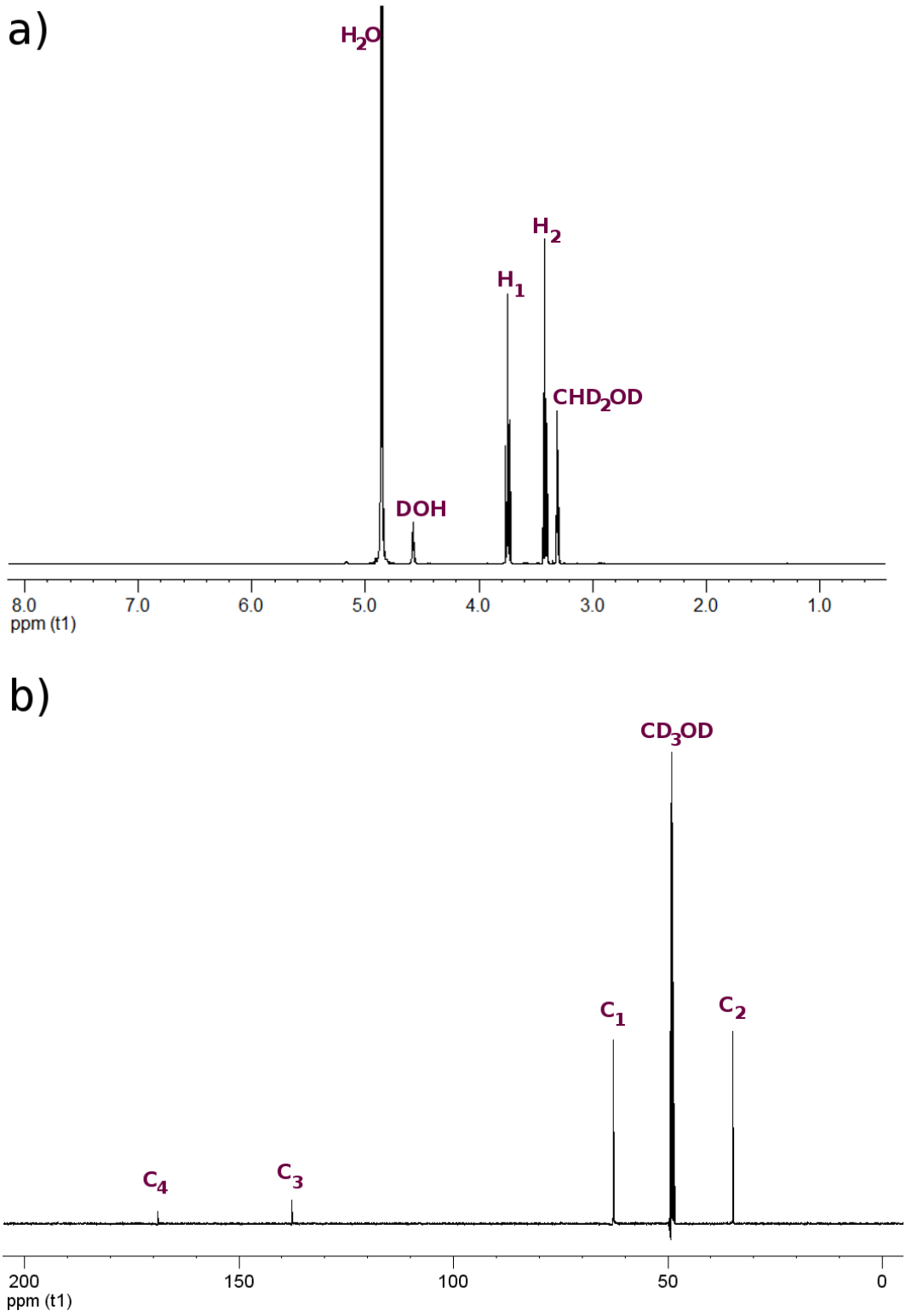

a) ^{1}H NMR (400 MHz, CD_3OD) spectrum and b) ^{13}C NMR (126 MHz, CD_3OD) spectrum for **3ii**.

3,4-Bis(benzylsulfanyl)-2,5-dihydro-1H-pyrrole-2,5-dione (3iii)

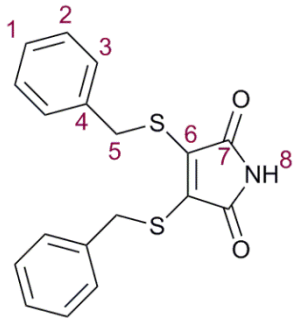

2,3-Dibromomaleimide (1.00 g, 3.92 mmol) was dissolved in diethyl ether (200 mL). To the solution, benzylmercaptan (1.22 g, 9.81 mmol) was added and stirred for 5 minutes. Triethylamine (0.993 g, 9.81 mmol) was added dropwise to the solution, whereby an immediate yellow colour was observed and a white precipitate. Upon complete addition of triethylamine, the solution was left to stir for 64 hours. The solvent was removed *in vacuo*, and the crude product purified by column chromatography (SiO_2, petroleum ether: ethyl acetate = 8:2) to yield the product as a yellow crystalline solid (0.56 g, 42%). R_f = 0.39. ^{1}H NMR (400 MHz, $CDCl_3$) δ 7.33-7.25 (10H, m, H1,2,3), 7.19 (1H, br, H8), 4.43 (4H, s, H5); ^{13}C NMR (100 MHz, $CDCl_3$) δ 166.2 (C7), 137.2 (C6), 136.5 (C4), 128.9 & 128.7 (C2&3), 127.7 (C1), 36.2 (C5); FTIR (neat) ν_{max} / cm^{-1} 3178 (H-N of maleimide), 1765 and 1705 (C=O of maleimide), 1601, 1585 and 1517 (C=C aromatic); HR-MS (MaXis) *m/z* found 364.0429, calc. 364.0436 ([M+Na]$^+$, 100%); $\lambda_{ex,max}$ ($CHCl_3$) 410 nm, $\lambda_{em,max}$ ($CHCl_3$) 520 nm.

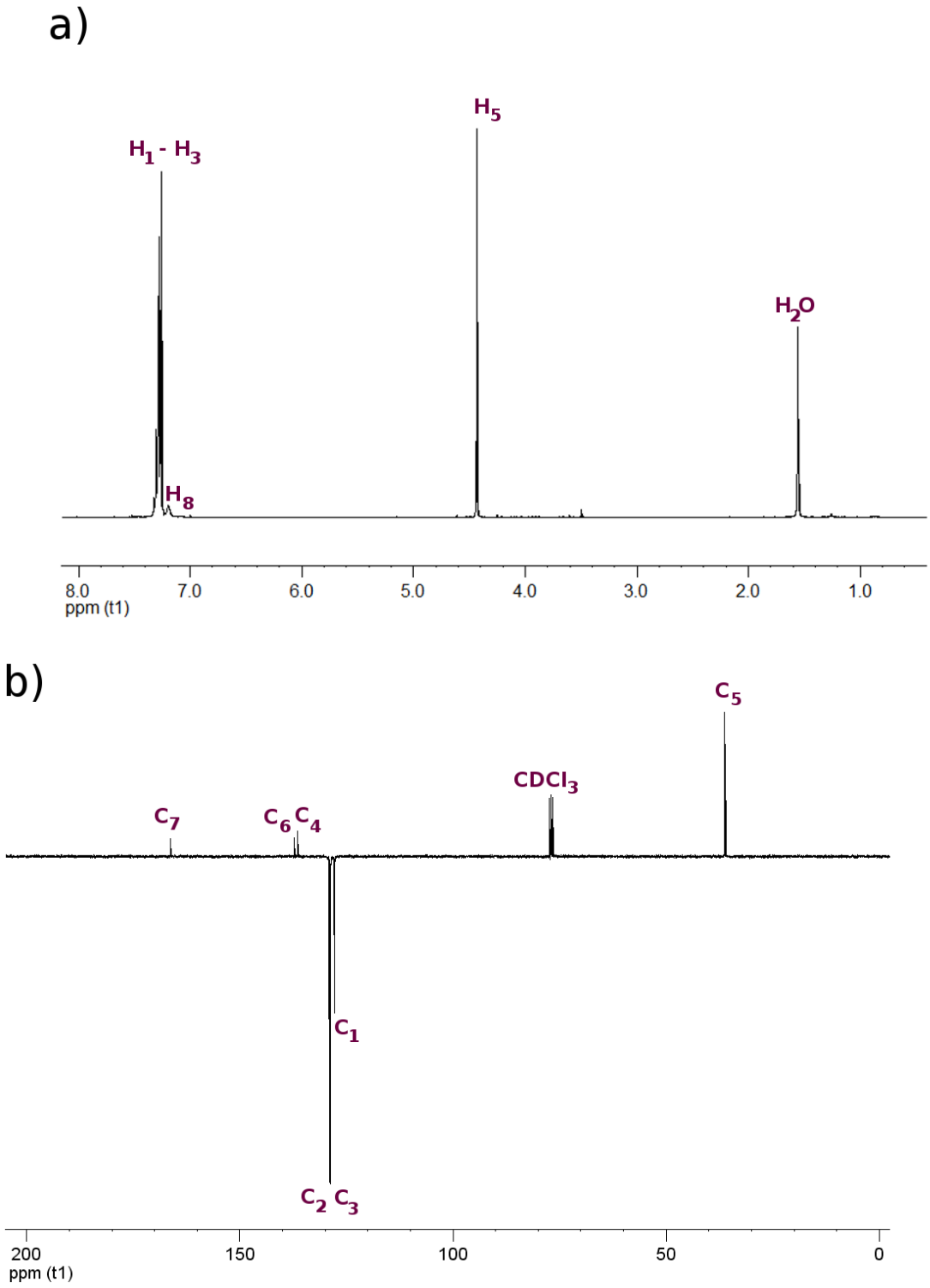

a) ^{1}H NMR (400 MHz, $CDCl_3$) spectrum and b) ^{13}C NMR (100 MHz, $CDCl_3$) spectrum for **3iii**.

3,4-Bis(phenylsulfanyl)-2,5-dihydro-1H-pyrrole-2,5-dione (3iv)

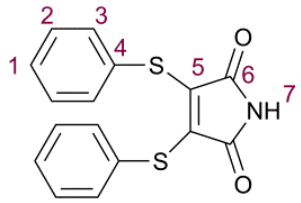

This compound was prepared using the procedure previously reported by Baker *et al.*[45]

^{1}H NMR (400 MHz, $CDCl_3$) δ 7.72 (1H, br, H7), 7.22–7.09 (10H, m, H1-3); ^{13}C NMR (100 MHz, $CDCl_3$) δ 166.4 (C6), 136.8 (C5), 132.0, 129.2, 128.9, 128.6 (12 × C_{arom}); FTIR (neat) ν_{max} / cm^{-1} 3229 (H-N maleimide), 1774 and 1701 (C=O maleimide), 1685 (C=C aromatic); HR-MS (ES+) *m/z* found 336.0128, calc. 336.0123 ($[M+Na]^+$, 100%).

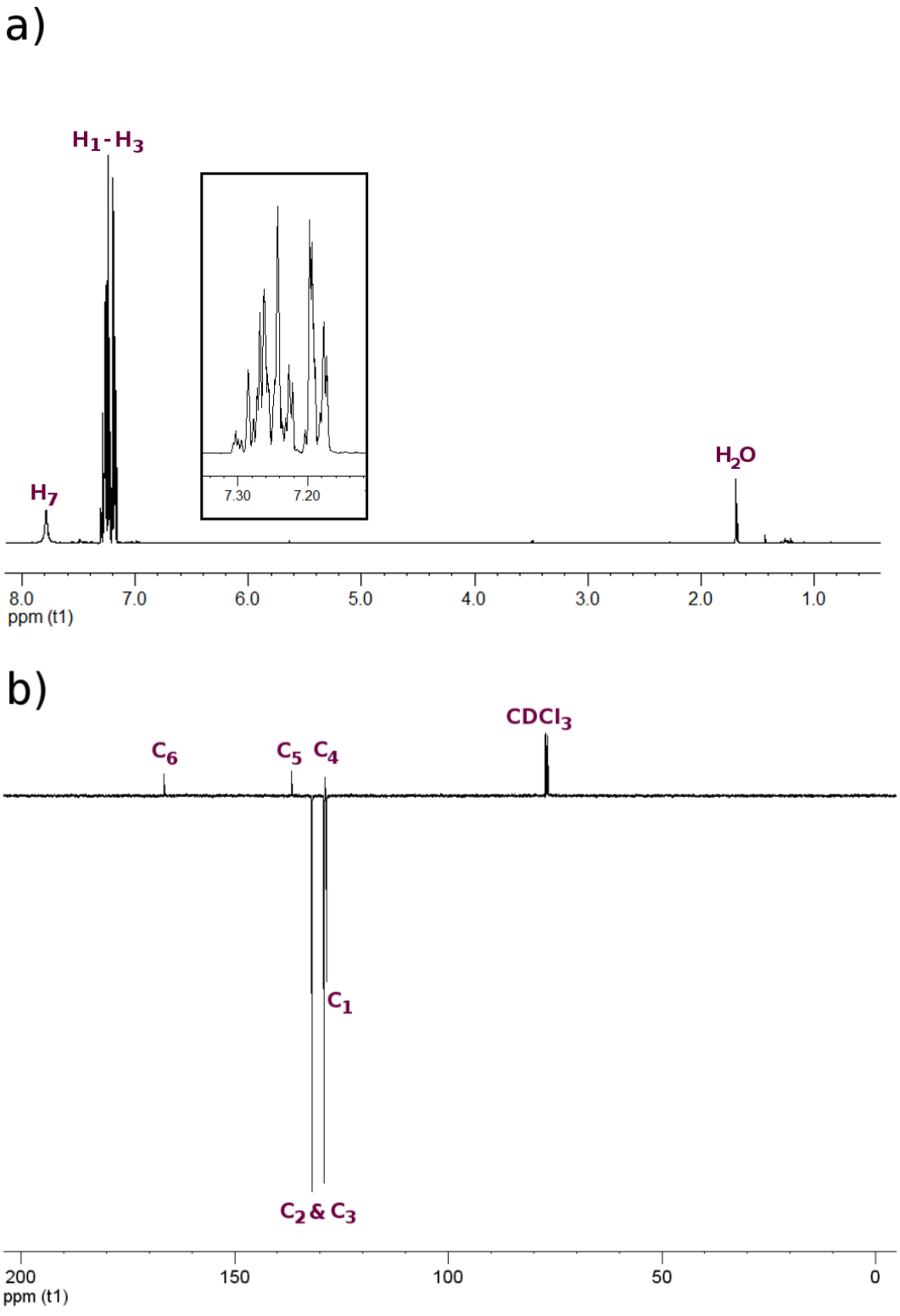

a) ^{1}H NMR (400 MHz, $CDCl_3$) spectrum and b) ^{13}C NMR (100 MHz, $CDCl_3$) spectrum for **3iv**.

3,4-bis(butylsulfanyl)-1-methyl-2,5-dihydro-1H-pyrrole-2,5-dione (3v)

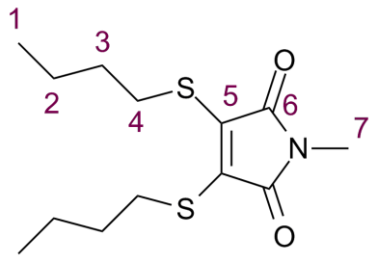

2,3-Dibromo-*N*-methylmaleimide (0.956 g, 3.56 mmol) was dissolved in diethyl ether (40 mL). To the solution was added dropwise triethylamine (0.756 g, 7.47 mmol) and butanethiol (0.674 g, 7.47 mmol), whereby an immediate yellow colour was observed and a white precipitate. Upon complete addition, the solution was stirred at room temperature for 24 hours. The solution was filtered and concentrated *in vacuo* and the crude mixture purified by column chromatography (SiO_2, petroleum ether: ethyl acetate = 97:3) to yield the product as a yellow oil (0.35 g, 34%). R_f = 0.21. ^{1}H NMR (400 MHz, $CDCl_3$) δ 3.28 (4H, t, J = 7.5 Hz, H4), 3.01 (3H s, H7), 1.63 (4H quin, J = 7.5 Hz, H3), 1.45 (4H, sex, J = 7.5 Hz, H2), 0.93, (3H, t, J = 7.5 Hz, H1); ^{13}C NMR (100 MHz, $CDCl_3$) δ 166.8 (C6), 135.9 (C5), 32.5 (C3), 31.6 (C4), 24.4 (C7), 21.7 (C2), 13.6 (C1); FTIR (neat) ν_{max} / cm^{-1} 1768 and 1697 (C=O of maleimide); HR-MS (MaXis) m/z found 310.0903, calc. 310.0906 ($[M+Na]^+$, 100%); $\lambda_{ex,max}$ ($CHCl_3$) 415 nm, $\lambda_{em,max}$ ($CHCl_3$) 530 nm.

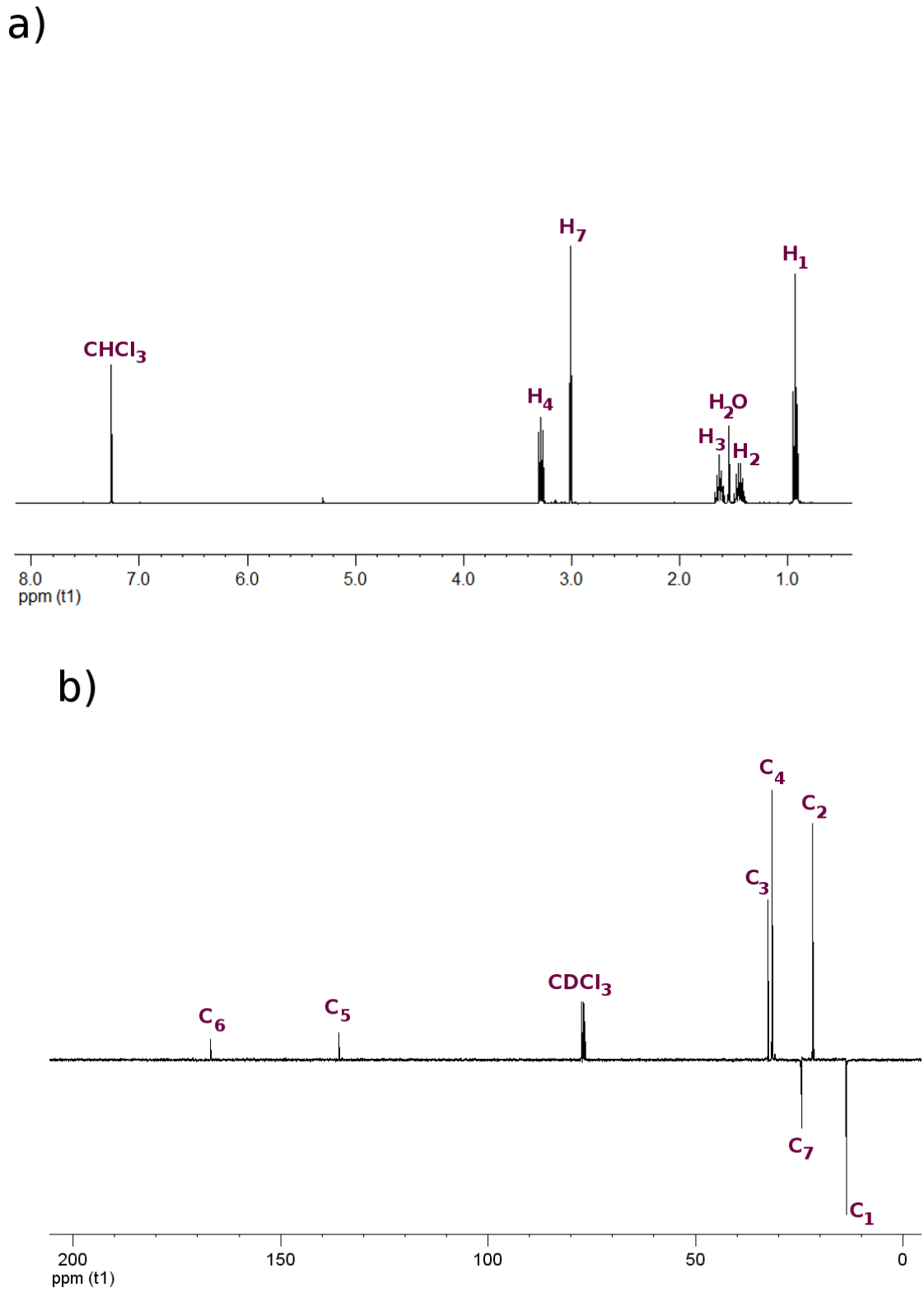

a) ^{1}H NMR (400 MHz, $CDCl_3$) spectrum and b) ^{13}C NMR (100 MHz, $CDCl_3$) spectrum for **3v**.

3,4-Bis[(2-hydroxyethyl)sulfanyl]-1-phenylpyrrolidine-2,5-dione (3vi)

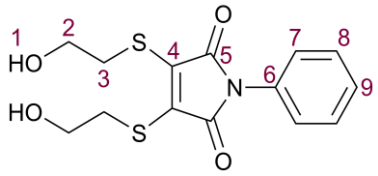

This compound was prepared using the procedure previously reported by Burke *et al.*[48]

^{1}H NMR (400 MHz, $CDCl_3$) δ7.59-7.44 (2H, m, H8), 7.39-7.22 (3H, m, H7 and H9), 3.87 (4H, t, J = 5.5 Hz, H2), 3.52 (4H, t, J = 5.5 Hz, H3), 2.57 (2H, br, H1); ^{13}C NMR (176 MHz, $CDCl_3$) δ165.49 (C5), 136.50 (C4), 131.26 (C6), 132.30, 129.16, 128.15, 127.47, 126.17 (5 × C_{arom}), 62.16 (C2), 34.73 (C3); FTIR (neat) ν_{max} / cm^{-1} 3342 br (H-N maleimide and H-O alcohol), 1767 & 1701 (C=O maleimide), 1597, 1524 & 1491 (C=C aromatic); HR-MS (MaXis) *m/z* found 348.0339, calc. 348.0335 ($M+Na^+$, 100%).

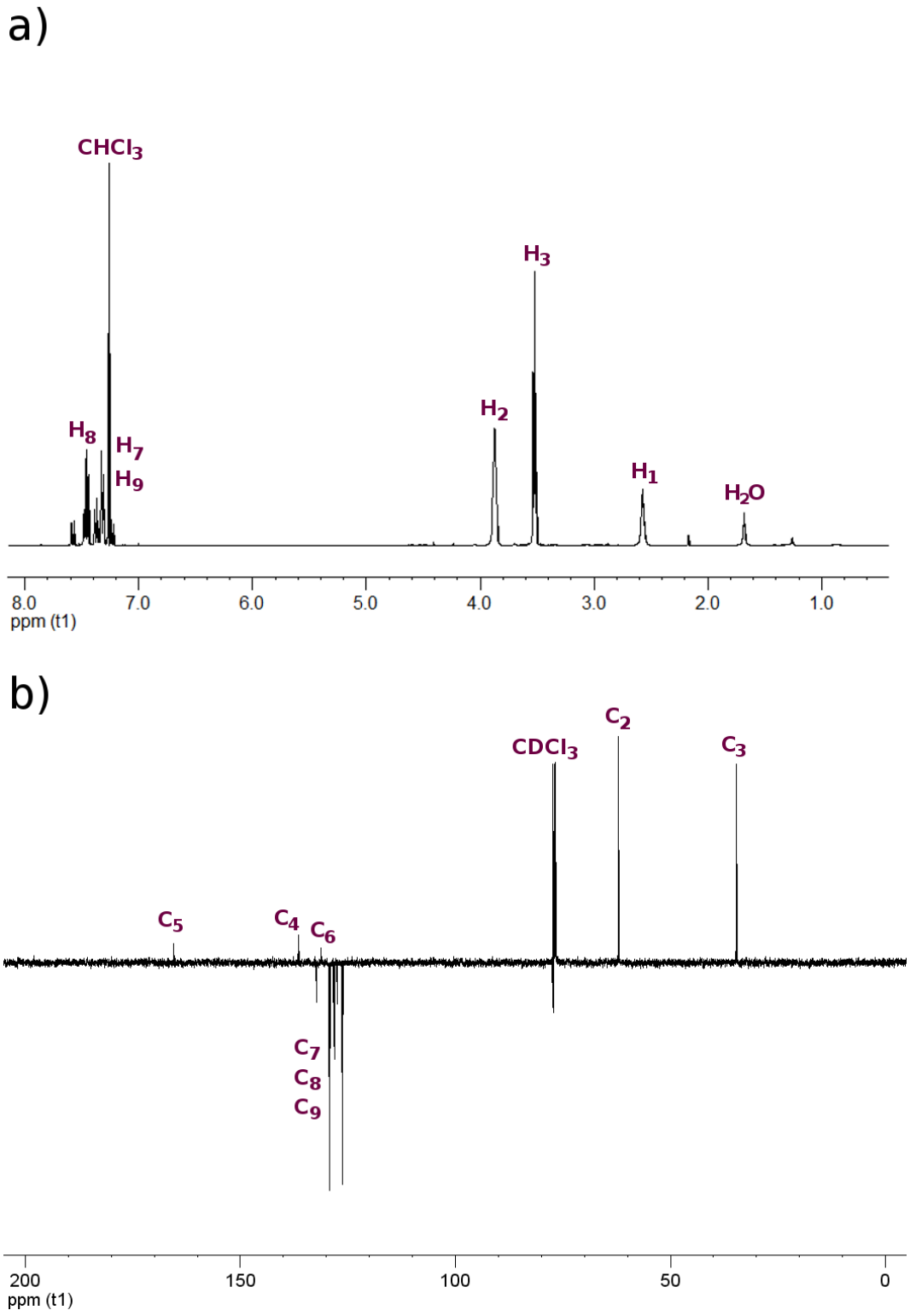

a) ^{1}H NMR (400 MHz, $CDCl_3$) spectrum and b) ^{13}C NMR (176 MHz, $CDCl_3$) spectrum for **3vi**.

2R-*tert*-Butoxycarbonylamino-3-[4-(2R-*tert*-butoxycarbonylamino-2-methoxycarbonyl-ethylsulfanyl)-2,5-dioxo-2,5-dihydro-1H-pyrrol-3-ylsulfanyl]-propionic acid methylester (3vii)

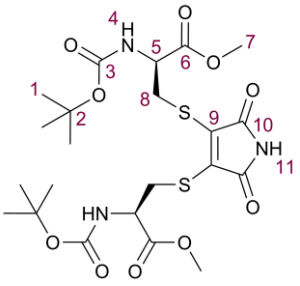

This compound was prepared using the procedure previously reported by Burke *et al.*[58]

^{1}H NMR (400 MHz, $CDCl_3$) δ 7.43-7.18 (1H, br, H11), 5.79 (2H, d, J = 7.5 Hz, H4), 4.71-4.68 (2H, m, H5), 3.89-3.68 (4H, m, H8), 3.78 (6H, s, H7), 1.44, (18H, s, H1); ^{13}C NMR (100 MHz, $CDCl_3$) δ 170.8 (C6), 165.5 (C10), 155.0 (C3), 137.1 (C9), 80.3 (C2), 53.8 (C5), 52.8 (C7), 33.8 (C8), 28.3 (C1); FTIR (neat) ν_{max} / cm^{-1} 3364 (H-N carbamate), 3219 (H-N maleimide), 1772 & 1709 (C=O maleimide), 1741 (C=O ester), 1688 & 1650 (C=O carbamate), 1506 (H-N carbamate); HR-MS (MaXis) *m/z* found 586.1498, calc. 586.1500 ($[M+Na]^+$, 100%); $\lambda_{ex,max}$ ($CHCl_3$) 405 nm, $\lambda_{em,max}$ ($CHCl_3$) 515 nm.

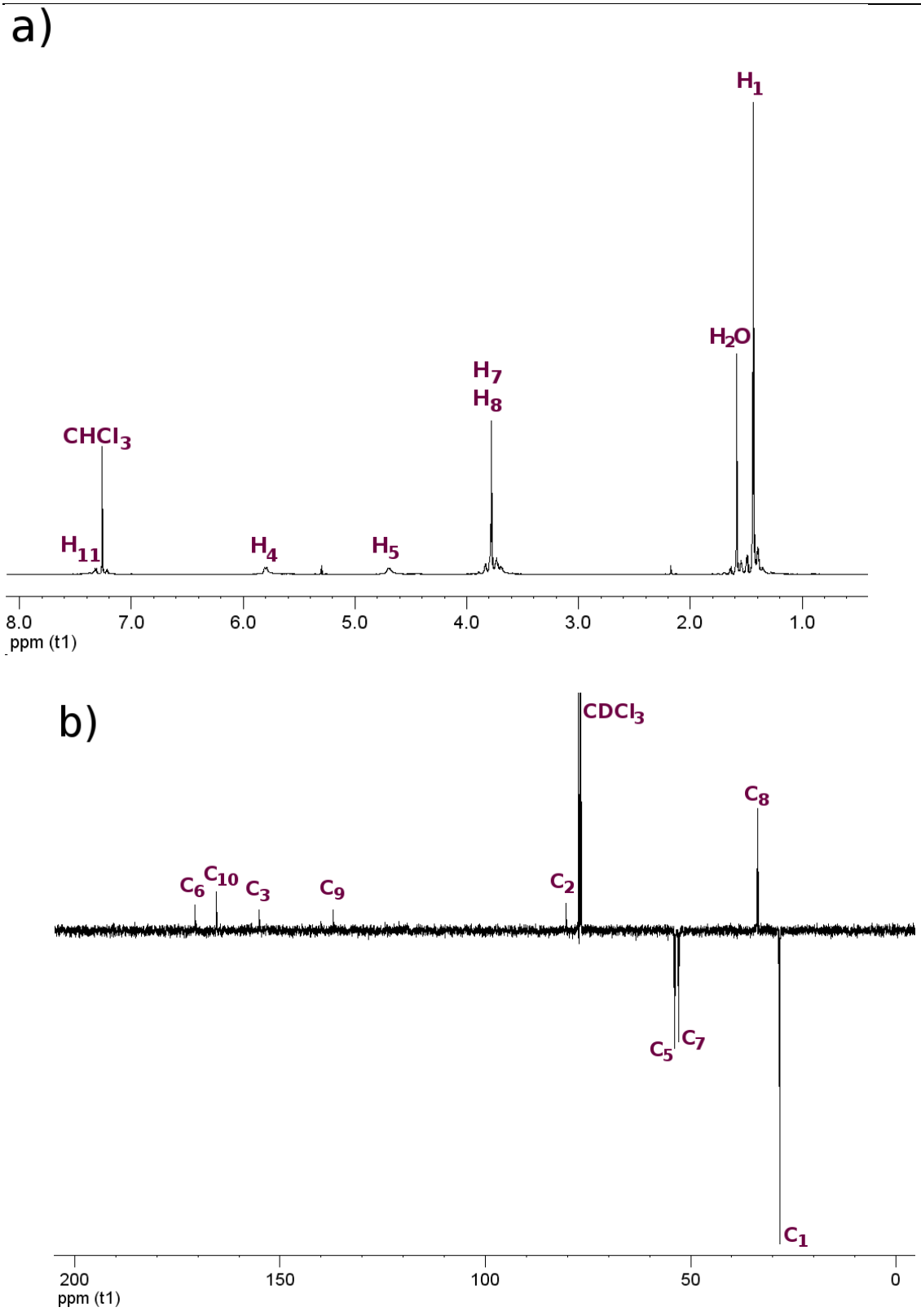

a) ^{1}H NMR (400 MHz, $CDCl_3$) spectrum and b) ^{13}C NMR (100 MHz, $CDCl_3$) spectrum for **3vii**.

Methyl 3-[(4-bromo-2,5-dioxo-2,5-dihydro-1H-pyrrol-3-yl)sulfanyl]-2-[([*tert*-butoxy]carbonyl)amino]propanoate (3viii)

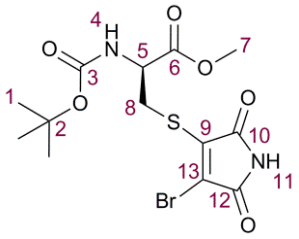

To a solution of 2,3-dibromomaleimide (0.217 g, 0.850 mmol) in methanol (4 mL) was added dropwise over 20 minutes a solution of sodium acetate (38.3 mg, 0.467 mmol) and *N*-Boc-Cys-OMe (0.100 g, 0.425 mmol) in methanol (20 mL). Upon complete addition the solution was stirred at room temperature for 1 hour. The solution was concentrated *in vacuo*, and the crude product purified by column chromatography (SiO_2, petroleum ether: ethyl acetate = 3:1) to yield the product as yellow solid (0.158 g, 91%). R_f = 0.18. ^{1}H NMR (400 MHz, $CDCl_3$) δ 8.08-7.82 (1H, br, H11), 5.26 (1H, d, J = 7.0 Hz, H4), 4.67-4.57 (1H, m, H5), 3.92-3.60 (2H, m, H8), 3.72 (3H, s, H7), 1.37, (9H, s, H1); ^{13}C NMR (150 MHz, $CDCl_3$) δ 170.5 (C6), 165.6 (C10), 163.34 (C12) 155.0 (C3), 143.0 (C9), 120.7 (C13), 80.8 (C2), 53.7 (C5), 53.0 (C7), 33.2 (C8), 28.3 (C1); FTIR (neat) ν_{max} / cm^{-1} 3300 br (H-N carbamate & H-N maleimide), 1780 (C=O maleimide), 1724 (C=O ester), 1689 (C=O carbamate), 1506 (H-N carbamate); HR-MS (MaXis) *m/z* found 430.9882, calc. 430.9883 ([M+Na]$^+$, 100%); $\lambda_{ex,max}$ ($CHCl_3$) 360 nm, $\lambda_{em,max}$ ($CHCl_3$) 465 nm.

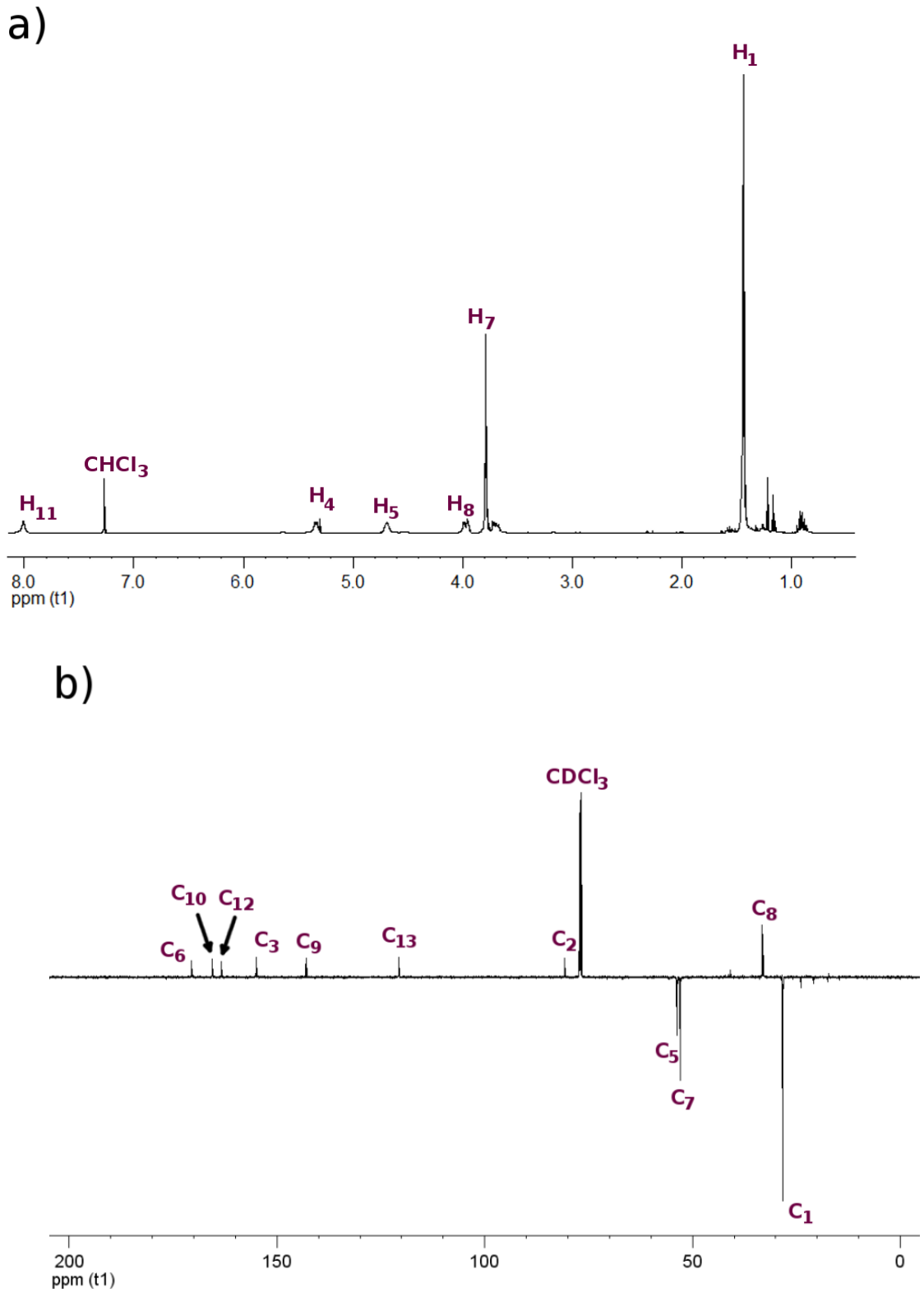

a) ^{1}H NMR (400 MHz, $CDCl_3$) spectrum and b) ^{13}C NMR (150 MHz, $CDCl_3$) spectrum for **3viii**.

1-([4-([([dodecylsulfanyl]methanethioyl)sulfanyl]methyl)phenyl]methyl)-3,4-bis[(2-hydroxyethyl)sulfanyl]-2,5-dihydro-1H-pyrrole-2,5-dione (3ix)

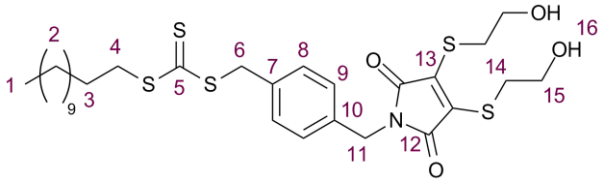

2i, (0.700 g, 1.10 mmol) was dissolved in THF (10 mL) and cooled to 0 °C. Triethylamine (0.383 mL, 2.75 mmol) and mercaptoethanol (0.193 mL, 2.75 mmol) were added to the mixture. The reaction was stirred for 3 hours, allowing to warm to room temperature. The solvent was removed *in vacuo*, the crude product was dissolved in DCM (150 mL) and the organic layer washed with water (2 x 100 mL) and brine (100 mL), and dried over anhydrous $MgSO_4$. The solvent was removed *in vacuo* and the product was isolated *via* column chromatography (SiO_2, petroleum ether: ethyl acetate = 1:2) as a yellow solid (0.25 g, 35%). R_f = 0.47. ^{1}H NMR (400 MHz, $CDCl_3$) δ7.30-7.25 (4H, m, H8 & H9), 4.63 (2H, s, H11), 4.58 (2H, s, H6), 3.83 (4H, t, J = 5.5 Hz, H15), 3.47 (4H, t, J = 5.5 Hz, H14), 3.36 (2H, t, J = 7.5 Hz, H4), 2.29 (2H, br, H16), 1.65 (2H, quin, J = 7.5 Hz, H3), 1.43-1.26 (18H, m, H2), 0.88 (3H, t, J = 6.5 Hz, H1); ^{13}C NMR (176 MHz, $CDCl_3$) δ 223.6 (C5), 166.2 (C12), 136.4 (C13), 135.4 (C7), 135.1 (C10), 129.6 (C9), 128.7 (C8), 62.1 (C15), 41.9 (C11), 40.8 (C6), 37.1 (C4), 34.7 (C14), 32-22 (C2-3), 14.1 (C1); FTIR (neat) ν_{max} / cm^{-1} 3258 (alcohol), 1763 and 1700 (C=O maleimide), 1524 and 1466 (C=C aromatic); HR-MS (MaXis) *m/z* found 652.1688, calc. 652.1688 ($[M+Na]^+$, 100%); $\lambda_{ex,max}$ ($CHCl_3$) 412 nm, $\lambda_{em,max}$ ($CHCl_3$) 538 nm.

^{1}H and ^{13}C NMR spectra shown in Figure 3.13.

Dithiomaleimide-terminated poly(*tert*-butyl acrylate) (3x)

3ix (25 mg, 39.7 μmol), AIBN (0.652 mg, 3.97 μmol), ^{t}BA (0.254 g, 1.98 mmol) and dioxane (0.288 mL) were added to a polymerisation ampoule. The solution was degassed by three freeze-pump-thaw cycles, the ampoule sealed under N_2 and the reaction stirred at 65 °C for 16 h. The product was isolated by repeated precipitation into ice cold methanol/water (9:1 *v/v*) and dried over anhydrous $MgSO_4$, then *in vacuo* to give the product as a yellow solid. $M_{n,NMR}$ = 7.0 kg·mol^{-1}, $M_{n,SEC}$ = 6.7 kg·mol^{-1}, $Đ_M$ = 1.11.

^{1}H NMR spectrum shown in Figure 3.15.

Dithiomaleimide-terminated poly(triethylene glycol methyl ether acrylate) (3xi)

3ix (25 mg, 39.7 μmol), AIBN (0.652 mg, 3.97 μmol), TEGA (0.433 g, 1.98 mmol) and dioxane (0.777 mL) were added to a polymerisation ampoule. The solution was degassed by three freeze-pump-thaw cycles, the ampoule sealed under N_2 and the reaction stirred at 65 °C for 4 h. The product was isolated by dialysis against distilled water (MWCO 3.5 kg·mol^{-1}) and lyophilisation to give the product as a yellow oil. $M_{n,NMR}$ = 5.7 kg·mol^{-1}, $M_{n,SEC}$ = 3.9 kg·mol^{-1}, $Đ_M$ = 1.20.

^{1}H NMR spectrum shown in Figure 3.18.

Dithiomaleimide-terminated poly(*N*-isopropyl acrylamide) (3xii)

3ix (25 mg, 39.7 μmol), AIBN (0.652 mg, 3.97 μmol), NIPAM (0.225 g, 1.98 mmol) and dioxane (0.449 mL) were added to a polymerisation ampoule. The solution was degassed by three freeze-pump-thaw cycles, the ampoule sealed under N_2 and the reaction stirred at 65 °C for 16 h. The product was isolated by repeated precipitation into ice cold diethyl ether, then dried *in vacuo* to give the product as a yellow solid. $M_{n,NMR}$ = 2.7 kg·mol^{-1}, $M_{n,SEC}$ = 3.3 kg·mol^{-1}, $Đ_M$ = 1.16.

^{1}H NMR spectrum shown in Figure 3.20.

Dithiomaleimide-terminated polystyrene (3xiii)

3ix (25 mg, 39.7 μmol) and styrene (0.372 g, 3.57 mmol) were added to a polymerisation ampoule. The solution was degassed by three freeze-pump-thaw cycles, the ampoule sealed under N_2 and the reaction stirred at 110 °C for 16 h. The product was isolated by repeated precipitation into ice cold methanol/water (9:1 *v/v*) and dried over anhydrous $MgSO_4$, then *in vacuo* to give the product as a yellow solid. $M_{n,NMR}$ = 5.1 kg·mol^{-1}, $M_{n,SEC}$ = 4.9 kg·mol^{-1}, $Đ_M$ = 1.39.

^{1}H NMR spectrum shown in Figure 3.23.

Dithiomaleimide-labelled poly(D,L-lactide) (3xiv)

To a solution of **3ix** (70.0 mg, 0.11 mmol), D,L-lactide (0.641 g, 4.4 mmol), and thiourea catalyst (82.3 mg, 0.22 mmol) dissolved in dry DCM (6.41 mL) was added (-)-sparteine (25.5 µL, 0.11 mmol). The reaction was stirred at room temperature for 2 hours to a monomer conversion $> 99\%$, before precipitation into an excess of hexanes ($\times$ 2). The resultant polymer was purified *via* a prep GPC column (Bio-Beads), to yield a yellow solid. $M_{n,NMR} = 6.7$ kg·mol^{-1}, $M_{n,SEC} = 9.8$ kg·mol^{-1}, $Đ_M = 1.09$.

^{1}H NMR spectrum shown in Figure 3.24.

Post-polymerisation modification of DBM-terminated PTEGA with *N*-Boc-Cys-OMe (3xv)

To a solution of (**2viii**) (10 mg, 2.74 µmol) in buffer (1 mL, sodium phosphate 100 mM, sodium chloride 150 mM, pH 7.5) was added a solution of *N*-Boc-Cys-OMe (1.75 mg, 6.88 µmol) in DMF (50 µl). The reaction was stirred at room temperature. Periodically, samples were taken for MALDI-TOF MS analysis.

Post-polymerisation modification of DBM-terminated PMA

*Dodecanethiol (**3xvi**)*

To a solution of (**2vi**) (10 mg, 3.28 µmol) in THF was added a solution of imidazole (2.23 mg, 32.8 µmol) in THF, then a solution of dodecanethiol (6.64 mg, 32.8 µmol) in THF, to give a final volume of 1 mL (polymer concentration 10 g/L). The reaction was stirred at room temperature. Periodically, samples were taken for MALDI-TOF MS analysis.

*Mercaptoethanol (**3xvii**)*

To a solution of (**2vi**) (10 mg, 3.28 µmol) in THF was added a solution of imidazole (0.558 mg, 8.20 µmol) in THF, then a solution of mercaptoethanol (0.641 mg, 8.20 µmol) in THF, to give a final volume of 1 mL (polymer concentration 10 g/L). The reaction was stirred at room temperature. Periodically, samples were taken for MALDI-TOF MS analysis.

*Thiophenol (**3xviii**)*

To a solution of (**2vi**) (20 mg, 6.56 μmol) in THF was added a solution of imidazole (1.12 mg, 16.4 μmol) in THF, then a solution of thiophenol (1.81 mg, 16.4 μmol) in THF, to give a final volume of 2 mL (polymer concentration 10 g/L). The reaction was stirred at room temperature. Periodically, samples were taken for MALDI-TOF MS analysis.

3.6. References

1. J. R. Lakowicz, *Principles of Fluorescence Spectroscopy*, Springer, 2009.

2. P. W. Atkins and J. De Paula, *Elements of physical chemistry*, 4th edn., Oxford University Press, 2005.

3. B.-C. Wang, H.-R. Liao, H.-C. Yeh, W.-C. Wu and C.-T. Chen, *J. Lumin.*, 2005, **113**, 321-328.

4. A. M. Brouwer, *Pure Appl. Chem.*, 2011, **83**, 2213-2228.

5. A. J. W. G. Visser and O. J. Rolinski, Basic Photophysics, http://photobiology.info/Visser-Rolinski.html.

6. M. Beija, M.-T. Charreyre and J. M. G. Martinho, *Prog. Polym. Sci.*, 2011, **36**, 568-602.

7. X. Wan and S. Liu, *J. Mater. Chem.*, 2011, **21**, 10321-10329.

8. G. O'Bryan and R. Braslau, *Macromolecules*, 2006, **39**, 9010-9017.

9. P. J. Roth, K.-S. Kim, S. H. Bae, B.-H. Sohn, P. Theato and R. Zentel, *Macromol. Rapid Commun.*, 2009, **30**, 1274-1278.

10. Y.-Y. Tong, R. Wang, N. Xu, F.-S. Du and Z.-C. Li, *J. Polym. Sci., Part A: Polym. Chem.*, 2009, **47**, 4494-4504.

11. B. Moon, T. R. Hoye and C. W. Macosko, *J. Polym. Sci., Part A: Polym. Chem.*, 2000, **38**, 2177-2185.

12. J.-D. Tong, C. Zhou, S. Ni and M. A. Winnik, *Macromolecules*, 2001, **34**, 696-705.

13. G. K. Such, R. A. Evans and T. P. Davis, *Macromolecules*, 2004, **37**, 9664-9666.

14. F. Ercole, N. Malic, S. Harrisson, T. P. Davis and R. A. Evans, *Macromolecules*, 2010, **43**, 249-261.

15. M. E. Scott, J. S. Parent, S. L. Hennigar, R. A. Whitney and M. F. Cunningham, *Macromolecules*, 2002, **35**, 7628-7633.

16. M. Rodlert, E. Harth, I. Rees and C. J. Hawker, *J. Polym. Sci., Part A: Polym. Chem.*, 2000, **38**, 4749-4763.

17. G. T. Gavranovic, S. Csihony, N. B. Bowden, C. J. Hawker, R. M. Waymouth, W. E. Moerner and G. G. Fuller, *Macromolecules*, 2006, **39**, 8121-8127.

18. D. Zhou, X. Zhu, J. Zhu and Z. Cheng, *J. Polym. Sci., Part A: Polym. Chem.*, 2008, **46**, 6198-6205.

19. M. Beija, C. A. M. Afonso, J. P. S. Farinha, M.-T. Charreyre and J. M. G. Martinho, *Polymer*, 2011, **52**, 5933-5946.

20. M. Chen, K. P. Ghiggino, A. W. H. Mau, E. Rizzardo, S. H. Thang and G. J. Wilson, *Chem. Commun.*, 2002, 2276-2277.

21. S. L. Mangold, R. T. Carpenter and L. L. Kiessling, *Org. Lett.*, 2008, **10**, 2997-3000.

22. A. E. Madkour, A. H. R. Koch, K. Lienkamp and G. N. Tew, *Macromolecules*, 2010, **43**, 4557-4561.

23. H. Zettl, W. Häfner, A. Böker, H. Schmalz, M. Lanzendörfer, A. H. E. Müller and G. Krausch, *Macromolecules*, 2004, **37**, 1917-1920.

24. X. Chen, Y. Zhou, X. Peng and J. Yoon, *Chem. Soc. Rev.*, 2010, **39**, 2120-2135.

25. T. O. Sippel, *J. Histochem. Cytochem.*, 1981, **29**, 314-316.

26. M. E. Langmuir, J.-R. Yang, A. M. Moussa, R. Laura and K. A. LeCompte, *Tetrahedron Lett.*, 1995, **36**, 3989-3992.

27. D. Kand, A. M. Kalle and P. Talukdar, *Org. Biomol. Chem.*, 2013, **11**, 1691-1701.

28. A. Prasanna de Silva, H. Q. Nimal Gunaratne and T. Gunnlaugsson, *Tetrahedron Lett.*, 1998, **39**, 5077-5080.

29. J. Guy, K. Caron, S. Dufresne, S. W. Michnick, Skene and J. W. Keillor, *J. Am. Chem. Soc.*, 2007, **129**, 11969-11977.

30. J. Youziel, A. R. Akhbar, Q. Aziz, M. E. B. Smith, S. Caddick, A. Tinker and J. R. Baker, *Org. Biomol. Chem.*, 2014, **12**, 557-560.

31. C.-W. Chiu, T. J. Chow, C.-H. Chuen, H.-M. Lin and Y.-T. Tao, *Chem. Mater.*, 2003, **15**, 4527-4532.

32. W. C. Wu, H. C. Yeh, L. H. Chan and C. T. Chen, *Adv. Mater.*, 2002, **14**, 1072-1075.

33. H.-C. Yeh, W.-C. Wu and C.-T. Chen, *Chem. Commun.*, 2003, 404-405.

34. H.-d. Xie, L. Ho, M. Truelove, B. Corry and S. Stewart, *J Fluoresc*, 2010, **20**, 1077-1085.

35. K. Onimura, M. Matsushima, M. Nakamura, T. Tominaga, K. Yamabuki and T. Oishi, *J. Polym. Sci., Part A: Polym. Chem.*, 2011, **49**, 3550-3558.

36. B. K. Kaletas, R. M. Williams, B. Konig and L. De Cola, *Chem. Commun.*, 2002, 776-777.

37. T. Kato and K. Naka, *Chem. Lett.*, 2012, **41**, 1445-1447.

38. H. Leismann, G. Marzolph, H.-D. Scharf and M. Behruzi, *Chem. Ber.*, 1983, **116**, 2591-2615.

39. S. G. Bodige, M. A. Méndez-Rojas and W. H. Watson, *J. Chem. Crystallogr.*, 1999, **29**, 57-66.

40. T. L. Smith, *US Pat.,* 4680272, 1987.

41. M. E. B. Smith, F. F. Schumacher, C. P. Ryan, L. M. Tedaldi, D. Papaioannou, G. Waksman, S. Caddick and J. R. Baker, *J. Am. Chem. Soc.*, 2010, **132**, 1960-1965.

42. D. M. Lynch and A. J. Crovetti, *J. Heterocycl. Chem.*, 1972, **9**, 1027-1032.

43. M. W. Jones, R. A. Strickland, F. F. Schumacher, S. Caddick, J. R. Baker, M. I. Gibson and D. M. Haddleton, *J. Am. Chem. Soc.*, 2012, **134**, 1847-1852.

44. R. P. Joyce, J. A. Gainor and S. M. Weinreb, *J. Org. Chem.*, 1987, **52**, 1177-1185.

45. F. F. Schumacher, M. Nobles, C. P. Ryan, M. E. B. Smith, A. Tinker, S. Caddick and J. R. Baker, *Bioconjugate Chem.*, 2011, **22**, 132-136.

46. D.-S. Choi, S. Huang, M. Huang, T. S. Barnard, R. D. Adams, J. M. Seminario and J. M. Tour, *J. Org. Chem.*, 1998, **63**, 2646-2655.

47. L. Castañeda, Z. V. F. Wright, C. Marculescu, T. M. Tran, V. Chudasama, A. Maruani, E. A. Hull, J. P. M. Nunes, R. J. Fitzmaurice, M. E. B. Smith, L. H. Jones, S. Caddick and J. R. Baker, *Tetrahedron Lett.*, 2013, **54**, 3493–3495.

48. U. Muus, C. Hose, W. Yao, T. Kosakowska-Cholody, D. Farnsworth, M. Dyba, G. T. Lountos, D. S. Waugh, A. Monks, T. R. B. Jr. and C. J. Michejda, *Bioorg. Med. Chem.*, 2010, **18**, 4535-4541.

49. M. P. Robin, P. Wilson, A. B. Mabire, J. K. Kiviaho, J. E. Raymond, D. M. Haddleton and R. K. O'Reilly, *J. Am. Chem. Soc.*, 2013, **135**, 2875–2878.

50. M. W. Jones, R. A. Strickland, F. F. Schumacher, S. Caddick, J. R. Baker, M. I. Gibson and D. M. Haddleton, *Chem. Commun.*, 2012, **48**, 4064-4066.

51. A. P. Dove, *ACS Macro Lett.*, 2012, **1**, 1409-1412.

52. R. C. Pratt, B. G. G. Lohmeijer, D. A. Long, P. N. P. Lundberg, A. P. Dove, H. Li, C. G. Wade, R. M. Waymouth and J. L. Hedrick, *Macromolecules*, 2006, **39**, 7863-7871.

53. R. J. Pounder, M. J. Stanford, P. Brooks, S. P. Richards and A. P. Dove, *Chem. Commun.*, 2008, 5158-5160.

54. W. Laye, MSc Dissertation, University of Warwick, 2013.

55. Y. Cui, Y. Yan, Y. Chen and Z. Wang, *Macromol. Chem. Phys.*, 2013, **214**, 470-477.

56. S. Long, Q. Tang, Y. Wu, L. Wang, K. Zhang and Y. Chen, *React. Funct. Polym.*, 2014, **80**, 15-20.

57. F. Hua, X. Jiang, D. Li and B. Zhao, *J. Polym. Sci., Part A: Polym. Chem.*, 2006, **44**, 2454-2467.

58. L. M. Tedaldi, A. E. Aliev and J. R. Baker, *Chem. Commun.*, 2012, **48**, 4725-4727.

4. Dithio- and dibromomaleimides as fluorescent and profluorescent monomers

4.1. Abstract

In this chapter the incorporation of dithiomaleimide (DTM) and dibromomaleimide (DBM) functionality into vinyl monomers is explored. An acrylic, methacrylic and styrene derivative of both DTM and DBM are synthesised, and their RAFT copolymerisation with analogous non-functional monomers is investigated. DTM monomers were anticipated to give highly fluorescent products without further reaction. Alternatively, DBM monomers were anticipated to give polymers with reactive pendant groups which can undergo the highly efficient addition-elimination reaction with thiols. As this addition-elimination reaction leads to the formation of the DTM fluorophore (and therefore to emissive polymers), DBM monomers would provide a precursor to profluorescent polymeric materials. These two strategies for the preparation of fluorescent polymers based on DTM and DBM monomers are depicted in Figure 4.1.

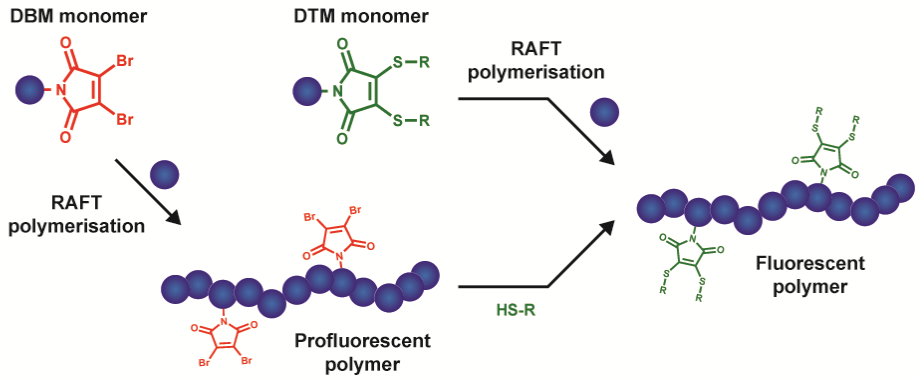

Figure 4.1. Strategy for the preparation of profluorescent and fluorescent polymers using DBM and DTM monomers

The work in this chapter complements that of the previous chapter, where DTM-terminated polymers were prepared *via* pre- and post-polymerisation functionalisation routes. The advantage of using functional monomers over functional initiators is the ease with which DTM or DBM incorporation could be tailored by altering monomer feed ratios, and the greater applicability to the current range of reversible-deactivation radical polymerisation (RDRP) processes.

4.2. Introduction

4.2.1. Fluorescent monomers

The polymerisation of fluorescent monomers results in the incorporation of fluorophore units along a polymer backbone. As opposed to main-chain π-conjugated polymers, polymerisation of dye molecules that are functionalised with a vinyl group can be performed by RDRP,[1] allowing a greater versatility in fluorescent polymer synthesis. Copolymers, block copolymers and homopolymers of fluorescent vinyl monomers have found a myriad of applications in organic electronic devices, sensor materials, the study of polymer properties, and as fluorescently-labelled polymer nanoparticles (as discussed in detail in Chapter 1).[2] There are several advantages of the copolymerisation approach for fluorescent labelling over an end-group modification approach. A single fluorescent monomer will often be compatible with many polymerisation techniques (e.g. free radical polymerisation[3], RAFT[4], ATRP[5], NMP[6]), and does not require any modification to either the initiator/CTA or the final polymer. When using a fluorescent monomer the degree of fluorophore incorporation (and hence its concentration in the final polymer) can be simply varied by altering the monomer feed, as opposed to an end-group labelling approach which is limited to one or two fluorophores per chain. Another advantage of fluorescent monomer incorporation is that the resultant polymer end-groups remain 'unused', allowing for further modification of the polymer by end-group functionalisation or conjugation.

The importance and utility of fluorophore-containing polymers is illustrated by the wealth of different monomers that have been investigated, with a recent review of the literature by Schubert *et al.* finding 211 different examples.[2] Included in this list were several commercially available fluorescent monomers, shown in Figure 4.2. Selected examples of the different fluorescent groups, polymerisation methodologies, and applications are given below.

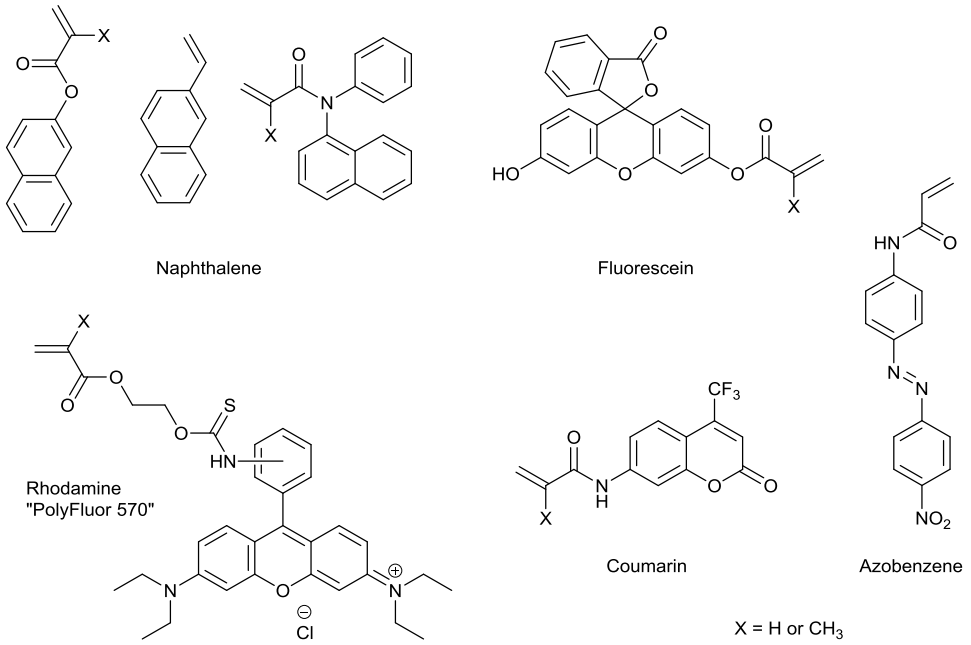

Figure 4.2. Commercially available fluorescent vinyl monomers

Due to a lack of heteroatoms, functionalization of polyaromatic hydrocarbons provides fluorescent monomers that are compatible with widest range of polymerisation techniques. Monomers based on naphthalene, pyrene, perylene, fluorene and anthracene have all been utilised.[2] For example, Swanson and colleagues synthesised methacrylic acid (MAA) ternary copolymers with 0.5 and 1.5 mol% loading respectively of acenaphthylene and anthracene methacrylate monomers by free radical polymerisation. A combination of fluorescence energy transfer and lifetime measurements for these two fluorophores allowed the conformational transition of PMAA in response to pH to be probed on the nanometre scale.[7] Thelakkat *et al.* used a polythiophene macroinitiator to polymerise a perylene bisimide acrylate monomer by NMP. The resultant double crystalline donor-acceptor block copolymers were used in the fabrication of single component single layer solar cells, which showed good maximum external quantum efficiency and power conversion efficiency.[8] Living anionic polymerisation was used by Hirao, Chen and co-workers to form diblock copolymers and asymmetric star polymers of poly(2-vinylpyridine) and a fluorene-functional styrenic monomer, which were used in the fabrication of non-volatile memory devices.[9]

Fluorescein-derived monomers constitute the largest group of polymerisable dyes.[2] Ionov *et al.* showed that copolymer brushes of NIPAM and a fluorescein acrylate (2 wt%) could be grown from surface adsorbed microtubules by ATRP.[10] The use of PNIPAM gave the

microtubules a thermoresponsive coating, while the incorporation of the fluorescein monomer allowed the microtubes to be visualised by epi-fluorescent microscopy. Matyjaszewski *et al.* also used ATRP in the copolymerisation of a fluorescein methacrylate (0.25 mol%) with *n*-butyl acrylate, grafting from a brush polymer macroinitiator, to form highly emissive molecular bottlebrushes.[11] The bottlebrush fluorescence was pH responsive, with the non-emissive neutral fluorescein being formed at pH $\leq$ 7. Rhodamine 6G-derived monomers are also a popular choice, due to its high quantum yield ($>$ 0.9). For example, Armes and coworkers synthesised a rhodamine methacrylate monomer which was used to label a diblock copolymer. Chain extension of water soluble poly(2-(methacryloyloxy)ethyl phosphorylcholine) by copolymerisation of (2-(diisopropylamino)ethyl methacrylate) and the rhodamine methacrylate monomer by ATRP produced block copolymers with an average of 1 rhodamine dye per chain.[12] The aqueous self-assembly of vesicles could be triggered by increasing the pH above 6, as protonation of the poly(2-(diisopropylamino)ethyl methacrylate) block rendered it hydrophobic. Fluorescence emission was responsive to this change in aggregation, due to formation of non-emissive rhodamine dimers in the vesicle bilayers, which lead to a decrease in emission upon self-assembly.

Coumarin based monomers have been utilized for their ability to reversibly photodimerise. Minoda *et al.* synthesised a vinyl ether coumarin monomer, which was polymerised by living cationic polymerisation.[13] Homopolymers, and amphiphilic diblock copolymers were shown to undergo photoinduced cross-linking upon irradiation at 366 nm, with photocleavage resulting from irradiation with 254 nm light. Azobenzene-derived monomers are also of interest, as they undergo a photo-induced cis-trans isomerism which leads to a change in absorption and emission spectra. Abd-El-Aziz *et al.* polymerised norbornene-functional aryl- and hetaryl-azo dyes by ROMP to give homopolymers, random copolymers, and block copolymers.[14] As well as photo-induced response, emission also displayed a bathochromic response to pH, due to the formation of the azonium form of the azo group. For example, a solution of the monomer in DMF changed from purple to blue to brown/red as the concentration of H^+ increased (Figure 4.3 a), while a thin film formed from the polymer turned purple upon exposure to HCl gas (Figure 4.3 b), returning to its original yellow colour to upon exposure to NH_3 gas (Figure 4.3 c).

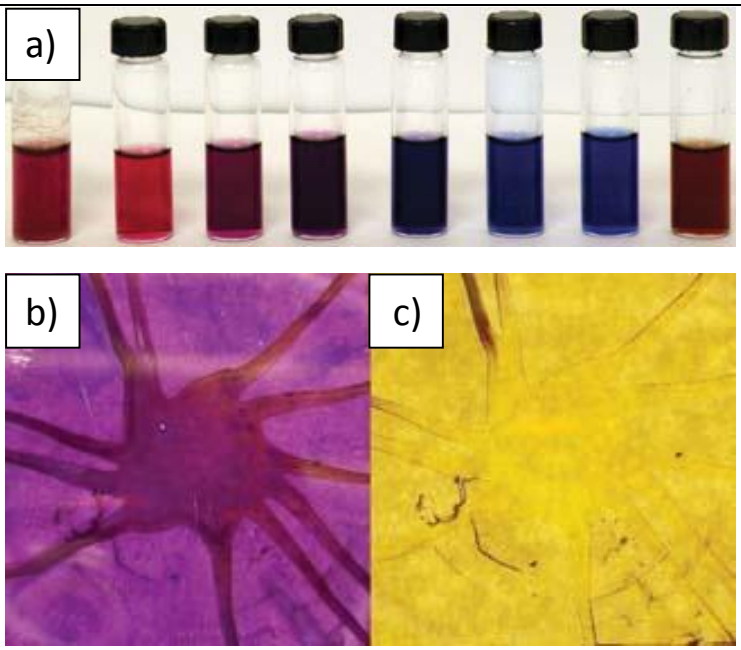

Figure 4.3 a) Solutions (in DMF) of norbornene-functional hetaryl-azo dye with increases H^+ concentration from left to right. b) Thin film of the subsequent ROMP polymer after exposure to HCl gas and c) returned to its original colour after exposure to NH_3 gas. Figure adapted from ref.[14]

Polymers derived from naphthalimide-labelled monomers have found applications as chemosensors, due to the sensitivity of naphthalimide emission to ion chelation. Tian and co-workers used RAFT polymerisation to produce homopolymers of a naphthalimide methacrylate which showed a red shift in emission in the presence of fluoride anions, while other halides elicited no change.[15] Enhanced emission due to transition metal chelation (Zn^{2+}, Fe^{3+}, Co^{2+}, Pb^{2+}, Cu^{2+}, Ni^{2+} and Mn^{2+}) was also shown by Grabchev *et al.*, who produced naphthalimide acrylate/styrene copolymers (1/1 monomer loading by mass) *via* free radical polymerisation.[16]

4.2.2. Profluorescence in polymer chemistry

The generation of an emissive fluorophore upon completion of a targeted reaction is a highly desirable characteristic. As opposed to the attachment of an already emissive species, use of a profluorophore gives a clear indication that fluorescent labelling has been achieved at the desired location, as an OFF→ON change in emission will occur. This can be achieved by using a quenched fluorophore, with reaction removing the quenching group. For example, 3-azidocoumarin shows little emission due to the quenching effect of the azide group. However, CuAAC with an alkyne forms a 1,4-disubstituted 1,2,3-triazole ring which no longer quenches the fluorophore, leading to emission. This reaction has been

utilised by O'Reilly *et al.* for the fluorescent labelling of alkyne-functional micelle cores,[17, 18] and by Cornelissen *et al.* for the simultaneous PEGylation and fluorescent labelling of an alkyne-functional bovine serum albumin protein (Scheme 4.1 a).[19]

A similar approach was also taken by Kiessling *et al.*, whose rhodamine-labelled polymeric antigen (prepared by ROMP) was quenched by a 'trimethyl lock'. Intracellular esterases caused lactonization of the trimethyl lock, with corresponding cleaveage of the linker between the quencher and rhodamine, allowing cellular internalisation of the polymeric antigen to be imaged by fluorescence microscopy (Scheme 4.1 b).[20] Nitroxide profluorophores have also been used, as the nitroxide radical quenches excited singlet states. For example Blinco *et al.* used the nitroxide exchange reaction to end-functionalise polystyrene (synthesised by NMP) with a profluorescent nitroxide, giving an emissive product (Scheme 4.1 c).[21]

Alternatively fluorescence can also by triggered where the labelling reaction is also the fluorophore-forming reaction, *i.e.* two profluorescent groups react to form a fluorophore. These are much rarer, as they require the reaction that generates the fluorophore to be highly efficient, if it is to have utility as a labelling reaction. It appears that the only reaction which currently fulfils this criteria is the tetrazole-alkene/azirine-alkene cycloaddition (Scheme 4.1 d). Recently reported to result in emissive products,[22] this strategy has been used by Lin *et al.* for protein-polymer conjugation (PEGylation), with reaction of azirine-functional lysozyme and alkene-functional PEG induced by ultraviolet (302 nm) light.[23] Barner-Kowollik and colleagues have also applied this concept to polymer-polymer conjugation both in solution, and for surface functionalisation. In the latter approach, a silicon wafer or cellulose membrane functionalised with tetrazole groups was immersed in a solution of maleimide-terminated PMMA. Irradiation of the solution with ultraviolet (254 nm) light led to grafting of PMMA to the surface. As shown in Figure 4.4 a&b, only the successfully functionalised surface containing the tetrazole/alkene cycloadduct became emissive, while the PMMA provided a hydrophobic coating to the otherwise absorbent cellulose (Figure 4.4 c).[24]

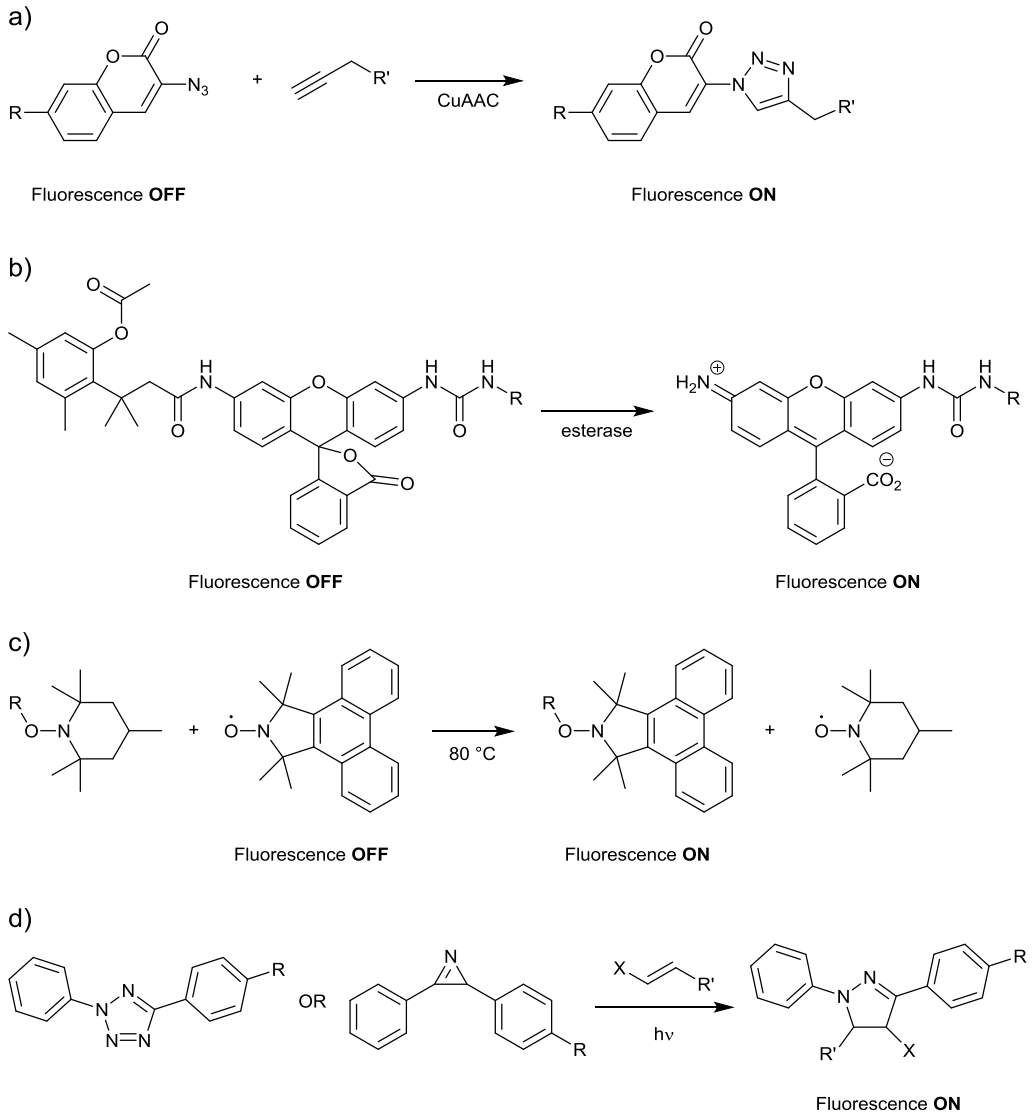

Scheme 4.1. Use of profluorescence in labelling reactions. In each case R represents the macromolecular substrate mentioned in the text.

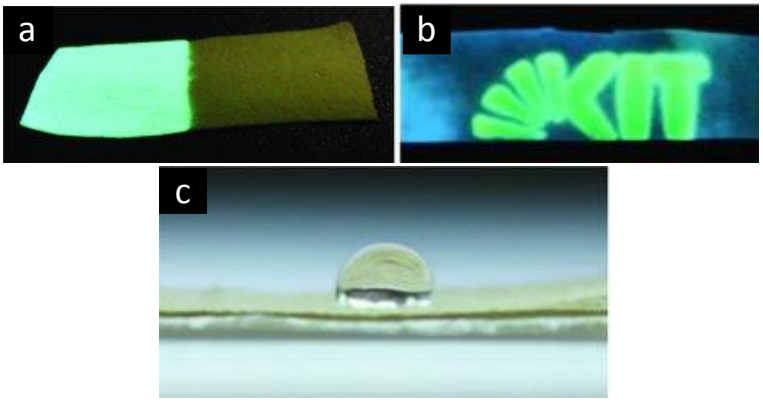

Figure 4.4 a) Photograph under ultraviolet (366 nm) light of a piece of cellulose whose left half has been functionalised with PMMA using the tetrazole/alkene cycloaddition, and b) where selective photoinitiaton was achieved using a foil mask. c) Photograph of a water droplet 10 min after its deposition on a piece of PMMA coated cellulose. Figure adapted from ref.[24]

4.3. Results and discussion

4.3.1. Monomer synthesis

Novel dithiomaleimide (DTM) and dibromomaleimide (DBM) functional methyacrylate, acrylate, and styrenic monomers were prepared according to Scheme 4.2.

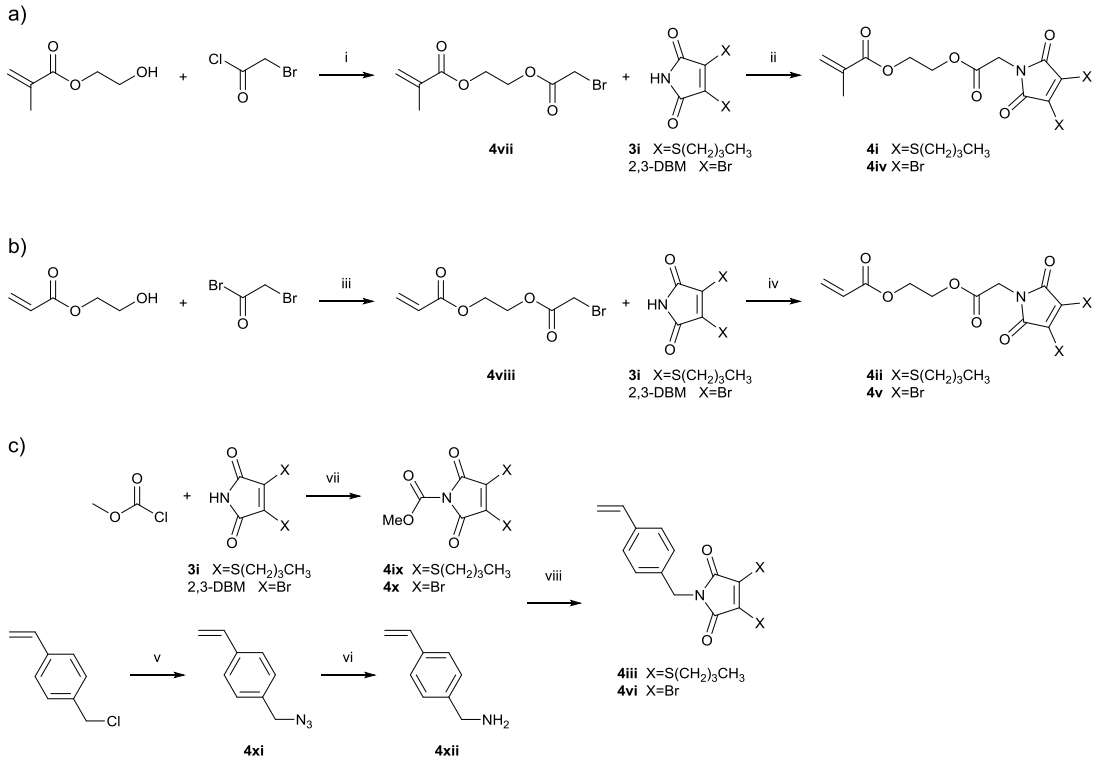

Scheme 4.2. Synthesis of DTM- and DBM-functional methacrylate (a), acrylate (b) and styrenic (c) monomers **4i-4vi**. i) $N(Et)_3$, $CHCl_3$, rt; ii) K_2CO_3, TBAI (0.1 eq), acetone, rt; iii) $N(Et)_3$, THF, rt; iv) K_2CO_3, acetone, rt; v) NaN_3, DMF, rt; vi) $P(Ph)_3$, THF:H_2O 10:1, rt; vii) NMM, THF, rt; viii) DCM, rt.

Dithiomaleimide methacrylate (DTMMA, **4i**), was prepared by alkylation of the *n*-butyl DTM (**3i**), with a bromoacetyl methacrylate (**4vii**) (prepared in one step from (hydroxyethyl)methacrylate). This route was analogous to work in the O'Reilly group on the synthesis of a thymine methacrylate monomer.[25] Formation of the desired product was confirmed by ^{1}H and ^{13}C NMR spectroscopy (Figure 4.5) and HR-MS.

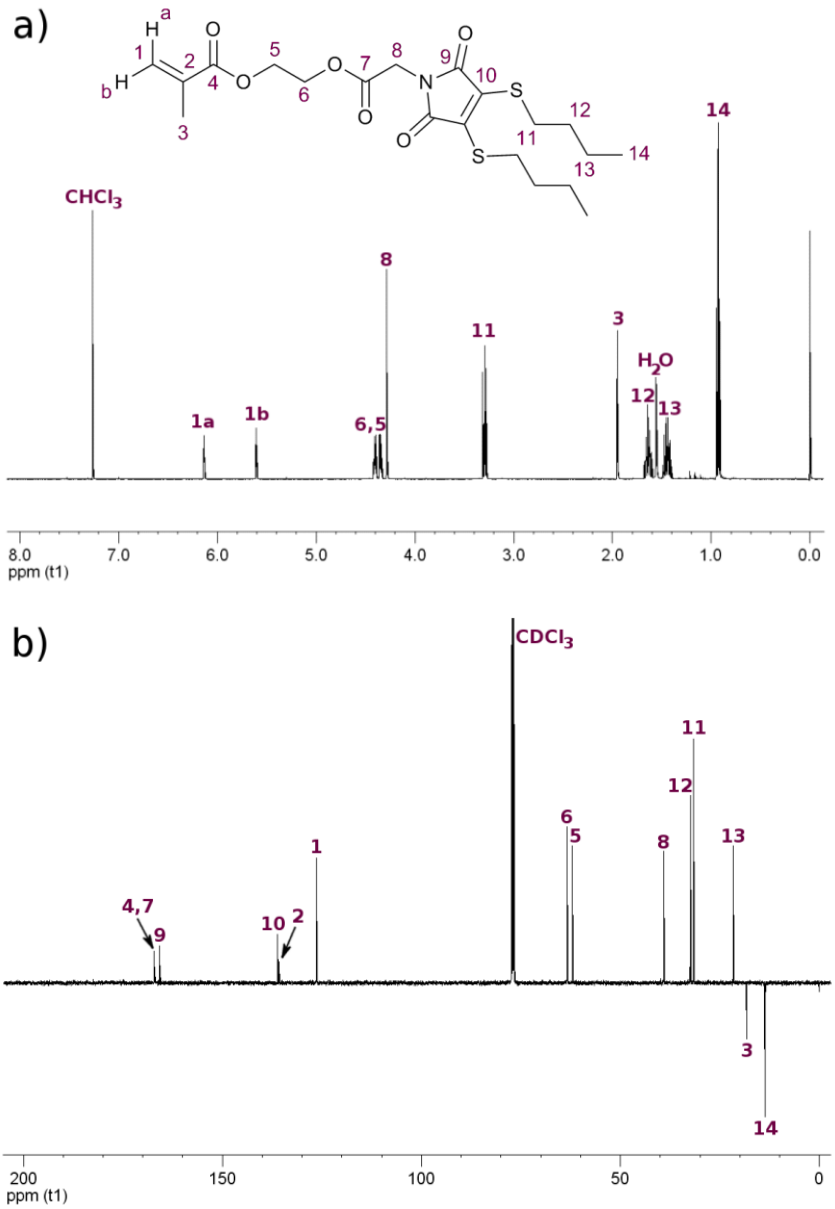

Figure 4.5 a) ^{1}H NMR (400 MHz, $CDCl_3$) spectrum and b) ^{13}C NMR (100 MHz, $CDCl_3$) spectrum for **4i**.

Alkylation of commercially available 2,3-DBM with **4vii** under the same conditions gave the dibromomaleimide methacrylate monomer (DBMMA, **4iv**), as confirmed by ^{1}H and ^{13}C NMR spectroscopy (Figure 4.6), and HR-MS.

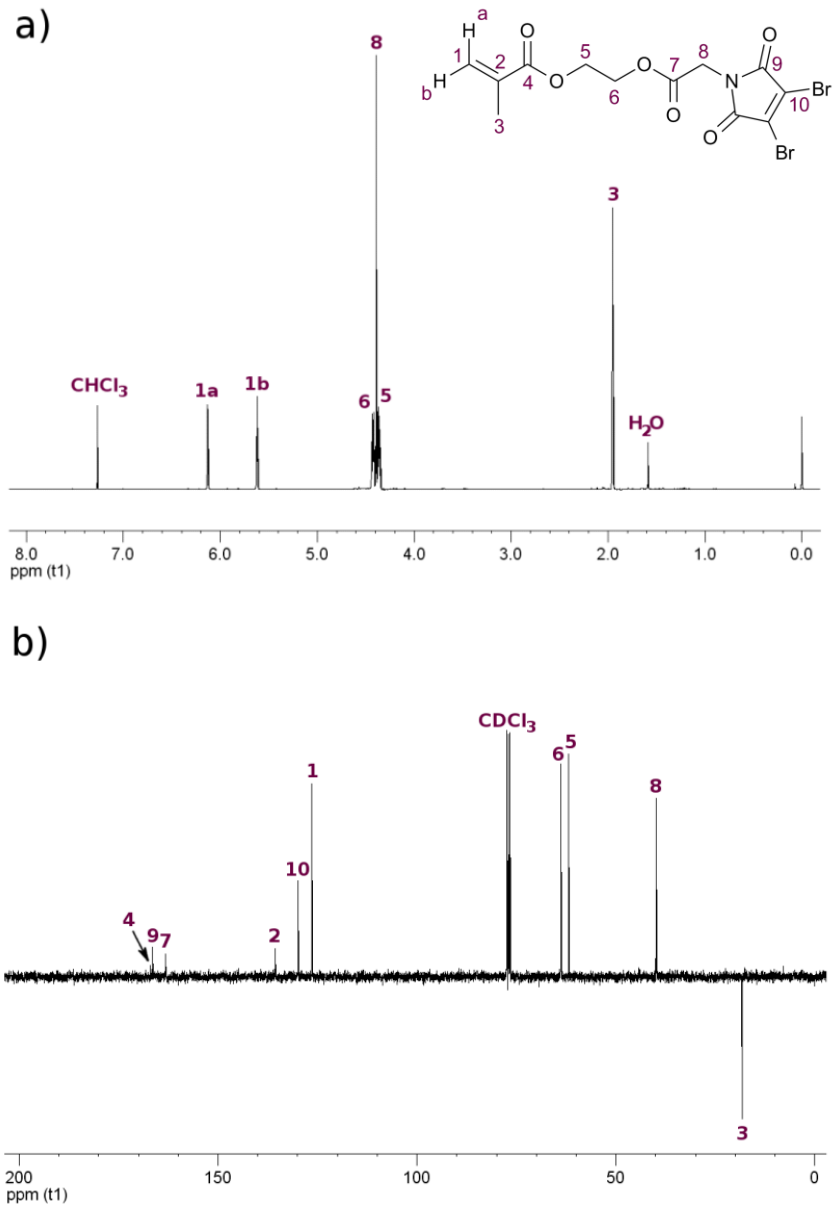

Figure 4.6 a) ^{1}H NMR (400 MHz, $CDCl_3$) spectrum and b) ^{13}C NMR (100 MHz, $CDCl_3$) spectrum for **4iv**.

Similarly, dithiomaleimide acrylate (DTMA, **4ii**) and dibromomaleimide acrylate (DBMA, **4v**) were prepared by the alkylation of **3i** or 2,3-DBM with bromoacetyl acrylate (**4viii**, prepared in one step from hydroxyethyl acrylate according to Liu *et al.*[26]). Formation of the desired products was confirmed by ^{1}H and ^{13}C NMR spectroscopy (Figure 4.7 and Figure 4.8 respectively), and HR-MS.

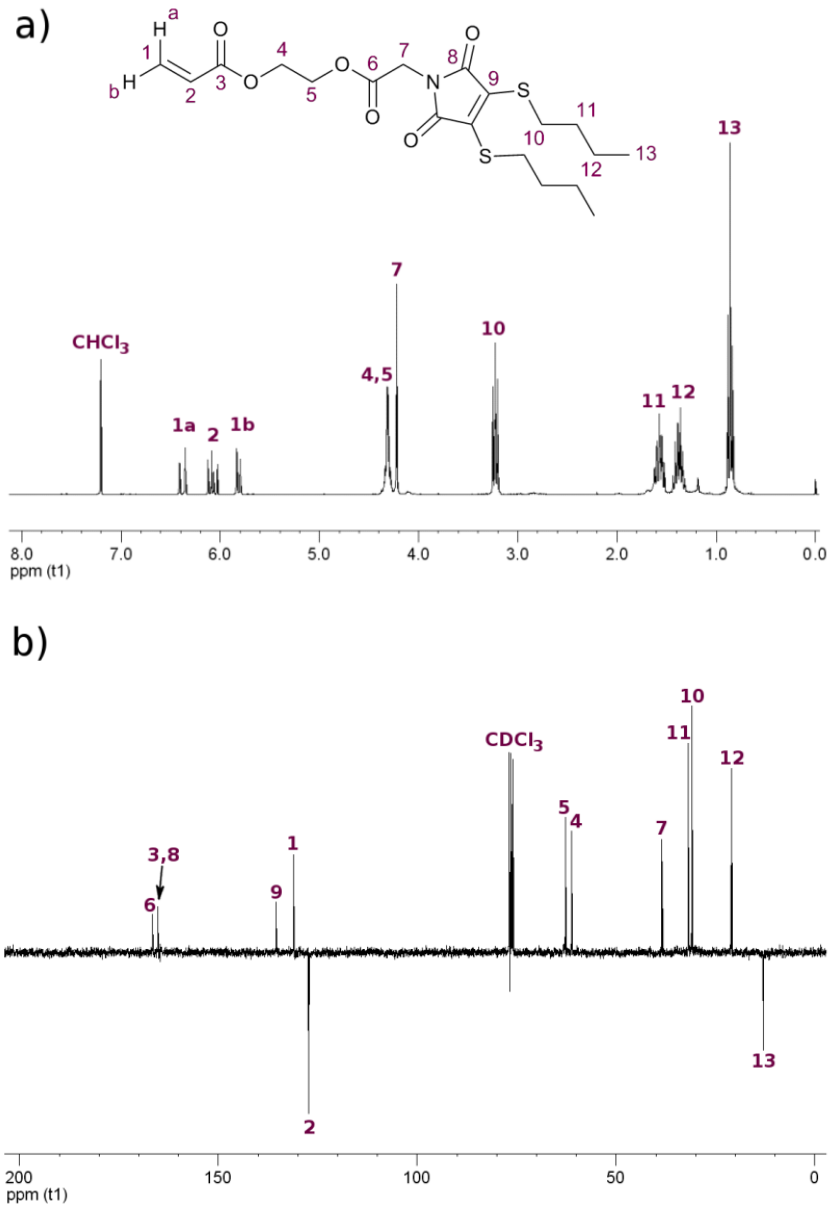

Figure 4.7 a) ^{1}H NMR (300 MHz, $CDCl_3$) spectrum and b) ^{13}C NMR (75 MHz, $CDCl_3$) spectrum for **4ii**.

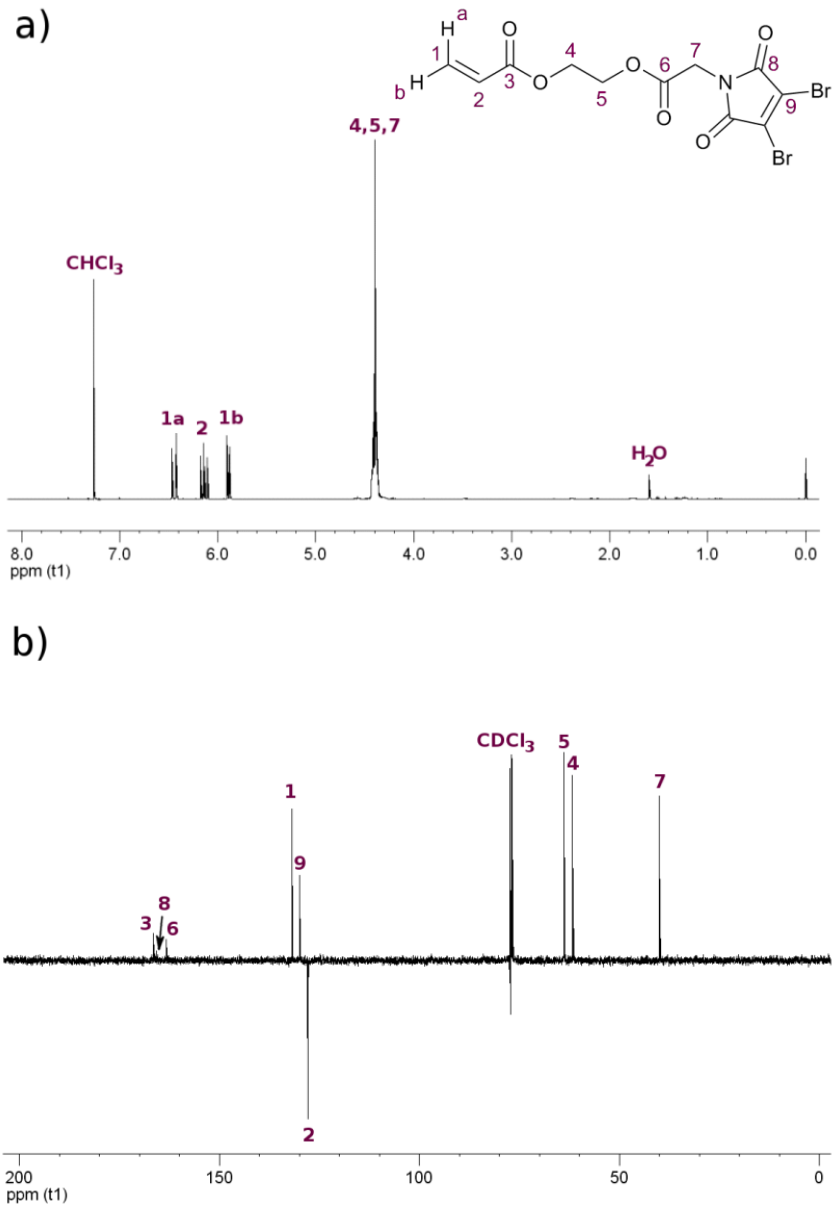

Figure 4.8 a) ^{1}H NMR (400 MHz, $CDCl_3$) spectrum and b) ^{13}C NMR (100 MHz, $CDCl_3$) spectrum for **4v**.

Attempts were made to prepare the styrenic derivatives vinylbenzyl dithiomaleimide (VBDTM, **4iii**) and vinylbenzyl dibromomaleimide (VBDBM, **4vi**) in an analogous method, by alkylation reactions with vinylbenzyl chloride, or vinylbenzyl iodide. However, this proved unsatisfactory with poor conversion in the case of the former, and formation of by-products in the case of the latter. Instead, the styrenic derivatives were prepared following a recently reported route for mild *N*-functionalisation of DTM/DBM *via* an *N*-methoxycarbonylmaleimide intermediate (**4ix**/**4x** respectively).[27] In this case vinylbenzyl amine (**4xii**) was prepared in two steps *via* vinylbenzyl azide (**4xi**) as previously reported,[28] and was used to afford both DTM and DBM derivatives. Formation of the desired

monomers was confirmed by ^{1}H and ^{13}C NMR spectroscopy (Figure 4.9 and Figure 4.10), and HR-MS for **4iii** (**4vi** could not be ionised by electrospray).

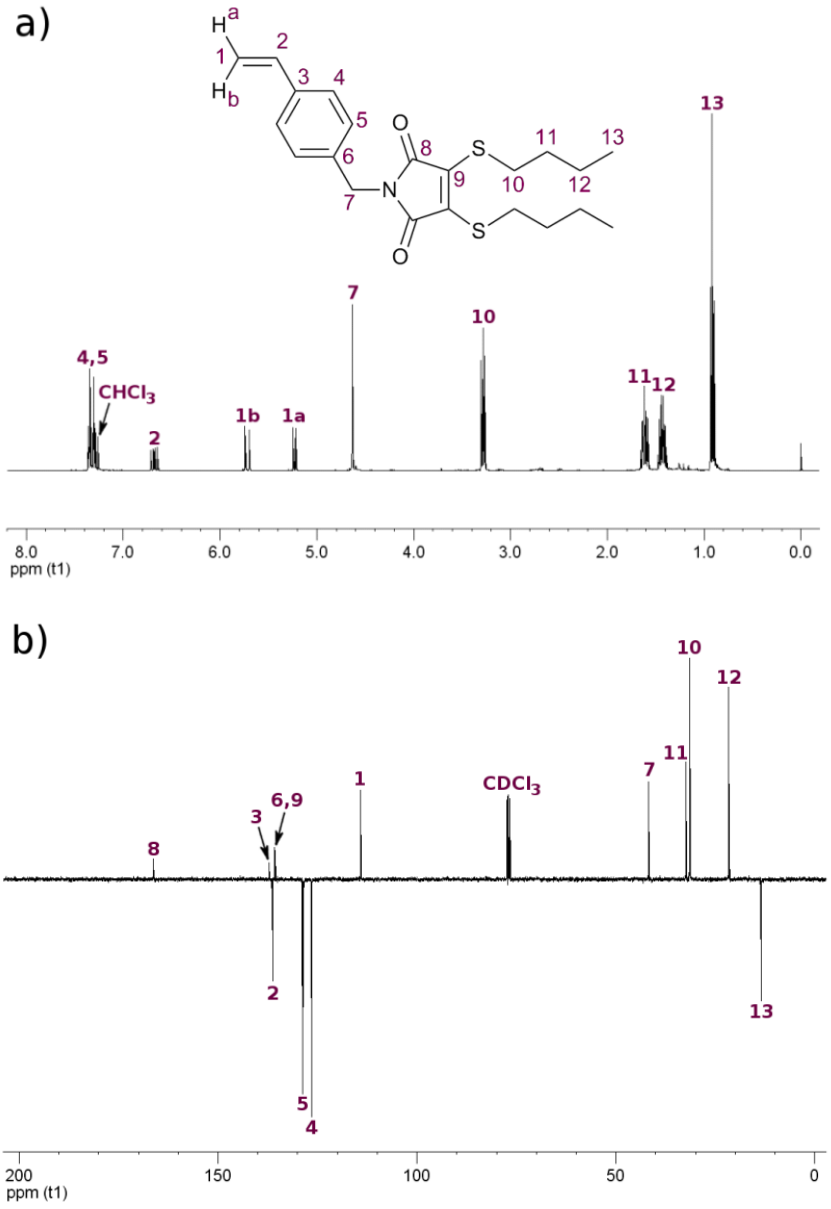

Figure 4.9 a) ^{1}H NMR (400 MHz, $CDCl_3$) spectrum and b) ^{13}C NMR (100 MHz, $CDCl_3$) spectrum for **4iii**.

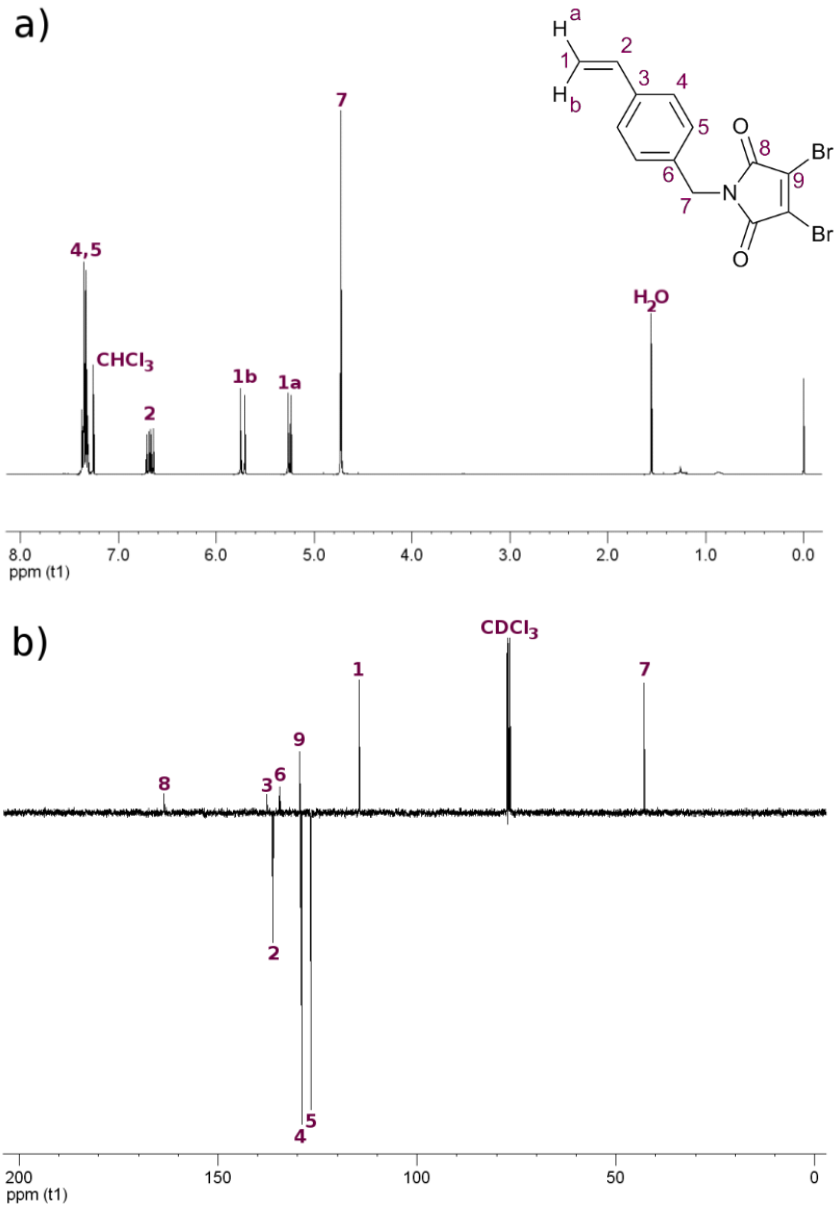

Figure 4.10 a) ^{1}H NMR (400 MHz, $CDCl_3$) spectrum and b) ^{13}C NMR (100 MHz, $CDCl_3$) spectrum for **4vi**.

For the DTM monomers **4i**, **4ii** and **4iii**, fluorescence spectra were very similar to the *n*-butyl DTM precursor **3i**, showing a broad excitation spectra with a maximum at *ca.* 420 nm and corresponding emission at *ca.* 520 nm (Figure 4.11), indicating that functionalization did not have a detrimental effect on the DTM emission.

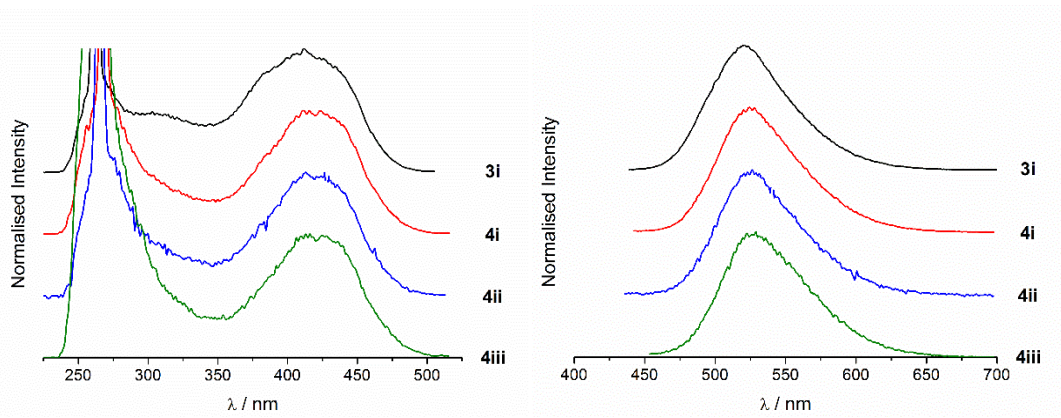

Figure 4.11. Excitation (left) and emission (right) spectra of DTM **3i**, and DTM monomers **4i-4iii** as solutions in $CHCl_3$. Excitation and emission spectra were recorded at the corresponding excitation and emission maxima respectively.

4.3.2. Polymerisation of fluorescent DTM monomers

Polymers containing the DTM fluorophore could be accessed directly by polymerization of the fluorescent DTM monomers. Copolymerization of **4i**, **4ii**, or **4iii** with corresponding non-functional methacrylate, acrylate or styrenic monomers was investigated by RAFT. Commercially available chain transfer agents (CTAs) were used, in each chosen to be appropriate for the class of monomer (methacrylic, acrylic, or styrenic).[4] DTMMA copolymerisations were performed using typical conditions, namely as a solution in 1,4-dioxane, heating at 65 °C, with the radical initiator AIBN, and 2-cyano-2-propyl benzodithioate (**4xiii**) as RAFT agent (Scheme 4.3).

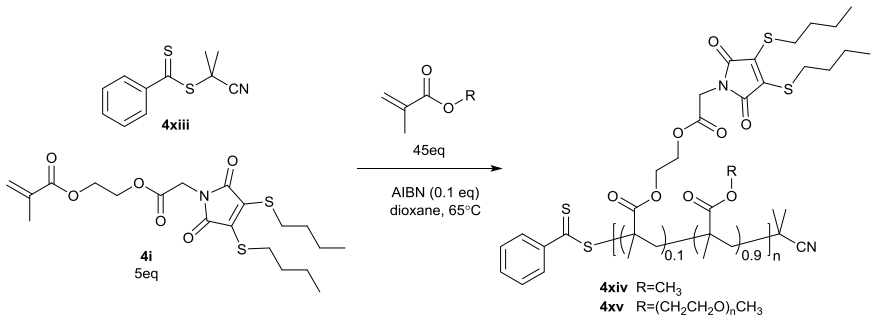

Scheme 4.3. RAFT copolymerisation of DTMMA (**4i**) with MMA (R=CH_3) or OEGMA (R=$(CH_2CH_2O)_nCH_3$)

Copolymerisation with the hydrophobic monomer methyl methacrylate (MMA) at a 10 mol% loading of DTMMA ([CTA]:[MMA]:[DTMMA]:[AIBN] = 1:45:5:0.1) was initially tested (**4xiv**). During the reaction samples were taken for analysis without precipitation or fractionation. The polymerisation displayed linear first order consumption of both

monomers, with conversion being measured by ^{1}H NMR spectroscopy. A linear increase of M_n with conversion (as measured by SEC), and low dispersities throughout ($Đ_M$ <1.2) were also observed, indicating a good control over molecular weight during the polymerisation (Figure 4.12).

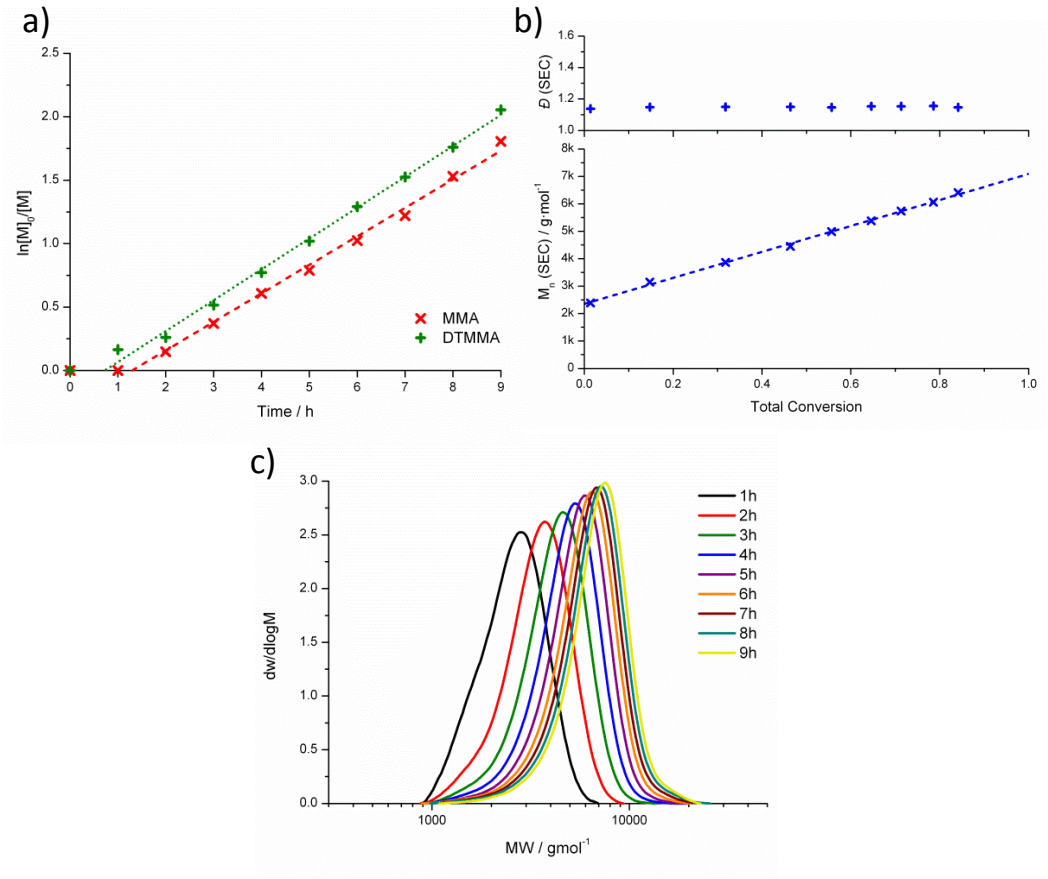

Figure 4.12. DTMMA/MMA copolymerisation **4xiv**; a) First order kinetics of DTMMA and MMA consumption with linear fits; b) M_n and $Đ_M$ (as measured by SEC) as a function of total monomer conversion with linear fit; c) Evolution of molecular weight distribution (as measured by SEC) as a function of time.

Both MMA and DTMMA were consumed at an approximately equivalent rate, to a final conversion at 9 h of $p = 84\%$ for MMA and $p = 87\%$ for DTMMA. The polymer was isolated by precipitation into methanol, with ^{1}H NMR spectroscopy of the purified product revealing incorporation of DTMMA at the expected 10% loading (Figure 4.13).

SEC analysis of the purified polymer indicated a narrow molecular weight distribution ($Đ_M = 1.13$), with incorporation of the DTM functional group and the dithiobenzoate RAFT end-group indicated by absorption maxima at 413 nm and 307 nm respectively, collected using a photodiode array (PDA) detector (Figure 4.14).

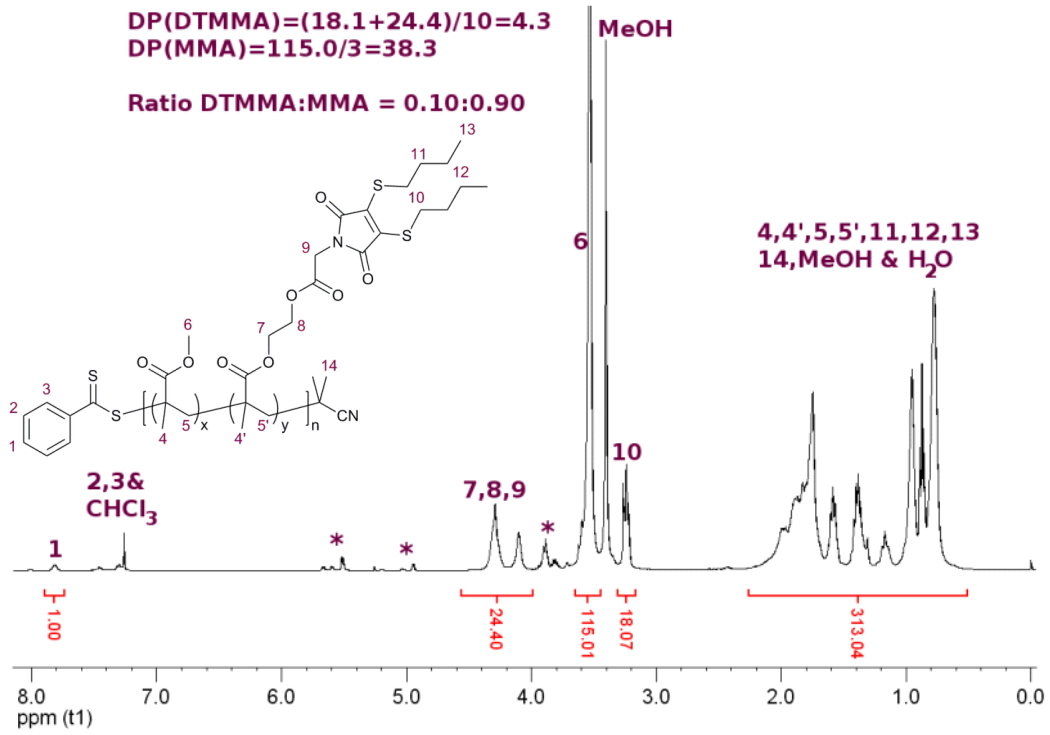

Figure 4.13. ^{1}H NMR (400 MHz, $CDCl_3$) spectrum of **4xiv**. Integration of H1 was set to be equal to 1.00. Peaks marked with * correspond to THF peroxide impurities.

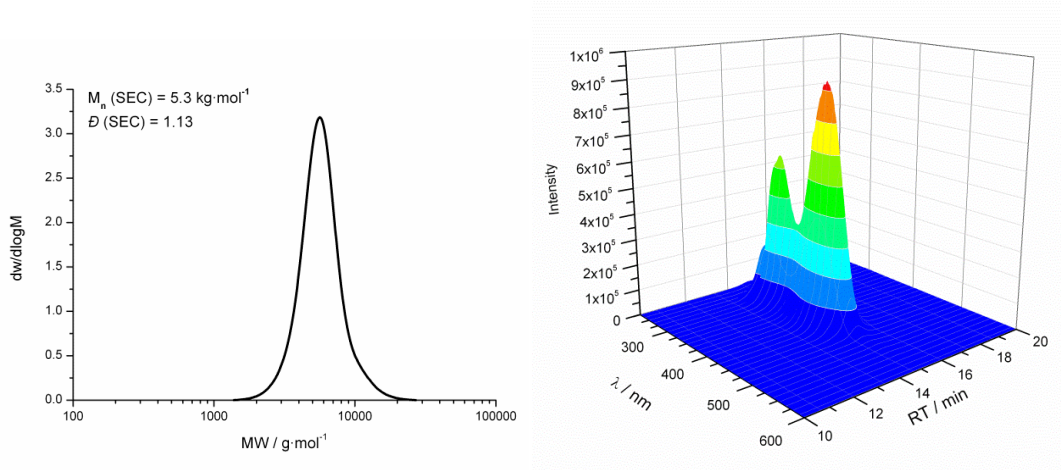

Figure 4.14. SEC molecular weight distribution (left) and three dimensional SEC chromatogram (right) obtained using a PDA detector (right) for **4xiv**.

Characterisation data for polymer **4xiv** is summarised in Table 4.1. The fact that both MMA and DTMMA monomers were consumed at an approximately equivalent rate, that the final polymer had both monomers incorporated at their initial feed ratio, and had a narrow molecular weight distribution, suggests a successful copolymerisation. In order to determine the exact composition it would be necessary to calculate the monomer reactivity ratios for this pair of monomers.[29]

Table 4.1. RAFT copolymers containing DTM-functional monomers **4i-4iii**.

	Monomer feed ratio	Polymer composition[a]	M_n [a] (kDa)	M_n [b] (kDa)	$Đ_M$ [b]	Final monomer conversion [c] (%)	
4xiv	MMA: 0.90 DTMMA: 0.10	P(MMA$_{0.90}$-*co*-DTMMA$_{0.10}$)	6.0	5.3	1.13	MMA 84	DTMMA 87
4xv	OEGMA: 0.90 DTMMA: 0.10	P(OEGMA$_{0.90}$-*co*-DTMMA$_{0.10}$)	10.5	7.8	1.23	OEGMA 80	DTMMA 86
4xvi	^{t}BA: 0.90 DTMA: 0.10	P(^{t}BA$_{0.91}$-*co*-DTMA$_{0.09}$)	8.2	5.6	1.24	^{t}BA 88	DTMA 82
4xvii	TEGA: 0.90 DTMA: 0.10	P(TEGA$_{0.90}$-*co*-DTMA$_{0.10}$)	8.6	4.7	1.25	TEGA 83	DTMA 80
4xviii	Sty: 0.91 VBDTM: 0.09	Hb-P(Sty$_{0.90}$-*co*-DTMA$_{0.10}$)[d]	—[e]	1.7[f]	2.89[f]	Sty 62	VBDTM 76

[a] Calculated by ^{1}H NMR spectroscopy end-group analysis using dithiobenzoate Ph-H or dodecyltrithiocarbonate CH$_3$, [b] Measured by SEC, [c] Calculated by ^{1}H NMR spectroscopy [d] Hyperbranched polymer, [e] No unique end-group signals in ^{1}H NMR spectrum, [f] Universal calibration.

Copolymerisation of DTMM with the hydrophilic monomer oligoethylene glycol methacrylate (OEGMA, M_n = 300 Da) at a 10 mol% loading of DTMMA ([CTA]:[OEGMA]:[DTMMA]:[AIBN] = 1:45:5:0.1) was also investigated (**4xv**). The polymerisation again displayed linear first order consumption of both monomers, with a linear increase of M_n with conversion (as measured by SEC), and low dispersities throughout ($Đ_M$ <1.3), indicating a good control over molecular weight during the polymerisation (Figure 4.15).

Both OEGMA and DTMMA were consumed at an approximately equivalent rate, to a final conversion at 9 h of p = 80% for OEGMA and p = 86% for DTMMA. The polymer was isolated by dialysis, with ^{1}H NMR spectroscopy of the purified product revealing incorporation of DTMMA at the expected 10 mol% loading (Figure 4.16).

SEC analysis of the purified polymer indicated a narrow molecular weight distribution ($Đ_M$ = 1.23, Figure 4.17). A small high molecular weight shoulder was observed, which may be due to transfer or polymer-polymer coupling in the later stages of polymerisation[30] (shoulder observed in 7, 8 and 9 h molecular weight distributions in Figure 4.15). Again, SEC with a PDA detector indicated incorporation of the DTM functional group and the dithiobenzoate RAFT end-group due to absorbance of the polymer.

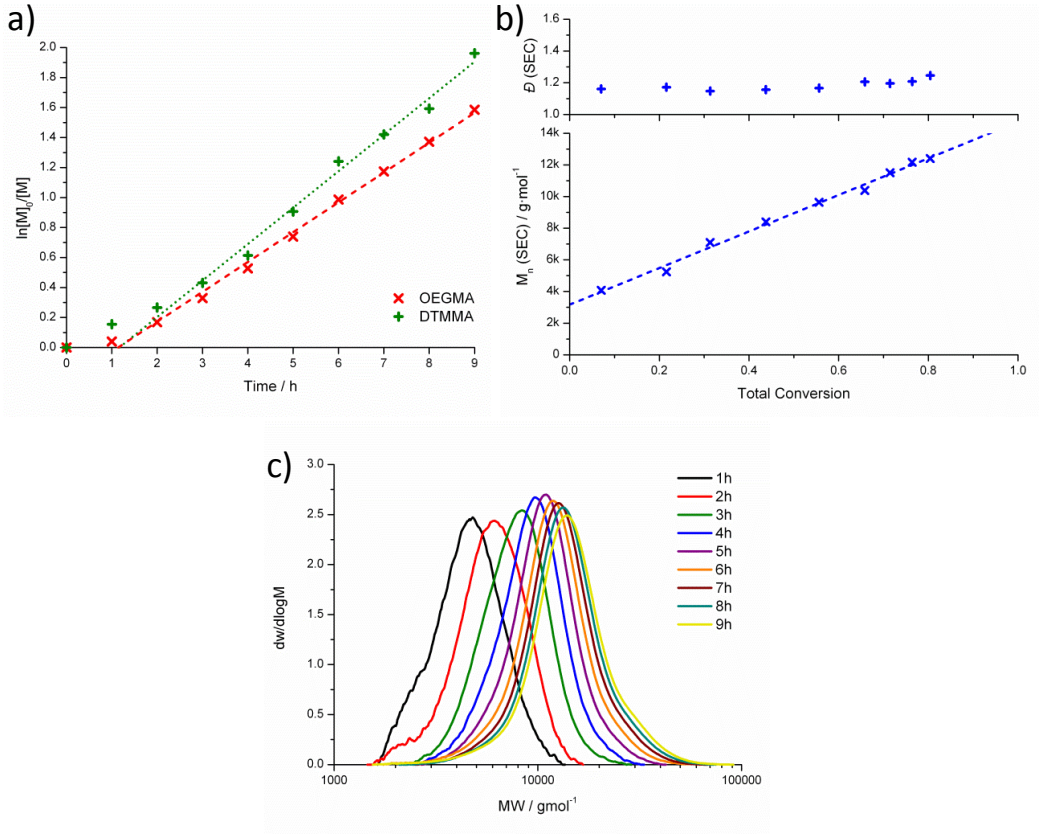

Figure 4.15. DTMMA/OEGMA copolymerisation **4xv**; a) First order kinetics of DTMMA and OEGMA consumption with linear fits; b) M_n and $Đ_M$ (as measured by SEC) as a function of total monomer conversion with linear fit; c) Evolution of molecular weight distribution (as measured by SEC) as a function of time.

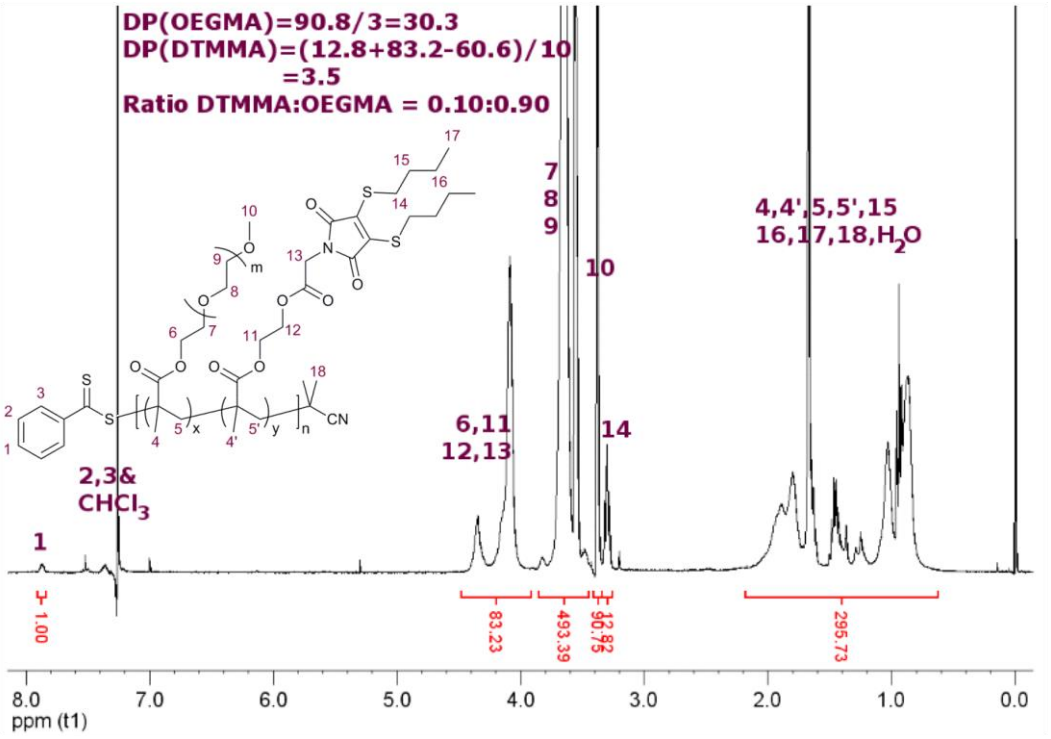

Figure 4.16. ^{1}H NMR (400 MHz, $CDCl_3$) spectrum of **4xv**. Integration of H1 was set to be equal to 1.00.

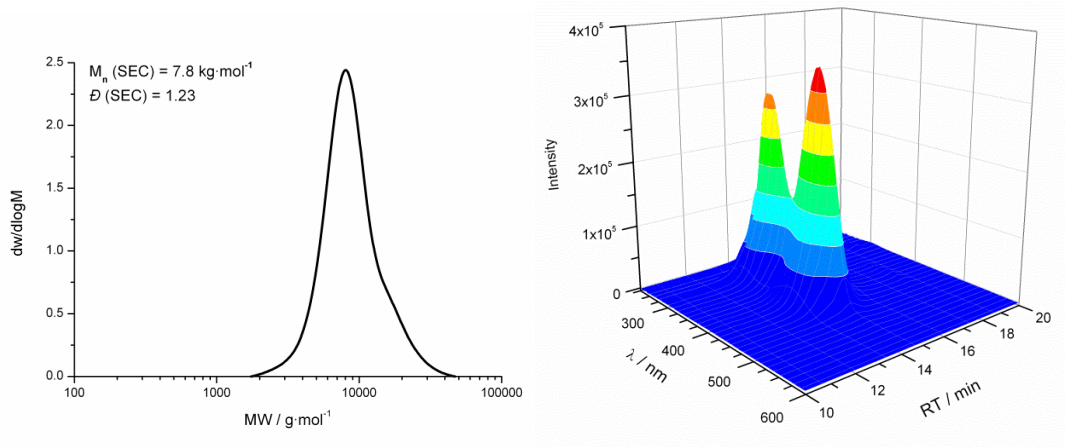

Figure 4.17. SEC molecular weight distribution (left) and three dimensional SEC chromatogram (right) obtained using a PDA detector (right) for **4xv**.

Despite the choice of a hydrophobic *n*-butyl thiol group in the DTMMA monomer, **4xv** retained its water solubility and thermoresponsive behaviour. The cloud point of **4xv** in water (18.2·MΩ·cm) was measured at 10 g/L by temperature-dependant light transmission as the average temperature corresponding to a normalised transmission of 0.5 from three heating/cooling cycles. For the heating cycles $T_c = 50.2 \pm 0.0$ °C, and for the cooling cycles $T_c = 50.0 \pm 0.1$ °C (Figure 4.18), demonstrating the expected lack of hysteresis.[31] An analogous homopolymer of POEGMA (**4xix**, $M_n = 10.1$ kDa, $Đ_M = 1.20$) was found to have $T_c = 65.8 \pm 0.0$ °C and 65.7 ± 0.1 °C for heating and cooling respectively, indicating that copolymerisation with DTMMA had caused an increase in hydrophobicity.

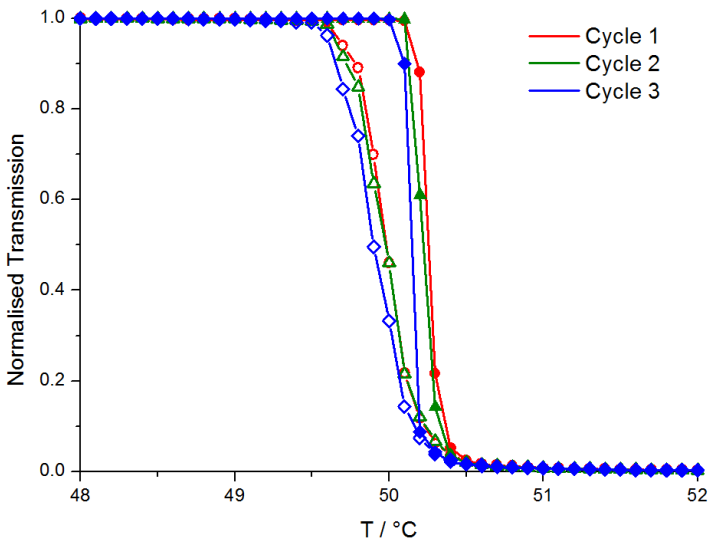

Figure 4.18. Temperature-dependent light transmission for a solution of **4xv** in water (10 g/L). Closed symbols represent heating cycles and open symbols represent cooling cycles.

Similar results were seen in the copolymerisation of DTMA (**4ii**) with the hydrophobic acrylic monomer ^{t}BA, and the hydrophilic acrylic monomer TEGA, with cyanomethyl dodecyl trithiocarbonate (**4xx**) as RAFT agent. In both cases a 10 mol% loading of DTMA was used, and polymerisations were conducted as a solution in 1,4-dioxane, heating at 65 °C, with the radical initiator AIBN, ([CTA]:[^{t}BA or TEGA]:[DTMA]:[AIBN] = 1:45:5:0.1) according to Scheme 4.4.

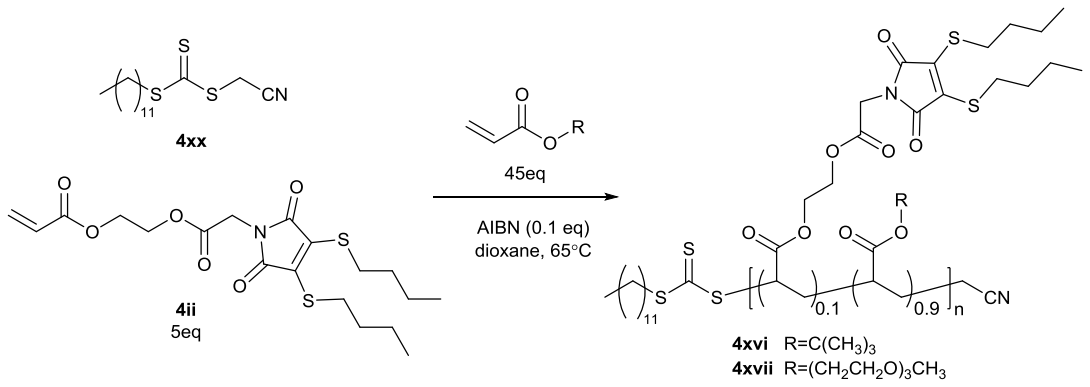

Scheme 4.4. RAFT copolymerisation of DTMA (**4ii**) with ^{t}BA (R=C(CH$_3$)$_3$) or TEGA (R=(CH$_2$CH$_2$O)$_3$CH$_3$)

In each case, the polymerisations displayed linear first order consumption of both monomers at an approximately equivalent rate. Final monomer conversions were $p_{\mathrm{DTMA}} = 82\%$ and $p_{\mathrm{tBA}} = 88\%$ for **4xvi**, and $p_{\mathrm{DTMA}} = 80\%$ and $p_{\mathrm{TEGA}} = 83\%$ for **4xvii**. A linear increase of M_{n} with conversion (as measured by SEC) was observed, with low dispersities throughout ($Đ_{\mathrm{M}} < 1.3$), indicating a good control over molecular weight during the polymerisation (Figure 4.19).

These copolymerisations were significantly slower than homopolymerisation of either ^{t}BA or TEGA under the same conditions, which reached $p > 90\%$ within 2 h and 4 h respectively. This could be result of increased viscosity of the reaction mixture due to addition of DTMA. Consideration of the retardation effect caused by DBM in RAFT polymerisation of acrylates is elaborated on in Chapter 6.

^{1}H NMR spectroscopy of polymers **4xvi** and **4xvii** confirmed incorporation of DTMA at 9 and 10 mol% respectively, compared to the monomer feed of 10 mol% DTMA (Figure 4.20 and Figure 4.21). SEC analysis of the purified polymers indicated narrow molecular weight distributions ($Đ_{\mathrm{M}} = 1.24$ for **4xvi** and $Đ_{\mathrm{M}} = 1.25$ for **4xvii**, Figure 4.22). Again,

SEC with a PDA detector indicated incorporation of the DTM functional group and the trithiocarbonate RAFT end-group by the absorbance of the polymer.

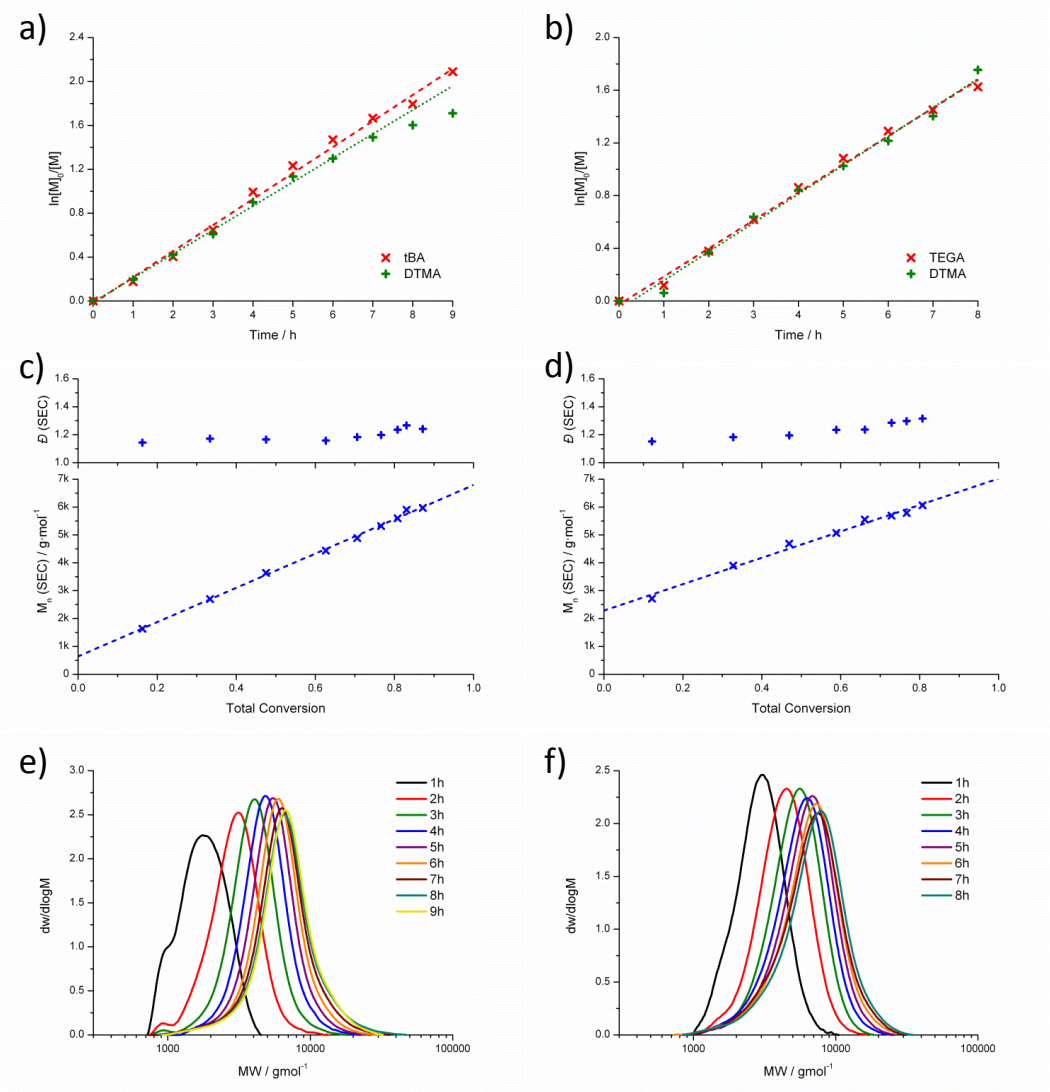

Figure 4.19. DTMA/^{t}BA copolymerisation **4xvi** (left) and DTMA/TEGA copolymerisation **4xvii** (right); a&b) First order kinetics of DTMA and ^{t}BA/TEGA consumption with linear fits; c&d) M_n and $Đ_M$ (as measured by SEC) as a function of total monomer conversion with linear fits; e&f) Evolution of molecular weight distribution (as measured by SEC) as a function of time.

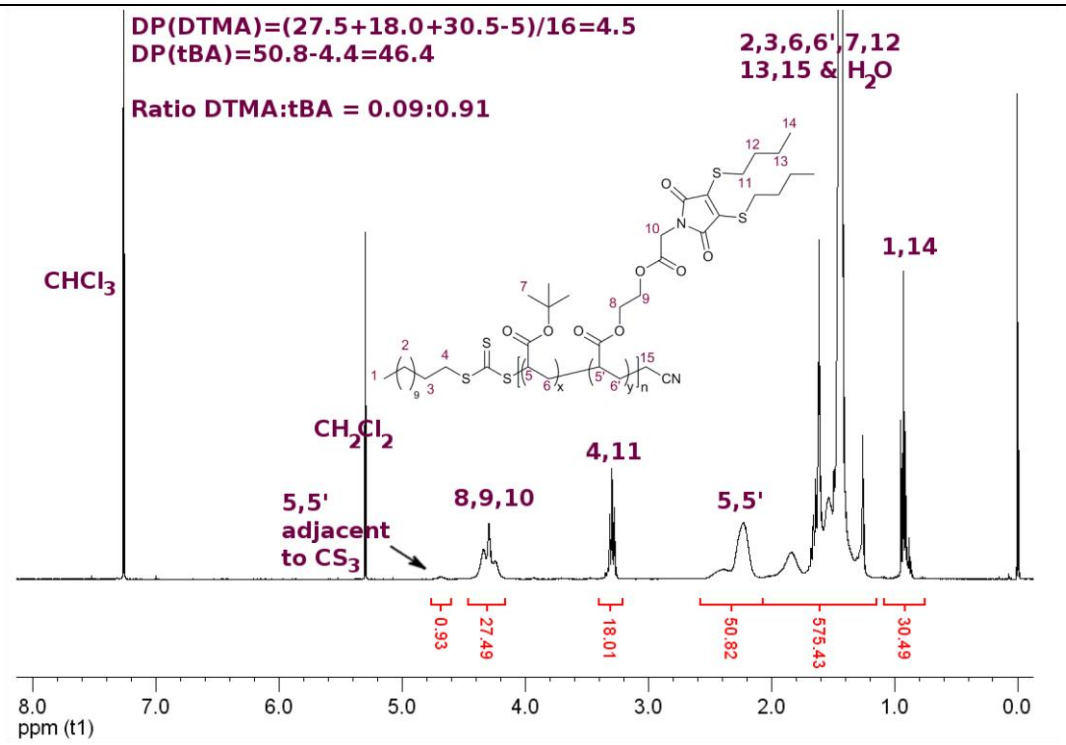

Figure 4.20. ^{1}H NMR (400 MHz, $CDCl_3$) spectrum of **4xvi**. Integration of H1 & H14 was set to be equal to integration of H8, H9 & H10 + 3.00.

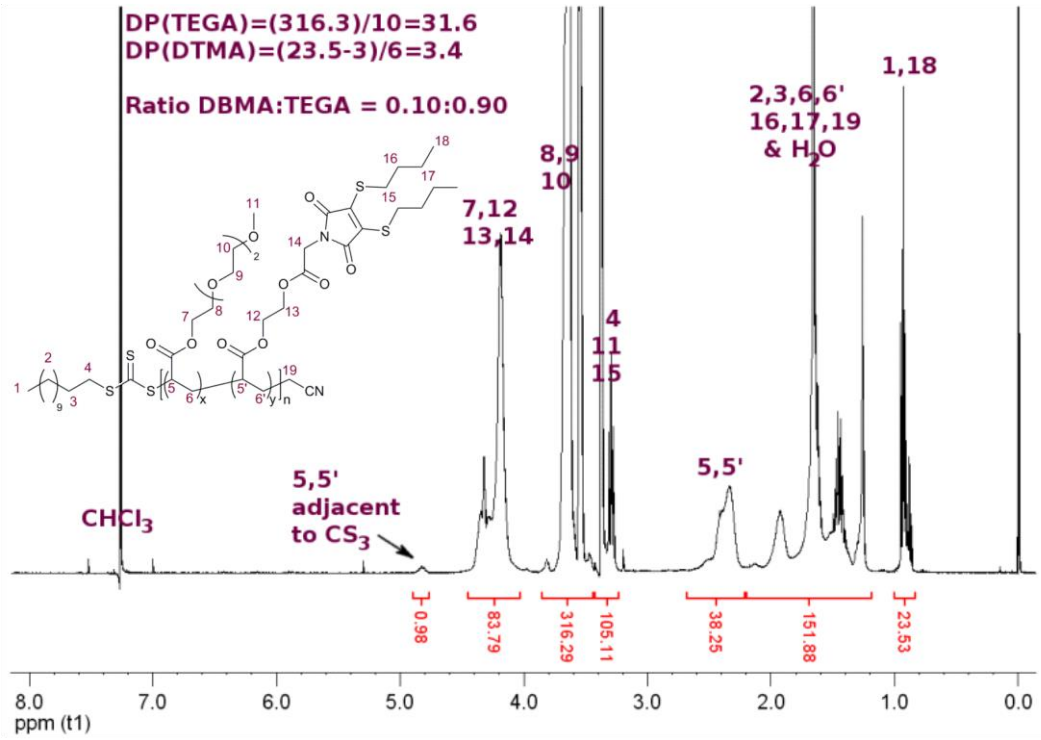

Figure 4.21. ^{1}H NMR (400 MHz, $CDCl_3$) spectrum of **4xvii**. Integrations for end-group analysis were calculated by simultaneous equation.

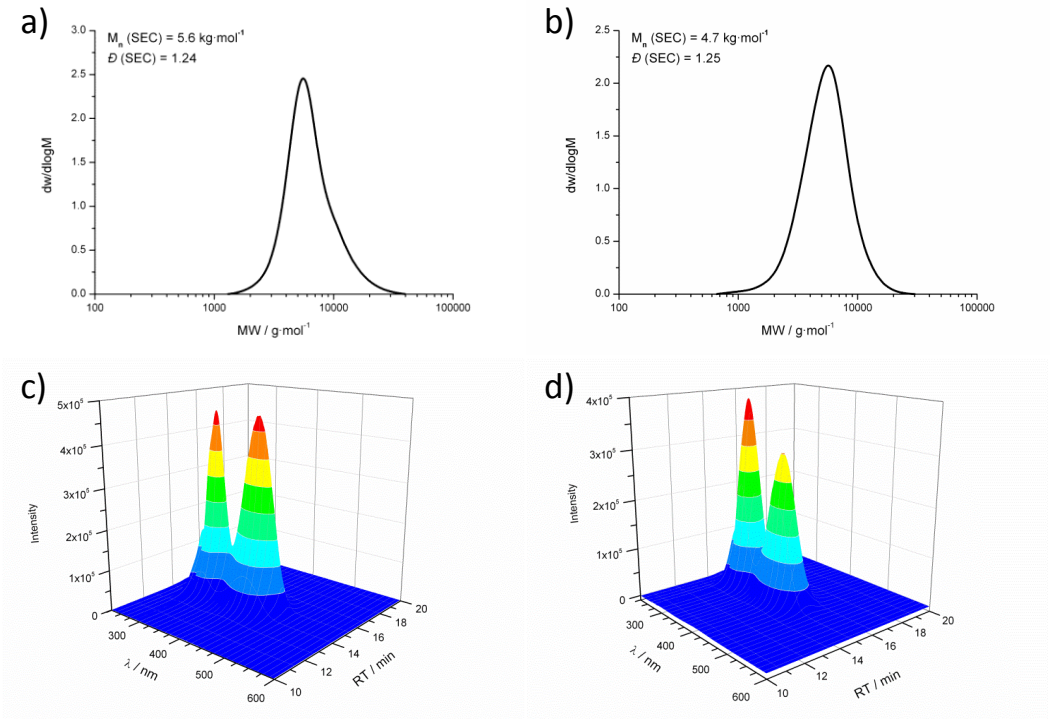

Figure 4.22. SEC molecular weight distribution of a) **4xvi**; b) **4xvii**. Three dimensional SEC chromatogram obtained using a PDA detector for c) **4xvi**; d) **4xvii**.

Like POEGMA, PTEGA is also a thermoresponsive polymer, with a PTEGA homopolymer (**4xxi**, $M_n = 10.0$ kDa, $Đ_M = 1.17$) prepared by RAFT having $T_c = 65.5 \pm 0.0$ °C (heating cycle) and 65.2 ± 0.0 °C (cooling cycle) when dissolved in water (18.2·MΩ·cm) at a concentration of 10 g/L. The P(TEGA-*co*-DTMA) copolymer **4xvii** was found to be water soluble, with $T_c = 37.3 \pm 0.3$ °C during the heating cycle, and 36.9 ± 0.2 °C for the cooling cycle (Figure 4.23). While **4xvii** and **4xxi** are not precisely matched in molecular weight ($M_n = 8.6$ kDa and 10.0 kDa respectively), it has been previously reported that PTEGA cloud point has a weak dependence on M_n in this range (< 5 °C),[32] suggesting that the introduction of the hydrophobic DTMA monomer has caused a decrease in T_c, as was observed for DTMMA.

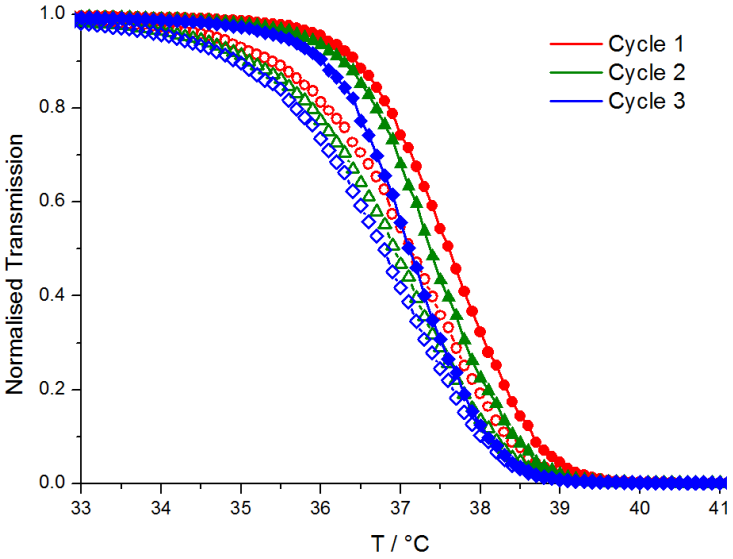

Figure 4.23. Temperature-dependent light transmission for a solution of **4xvii** in water (10 g/L). Closed symbols represent heating cycles and open symbols represent cooling cycles.

Copolymerisation of VBDTM (**4iii**) with styrene in bulk at 110 °C (thermal initiation)[33] using the RAFT agent 2-cyano-2-propyl dodecyl trithiocarbonate (**4xxii**) was investigated. As styrene was acting as solvent, the monomer loadings were increased relative to methacrylate and acrylate polymerisations, to give reaction mixture composition of ([CTA]:[Sty]:[VBDTM] = 1:100:10). The reaction proceeded with linear first order consumption of both monomers for 6 h, after which point the reaction medium became too viscous to stir, and monomer consumption halted (Figure 4.24). Although a linear increase of molecular weight with total monomer conversion was observed, dispersity also increased with p as the molecular weight distributions became increasingly broad and multimodal. Furthermore between 6 h and 7 h while there was no change in monomer conversion, M_n increased and a clear shift in molecular weight distribution was observed.

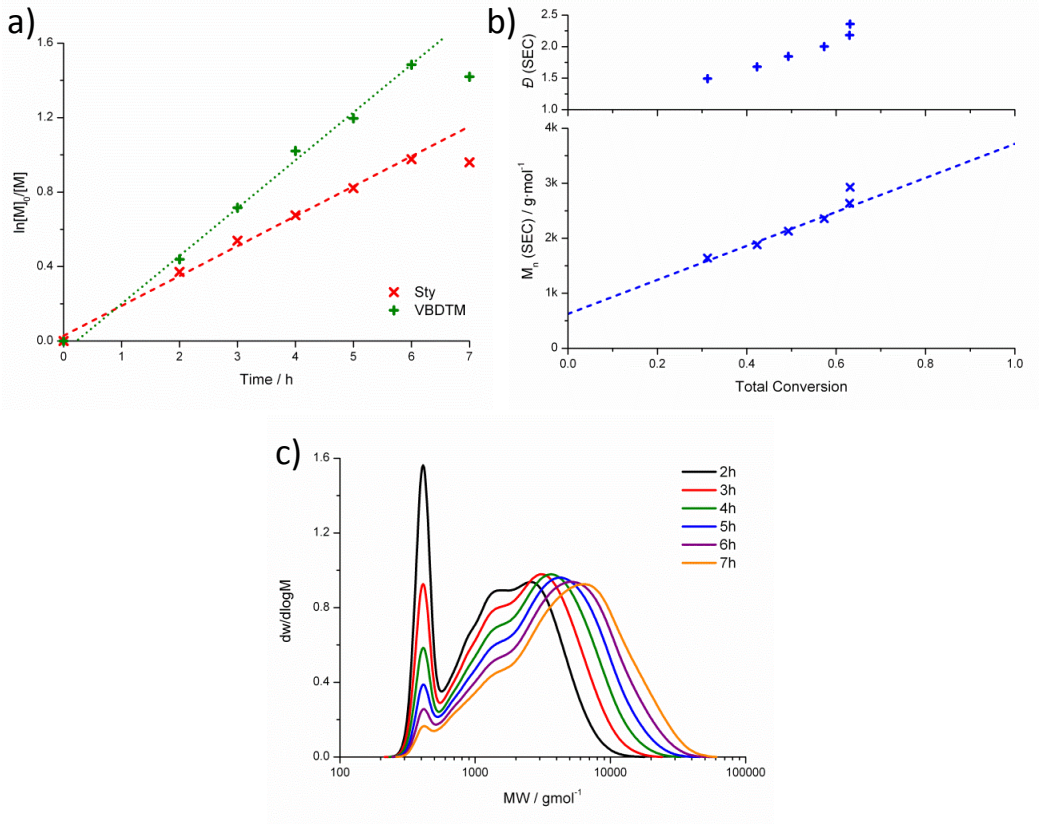

Figure 4.24. VBDTM/Sty copolymerisation **4xviii**; a) First order kinetics of VBDTM and Sty consumption with linear fits; b) M_n and $Đ_M$ (as measured by SEC) as a function of total monomer conversion with linear fit; c) Evolution of molecular weight distribution (as measured by SEC) as a function of time.

Multimodal molecular weight distributions are often indicative of branching, and this was confirmed using SEC with a viscometry detector. The polymer was isolated and purified by repeated precipitation into MeOH/H_2O, then analysed by SEC. The Mark-Houwink plot ($\ln[\eta]$ *vs.* $\ln[MW]$ where η is the intrinsic viscosity measured by the visometry detector and MW is the molecular obtained by a Universal Calibration) had a gradient (α) of 0.31 (Figure 4.25). In comparison to linear poly(styrene) which had $\alpha = 0.64$ under the same SEC conditions, this lower value indicates that **4xviii** had a more contracted morphology in solution than the linear analogue, which is the result of branching. SEC analysis using a PDA detector also revealed incorporation of the DTM functional group and the trithiocarbonate RAFT end-group from the absorbance of the polymer.

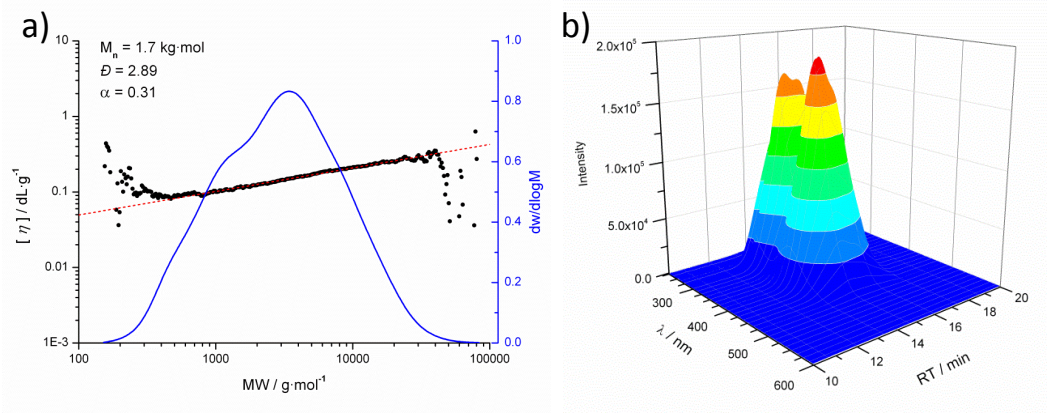

Figure 4.25. a) SEC molecular weight distribution and Mark-Houwink plot and b) Three dimensional SEC chromatogram obtained using a PDA detector for **4xviii**.

^{1}H NMR spectroscopy of polymer **4xviii** suggested that branching was due to polymerization of the DTM C=C double bond (Scheme 4.5). Resonances attributed to polystyrene (A units), VBDTM that had polymerized through both vinyl and maleimide C=C double bond (B units), as well as VBDTM where only maleimide or vinyl C=C double bonds had reacted (C and D units respectively) were assigned (Figure 4.26).

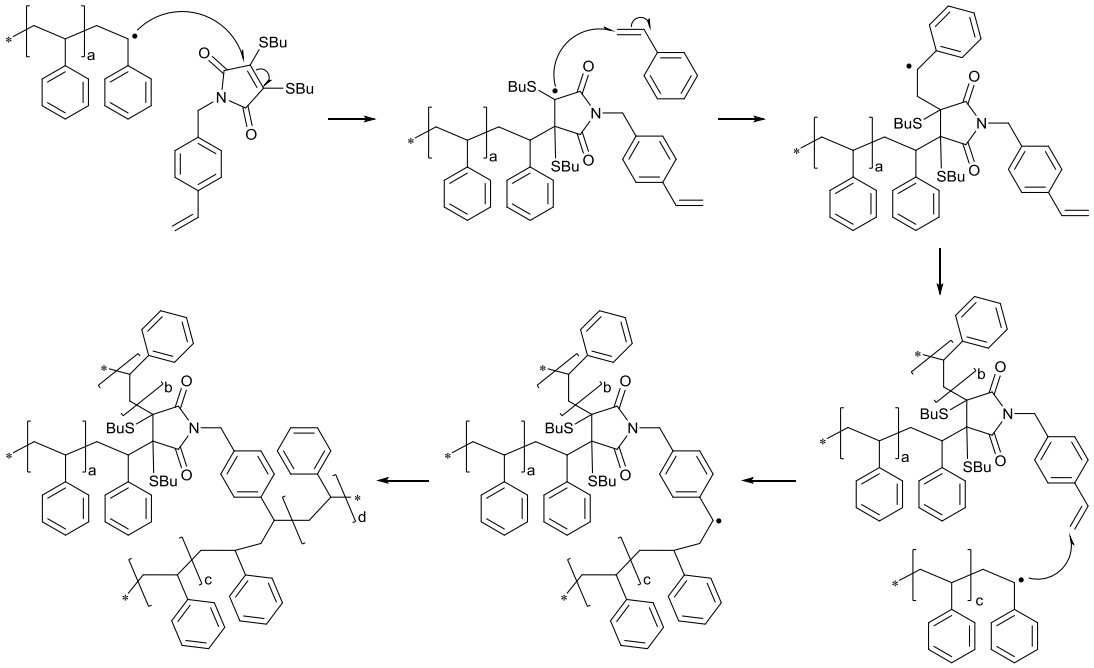

Scheme 4.5. Formation of branch points during the Sty/VBDTM polymerisation due to polymerisation of the DTM C=C double bond.

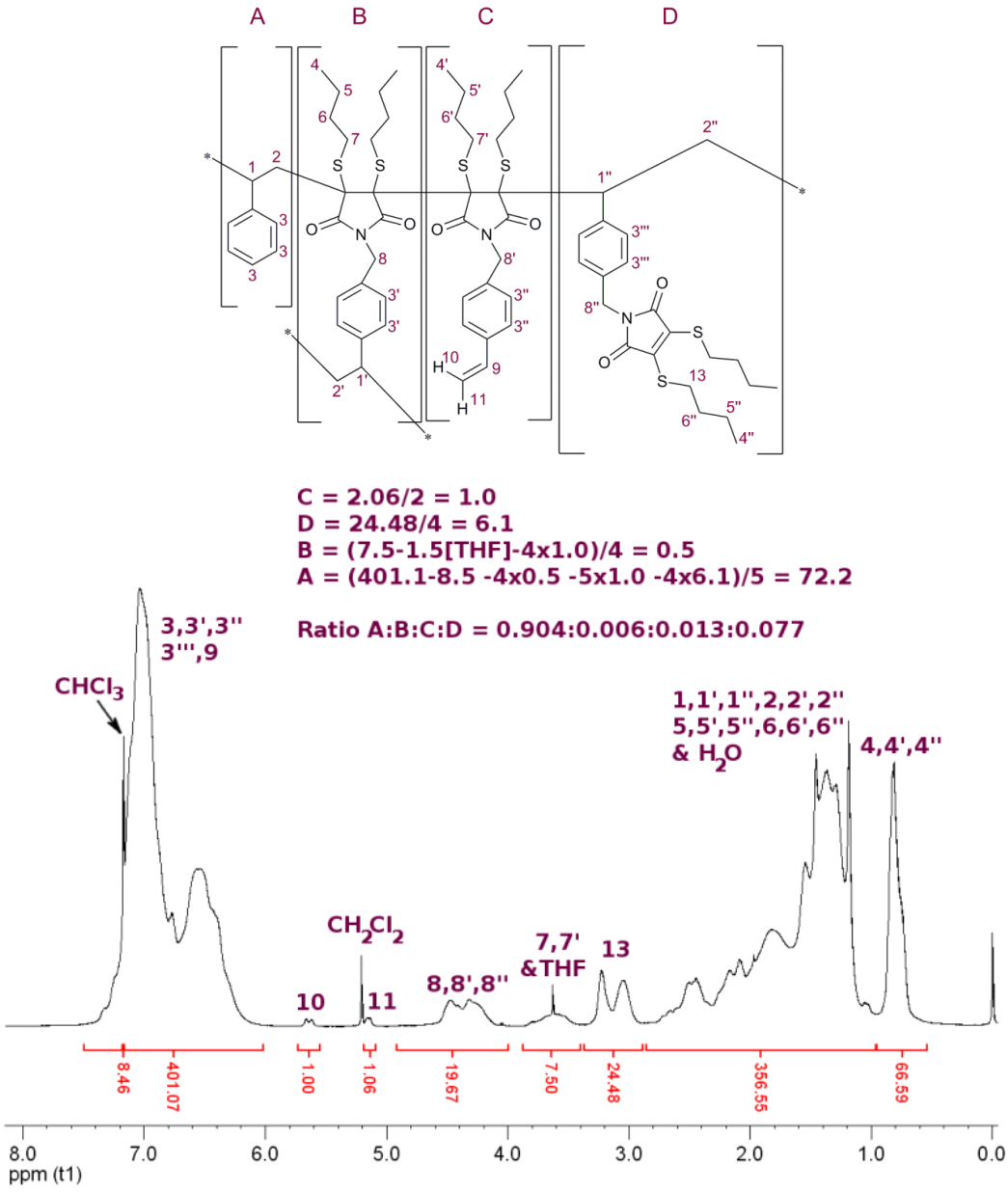

Figure 4.26. ^{1}H NMR (400 MHz, $CDCl_3$) spectrum of **4xviii**. Integration of H10 was set to be equal to 1.00.

Although absolute *DP* could not be calculated due to the lack of unique end-group resonances, the ratio of the different units A:B:C:D could be calculated. Resonances due to the unreacted vinyl group of C units were seen at 5.1 and 5.6 ppm, with these peaks being broader than those for the monomer **4iii**. A broad peak from 2.9-3.3 ppm was attributed to S$\underline{CH_2}$ of the DTM groups of the D units, in accordance with the other DTM-containing polymers **4xiv-4xvii**. A peak just downfield at 3.8-3.4 was assigned to these S$\underline{CH_2}$ protons in B and C units, where loss of the maleimide conjugation had increased the electron withdrawing nature of the S. Together this gives A:B:C:D = 0.904:0.006:0.013:0.077, which is reasonable, as it suggests an approximate 10:1 Sty:VBDTM ratio in accordance

with monomer feed. It also indicates that 80% of VBDTM units polymerised through their vinyl bond as desired, 13% polymerised through the maleimide C=C double bond, and 7% through both bonds. The fact that 80% of DTM units survived intact explains the observed fluorescence of the product **4xviii**. The difference in reactivity between the maleimide C=C double bonds of **4i**, **4ii**, and **4iii** is explored further in Chapter 6.

The fluorescence spectra of polymers **4xiv-4xviii** as solutions in $CHCl_3$ (Figure 4.27) were nearly identical, displaying $\lambda_{ex,max}$ = 415 nm and $\lambda_{em,max}$ = 525 nm. The spectra were very similar to that of the DTM monomers, indicating that no adverse effects on DTM fluorescence are caused by incorporation into a polymeric structure, in line with previous observations for end-group labelled polymers in Chapter 3.

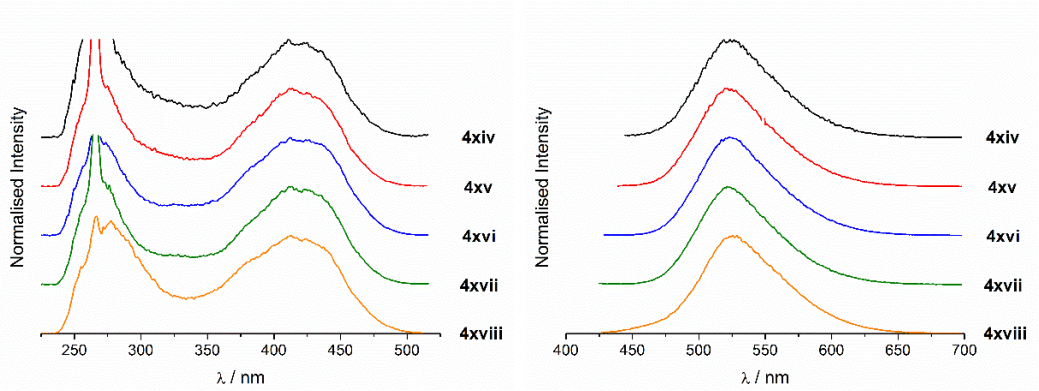

Figure 4.27. Excitation (left) and emission (right) spectra of DTM-functional polymers **4xiv-4xviii** as solutions in $CHCl_3$. Excitation and emission were measured at λ_{em} = 525 nm and λ_{ex} = 415 nm respectively.

4.3.3. Polymerisation of profluorescent DBM monomers

Copolymerisations of the profluorescent DBM methacrylate monomer (DBMMA, **4iv**) with MMA (**4xxiii**) and OEGMA (**4xxiv**) by RAFT were investigated. Polymerisations were performed with the dithiobenzoate RAFT agent **4xiii**, as a 1,4-dioxane solution, at 65 °C, with [CTA]:[AIBN]:[MMA or OEGMA]:[DBMMA] = 1:0.1:45:5 according to Scheme 4.6.

Copolymerisations with both MMA and OEGMA displayed linear first order consumption of both monomers at an approximately equivalent rate. Final monomer conversions were p_{DBMMA} = 90% and p_{MMA} = 83% for **4xxiii**, and p_{DBMMA} = 82% and p_{OEGMA} = 75% for **4xxiv**. A linear increase of M_n with conversion (as measured by SEC) was observed, with

low dispersities throughout ($Đ_M$ <1.3), indicating a good control over molecular weight during the polymerisation (Figure 4.28).

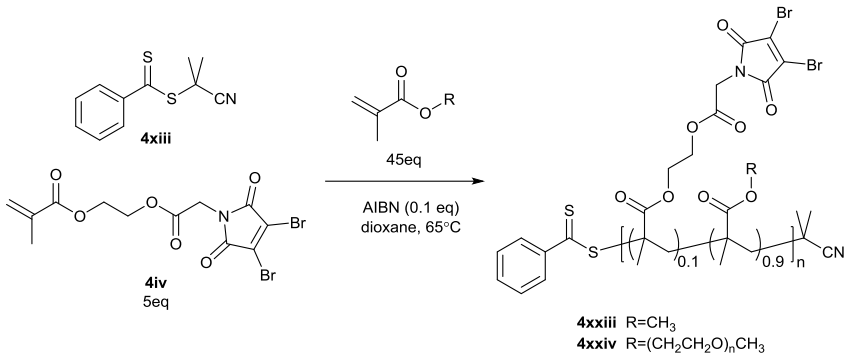

Scheme 4.6. RAFT copolymerisation of DBMMA (**4iv**) with MMA (R=CH_3) or OEGMA (R=$(CH_2CH_2O)_nCH_3$)

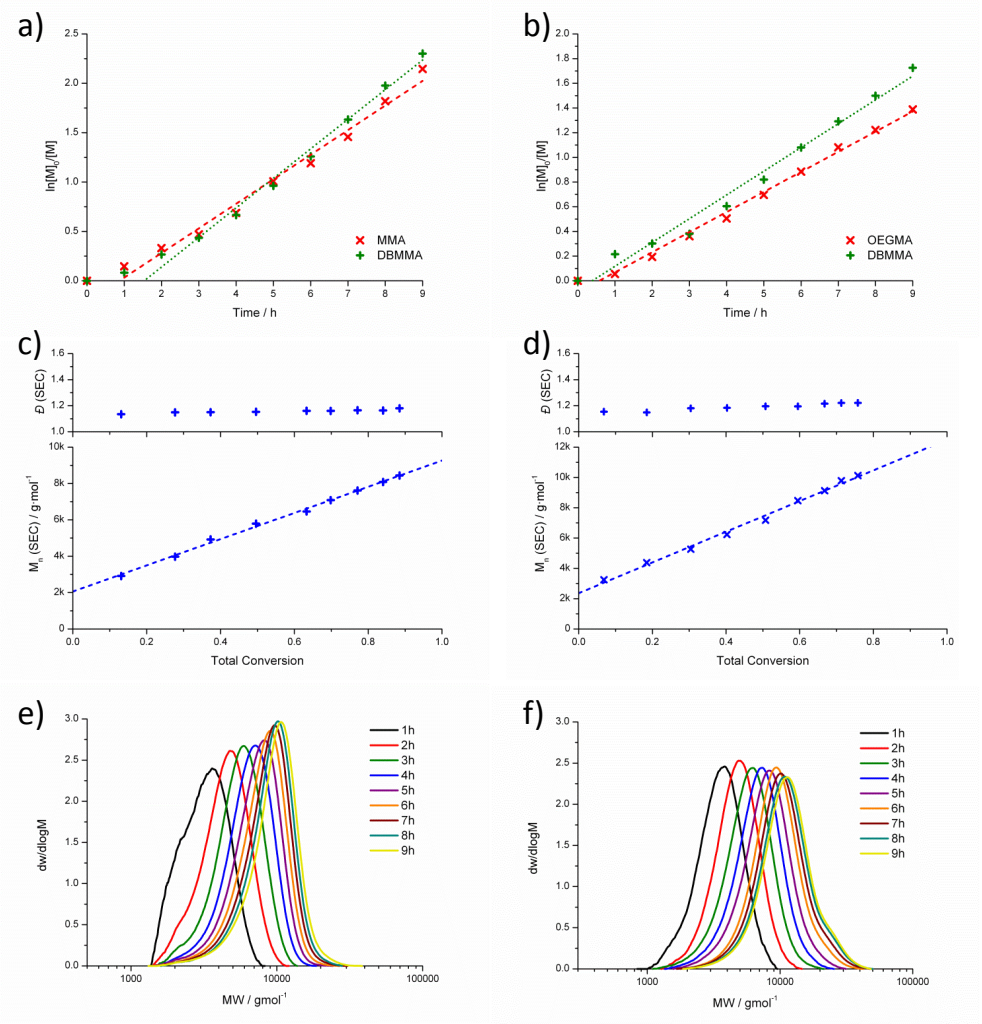

Figure 4.28. DBMMA/MMA copolymerisation **4xxiii** (left) and DBMMA/OEGMA copolymerisation **4xxiv** (right); a&b) First order kinetics of DBMMA and MMA/OEGMA consumption with linear fits; c&d) M_n and $Đ_M$ (as measured by SEC) as a function of total monomer conversion with linear fits; e&f) Evolution of molecular weight distribution (as measured by SEC) as a function of time.

^{1}H NMR spectroscopy of the purified polymers **4xxiii** and **4xxiv** revealed incorporation of DBMMA at 11% and 13% respectively, close to the monomer loading of 10% (Figure 4.29 and Figure 4.30 respectively). As the DBM group itself does not contain any protons, ^{13}C NMR spectroscopy provided addition proof of the presence of the DBM group. The ^{13}C NMR spectrum of **4xiii** showed the characteristic resonance of the C=C at 129.9 ppm (C17) and the C=O at 166.7 ppm (C16). SEC analysis of the purified polymers revealed narrow molecular weight distributions, with $Đ_M$ = 1.12 for **4xxiii**, and $Đ_M$ = 1.24 for **4xxiv** (Figure 4.31). Characterisation data is summarised in Table 4.2.

Table 4.2. RAFT copolymers containing DBM-functional monomers **4iv-4vi**.

	Monomer feed ratio	**Polymer composition**[a]	M_n [a] **(kDa)**	M_n [b] **(kDa)**	$Đ_M$ [b]	**Final monomer conversion** [c] **(%)**	
4xxiii	MMA: 0.90 DBMMA: 0.10	P(MMA$_{0.89}$-*co*-DBMMA$_{0.11}$)	5.9	6.6	1.12	MMA 83	DBMMA 90
4xxiv	OEGMA: 0.90 DBMMA: 0.10	P(OEGMA$_{0.87}$-*co*-DBMMA$_{0.13}$)	13.1	9.3	1.24	OEGMA 75	DBMMA 82
4xxv	^{t}BA: 0.90 DBMA: 0.10	P(^{t}BA$_{0.89}$-*co*-DBMA$_{0.11}$)	5.4	4.2	1.14	^{t}BA 58	DBMA 57
4xxvi	TEGA: 0.90 DBMA: 0.10	P(TEGA$_{0.89}$-*co*-DBMA$_{0.11}$)	4.3	3.4	2.26	TEGA 37	DBMA 55
4xxvii	Sty: 0.99 VBDBM: 0.01	—[c]	—[c]	—[c]	—[c]	—[c]	—[c]

[a] Calculated by ^{1}H NMR spectroscopy end-group analysis using dithiobenzoate Ph-H or dodecyltrithiocarbonate CH$_3$, [b] Measured by SEC, [c] No polymer formed.

RAFT copolymerisations of DBMA (**4v**) with ^{t}BA (**4xxv**) and TEGA (**4xxvi**) with trithiocarbonate **4xx** as RAFT agent were performed in 1,4-dioxane solution, at 65 °C, with [CTA]:[AIBN]:[^{t}BA or TEGA]:[DBMA] = 1:0.1:45:5 according to Scheme 4.7.

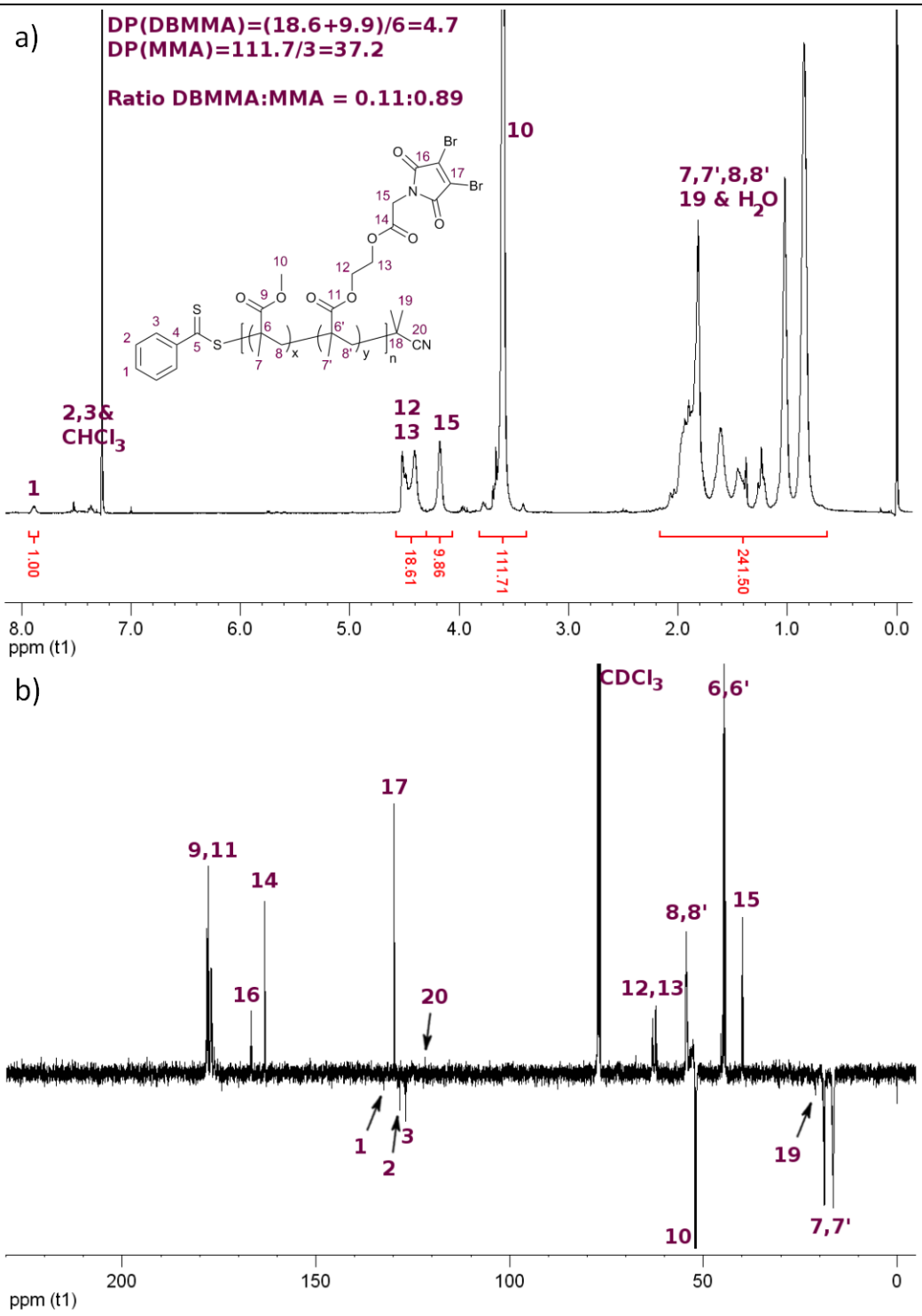

Figure 4.29. a) ^{1}H NMR (400 MHz, $CDCl_3$) spectrum for **4xxiii**. Integration of H1 was set to be equal to 1.00. b) ^{13}C NMR (125 MHz, $CDCl_3$) spectrum for **4xxiii**. Resonances of the quaternary end-group carbons C4, C5 and C18 were not observed above baseline noise.

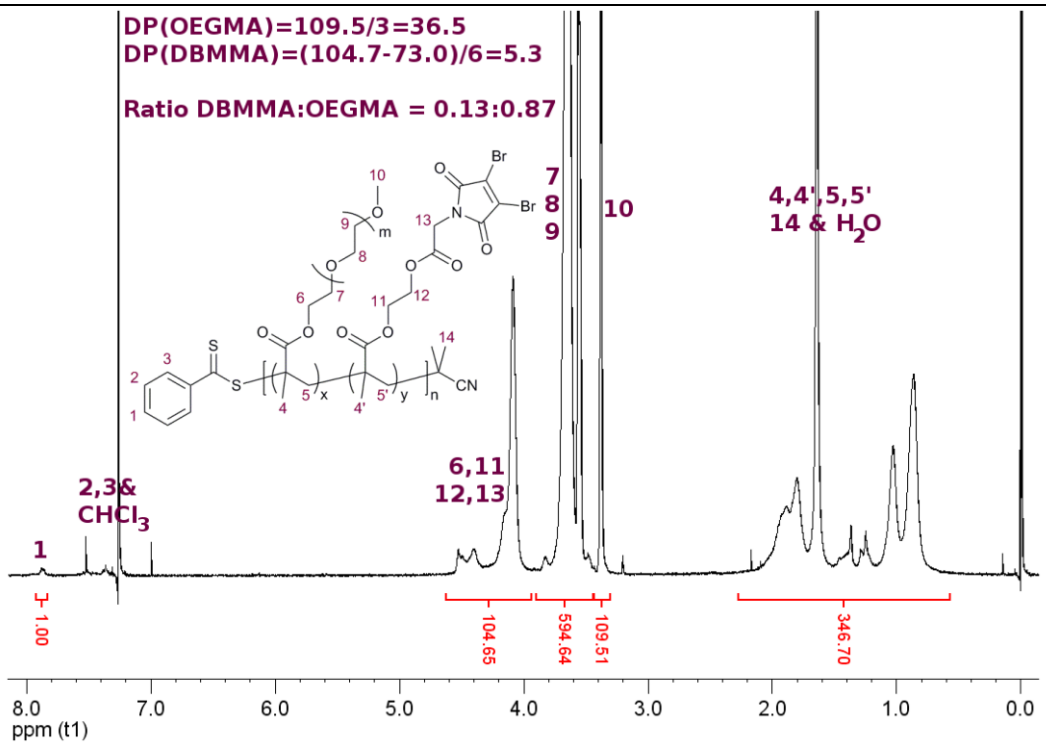

Figure 4.30. ^{1}H NMR (400 MHz, $CDCl_3$) spectrum of **4xxiv**. Integration of H1 was set to be equal to 1.00.

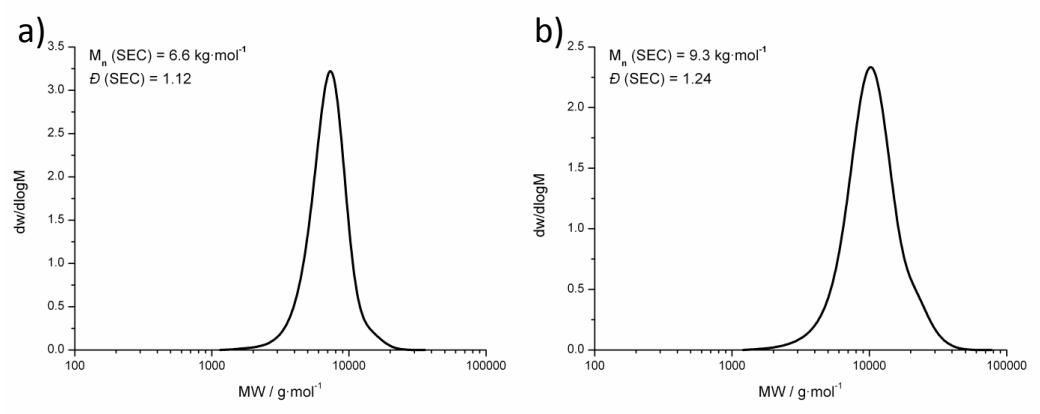

Figure 4.31. SEC molecular weight distribution of a) **4xxiii**; b) **4xxiv**.

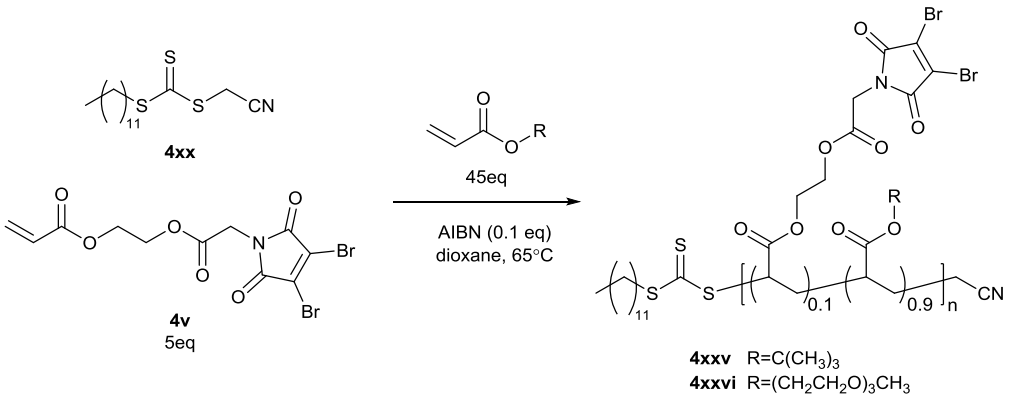

Scheme 4.7. RAFT copolymerisation of DBMA (**4v**) with ^{t}BA (R=C(CH$_3$)$_3$) or TEGA (R=(CH$_2$CH$_2$O)$_3$CH$_3$)

Copolymerisation of DBMA with ^{t}BA (**4xxv**) proceeded with linear first order consumption of monomer, however once total monomer conversion reached *ca.* 60% a complete retardation of polymerization was observed. No loss of control over the evolution of molecular weight was observed after this point, with $Đ_M \leq 1.2$ throughout the entire polymerisation (Figure 4.32). A similar effect was seen in the copolymerisation of DBMA and TEGA (**4xxvi**), where retardation occurred at *ca.* 40% total monomer conversion. Again, no loss of control over molecular weight was observed with $Đ_M \leq 1.2$ (Figure 4.32).

^{1}H NMR spectroscopy of the purified polymers **4xxv** and **4xxvi** did not indicate any loss of monomer functionality, with the spectra showing all the expected resonances. DBMA monomer incorporation was 11% in both cases, close to the monomer loading of 10% (Figure 4.33 and Figure 4.34). Once again, ^{13}C NMR spectroscopy also demonstrated the presence of the DBM groups, with the characteristic resonance of the C=C seen at 129.8 ppm (C17), and the C=O at 166.6 ppm (C16). SEC analysis of the purified polymers revealed narrow molecular weight distributions, with $Đ_M = 1.14$ for **4xxv**, and $Đ_M = 1.26$ for **4xxvi** (Figure 4.35). Characterisation data is summarised in Table 4.2.

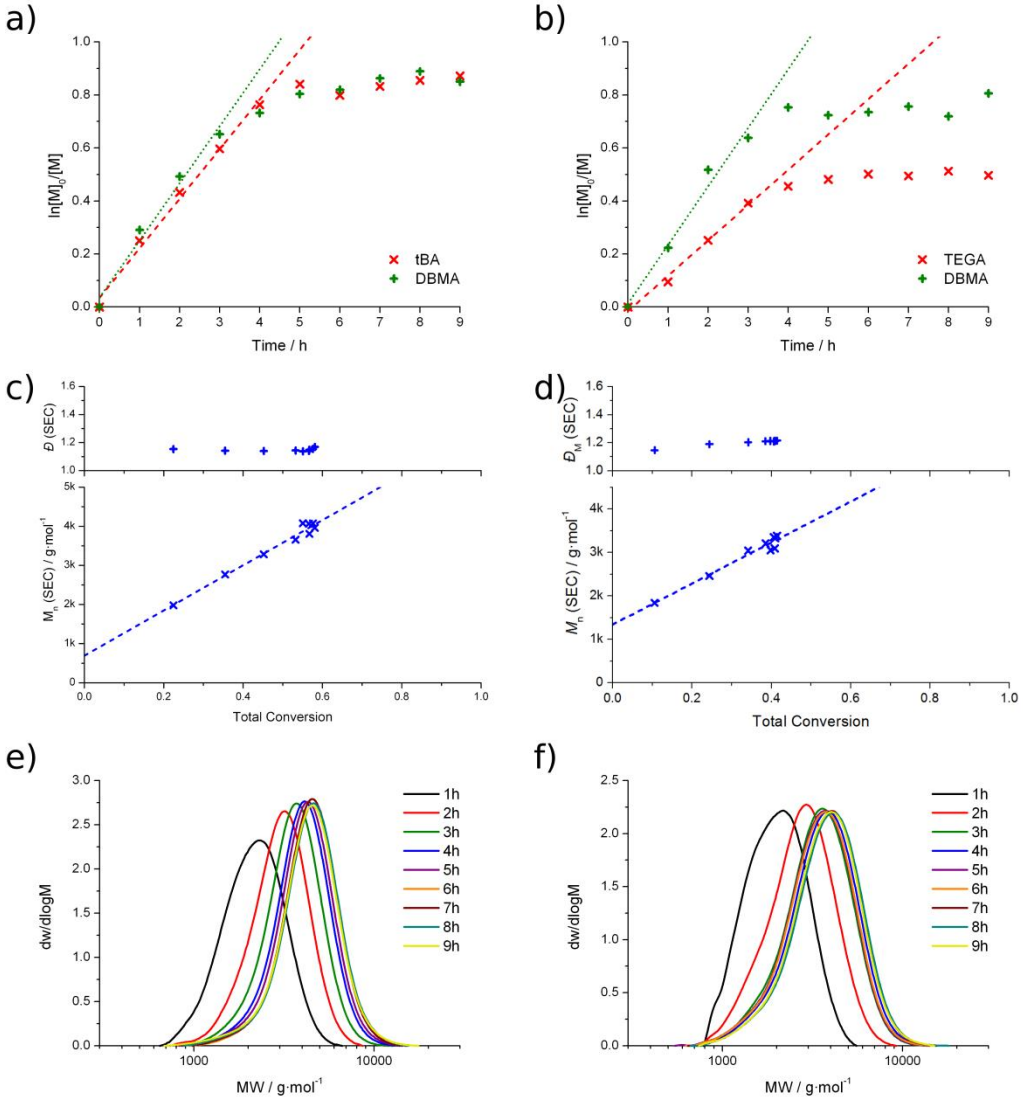

Figure 4.32. DBMA/^{t}BA copolymerisation **4xxv** (left) and DBMA/TEGA copolymerisation **4xxvi** (right); a&b) First order kinetics of DBMA and ^{t}BA/TEGA consumption with linear fits to the initial rate; c&d) M_n and $Đ_M$ (as measured by SEC) as a function of total monomer conversion with linear fits; e&f) Evolution of molecular weight distribution (as measured by SEC) as a function of time.

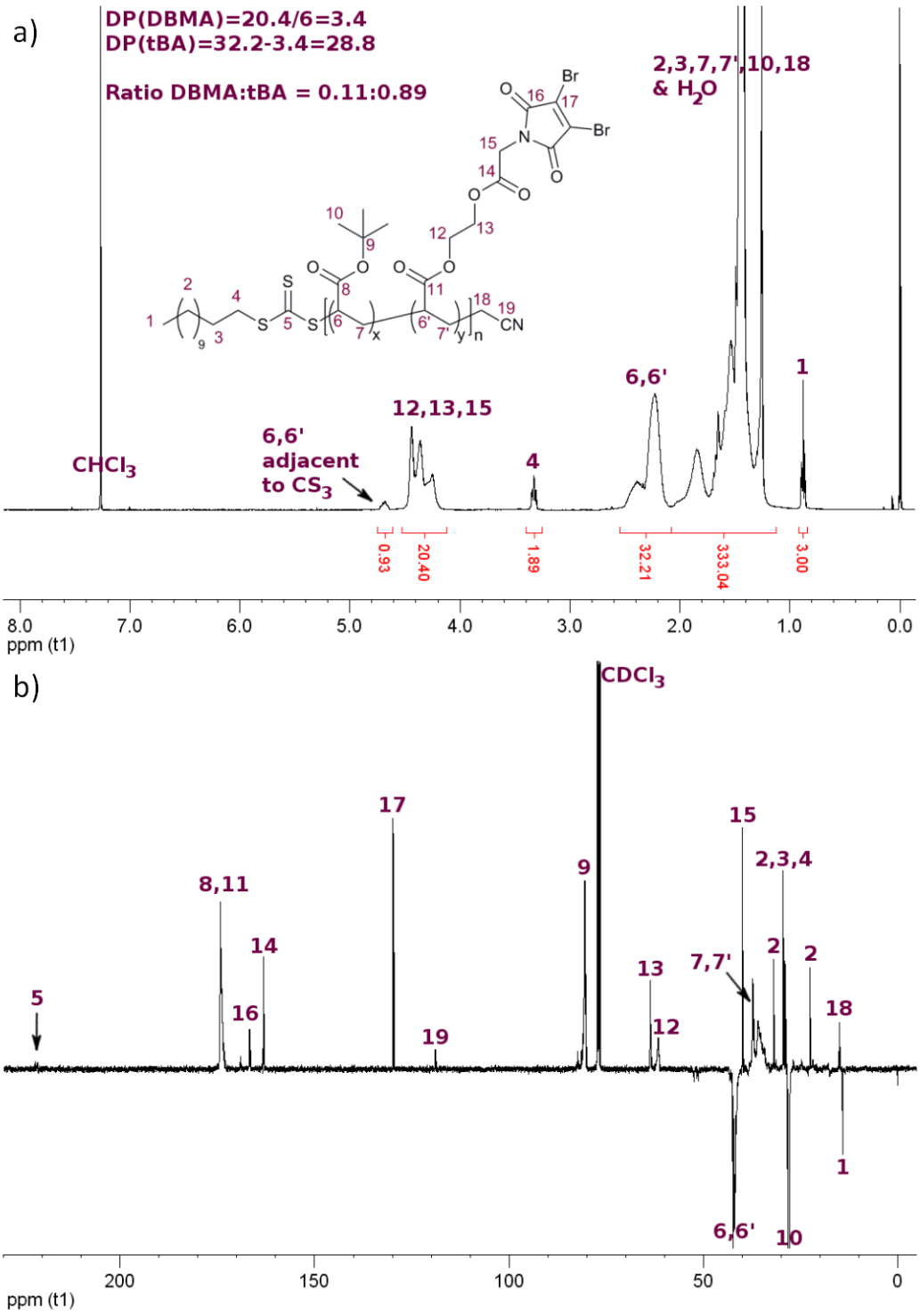

Figure 4.33. a) ^{1}H NMR (400 MHz, $CDCl_3$) spectrum for **4xxv**. Integration of H1 was set to be equal to 3.00. b) ^{13}C NMR (125 MHz, $CDCl_3$) spectrum for **4xxv**.

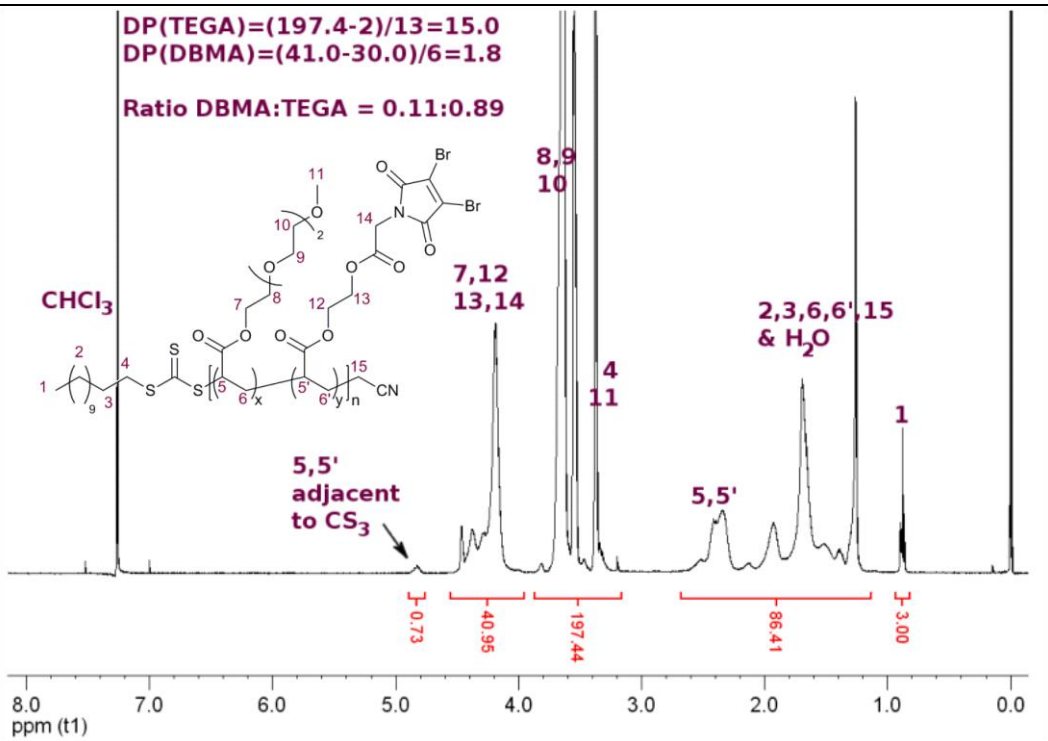

Figure 4.34. ^{1}H NMR (400 MHz, $CDCl_3$) spectrum of **4xxvi**. Integration of H1 was set to be equal to 3.00.

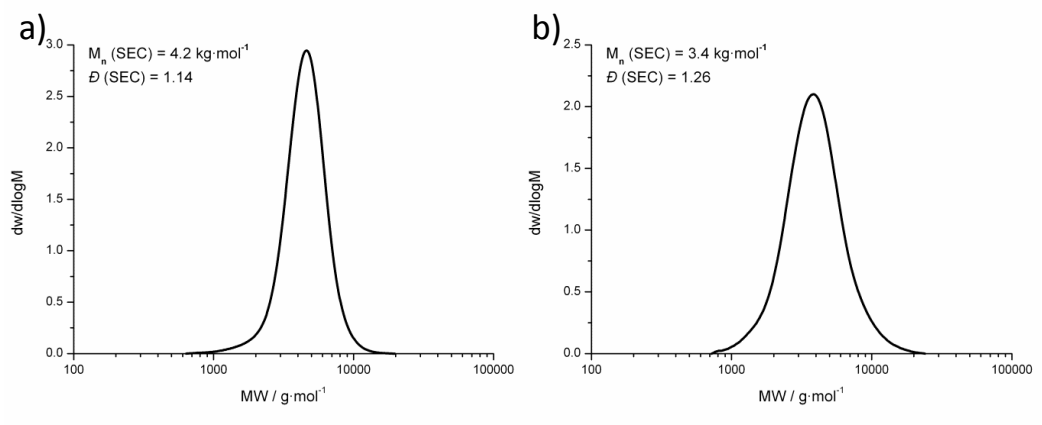

Figure 4.35. SEC molecular weight distribution of a) **4xxv**; b) **4xxvi**.

Polymerisation rate retardation was most significant for VBDBM. Copolymerisations of styrene and VBDBM were performed in bulk, with thermal initiation (110 °C) using RAFT agent **4xxii**. Even at extended reaction times (88 h) with low VBDBM loadings ([CTA]:[Sty]:[VBDBM] = 1:100:1]) total monomer conversion was < 10% (**4xxvii**). As a result only oligomers were produced. The retardation of RAFT polymerisations in the presence of DBM is considered further in Chapter 6.

4.3.4. Post polymerization functionalisation of profluorescent P(OEGMA-*co*-DBMMA)

An investigation into the post-polymerisation functionalization of polymers derived from DBM-functional monomers was undertaken. In Chapter 3 it was found that the post-polymerisation functionalization of polymers with a DBM end-group worked best in aqueous buffer. The success of reactions in organic media depended strongly on the solvent used, as well as the acidity of the thiol. It was therefore decided to use a water soluble DBM-functional polymer, so that the reactions could again be studied in aqueous buffer. Additionally, post-polymerisation functionalization of thermoresponsive copolymers by reaction of the pendant groups of reactive monomers has previously been shown to allow modification of cloud point temperatures. For example Oh and co-workers copolymerised OEGMA with a disulfide-containing monomer. They showed that both reduction of the disulfide, and subsequent thiol-ene Michael addition of ^{t}BA caused a shift in cloud point (Figure 4.36).[34] Alternatively, Du Prez *et al.* copolymerised NIPAM with a thiolactone-functional acrylamide. They showed that ring-opening of the thiolactone with a primary amine followed by thiol-ene reaction with an acrylate allowed the PNIPAM cloud point to be altered, depending on the degree of modification targeted.[35]

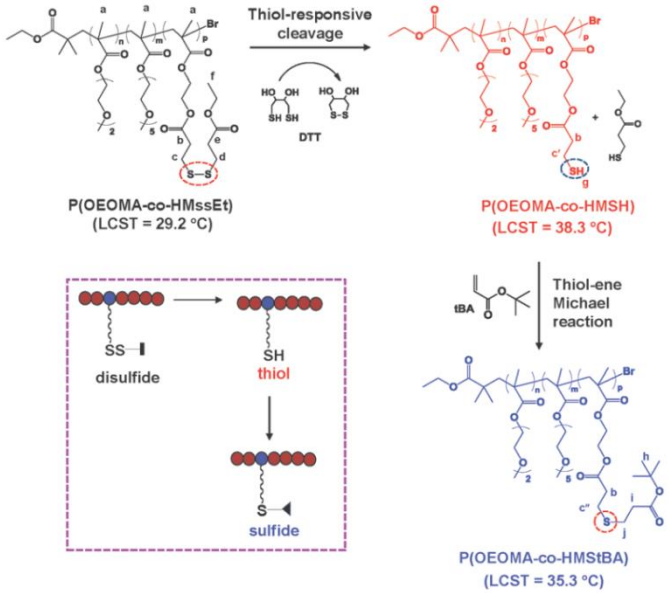

Figure 4.36. POEGMA cloud point modification by post-polymerisation functionalization of reactive disulfide co-monomer. Reproduced from ref.[34]

As detailed above, copolymerisation of TEGA and DBMA (**4xxvi**) was significantly retarded above *ca.* 35% total monomer conversion, making it impractical to study a TEGA/DBMA copolymer. Therefore P(OEGMA-*co*-DBMMA) was synthesised according to the procedure outlined above, with *DP*(OEGMA) = 27.6 and *DP*(DBMMA) = 4.7 (**4xxviii**). Reaction of **4xxviii** with a range of thiols was investigated, according to Scheme 4.8 and detailed in Table 4.3.

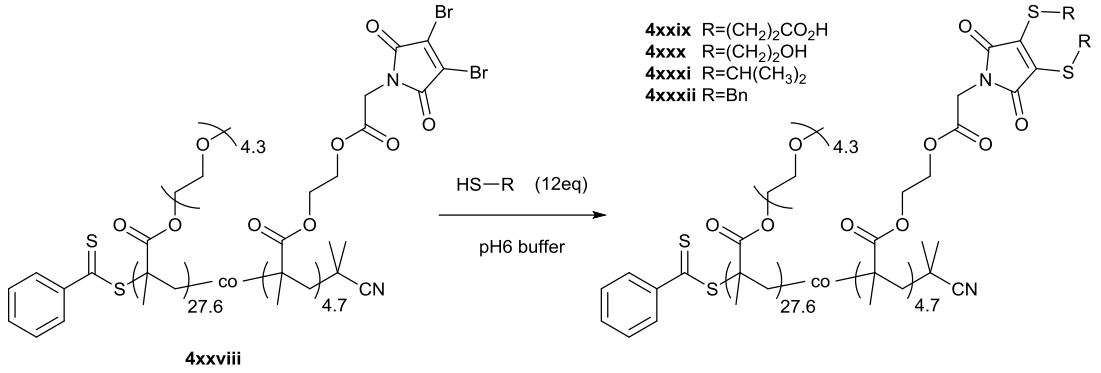

Scheme 4.8. Post-polymerisation functionalization of **4xxviii** with a range of thiols.

Table 4.3. Post polymerization functionalisation reactions of **4xxviii** with a range of thiols.

	Thiol	**Conversion** [a] **(%)**	**Cloud point** [b] **(°C)**	M_n [c] **(kDa)**	$Đ_M$ [c]
4xxviii	-	-	46.3±0.3	9.3	1.24
4xxix	$HS(CH_2)_2CO_2H$	95	55.2±0.7	- [d]	- [d]
4xxx	$HS(CH_2)_2OH$	- [e]	54.9±0.6	7.0	1.38
4xxxi	$HSCH(CH_3)_2$	96	48.1±0.8	7.7	1.39
4xxxii	HSBn	97	44.3±0.3	8.9	1.34

[a] Measured by ^{1}H NMR spectroscopy. [b] Measured by temperature-dependant light transmission at 10 g/L in water (18.2 MΩ·cm). [c] Measured by SEC ($CHCl_3$ eluent, PSty calibration). [d] Polymer interacted with SEC column due to acid groups. [e] DTM CH_2 resonances entirely overlapped with POEGMA resonance.

4xxviii was dissolved in pH6 buffer (100 mM sodium phosphate, 150 mM NaCl) at 10 g/L, before addition of a small excess of thiol (12 *eq.* relative to the polymer which corresponds to 2.6 *eq.* per DBM group) as a 1 M solution in DMF. An immediate colour change was observed due to the formation of the DTM fluorophore, suggesting a fast reaction, as was observed with the end-group functionalization in Chapter 3. After 30 mins the reaction

mixture was added to an excess of water and dialysed to remove unreacted thiol, before lyophilisation to obtain the purified products (**4xxix-4xxxii**). Conversion was calculated by ^{1}H NMR spectroscopy to be ≥ 95%, except in the case of $HS(CH_2)_2OH$ (**4xxx**), where the new resonances of the product completely overlapped with those of POEGMA (Figure 4.37).

SEC (with $CHCl_3$ as eluent) revealed small changes in M_n as the result of the substitution of –Br with the thiols. There was some low molecular weight tailing for **4xxx** due to interactions between the column and the pendant diol groups, which prevented effective size exclusion. This effect was worse for the acid-functional **4xxix**, which failed to elute entirely due to column interactions. There was also evidence of a slight increase in the high molecular weight shoulder for the purified polymers, which is possibly due to hydrolysis of the dithiobenzoate groups, known to occur in basic aqueous media,[36] during the additional dialysis step. Oxidation of the resultant polymeric thiols would therefore lead to species with double the molecular weight of the starting material. The use of a UV-vis SEC detector (with $\lambda_{abs} = 420$ nm) confirmed transformation of DBM groups along the polymer backbone to DTMs which have λ_{max} at *ca.* 420 nm (Figure 4.38).

Generation of the DTM fluorophores along the polymer backbone was also confirmed by fluorescence spectra. Polymer solutions in $CHCl_3$ showed excitation maxima at *ca.* 420 nm with corresponding emission maxima at *ca.* 520 nm – characteristic of DTM – therefore indicating that the profluorescent **4xxviii** had successfully undergone an OFF-to-ON switching of fluorescence emission (Figure 4.39).

Polymers **4xxviii-4xxxii** were dissolved in water (18.2 MΩ·cm) at 10 g/L, and cloud points were measured by temperature-dependant light transmission. The cloud point for the unsubstituted polymer **4xxviii** was 46.3±0.3 °C, while cloud points for the substituted polymers ranged from 44.3±0.3 °C to 55.2±0.7 °C (Table 4.3). A trend of increasing T_c with increasing polarity of the thiol used for the conjugation reaction was observed, suggesting that water solubility of the pendant DTM groups was the determining factor in cloud point temperature (Figure 4.40).

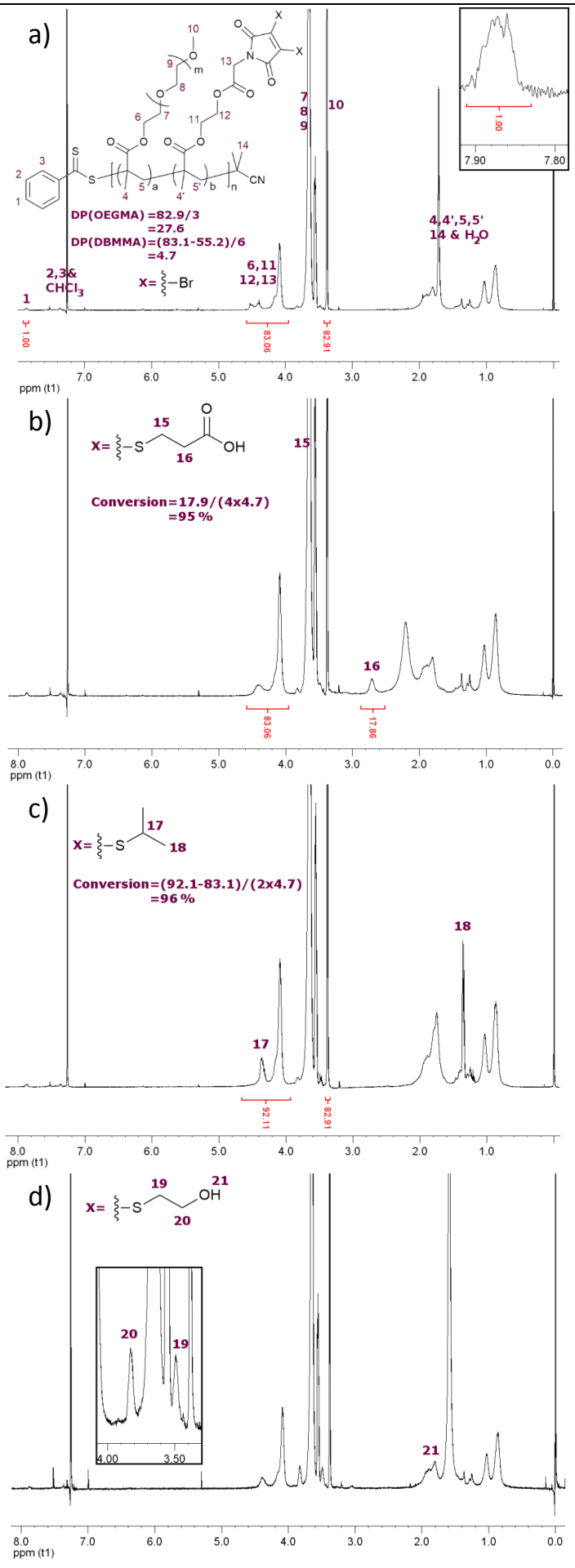
a)
DP(OEGMA) =82.9/3
=27.6
DP(DBMMA)=(83.1-55.2)/6
=4.7
X= Br
2,3& CHCl3
1
6,11
12,13
7
8
9
10
4,4',5,5'
14 & H2O
1.00
83.06
82.91
7.90
7.80
ppm (t1)
b)
X=
15
16
OH
Conversion=17.9/(4x4.7)
=95 %
15
16
83.06
17.86
c)
X=
17
18
Conversion=(92.1-83.1)/(2x4.7)
=96 %
18
17
92.11
82.91
d)
X=
19
20
21
OH
20
19
4.00
3.50
21

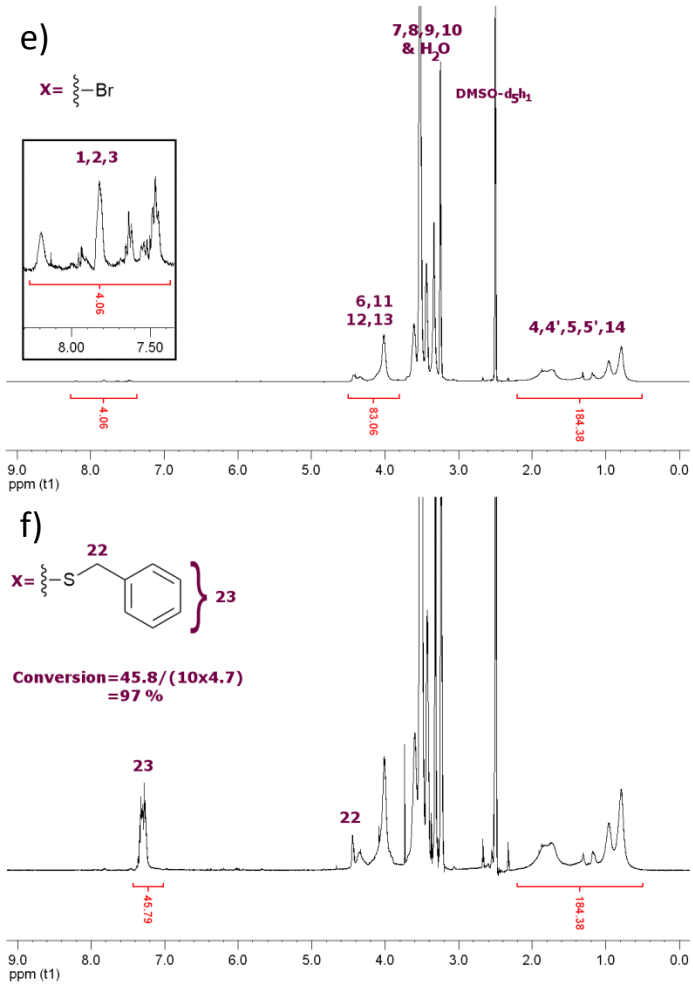

Figure 4.37. ^{1}H NMR spectra of a) **4xxviii** in $CDCl_3$ and e) **4xxviii** in DMSO-d_6; and the thiol-functionalised products; b) **4xxix** in $CDCl_3$; c) **4xxxi** in $CDCl_3$; d) **4xxx** in $CDCl_3$; and f) **4xxxii** in DMSO-d_6. Integration of H1 was set to be equal to 1.00 for a), with integrations in the other spectra derived from those in a).

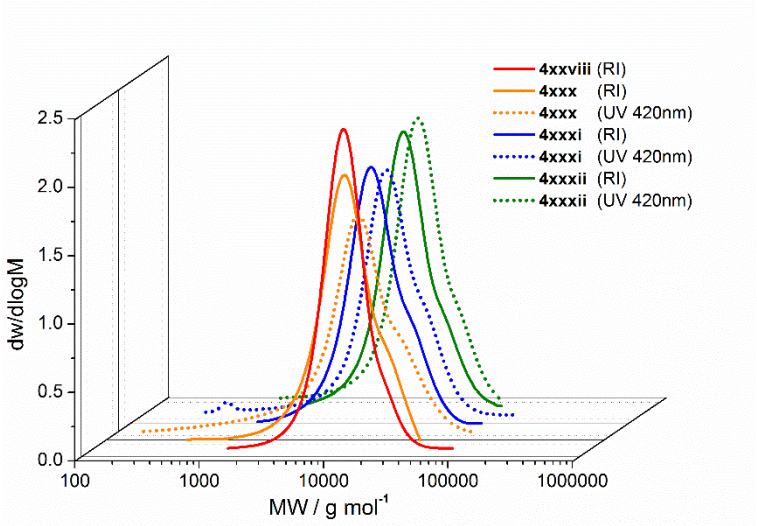

Figure 4.38. SEC molecular weight distributions for **4xxviii**, and the products of the post-polymerisation functionalization reaction with various thiols (**4xxx-4xxxii**) collected using an RI or UV (λ_{abs} = 420 nm) detectors.

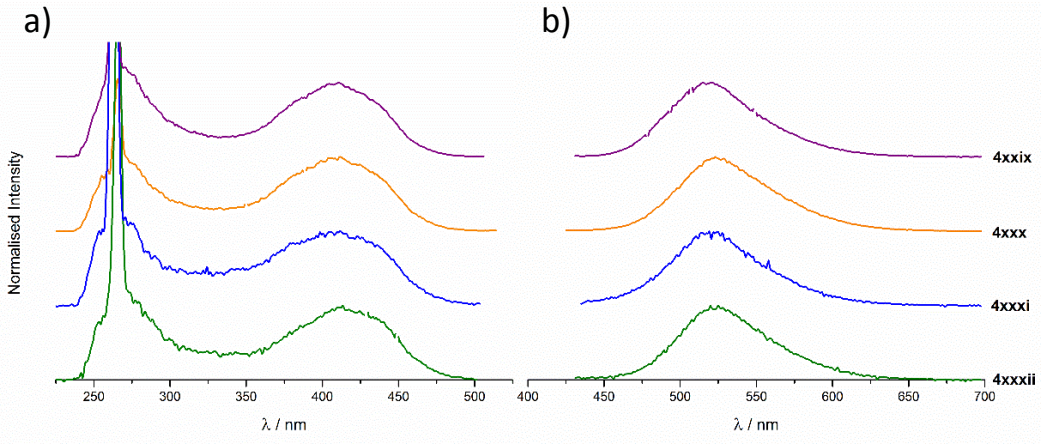

Figure 4.39. a) Excitation spectra (λ_{em} = 525 nm) and b) Emission spectra (λ_{ex} = 410 nm) for the products of the post-polymerisation functionalization reaction of **4xxviii** with various thiols (**4xxix-4xxxii**) recorded as solutions in $CHCl_3$.

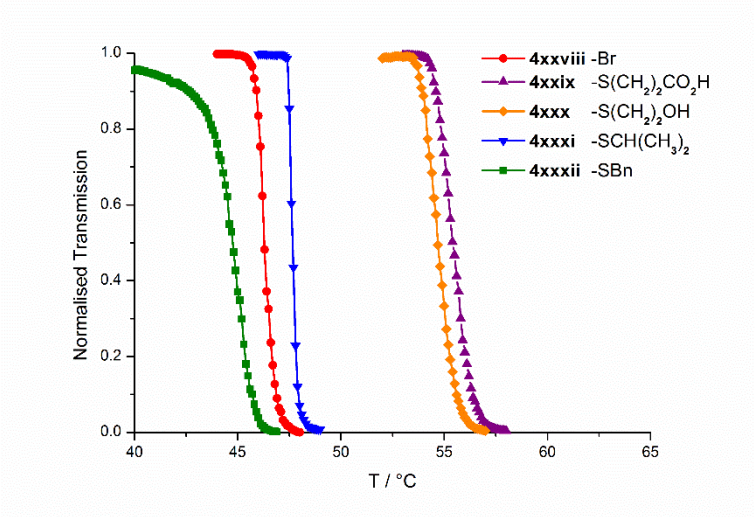

Figure 4.40. LCST cloud point determination by temperature-dependent light transmission for solutions of **4xxviii-4xxxii** at 10 g/L in water.

To quantify the rate at which the side group functionalisation was occurring, in-situ UV-vis spectroscopy was conducted (**4xxxiii**). First, the UV-vis spectrum of a solution of **4xxix** (the previously synthesised product of $HS(CH_2)_2CO_2H$ addition) was measured in pH 6 buffer. It was necessary to use a concentration of 1 g/L to obtain an absorbance < 1 for λ_{max} of the DTM group at 409 nm. The λ_{max} value was taken to correspond to 95% conversion for the functionalisation reaction between **4xxviii** and $HS(CH_2)_2CO_2H$, which had been calculated for **4xxix** by ^1H NMR spectroscopy (see Figure 4.37). Then, to a 1 g/L solution of **4xxviii** in pH 6 buffer was added 12 *eq.* of $HS(CH_2)_2CO_2H$ as a 1 M solution in DMF. The absorbance at 409 nm was monitored as a function of time, and converted to values of conversion by comparison with the spectrum for **4xxix**. Even at this

10× dilution from the optimum conditions used above, the reaction (**4xxxiii**) was found to be very fast, reaching 50% conversion within 10 min, and > 95% conversion after 3 h. Comparison of the full UV-vis spectra of **4xxxiii** at 3 h with **4xxix** showed them to be near identical (Figure 4.41), confirming the validity of using *in situ* UV-vis spectroscopy for rate determination.

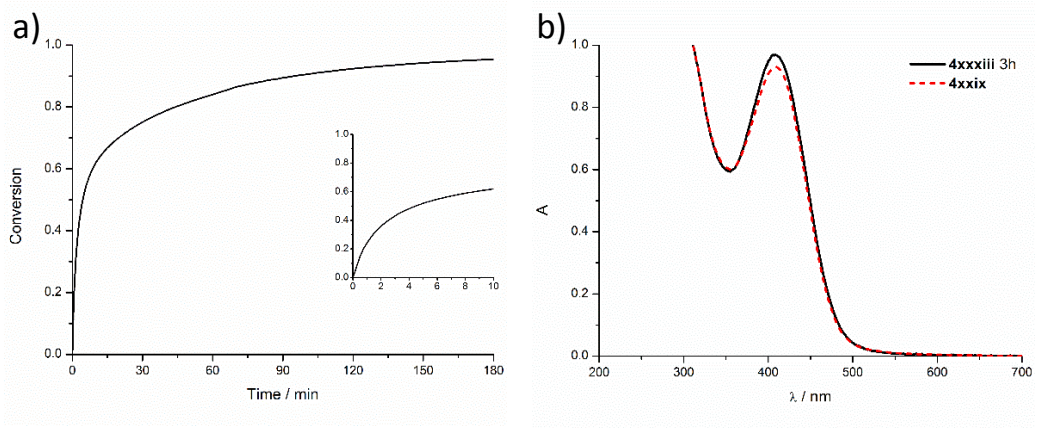

Figure 4.41. a) Conversion *vs.* time as measured by UV-vis spectroscopy (λ_{abs} = 409 nm) for the post-polymerisation functionalisation of **4xxviii** with $HS(CH_2)_2CO_2H$ in pH 6 buffer at 1 g/L (**4xxxiii**). b) Full UV-vis spectrum of **4xxxiii** at 3 h compared with that of **4xxix** at 1 g/L in pH 6 buffer.

4.4. Conclusion

Methacrylic, acrylic and styrenic monomers bearing dithiomaleimide (DTM) or dibromomaleimide (DBM) functional groups have been successfully synthesised and their RAFT copolymerisation has been studied. The fluorescent methacrylic and acrylic DTM monomers were found to give fluorescent copolymers with MMA, OEGMA, ^{t}BA, and TEGA with good control over molecular weight distribution. The copolymers with OEGMA and TEGA retained their water solubility and thermoresponsive properties, with a 10 mol% loading of DTM monomers causing a decrease in LCST cloud point. However, copolymerisation of the styrenic DTM monomer with styrene afforded branched polymers, due to polymerisation of the DTM C=C double bond. The difference in the reactivity of the of the DTM double bonds in these monomers is discussed further in Chapter 6.

The DBM monomers gave profluorescent copolymers with MMA, OEGMA, ^{t}BA and TEGA, again with good control over molecular weight distribution. However, copolymerisations with DBM acrylate were found to reach a limiting conversion, while copolymerisations with styrenic DBM were completely retarded. This affect was similar to that observed in RAFT polymerisations mediated by a DBM-functional CTA in Chapter 2, and is discussed further in Chapter 6.

The reaction between the profluorescent DBM/OEGMA copolymer and a range of thiols was found to be fast and highly efficient in aqueous buffer. The result was an OFF-to-ON switching of fluorescence emission, therefore providing an alternative route to fluorescent DTM-functional polymers. These substituted OEGMA copolymers retained an LCST cloud point, with the ability to tune the cloud point over a range of 11 °C according to thiol polarity.

These new monomers provide an alternative strategy for fluorescent labelling of polymers with the DTM fluorophore to the end-group labelling demonstrated in Chapter 3. These DTM monomers are utilised in Chapter 5 for the synthesis of fluorescently-labelled polymer nanoparticles.

4.5. Experimental

4.5.1. Materials and apparatus

Tert-butyl acrylate (^{t}BA) and styrene (Sty) were vacuum distilled over CaH_2 prior to use, and stored at 4 °C. Methyl methacrylate (MMA) was passed through a column of neutral alumina (Al_2O_3) prior to use, and stored at 4 °C. 2,2'-azobis(2-methylpropionitrile) (AIBN) was recrystallized twice from methanol and stored at 4 °C in the dark. 1,4-Dioxane was passed through a basic alumina plug immediately before use. The RAFT agents 2-cyano-2-propyl benzodithioate (**4xiii**), cyanomethyl dodecyl trithiocarbonate (**4xx**) and 2-cyano-2-propyl dodecyl trithiocarbonate (**4xxii**) were purchased from Aldrich and used as received. All other chemicals and reagents were purchased from Aldrich and used as received. The number average molecular weight (M_n) of oligoethyleneglycol methacrylate (OEGMA) was determined to be 291 g·mol^{-1} by ^{1}H NMR spectroscopy end-group analysis. Solvents were purchased from Fisher Scientific and used as received. Dry solvents were used directly from a drying and degassing solvent tower delivery system.

^{1}H and ^{13}C NMR spectra were recorded on a Bruker DPX-300, DPX-400, DRX-500, AV-600 or AV-700 spectrometer in $CDCl_3$ unless otherwise stated. Chemical shifts are given in ppm downfield from the internal standard tetramethylsilane, and coupling constants (J) correspond to $^{3}J_{H\text{-}H}$ unless otherwise stated. Size exclusion chromatography (SEC) measurements were conducted using a Varian 390-LC-Multi detector suite fitted with differential refractive index (DRI), and UV-Vis or photodiode array (PDA) detectors. A guard column (Varian Polymer Laboratories PLGel 5 µm, 50 × 7.5 mm) and two mixed D columns (Varian Polymer Laboratories PLGel 5 µm, 300 × 7.5 mm) were used. The mobile phase was tetrahydrofuran with 2% triethylamine, or chloroform with 2% triethylamine eluent at a flow rate of 1.0 mL/min. Data was analysed using Cirrus v3.3 with calibration curves produced using Varian Polymer laboratories Easi-Vials linear poly(Sty) standards (162 Da – 240 kDa). Infrared spectra were recorded (neat) on a Perkin Elmer, Spectrum 100 FT-IR Spectrometer. High Resolution Mass Spectrometry (HR-MS) was conducted on a Bruker UHR-Q-ToF MaXis with electrospray ionization. Fluorescence spectra were collected on a PerkinElmer LS 55 Fluorescence Spectrometer. UV-Vis spectra and temperature dependant light transmission were recorded on a

PerkinElmer LAMBDA 35 UV-Vis Spectrophotometer. High pressure liquid chromatograms were recorded on a Varian 9250 HPLC, fitted with a Supelco Discovery C18 column and a PDA and fluorescence detector. The mobile phase was a gradient of water and methanol.

4.5.2. Synthetic protocols

Triethylene glycol monomethylether acrylate (TEGA) was synthesised as previously reported.[32]

The synthesis of 3,4-bis(butylsulfanyl)-2,5-dihydro-1H-pyrrole-2,5-dione (**3i**) was described in Chapter 3.

2-[(2-bromoacetyl)oxy]ethyl 2-methylprop-2-enoate (**4vii**) was synthesised in a single step as previously reported.[25]

2-[(2-bromoacetyl)oxy]ethyl prop-2-enoate (**4viii**) was synthesised in a single step as previously reported.[26]

Methyl 3,4-dibromo-2,5-dioxo-2,5-dihydro-1H-pyrrole-1-carboxylate (**4x**) was synthesised in a single step as previously reported.[27]

1-(azidomethyl)-4-ethenylbenzene (**4xi**) and (4-ethenylphenyl)methanamine (**4xii**) were prepared as previously reported.[28]

2-([2-(3,4-bis[butylsulfanyl]-2,5-dioxo-2,5-dihydro-1H-pyrrol-1-yl)acetyl]oxy)ethyl 2-methylprop-2-enoate (4i)

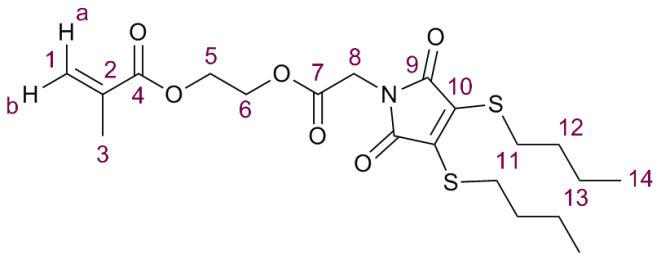

To a suspension of K_2CO_3 (1.12 g, 8.08 mmol) and tetrabutylammonium iodide (0.199 g 0.539 mmol) in acetone was added solutions of **3i** (1.62 g, 5.93 mmol) and **4vii** (1.35 g, 5.39 mmol) in acetone to a final volume of 250 mL. The solution was stirred at

room temperature for 50 h, before the solution was filtered and the solvent removed *in vacuo*. The crude product was purified by column chromatography (SiO_2, petroleum ether : dichloromethane = 3:7) to yield the product as an off-yellow oil (1.6 g, 67%). $R_f = 0.16$. ^{1}H NMR (400 MHz, $CDCl_3$) δ 6.14 (1H, m, H1a), 5.61 (1H, quin, $^2J_{H\text{-}H}$ = $^4J_{H\text{-}H}$ = 1.5 Hz, H1b), 4.41 (2H, m, H6) 4.35 (2H, m, H5), 4.28 (2H, s), 3.30 (4H, t, J = 7.5 Hz, H11), 1.95 (3H, t, $^4J_{H\text{-}H}$ = 1.5 Hz, H3), 1.64 (4H, m, H12), 1.44 (4H, sex, J = 7.5 Hz, H13), 0.93 (6H, t, J = 7.5 Hz, H14); ^{13}C NMR (125 MHz, $CDCl_3$) δ 167.1 (C7) 167.0 (C4), 165.7 (C9), 136.2 (C10) 135.8 (C2), 126.4 (C1), 63.4 (C6), 62.0 (C5), 39.1 (C8), 32.5 (C12), 31.6 (C11), 21.7 (C13), 18.3 (C3), 13.6 (C14) ; FTIR (neat) ν_{max} / cm^{-1} 1755 (C=O stretch ester), 1706 (C=O stretch maleimide), 1638 (C=C stretch methacrylate); HR-MS (MaXis) *m/z* found 466.1322, calc. 466.1329 ($[M+Na]^+$, 100%).

^{1}H and ^{13}C NMR spectra shown in Figure 4.5.

2-[(2-[3,4-bis(butylsulfanyl)-2,5-dioxo-2,5-dihydro-1H-pyrrol-1-yl]acetyl)oxy]ethyl prop-2-enoate (4ii)

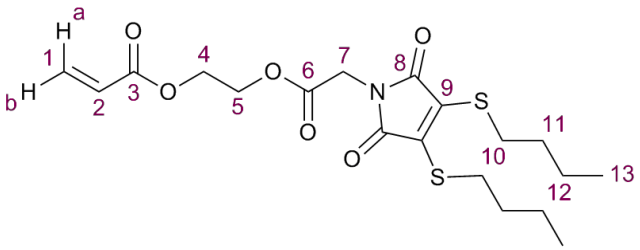

To a suspension of K_2CO_3 (1.44 g, 10.4 mmol) in acetone (200 mL) was added **4viii** (1.65 g, 6.97 mmol), and **3i** (2 g, 7.32 mmol). The solution was stirred at room temperature for 44 h, filtered, and the solvent removed from the filtrate *in vacuo*. The crude product was then purified by column chromatography (SiO_2, petroleum ether : dichloromethane gradient 2:1–1:2) to yield the product as a yellow oil (2.27 g, 76%). $R_f = 0.21$ (petroleum ether : dichloromethane = 1:2). ^{1}H NMR (300 MHz, $CDCl_3$) δ 6.45 (1H, dd, J = 17.5 Hz, $^2J_{H\text{-}H}$ = 1.5 Hz, H1a), 6.15 (1H, dd, J = 17.5 Hz, J = 10.5 Hz, H2), 5.89 (1H, dd, J = 10.5 Hz, $^2J_{H\text{-}H}$ = 1.5 Hz, H1b), 4.38 (4H, m, H4 & H5), 4.29 (2H, s, H7), 3.30 (4H, t, J = 7.5 Hz, H10), 1.64 (4H, quin, J = 7.5 Hz, H11), 1.45 (4H, sex, J = 8.0 Hz, H12), 0.93 (6H, t, J = 7.5 Hz, H13); ^{13}C NMR (75 MHz, $CDCl_3$) δ 166.5 (C6), 165.2 (C8), 165.1 (C3), 135.5 (C9), 131.0 (C1), 127.2 (C2), 62.8 (H5), 61.2 (H4), 38.5 (C7),

31.8 (C11), 31.0 (C10), 21.0 (C12), 13.0 (C13); FTIR (neat) ν_{max} / cm^{-1}, 1755 (C=O stretch ester), 1727 (C=O stretch acrylate), 1706 (C=O stretch maleimide), 1637 (C=C stretch acrylate), 1620 (C=C stretch maleimide); HR-MS (MaXis) *m/z* found 452.1179, calc. 452.1172 ($[M+Na]^+$, 100%).

^1H and ^{13}C NMR spectra shown in Figure 4.7.

3,4-bis(butylsulfanyl)-1-[(4-ethenylphenyl)methyl]-2,5-dihydro-1H-pyrrole-2,5-dione (4iii)

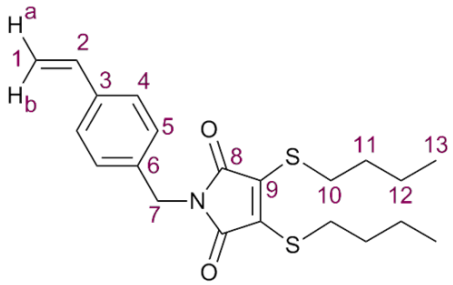

To a solution of **4xii** (0.603 g, 4.53 mmol) in chloroform (20 mL) was added dropwise triethylamine (0.688 g, 6.80 mmol), and a solution of **4ix** (1.5 g, 4.53 mmol) in chloroform (20 mL). The solution was stirred at room temperature for 4 h, then the reaction mixture was filtered, the solvent removed *in vacuo*, and the crude product purified by column chromatography (SiO_2, petroleum ether : ethyl acetate gradient 10:1–8:1) to yield the product as a yellow oil (0.852 g, 48%). R_f = 0.27 (petroleum ether : ethyl acetate = 9:1). ^1H NMR (400 MHz, $CDCl_3$) δ 7.35 (2H, d, J = 8.0 Hz, H4), 7.30 (2H, d, J = 8.0 Hz, H5), 6.68 (1H, dd, J = 11.0, J = 17.5, H2), 5.72 (1H, d, J = 17.5, H1b), 5.23 (1H, d, J = 11.0 Hz, H1a), 4.63 (2H, s, H7), 3.28 (4H, t, J = 7.5, H10), 1.62 (4H, quin, J = 7.5 Hz, H11), 1.43 (4H, sex, J = 7.5 Hz, H12), 0.92 (6H, t, J = 7.5 Hz, H13); ^{13}C NMR (100 MHz, $CDCl_3$) δ 166.3 (C8), 137.2 (C3), 136.3 (C2), 135.78 & 135.75 (C6 & C9), 128.7 (C5), 126.5 (C4), 114.2 (C1), 41.9 (C7), 32.5 (C11), 31.6 (C10), 21.7 (C12), 13.6 (C13); FTIR (neat) ν_{max} / cm^{-1}, 1763 (C=O stretch maleimide), 1698 (C=O stretch maleimide), 1630 and 1513 (C=C stretches); HR-MS (MaXis) *m/z* found 412.1375, calc. 412.1375 ($[M+Na]^+$, 100%).

^1H and ^{13}C NMR spectra shown in Figure 4.9.

2-[(2-[3,4-dibromo-2,5-dioxo-2,5-dihydro-1H-pyrrol-1-yl]acetyl)oxy]ethyl 2-methylprop-2-enoate (4iv)

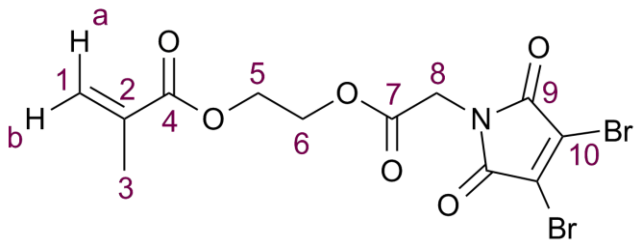

To a solution of 2,3-dibromomaleimide (3.91 g, 15.3 mmol), K_2CO_3 (2.12 g, 15.3 mmol) and tetrabutylammonium iodide (0.513 g, 1.39 mmol) in acetone (200 mL) was added dropwise **4vii** (3.50 g, 13.9 mmol). The solution was stirred at room temperature for 16 h, before the solvent was removed *in vacuo*. Water (200 mL) was added, and the crude product extracted with diethyl ether (200 mL x 3). The combined organic layers were washed with brine (200 mL x 2), and dried with $MgSO_4$. The solvent was removed from the organic layer *in vacuo* and the crude product was purified by column chromatography (SiO_2, petroleum ether : diethyl ether = 3:1) to yield the product as an off-white solid (1.6 g, 67%). $R_f = 0.23$. ^{1}H NMR (400 MHz, $CDCl_3$) δ 6.13 (1H, quin, $^4J_{H\text{-}H} = {}^2J_{H\text{-}H} = 1.5$ Hz, H1a), 5.62 (1H, quin, $^4J_{H\text{-}H} = {}^2J_{H\text{-}H} = 1.5$ Hz, H1b), 4.43 (2H, m, H6), 4.39 (2H, s, H8), 4.36 (2H, m, H5), 1.95 (3H, t, $^4J_{H\text{-}H} = 1.6$ Hz, H3); ^{13}C NMR (100 MHz, $CDCl_3$) δ 167.0 (C4), 166.4 (C9), 163.1 (C7), 135.7 (C2), 129.9 (C10), 126.4 (C1), 63.8 (C6), 61.9 (C5), 40.0 (C8), 18.3 (C3); FTIR (neat) ν_{max} / cm^{-1} 1793 (C=O stretch maleimide), 1749 (C=O stretch ester), 1717 (C=O stretch acrylate), 1706 (C=O stretch maleimide), 1632 (C=C stretch acrylate), 1593 (C=C stretch maleimide); HR-MS (MaXis) *m/z* found 423.9027, calc. 423.9026 ($[M+H]^+$, 100%).

^{1}H and ^{13}C NMR spectra shown in Figure 4.6.

2-[(2-[3,4-dibromo-2,5-dioxo-2,5-dihydro-1H-pyrrol-1-yl]acetyl)oxy]ethyl prop-2-enoate (4v)

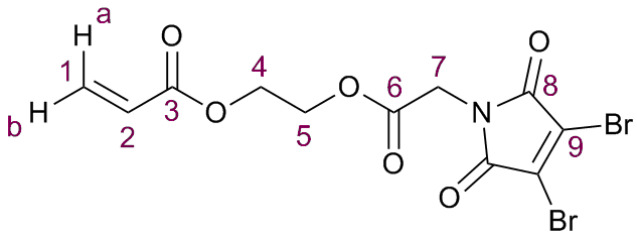

To a solution of 2,3-dibromomaleimide (5.39 g, 21.1 mmol) and K_2CO_3 (2.92 g, 21.1 mmol) in acetone (200 mL) was added dropwise **4viii** (4.56 g, 19.2 mmol). The solution was stirred at room temperature for 16 h, before the solvent was removed *in vacuo*. The residue was dissolved in diethyl ether (300 mL) and washed with water (200 mL x 6), brine (200 mL), and dried with $MgSO_4$. The solvent was removed from the organic layer *in vacuo* and the crude product was purified by column chromatography (SiO_2, petroleum ether : diethyl ether = 3:1) to yield the product as an off-white powder (5.01 g, 68%). $R_f = 0.14$. ^{1}H NMR (400 MHz, $CDCl_3$) δ 6.45 (1H, dd, $J = 17.5$ Hz, $^2J_{H\text{-}H} = 1.5$ Hz, H1a), 6.14 (1H, dd, $J = 17.5$ Hz, $J = 10.5$ Hz, H2), 5.89 (1H, dd, $J = 10.5$ Hz, $^2J_{H\text{-}H} = 1.5$ Hz, H1b), 4.42 (2H, m, H5), 4.40 (2H, s, H7), 4.38 (2H, m, H4); ^{13}C NMR (100 MHz, $CDCl_3$) δ 166.4 (C3), 165.8 (C8), 163.1 (C6), 131.8 (C1), 129.9 (C9), 127.8 (C2), 63.8 (C5), 61.7 (C4), 40.0 (C7); FTIR (neat) ν_{max} / cm^{-1} 1792 (C=O stretch maleimide), 1748 (C=O stretch ester), 1724 (C=O stretch acrylate), 1711 (C=O stretch maleimide), 1630 (C=C stretch acrylate), 1589 (C=C stretch maleimide); HR-MS (MaXis) *m/z* found 409.8870, calc. 409.8869 ($[M+H]^+$, 100%).

^{1}H and ^{13}C NMR spectra shown in Figure 4.8.

3,4-dibromo-1-[(4-ethenylphenyl)methyl]-2,5-dihydro-1H-pyrrole-2,5-dione (4vi)

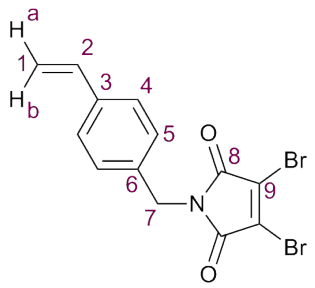

To a solution of **4xii** (2.34 g, 17.6 mmol) in dichloromethane (20 mL) was added dropwise a solution of **4x** (5.5 g, 17.6 mmol) in dichloromethane (20 mL). The solution was stirred at room temperature for 5 h, then dichloromethane (160 mL) was added, and the organic layer washed with sat. NH_4Cl solution (200 mL x 2), water (200 mL x 2), brine (200 mL), and dried with $MgSO_4$. The solvent was removed from the organic layer *in vacuo* and the crude product was purified by column chromatography (SiO_2, petroleum ether : diethyl ether = 9:1) to yield the product as an off-white solid (2.11 g, 32%). $R_f = 0.36$. ^{1}H NMR (400 MHz, $CDCl_3$) δ 7.36 (2H, d, J = 8.5 Hz, H4), 7.32 (2H, d, J = 8.5 Hz, H5), 6.68 (1H, dd, J = 17.5 Hz, J = 11.0 Hz, H2), 5.73 (1H, d, J = 17.5 Hz, H1b), 5.25 (1H, d, J = 11.0 Hz, H1a), 4.73 (2H, s, H7); ^{13}C NMR (100 MHz, $CDCl_3$) δ 163.61 (C8), 137.7 (C3), 136.2 (C2), 134.6 (C6), 129.5 (C9), 129.1 (C4), 126.7 (C5), 114.6 (C1), 43.0 (C7); FTIR (neat) ν_{max} / cm^{-1} 1782 & 1723 (C=O stretch maleimide), 1594 (C=C stretch maleimide), 1510 (C=C aromatic).

^{1}H and ^{13}C NMR spectra shown in Figure 4.10.

Methyl 3,4-bis(butylsulfanyl)-2,5-dioxo-2,5-dihydro-1H-pyrrole-1-carboxylate (4ix)

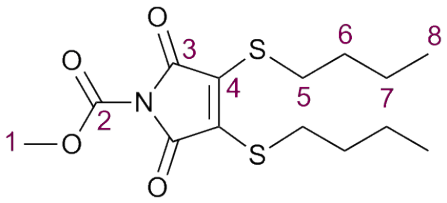

To a solution of **3i** (1.50 g, 5.49 mmol) and *N*-methylmorpholine (0.555 g, 5.49 mmol) in ethyl acetate (50 mL) was added methyl chloroformate (0.570 g, 6.04 mmol). The solution was stirred at room temperature for 2 h, before ethyl acetate (50 mL) was added and the organic layer washed with water (200 mL x 3) and dried with $MgSO_4$. The solvent was removed *in vacuo* to give the product as a dark yellow liquid (1.64 g, 90%). ^{1}H NMR (400 MHz, $CDCl_3$) δ 3.97 (3H, s, H1), 3.34 (4H, t, J = 7.5 Hz, H5), 1.65 (4H, quin, J = 7.5 Hz, H6), 1.45 (4H, sex, J = 7.5 Hz, H7), 0.93 (6H, t, J = 7.5 Hz, H8); ^{13}C NMR (100 MHz, $CDCl_3$) δ 161.5 (C3), 151.2 (C2), 137.1 (C4), 54.3 (C1), 32.5 (C6), 31.7 (C5), 21.7 (C7), 13.6 (C8); FTIR (neat) ν_{max} / cm^{-1}, 1800 (C=O stretch) 1761 (C=O stretch maleimide), 1717 (C=O stretch maleimide); HR-MS (MaXis) *m/z* found 354.0822, calc. 354.0804 ($[M+Na]^+$, 100%).

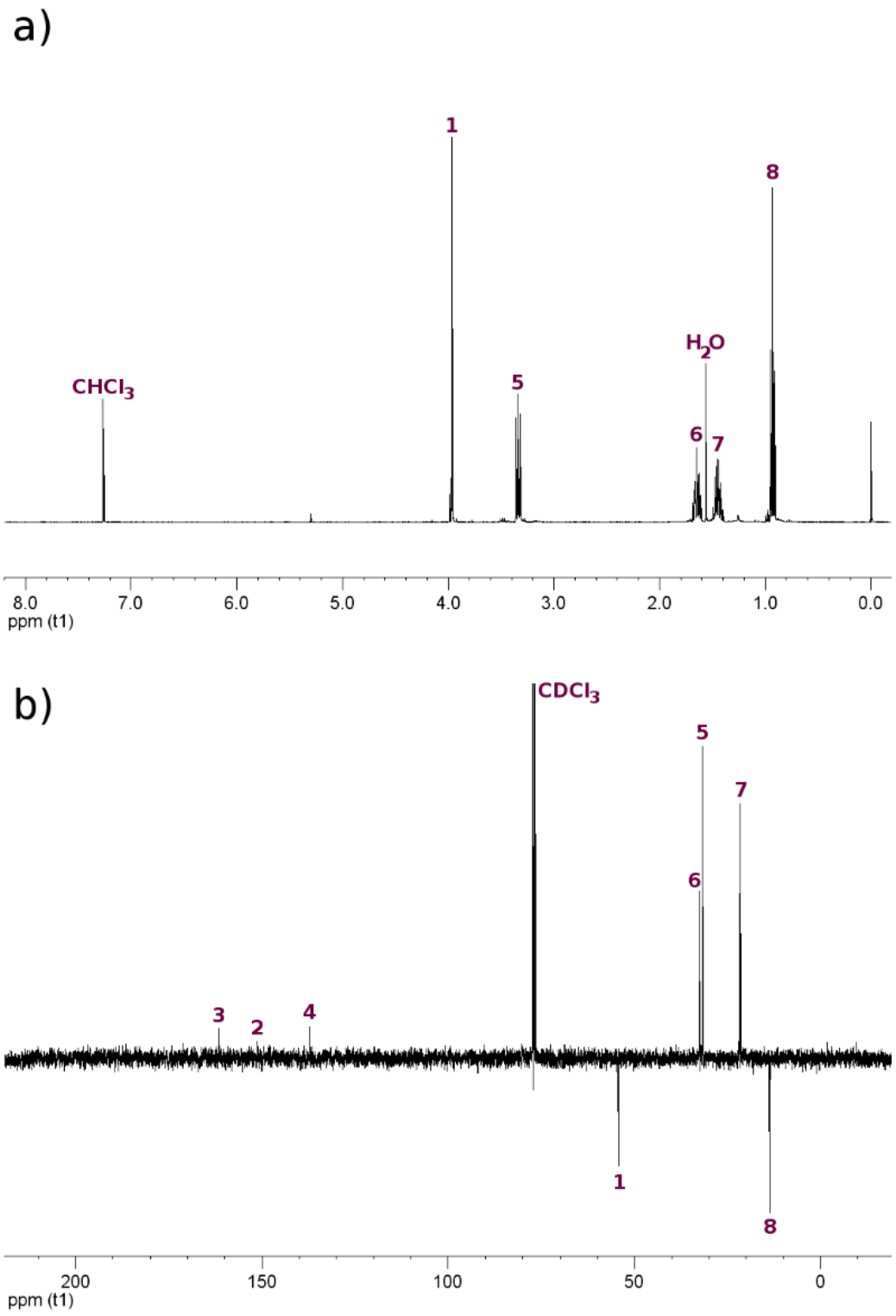

Figure 4.42 a) ^{1}H NMR (400 MHz, $CDCl_3$) spectrum and b) ^{13}C NMR (100 MHz, $CDCl_3$) spectrum for **4ix**.

General procedure for RAFT copolymerisations

Typically; to a polymerization ampoule was added a solution of RAFT agent, AIBN, and monomers and solvent. The solution was degassed by three freeze-pump-thaw cycles, the ampoule sealed under N_2 and the reaction stirred at the required temperature. Periodically samples were taken for ^{1}H NMR spectroscopy and SEC analysis.

	CTA (mg, μmol)	Monomers (g, mmol)		AIBN (mg, μmol)	Dioxane (mL)	Temp (°C)
4xiv	**4xiii** (20.0, 90.4)	MMA (0.407, 4.07)	**4i** (0.200, 0.452)	(1.48, 9.04)	(0.483)	(65)
4xv	**4xiii** (10.0, 45.2)	OEGMA (0.592, 2.03)	**4i** (0.100, 0.226)	(0.742, 4.52)	(1.25)	(65)
4xvi	**4xx** (20.0, 63.0)	^{t}BA (0.363, 2.83)	**4ii** (0.135, 0.315)	(1.03, 6.30)	(0.457)	(65)
4xvii	**4xx** (10.0, 31.5)	TEGA (0.309, 1.42)	**4ii** (0.068, 0.157)	(0.517, 3.15)	(0.616)	(65)
4xviii	**4xxii** (15.0, 43.4)	Sty (0.452, 4.34)	**4iii** (0.169, 0.434)	-	-	(110)
4xix	**4xiii** (10.0, 45.2)	OEGMA (0.657, 2.26)	-	(0.742, 4.52)	(1.25)	(65)
4xxi	**4xx** (10.0, 31.5)	TEGA (0.344, 1.57)	-	(0.517, 3.15)	(0.616)	(65)
4xxiii	**4xiii** (20.0, 90.4)	MMA (0.407, 4.07)	**4iv** (0.192, 0.452)	(1.48, 9.04)	(0.483)	(65)
4xxiv	**4xiii** (10.0, 45.2)	OEGMA (0.592, 2.03)	**4iv** (0.096, 0.226)	(0.742, 4.52)	(1.25)	(65)
4xxv	**4xx** (26.3, 82.7)	^{t}BA (0.477, 3.72)	**4v** (0.170, 0.413)	(1.36, 8.27)	(0.600)	(65)
4xxvi	**4xx** (10.0, 31.5)	TEGA (0.309, 1.42)	**4v** (0.065, 0.157)	(0.517, 3.15)	(0.616)	(65)
4xxvii	**4xxii** (15.0, 43.4)	Sty (0.452, 4.34)	**4vi** (0.016, 0.043)	-	-	(110)
4xxviii	**4xiii** (20.0, 90.4)	OEGMA (1.18, 4.07)	**4iv** (0.192, 0.452)	(1.48, 9.04)	(1.48)	(65)

P(MMA-*co*-DTMMA) (**4xiv**) and P(MMA-*co*-DBMMA) (**4xxiii**) were isolated by repeated precipitation from THF into ice-cold methanol.

P(OEGMA-*co*-DTMMA) (**4xv**) and P(OEGMA-*co*-DBMMA) (**4xxiv** and **4xxviii**) were isolated by repeated precipitation from dioxane into ice-cold hexanes, followed by exhaustive dialysis against deionized water (MWCO = 3.5 kDa) and lyophilisation.

P(^{t}BA-*co*-DTMA) (**4xvi**) and P(tBA-*co*-DBMA) (**4xxv**) were isolated by repeated precipitation from DCM into dry-ice cold methanol/water (9/1 *v/v*).

P(TEGA-*co*-DTMA) (**4xvii**) was isolated by repeated precipitation from dioxane into ice-cold hexanes, followed by exhaustive dialysis against deionized water (MWCO = 3.5 kDa) and lyophilisation.

P(Sty-*co*-VBDTM) (**4xviii**) was isolated by repeated precipitation from THF into ice-cold methanol/water (9/1 *v/v*).

P(OEGMA) (**4xix**) and P(TEGA) (**4xxi**) were isolated by exhaustive dialysis against deionized water (MWCO = 3.5 kDa) and lyophilisation.

P(TEGA-*co*-DBMA) (**4xxvi**) was isolated by exhaustive dialysis against deionized water (MWCO = 1.0 kDa) and lyophilisation.

General procedure for the post-polymerisation functionalization of P(OEGMA$_{27.6}$-*co*-DBMMA$_{4.7}$) (4xxviii) with thiols

Typically; **4xxviii** (40 mg, 3.9 μmol) was dissolved in pH 6 buffer (4 mL, 100 mM sodium phosphate, 150 mM NaCl). To this solution was added a solution of thiol in DMF (46.8 μl of a 1 M solution) upon which the solution immediately turned yellow/green in colour. The reaction was stirred at room temperature for 30 mins, before addition of an excess of deionised water, and dialysis against deionised water (MWCO 3.5 kDa). The product was isolated by lyophilisation.

Post-polymerisation functionalization of P(OEGMA$_{27.6}$-*co*-DBMMA$_{4.7}$) (4xxviii) with 3-mercaptopropionic acid, monitored by UV-vis spectroscopy (4xxxiii)

4xxviii (1.5 mg, 0.146 μmol) was dissolved in pH 6 buffer (1.5 mL, 100 mM sodium phosphate, 150 mM NaCl) and added to a quartz cuvette, and a full UV-vis spectrum was

recorded. Then, a solution of 3-mercaptopropionic acid in DMF (1.76 µl of a 1 M solution) was added to the cuvette, and the absorption at 409 nm measured for 3 h.

4.6. References

1. G. Moad, E. Rizzardo and S. H. Thang, *Acc. Chem. Res.*, 2008, **41**, 1133-1142.

2. A. M. Breul, M. D. Hager and U. S. Schubert, *Chem. Soc. Rev.*, 2013, **42**, 5366-5407.

3. B. Yamada and P. B. Zetterlund, in *Handbook of Radical Polymerization*, John Wiley & Sons, Inc., 2003, pp. 117-186.

4. G. Moad, E. Rizzardo and S. H. Thang, *Aust. J. Chem.*, 2012, **65**, 985-1076.

5. K. Matyjaszewski, *Macromolecules*, 2012, **45**, 4015-4039.

6. J. Nicolas, Y. Guillaneuf, C. Lefay, D. Bertin, D. Gigmes and B. Charleux, *Prog. Polym. Sci.*, 2013, **38**, 63-235.

7. L. Ruiz-Perez, A. Pryke, M. Sommer, G. Battaglia, I. Soutar, L. Swanson and M. Geoghegan, *Macromolecules*, 2008, **41**, 2203-2211.

8. M. Sommer, S. Hüttner, U. Steiner and M. Thelakkat, *Appl. Phys. Lett.*, 2009, **95**, 183308.

9. J.-C. Hsu, C. Li, K. Sugiyama, R. Mezzenga, A. Hirao and W.-C. Chen, *Soft Matter*, 2011, **7**, 8440-8449.

10. L. Ionov, V. Bocharova and S. Diez, *Soft Matter*, 2009, **5**, 67-71.

11. A. Nese, N. V. Lebedeva, G. Sherwood, S. Averick, Y. Li, H. Gao, L. Peteanu, S. S. Sheiko and K. Matyjaszewski, *Macromolecules*, 2011, **44**, 5905-5910.

12. J. Madsen, N. J. Warren, S. P. Armes and A. L. Lewis, *Biomacromolecules*, 2011, **12**, 2225-2234.

13. J. Motoyanagi, I. Nishimura and M. Minoda, *J. Polym. Sci., Part A: Polym. Chem.*, 2011, **49**, 4701-4707.

14. A. S. Abd-El-Aziz, P. O. Shipman, P. R. Shipley, B. N. Boden, S. Aly and P. D. Harvey, *Macromol. Chem. Phys.*, 2009, **210**, 2099-2106.

15. P. Zhao, J. Jiang, B. Leng and H. Tian, *Macromol. Rapid Commun.*, 2009, **30**, 1715-1718.

16. I. Grabchev, S. Dumas and J.-M. Chovelon, *Polym. Adv. Technol.*, 2008, **19**, 316-321.

17. C. F. Hansell and R. K. O'Reilly, *ACS Macro Lett.*, 2012, **1**, 896-901.

18. R. K. O'Reilly, M. J. Joralemon, C. J. Hawker and K. L. Wooley, *Chem. Eur. J.*, 2006, **12**, 6776-6786.

19. A. J. Dirks, J. J. L. M. Cornelissen and R. J. M. Nolte, *Bioconjugate Chem.*, 2009, **20**, 1129-1138.

20. S. L. Mangold, R. T. Carpenter and L. L. Kiessling, *Org. Lett.*, 2008, **10**, 2997-3000.

21. J. P. Blinco, K. E. Fairfull-Smith, A. S. Micallef and S. E. Bottle, *Polym. Chem.*, 2010, **1**, 1009-1012.

22. W. Song, Y. Wang, J. Qu, M. M. Madden and Q. Lin, *Angew. Chem., Int. Ed.*, 2008, **47**, 2832-2835.

23. R. K. V. Lim and Q. Lin, *Chem. Commun.*, 2010, **46**, 7993-7995.

24. M. Dietrich, G. Delaittre, J. P. Blinco, A. J. Inglis, M. Bruns and C. Barner-Kowollik, *Adv. Funct. Mater.*, 2012, **22**, 304-312.

25. Y. Kang, A. Lu, A. Ellington, M. C. Jewett and R. K. O'Reilly, *ACS Macro Lett.*, 2013, **2**, 581-586.

26. B. Mu, M. Zhao and P. Liu, *J. Nanopart. Res.*, 2008, **10**, 831-838.

27. L. Castañeda, Z. V. F. Wright, C. Marculescu, T. M. Tran, V. Chudasama, A. Maruani, E. A. Hull, J. P. M. Nunes, R. J. Fitzmaurice, M. E. B. Smith, L. H. Jones, S. Caddick and J. R. Baker, *Tetrahedron Lett.*, 2013, **54**, 3493–3495.

28. K. S. Williamson and T. P. Yoon, *J. Am. Chem. Soc.*, 2010, **132**, 4570-4571.

29. A. M. Van Herk and T. Dröge, *Macromol. Theory Simul.*, 1997, **6**, 1263–1276.

30. D. Neugebauer, Y. Zhang, T. Pakula, S. S. Sheiko, and K. Matyjaszewski, *Macromolecules*, 2003, **36**, 6746–6755.

31. S. Hocine and M.-H. Li, *Soft Matter*, 2013, **9**, 5839-5861.

32. F. Hua, X. Jiang, D. Li and B. Zhao, *J. Polym. Sci., Part A: Polym. Chem.*, 2006, **44**, 2454-2467.

33. J. Chiefari, Y. K. (Bill) Chong, F. Ercole, J. Krstina, J. Jeffery, T. P. T. Le, R. T. A. Mayadunne, G. F. Meijs, C. L. Moad, G. Moad, E. Rizzardo, and S. H. Thang, *Macromolecules*, 1998, **31**, 5559–5562.

34. K. Rahimian-Bajgiran, N. Chan, Q. Zhang, S. M. Noh, H.-i. Lee and J. K. Oh, *Chem. Commun.*, 2013, **49**, 807-809.

35. S. Reinicke, P. Espeel, M. M. Stamenović and F. E. Du Prez, *ACS Macro Lett.*, 2013, **2**, 539-543.

36. G. Moad, *Macromol. Chem. Phys.*, 2014, **215**, 9-26.

37. M. P. Robin and R. K. O'Reilly, *Chem. Sci.*, 2014, **5**, 2717-2723

5. Fluorescent dithiomaleimide-containing polymer nanoparticles

5.1. Abstract

In this chapter the fluorescent labelling chemistry developed in this thesis is applied to the synthesis of fluorescent polymer nanoparticles. Using a fluorescent ROP initiator/RAFT agent an amphiphilic block copolymer with a DTM fluorophore at the interface between hydrophobic and hydrophilic blocks was produced. Aqueous solution state self-assembly gave polymer micelles with this DTM group at the interface between core and shell-forming blocks. Micelles labelled in either the core or the shell are also synthesised. In this case self-assembly was performed with amphiphilic RAFT diblock copolymers with a fluorescent DTM-functional monomer (developed in Chapter 4) copolymerised into either the hydrophobic or hydrophilic block. A DTM-functional monomer was also utilised in the synthesis of polymer nanogels by radical cross-linking copolymerisation, providing a one-step synthesis of fluorescently-labelled polymer nanoparticles.

The resultant particles were analysed by multiangle light scattering (DLS/SLS), which allowed determination of intraparticle local dye concentrations. The steady-state and time-resolved fluorescence of the particles was also assessed. The fluorescence emission of the labelled micelles was found to depend on their supramolecular state (micelles *vs.* unimers), and this self-reporting ability was further assessed *in vitro*.

5.2. Introduction

5.2.1. Fluorescence spectroscopy – The fate of the excited state

As described in the introduction to Chapter 3, absorption of a photon results in the promotion of a ground state electron to an excited state (Figure 3.1). This excited state electron can then return to the ground state either by emission of a photon (with rate Γ) or by a non-radiative process (with rate k_{nr}). From these two rates a fluorescence lifetime (τ) and fluorescence quantum yield (Q) can be calculated according to equations 3.1 and 3.2, which are reproduced below

$$\tau = \frac{1}{\Gamma + k_{nr}} \tag{3.1}$$

$$Q = \frac{\Gamma}{\Gamma + k_{nr}} \tag{3.2}$$

It follows that if $k_{nr} = 0$, then Q is the maximum value of unity. As Q is effectively a measure of the brightness of emission, $Q = 1$ corresponds to the most efficient emission possible for a particular fluorophore. When $k_{nr} = 0$, $\tau = 1/\Gamma = \tau_n$, which is the intrinsic lifetime of a fluorophore. The fate of the excited state therefore depends on the rate of non-radiative annihilation (k_{nr}), which in turn depends on the environment surrounding the fluorophore.

One such non-radiative process is solution state quenching, where the excited state fluorophore is deactivated upon collision with another molecule (for example solvent). The decrease in emission intensity due to collisional quenching is described by the Stern-Volmer equation (5.1), where I_0 and I are the intensity of fluorescence in the absence and presence of a quencher (X) respectively, k_q is the quenching rate constant, τ_0 is the unquenched lifetime and [X] is the concentration of the quencher.

$$\frac{I_0}{I} = 1 + k_q \tau_0 [X] \tag{5.1}$$

Therefore k_q is one component of k_{nr}. The magnitude of k_q will depend on the efficiency with which collisions lead to excited state quenching, and importantly, k_q will also depend on the accessibility of fluorophore to the quencher (for example the accessibility of the fluorophore to solvent).

As a result of these considerations, changes in Q and τ are indicative of changes in the environment surrounding the fluorophore, which manifest due to changes in k_{nr}. Measuring the parameters Q and τ is thus highly informative of the environment surrounding the fluorophore, while control over the environment surrounding the fluorophore manifests as control over Q and τ.

Another way in which the lifetime of the excited state influences emission is seen in fluorescence anisotropy. If a fluorophore is excited with polarised light, those molecules whose absorption transition moments are oriented along the electric vector of the incident light are preferentially excited. In a homogeneous solution, these fluorophore dipoles are randomly orientated, leading to selective excitation (Figure 5.1).

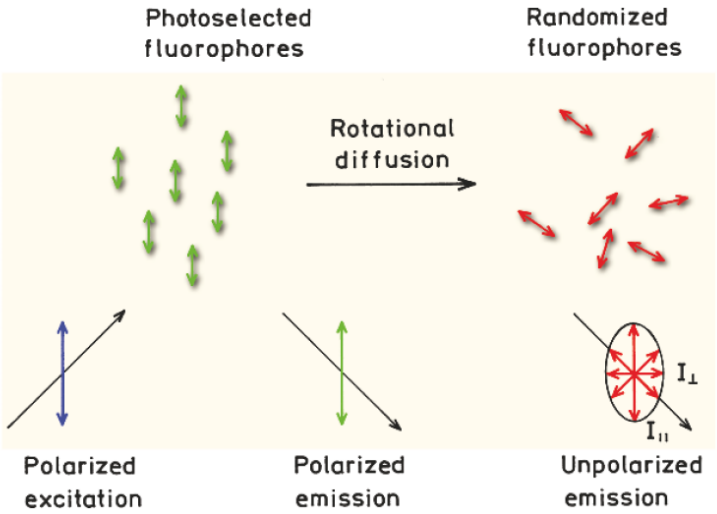

Figure 5.1. The effect of polarized excitation on emission. Figure reproduced from ref.[1]

The extent to which emission is also polarised is defined as the anisotropy (r) given in equation (5.2), where $I_{\parallel}$ is the intensity of emission parallel to the axis of polarised excitation, and $I_{\perp}$ is intensity along each of the axes perpendicular to the polarised excitation.

$$r = \frac{I_{\parallel} - I_{\perp}}{I_{\parallel} + 2I_{\perp}} \qquad (5.2)$$

As shown in Figure 5.1, immediate emission (in the absence of any diffusion) would lead to maximally polarised emission. For a homogeneous unorientated sample, anisotropy in the absence of diffusion (r_0) is 0.4.[v] However, molecular rotation for most small molecule fluorophores occurs on the order of 50-100 ps, which is much greater than typical lifetimes for the excited state ($1 < \tau < 10$ ns). Therefore, rotational diffusion leads to randomisation of the excited dipoles, and a resultant depolarised emission ($r \rightarrow 0$). As such, anisotropy will depend upon both τ, and the rotational correlation time (θ), as expressed by the Perrin equation (5.3).

$$r = \frac{r_0}{1 + \frac{\tau}{\theta}} \qquad (5.3)$$

Equation (5.3) illustrates that anisotropy is very sensitive to the environment of the excited state. For example, encapsulation of the fluorophore into a macromolecule will lead to an increased r, because θ will be larger for the macromolecule than for the small molecule. An increase in the rate of either non-radiative or radiative decay will result in increased anisotropy. This can be caused by processes such as increased collisional quenching (leading to an increase in k_{nr}) or a decrease in the intrinsic lifetime of the fluorophore (leading to an increase in Γ). With no change in fluorophore state (protonation, increased/decreased temperature *etc.*) a change in emission anisotropy is primarily associated with changes to k_{nr}.

5.2.2. Measuring r and τ by steady-state and time-resolved fluorescence

Steady-state fluorescence measurements are performed with constant illumination of the sample, thereby providing continuous excitation. As a result average values of I and r are measured – that is, I and r are collected as a function of wavelength (λ). In contrast, time-resolved measurements use pulsed light sources and high-speed detection which allows the

[v] The reason $r_0 = 0.4$ and not 1 is due to the photoselection rules for excitation. It has been shown that for excitation along the z-axis the probability of absorption is proportional to $\cos^2\theta$, where θ is the angle between the dipole and z-axis. In this case $I_{\parallel} = 3I_{\perp}$ giving $r_0 = 0.4$.

decay of I and r to be measured after single photon excitation – that is, I and r are collected as a function of time (t). This is difference is depicted in Figure 5.2.

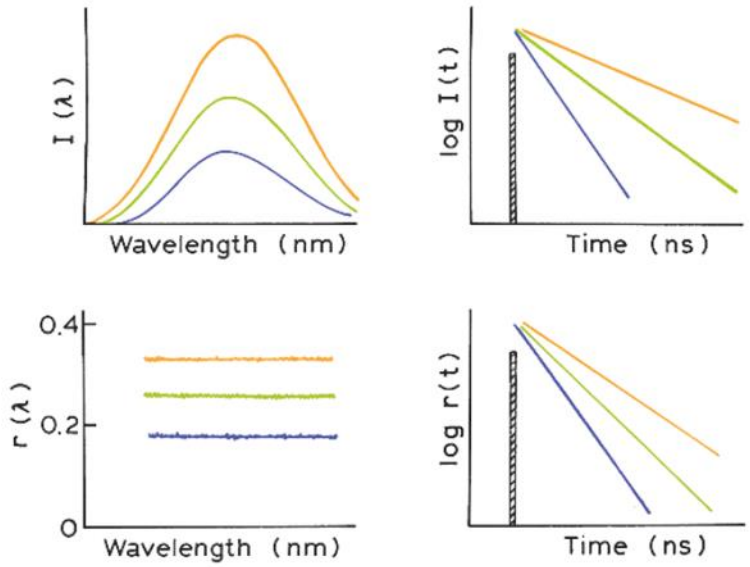

Figure 5.2. Comparison between steady state (left) and time-resolved (right) fluorescence spectroscopy. Figure adapted from ref.[1]

Measurement of emission anisotropy (r) is fairly trivial. As it is a steady-state measurement, this equipment is less complex/expensive than that required for time-resolved measurements, and therefore more commonly available. As shown in Figure 5.3, the use of an excitation polariser allows the production of vertically (V) or horizontally (H) polarised light, while the emission polariser allows detection of emitted light polarised in the vertical or horizontal plane. In the case of vertically polarised excitation, $I_{\parallel}$ is detected as I_{VV} (where the order of subscripts corresponds to excitation and emission respectively), and $I_{\perp}$ as I_{VH}. Likewise, for horizontally polarised excitation, both I_{HH} and I_{HV} correspond to $I_{\perp}$. Measurement of I_{VH}, I_{VV}, I_{HH} and I_{HV} allows anisotropy to be calculated according to equation (5.4), where the G-factor (which corrects for any difference in detection efficiency for vertically and horizontally polarised light[vi]) is found according to equation (5.5).

[vi] These differences are the result of any polarising properties of the optical components of the fluorometer such as the emission monochromator (MC).

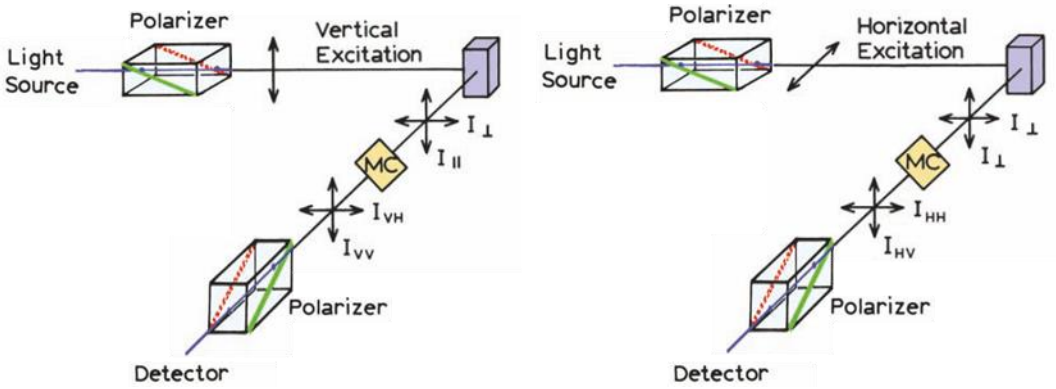

Figure 5.3. Schematic of the experimental set-up for measurement of fluorescence anisotropy. Figure adapted from ref.[1]

$$r = \frac{I_{VV} - GI_{VH}}{I_{VV} + 2GI_{VH}} \tag{5.4}$$

$$G = \frac{I_{HV}}{I_{HH}} \tag{5.5}$$

As a time-resolved measurement, the determination of τ is more complex in both the equipment and analysis required. The aim of the experiment is to excite the fluorophore with a pulse of light (the duration of which is much shorter than τ), then to monitor the decay of excited state fluorophores to the ground state. Both radiative processes (with rate Γ) and non-radiative processes (with rate k_{nr}) depopulate the excited state, so that the number of excited molecules (n) can be described according to equation (5.6).

$$\frac{dn(t)}{dt} = (\Gamma + k_{nr})\, n(t) \tag{5.6}$$

Integration of equation (5.6) results in an exponential decay of n. Because the emission intensity is directly proportional to n, the result is the measurable decay of I shown in equation (5.7), where I_0 is the intensity at time zero.

$$I(t) = I_0\, e^{-\frac{t}{\tau}} \tag{5.7}$$

Most samples possess more than one mechanism for excited state depopulation, such that decay of I is represented as a sum of lifetimes (τ_i), each with amplitude A_i, according to equation (5.8).

$$I(t) = \sum_i A_i \, e^{-\frac{t}{\tau_i}} \tag{5.8}$$

These lifetime components (τ_i) and their amplitudes (A_i) are found by fitting I(t) to a sum of exponential decays. Average lifetimes, weighted either by intensity ($\tau_{Av,I}$) or amplitude ($\tau_{Av,A}$), can be calculated according to equations (5.9) and (5.10).[2]

$$\tau_{Av,I} = \frac{\sum A_i \tau_i^2}{\sum A_i \tau_i} \tag{5.9}$$

$$\tau_{Av,A} = \frac{\sum A_i \tau_i}{\sum A_i} \tag{5.10}$$

The most common way to measure I(t) is by time-correlated single photon counting (TCSPC). A pulsed laser is used for excitation, and the arrival time of single photons at the detector is measured using high speed optics. A histogram of photon arrival times builds up as the experiment progresses, which represents the waveform of I(t), as shown in Figure 5.4. For the TCSPC setup used in this Chapter, the laser was pulsed at 2.5 MHz (with a FWHM duration of 59 ps), with a detection rate of $< 1\%$ (*i.e.* < 25 kHz) to prevent bias towards shorter lifetimes. The histogram was populated to a maximum intensity of 10 000 counts, in 64 ps bins. An instrument response function (IRF), which is the response of the instrument to a zero lifetime sample is recorded using a dilute scattering solution such as Ludox (colloidal silica). The effect of the IRF on the measured decay is removed by deconvolution during the fitting.

5.2.3. Fluorescence lifetime imaging microscopy (FLIM)

In fluorescence lifetime imaging microscopy (FLIM), TCSPC is coupled to confocal microscopy to provide a powerful tool for cell imaging. An I(t) decay is recorded for every pixel in the image, providing the image contrast. There are several advantages of FLIM over conventional fluorescence microscopy when using fluorescent dyes/probes for cellular imaging.

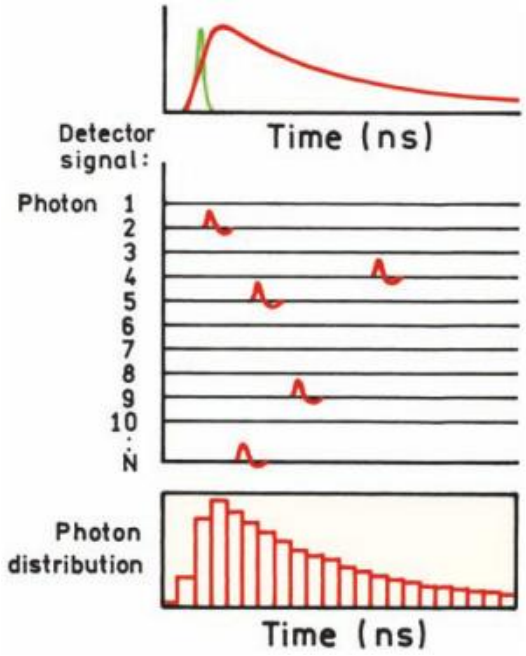

Figure 5.4. The principle of a TCSPC experiment. Reproduced from ref.[1]

Firstly, the intensity of fluorescence is dependent on the fluorophore concentration, which can be hard to determine *in vitro* due to the rapid diffusion of fluorophores, photobleaching, and the potential for loss of fluorophore during cell washing.[1] Furthermore, the intensity will also depend on a variety of environmental factors such as quenching, fluorophore aggregation, energy transfer, and differences in the refractive index of the medium.[3] In contrast, the fluorescence lifetime of a chromophore is independent of its concentration, and of the light path-length in the sample.[4]

Another advantage of FLIM over conventional fluorescence microscopy is the ability of FLIM to distinguish between spectrally similar probes, provided their fluorescent lifetimes are different.[3] This is particularly useful in cell imaging due to the natural occurrence of endogenous fluorescent biomolecules such as keratin, collagen, flavins, metal-free porphyrins and NAD(P)H coenzymes.[5] This cellular autofluorescence has a lifetime on the order of 2-3 ns, so temporal resolution can be achieved with dyes that have a greater τ.[6]

In vitro FLIM has so far been mostly conducted using organic fluorophores and fluorescent proteins as probes, with the use of fluorescent nanoparticles not widely exploited to date.[6] One of these rare examples comes from Davis and co-workers, who synthesised iron oxide nanoparticles (IONPs) with a grafted polymer shell to which was

attached doxorubicin (DOX) *via* a pH responsive imine linkage. After addition to H1299 lung cancer cells, the release of DOX by hydrolysis of the imine linkage was observed by *in vitro* FLIM. The DOX-IONPs had a lifetime of 4.6 ns and were found to be present in the cytoplasm, whereas free DOX with a lifetime of 1.6 ns was observed in the cell nuclei (Figure 5.5).[7]

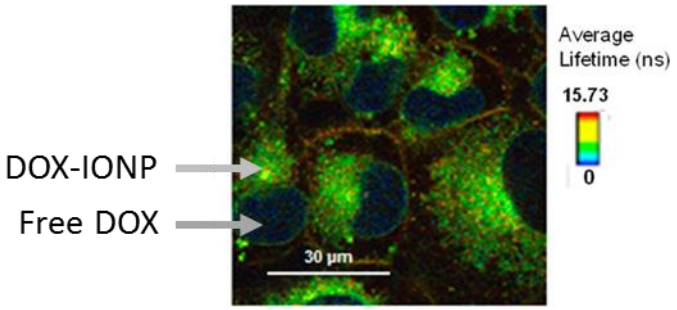

Figure 5.5. FLIM images showing cell uptake of DOX-IONP by H1299 cells. Figure adapted from ref.[7]

5.3. Results and Discussion

5.3.1. Fluorescent amphiphilic block copolymer polymer synthesis

In order to synthesise block copolymer (BCP) micelles with DTM fluorophores in the shell, core, or at the core-shell interface it was necessary to synthesise three different block copolymers. Core-shell interface-labelled micelles (ILMs) would be derived from the self-assembly of an amphiliphilic BCP with the DTM fluorophore at the interface between the hydrophilic shell-forming block and the hydrophobic core-forming block, while shell-labelled micelles (SLMs) and core-labelled micelles (CLMs) would require a BCP with the DTM fluorophore in the hydrophilic block and hydrophobic block respectively (Figure 5.6).

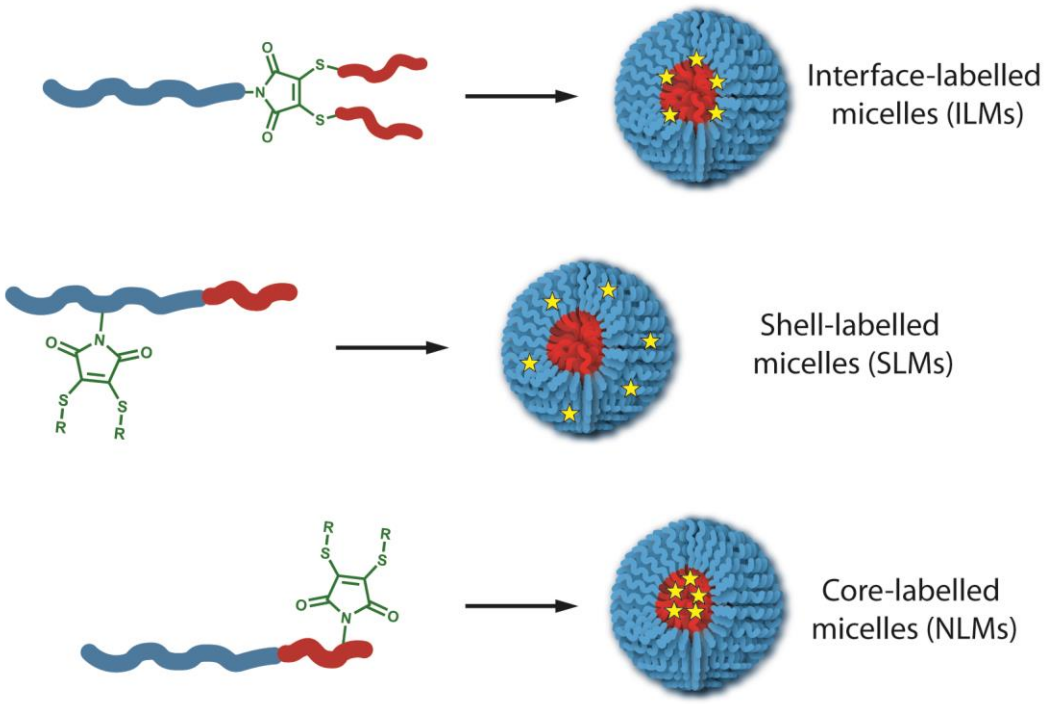

Figure 5.6. Schematic representation of the route to interface-labelled micelles (ILMs), shell-labelled micelles (SLMs) and core-labelled micelles (CLMs) containing the DTM fluorophore.

5.3.1.1. Interface-labelled micelles

The BCP used to form the ILMs was based on the DTM-containing dual ROP initiator/RAFT agent (**3ix**). As shown in Chapter 3, ring-opening polymerisation of hydrophobic poly(D,L-lactide) (PLA) could be initiated from the hydroxyl groups attached to the DTM unit *via* the two thioether groups, while RAFT polymerisation of hydrophilic

poly(triethyleneglycol monomethylether acrylate) (PTEGA) could be mediated by the trithiocarbonate attached to the DTM unit *via* the N. Sequential ROP/RAFT or RAFT/ROP would therefore afford an amphiliphilic BCP with the DTM fluorophore at the interface between shell and core-forming blocks. For practical reasons it was decided to perform the ROP step first to produce poly(D,L-lactide) **3xiv**, as ROP of lactide requires completely anhydrous conditions and it was expected to be easier to dry the initiator **3ix** as opposed to a PTEGA macroinitiator. Therefore, the interface-labelled block copolymer (**5i**) was synthesised by RAFT polymerisation of TEGA through chain-extension of the macro-CTA **3xiv** as shown in Scheme 5.1. The polymerisation was performed at 60 °C in chloroform; conditions that have previously been found to provide the best solubility for both the PLA chain and trithiocarbonate end-group for PLA macro-RAFT agents.[8, 9]

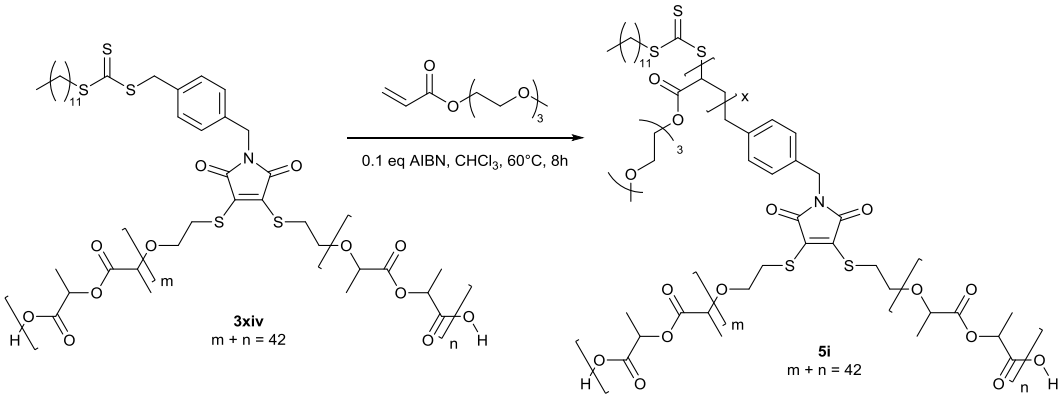

Scheme 5.1. Synthesis of the interface-labelled block copolymer **5i**.

The resultant PTEGA-*b*-$(PLA)_2$ BCP (**5i**)was purified by exhaustive dialysis against deionised water and isolated by lyophilisation. SEC analysis (with a DRI detector) of **5i** indicated a narrow molecular weight distribution with $Đ_M = 1.32$ (Figure 5.7). When analysing RAFT block copolymers by SEC it was important to also use a UV detector, with $\lambda_{abs} = 309$ nm to detect for trithiocarbonate end-groups. This is due to the difference in refractive index increment (dn/dc) for polymers with different repeating units (e.g. PLA, PTEGA and PTEGA-*b*-PLA) which results in a non-uniform DRI detector response. This is particularly important for PLA which is known to have a low dn/dc in THF (0.042 mL/g).[10] The response from the UV detector ($\lambda_{abs} = 309$ nm) is proportional to the number of polymer chains for both **3xiv** and **5i**, assuming good RAFT end-group

retention. Analysis using the Cirrus SEC software assumes a response proportional to the number of repeat units, therefore analysis of **5i** with a calibration generated for the UV detector could be used to generate a weight distribution. This weight distribution could be corrected to $dw_i/d\log M_i$ *via* multiplication by M_i at each point i.[11] This refractive index independent molecular weight distribution confirmed a good chain extension, with consumption of the PLA macro-CTA (Figure 5.7). SEC data from the UV detector with $\lambda_{abs} = 400$ nm showed the presence of the DTM chromophore in **5i**. It was again assumed that response from the UV detector was proportional to the number of polymer chains, and the molecular weight distribution was corrected accordingly.

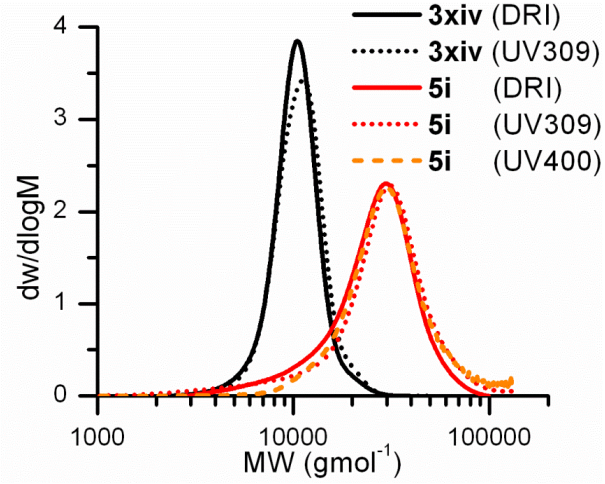

Figure 5.7. Molecular weight distribution for **3xiv** and **5i** obtained by SEC using DRI and UV ($\lambda_{abs} = 309$ nm and 400 nm) detectors.

The ^{1}H NMR spectrum **5i** indicated that DP(TEGA) = 136, giving a weight fraction for the hydrophobic (core-forming) PLA block (f_C) of 17% (Figure 5.8). The morphology resulting from BCP self-assembly is dependent on the preparation pathway, due to the propensity for formation of kinetically trapped structures.[12] However, equilibrium morphology depends on the relative lengths of solvophobic and solvophilic blocks, which dictate the free energy of the aggregate.[13] Although determining the free energy is non-facile for polymeric amphiphiles, a qualitative argument to determine equilibrium morphology based on block weight fractions has been proposed.[14, 15] In the case of **5i** $f_C \ll 50\%$, suggesting the formation of starlike spherical micelles upon aqueous self-assembly.

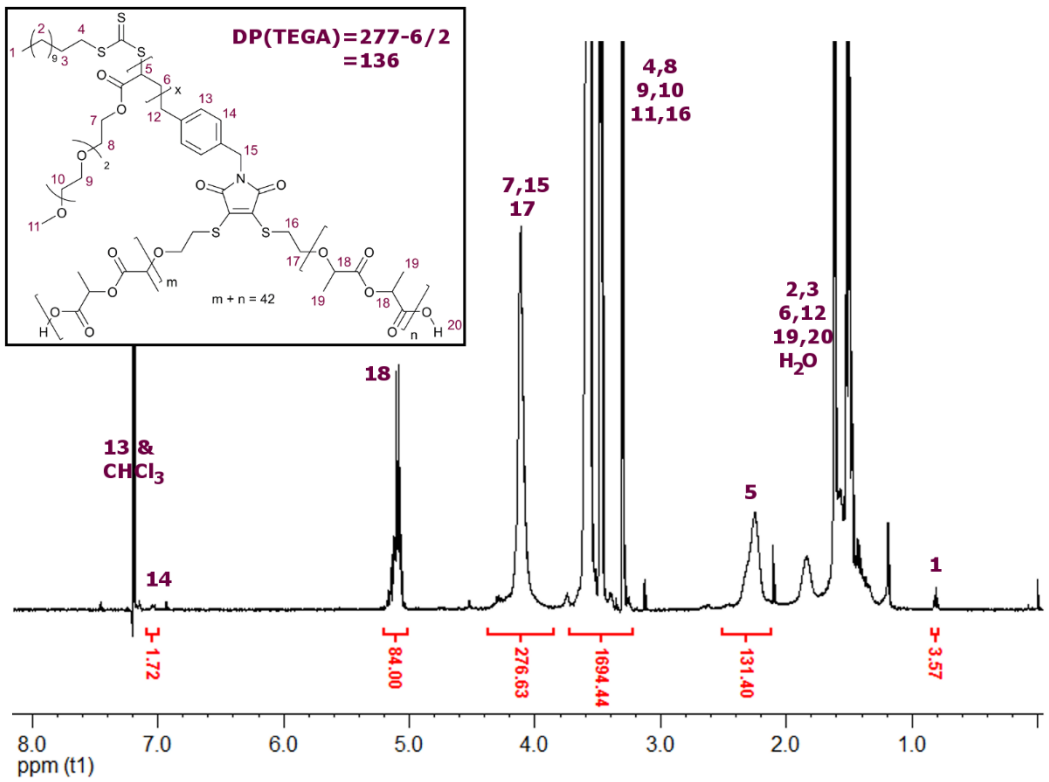

Figure 5.8. ^{1}H NMR spectrum (400 MHz, $CDCl_3$) of **5i**. Integration of H18 was set to be equal to 84.

Characterisation data for all the polymers discussed in this chapter is summarised in Table 5.1.

Table 5.1. Characterisation data for polymers **3xiv**, **5i-5vi**

	Polymer	M_n [a] (kg·mol^{-1})	M_n [b] (kg·mol^{-1})	$Đ_M$ [b]
3xiv	P(D,L-LA)$_{42}$	6.7	9.8	1.09
5i	P(TEGA)$_{136}$-*b*-P(D,L-LA)$_{42}$	36.4	21.4	1.32
5ii	P(TEGA$_{143}$-*co*-DTMA$_{1.1}$)-*b*-P(^{t}BA)$_{44.1}$	37.7	21.9	1.35
5iii	P(TEGA)$_{127}$-*b*-P(^{t}BA$_{35.8}$-*co*-DTMA$_{1.1}$)	33.1	26.7	1.38
5iv	P(TEGA)$_{116}$-*b*-P(^{t}BA)$_{44.1}$	31.3	20.1	1.38
5v	P(^{t}BA)$_{44.1}$	6.0	5.2	1.08
5vi	P(^{t}BA$_{35.8}$-*co*-DTMA$_{1.1}$)	5.4	5.1	1.13

[a] Calculated by ^{1}H NMR end-group analysis. [b] Measured by SEC.

5.3.1.2. Shell- and core-labelled micelles

The BCPs used to form SLMs and CLMs were based on P(TEGA)-*b*-P(^{t}BA), with an average of approximately one repeat unit per chain of dithiomaleimide acrylate (DTMA, **4ii**) copolymerised into either the PTEGA shell-forming block (**5ii**), or P^{t}BA core-forming block (**5iii**) as show in Scheme 5.2. A non-functional P(TEGA)-*b*-P(^{t}BA) was also synthesised (**5iv**), to allow self-assembly of non-labelled micelles (NLMs) for comparison.

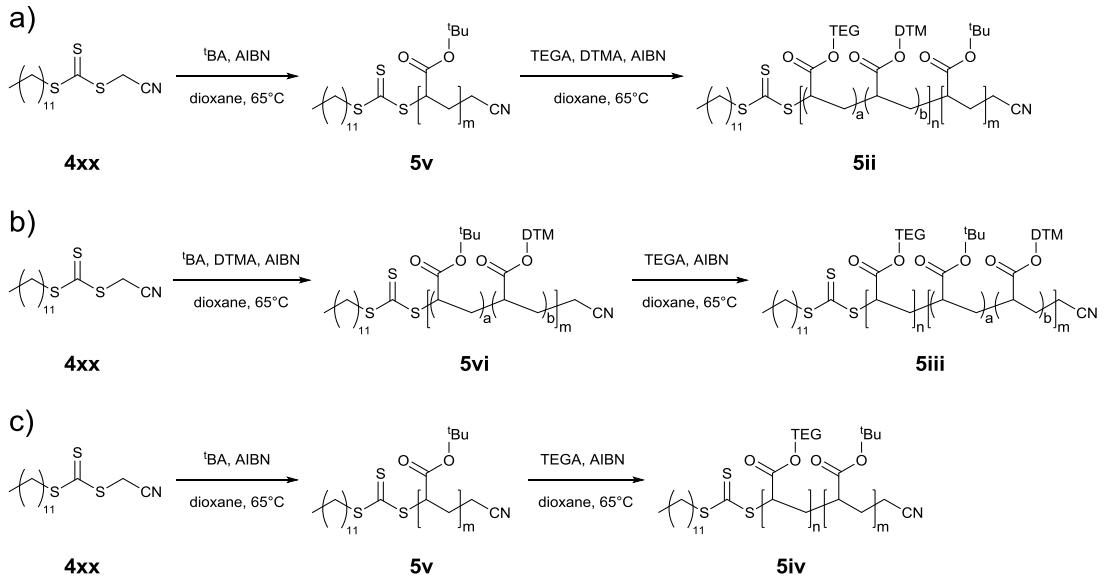

Scheme 5.2. Synthesis of P(TEGA)-*b*-P(^{t}BA) block copolymers with DTM label in the shell-forming block (**5ii**), the core-forming block(**5iii**), and a non-labelled block copolymer (**5iv**).

For the synthesis of the shell-block labelled BCP **5ii**, it was first necessary to synthesise the non-labelled P^{t}BA core-forming block **5v**. RAFT polymerisation of ^{t}BA was performed using the commercially available CTA **4xx**, with AIBN (0.1 *eq.*) as radical initiator, as a solution in dioxane at 65 °C. The resultant polymer **5v** was purified by repeated precipitation into ice-cold methanol/H_2O (9/1 *v/v*). ^{1}H NMR spectroscopy indicated $DP = 44.1$ while the presence of the trithiocarbonate end-group was confirmed by characteristic resonances of the dodecyl chain (H1 and H4 in Figure 5.9). SEC analysis of **5v** indicated a good control over molecular weight ($Đ_M = 1.08$), with trithiocarbonate retention indicated by polymer absorption at 309 nm (Figure 5.10).

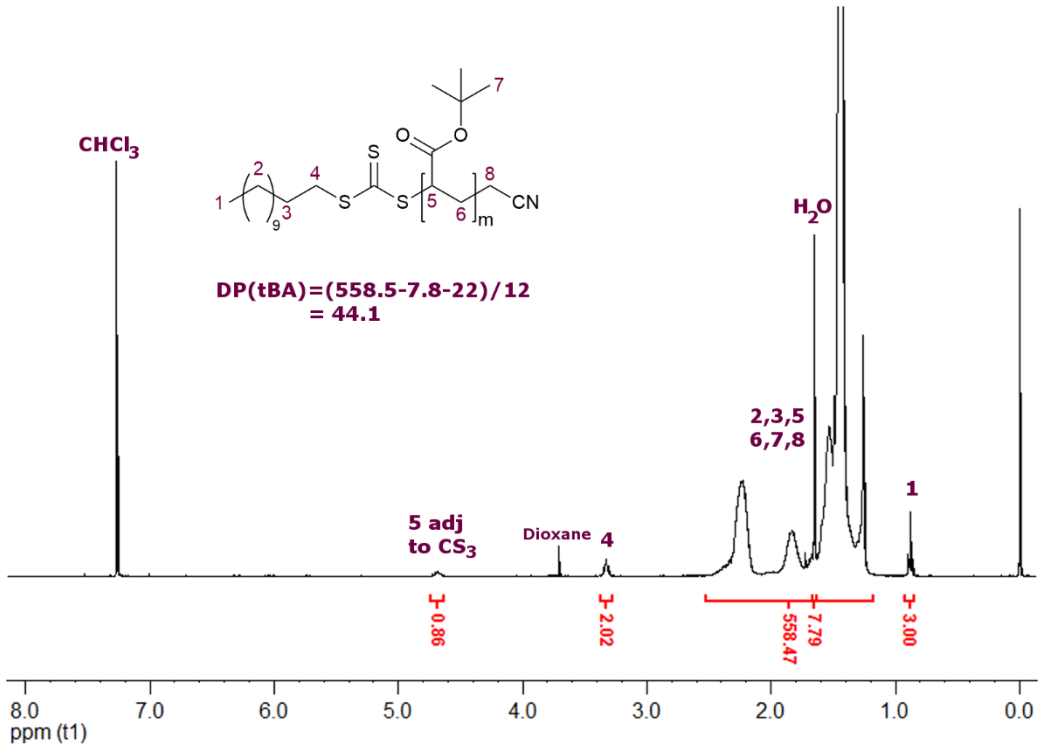

Figure 5.9. ^{1}H NMR spectrum (400 MHz, $CDCl_3$) of **5v**. Integration of H1 was set to be equal to 3.00.

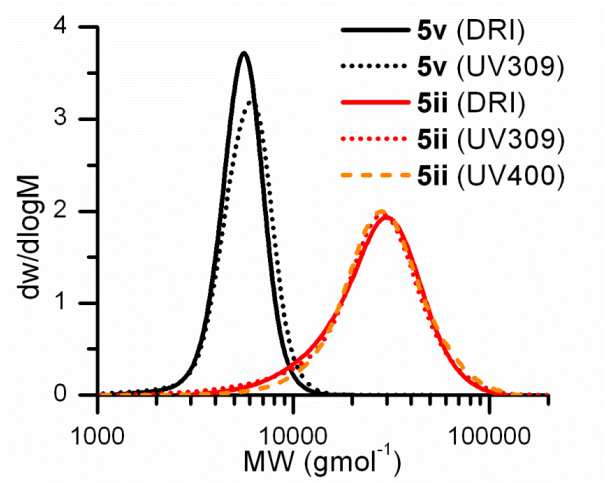

Figure 5.10. Molecular weight distribution for **5v** and **5ii** obtained by SEC using DRI and UV (λ_{abs} = 309 nm or 400 nm) detectors.

Chain extension of **5v** was performed according to Scheme 5.2, using TEGA and DTMA. Average *DP* of 1 for DTMA and 136 for TEGA was targeted, so that the molar concentration of DTM groups in the resultant BCP would be the same as in the interface-labelled BCP **5i**. This was done by using a reaction composition of [**5v**]:[TEGA]:[DTMA]:[AIBN] = 1:200:1.5:0.1 and aiming for *ca.* 66% conversion. The resultant polymer **5ii** was purified by precipitation into ice-cold hexane followed by

exhaustive dialysis of a dioxane/water solution against deionised water, and isolated by lyophilisation. ^{1}H NMR spectroscopy indicated that the final BCP **5ii** had *DP*(TEGA) = 143 and *DP*(DTMA) = 1.1 (Figure 5.11), giving **5ii** a hydrophobic weight fraction (f_C) of 15%, which will likely favour the formation of starlike spherical micelles upon aqueous self-assembly.

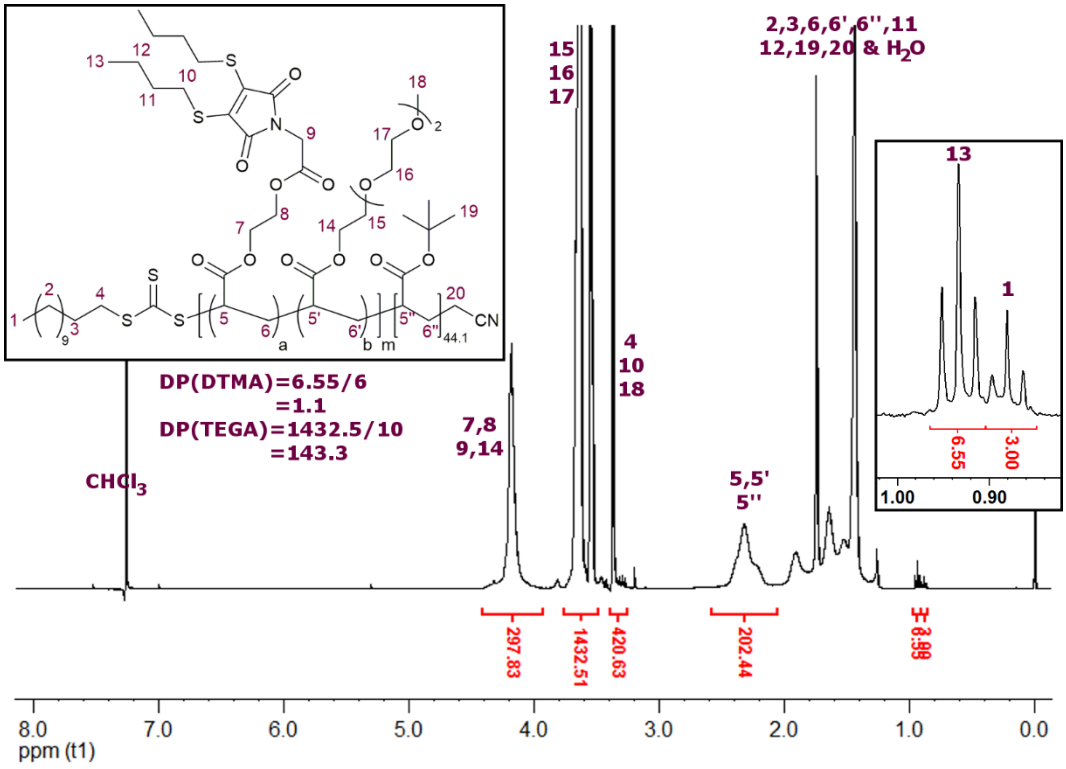

Figure 5.11. ^{1}H NMR spectrum (400 MHz, $CDCl_3$) of 5ii. Integration of H1 was set to be equal to 3.00.

SEC indicated good blocking efficiency, with molecular weight distributions obtained from both DRI and UV (λ_{abs} = 309 nm) showing consumption of **5v**, with a reasonable control over molecular weight ($Đ_M$ = 1.35). By using a UV detection at 400 nm (absorption due to the DTM chromophore), incorporation of DTMA into the BCP was also confirmed (Figure 5.10).

For the synthesis of the shell-block labelled BCP **5iii**, the first step was to synthesise a DTM-labelled core-forming block by copolymerisation of ^{t}BA and DTMA. RAFT polymerisation was performed using the commercially available CTA **4xx**, with AIBN (0.1 *eq.*) as radical initiator, as a solution in dioxane at 65 °C. A final molar loading of 1 *eq.* DTMA and a core block M_n similar **5v** were targeted by using a reaction

composition of [**4xx**]:[^{t}BA]:[DTMA]:[AIBN] = 1:50:1.5:0.1 and aiming for *ca.* 66% conversion. The resultant polymer **5vi** was purified by repeated precipitation into ice-cold methanol/H_2O (9/1 *v*/*v*). ^{1}H NMR spectroscopy indicated that $DP(^{t}BA) = 35.8$ and $DP(DTMA) = 1.1$ and showed resonances attributed to the trithiocarbonate end-group (H1 and H4 in Figure 5.12).

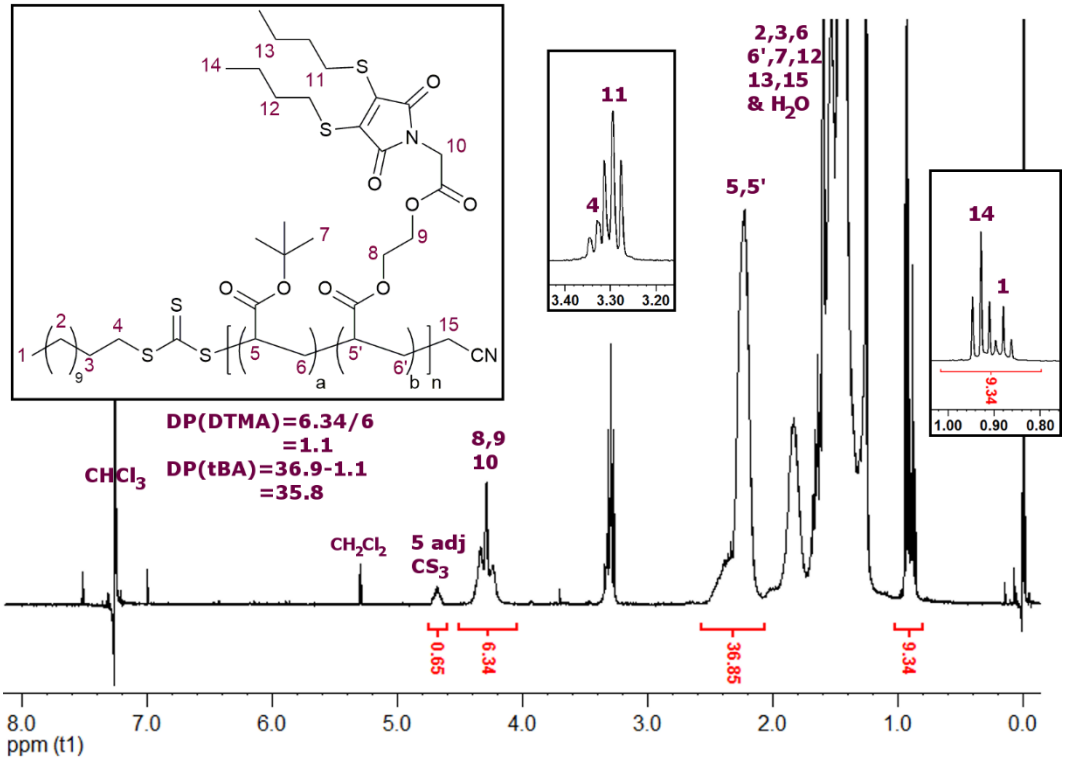

Figure 5.12. ^{1}H NMR spectrum (400 MHz, $CDCl_3$) of **5vi**. Combined integration of H1&4 was set to be equal to 3 + combined integration of H8-10.

SEC analysis of **5vi** indicated a good control over molecular weight ($Đ_M = 1.13$), with trithiocarbonate retention indicated by polymer absorption at 309 nm (Figure 5.13). Additionally, SEC analysis using a PDA detector showed incorporation of the DTM chromophore, with the polymer peak having the characteristic DTM absorption at *ca.* 400 nm (Figure 5.14).

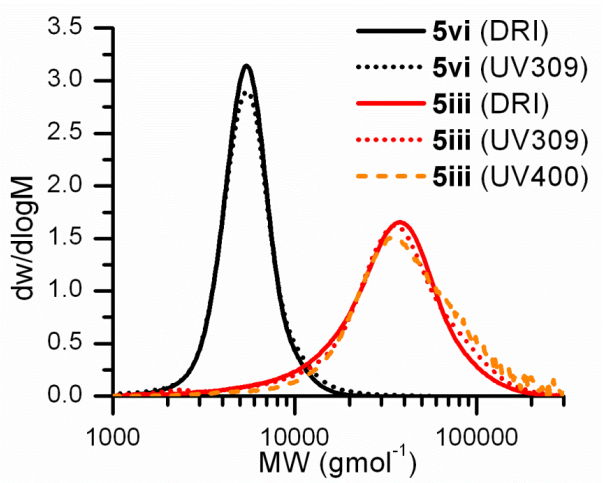

Figure 5.13. Molecular weight distribution for **5vi** and **5iii** obtained by SEC using DRI and UV (λ_{abs} = 309 nm or 400 nm) detectors.

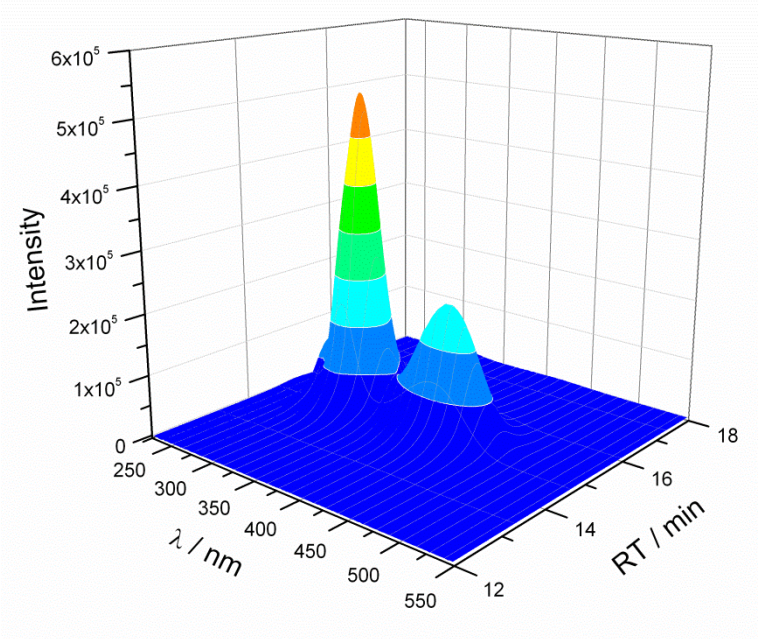

Figure 5.14. Three-dimensional chromatogram of **5vi** obtained by SEC using a PDA detector and THF as eluent.

Chain extension of **5vi** with TEGA was performed according to Scheme 5.2. A *DP*(TEGA) of approximately 135 was targeted (in line with **5i** and **5ii**) by using a reaction composition of [**5vi**]:[TEGA]:[AIBN] = 1:200:0.1 and aiming for *ca.* 66% conversion. The resultant polymer **5iii** was purified by exhaustive dialysis against deionised water, and isolated by lyophilisation. ^{1}H NMR spectroscopy indicated that the final BCP **5iii** had *DP*(TEGA) = 127 (Figure 5.15), corresponding to f_C = 16%, which should also favour the formation of starlike spherical micelles upon aqueous self-assembly.

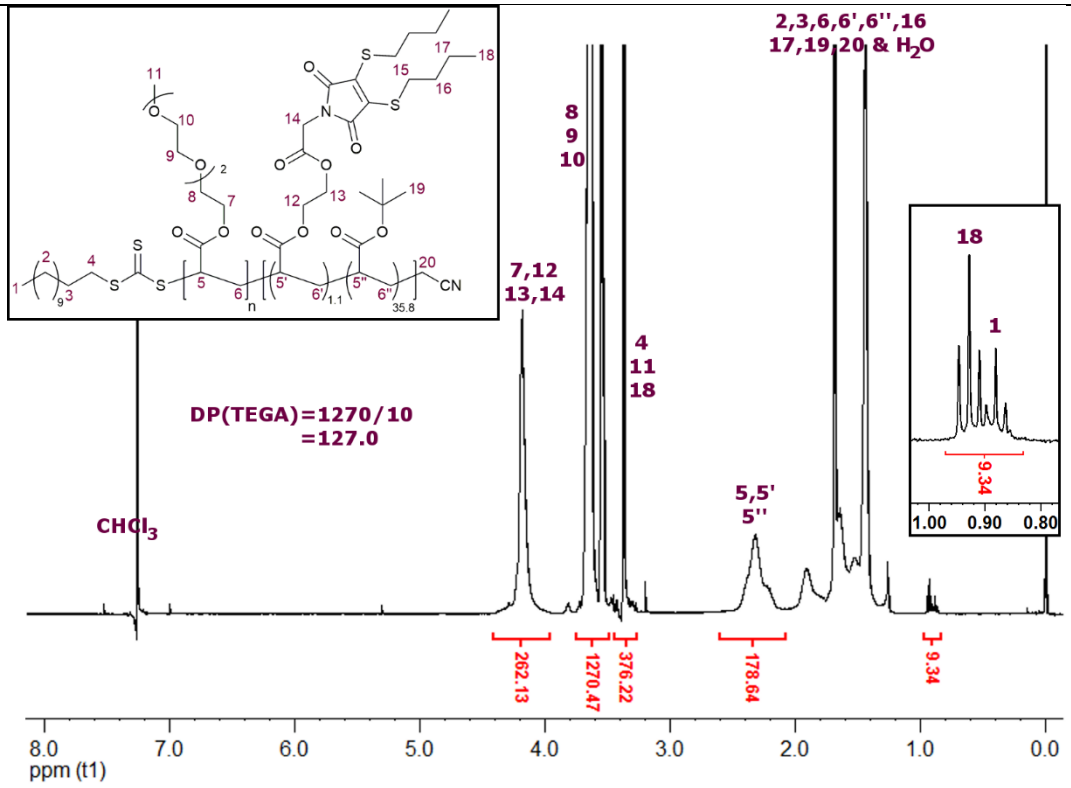

Figure 5.15. ^{1}H NMR spectrum (400 MHz, $CDCl_3$) of **5iii**. Combined integration of H1&18 was set to be equal to 9.34.

SEC indicated good blocking efficiency, with molecular weight distributions obtained from both DRI and UV (λ_{abs} = 309 nm) showing consumption of **5vi**, with a reasonable control over molecular weight ($Đ_M$ = 1.38). By using a UV detection at 400 nm the presence of the DTM group in the final BCP was also confirmed (Figure 5.13).

The non-labelled BCP (**5iv**) was synthesised by chain extension of **5v** with TEGA according to Scheme 5.2. ^{1}H NMR spectroscopy indicated *DP*(TEGA) = 116 (Figure 5.16), corresponding to f_C = 18%, while SEC showed reasonable control over molecular weight ($Đ_M$ = 1.38, Figure 5.17).

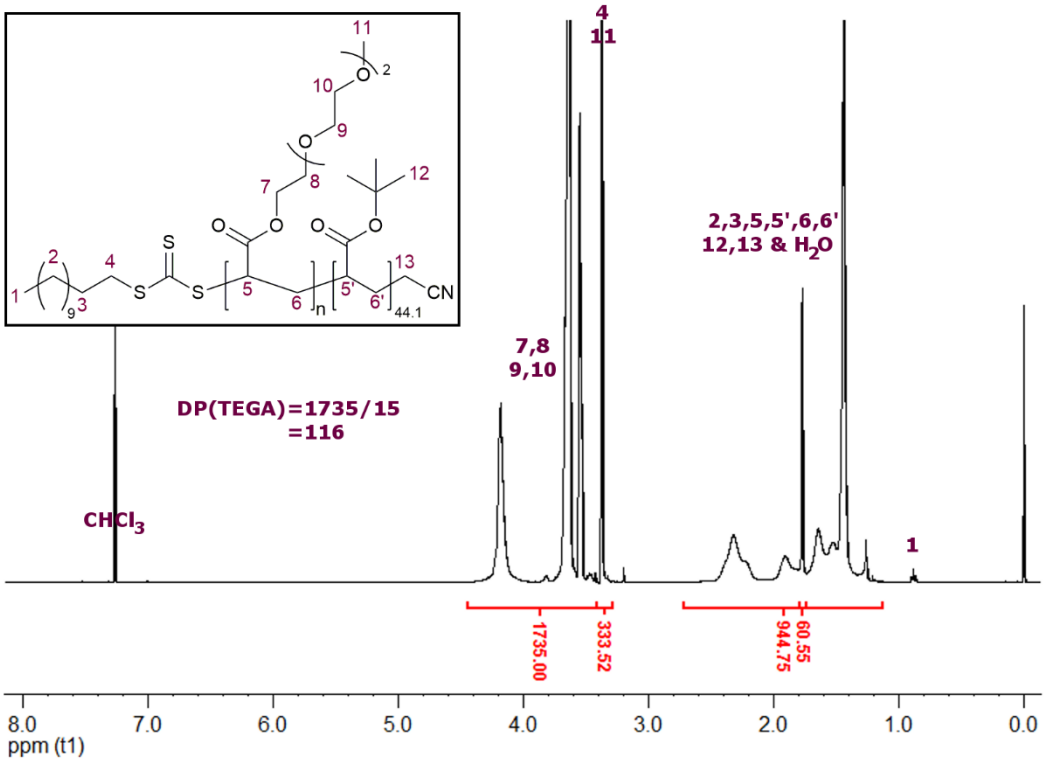

Figure 5.16. ^{1}H NMR spectrum (400 MHz, $CDCl_3$) of **5iv**. Combined integration of H2,3,5,5',6,6',12,13 was set to be equal to the combined integration of H4&11 + (558.5-7.8-2).

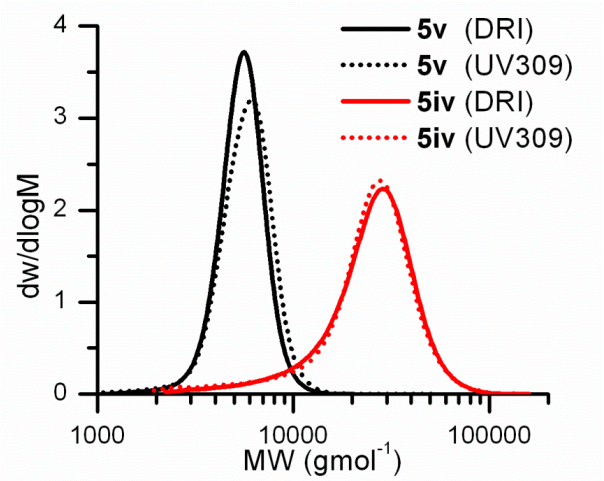

Figure 5.17 a) Molecular weight distribution for **5v** and **5iv** obtained by SEC using DRI and UV (λ_{abs} = 309 nm) detectors.

5.3.2. Self-assembly and particle characterisation

The amphiphilic BCPs **5i-5iv** were assembled by direct dissolution in water (18.2 MΩ·cm) at a concentration of 1 g/L. In order to fully disperse the particles of **5i** the solution was sonicated until completely transparent. For **5ii-5iv** solutions were stirred at 60 °C for 3 h, then sonicated until completely transparent.

5.3.2.1. Theory of dynamic and static light scattering (DLS/SLS)[16]

Light scattering experiments for dilute solutions of polymer nanoparticles provide information about the particle size and morphology, particle molecular weight, and the second virial coefficient.[17] In the light scattering experiment the sample is placed in a cuvette and illuminated with radiation of known intensity (I) and wavelength (λ) *i.e.* using a laser. Radiation that is scattered by the sample is then measured at an angle (θ) relative to the transmitted incident radiation. The scattering vector (q) for light scattering is defined according to equation (5.11), where n is the refractive index of the solvent.

$$q = \frac{4\pi n \sin\frac{\theta}{2}}{\lambda} \tag{5.11}$$

In dynamic light scattering (DLS), an intensity autocorrelation function ($g_2(q,t)$) is produced by the correlator, which calculates fluctuations in intensity of scattered light (I) over small time intervals (Δt), according to equation (5.12).

$$g_2(q,t) = \frac{\langle I_0(q,t) I_{0+\Delta t}(q,t)\rangle}{\langle I_0(q,t)\rangle^2} \tag{5.12}$$

This intensity autocorrelation function is related to the electric field autocorrelation function ($g_1(q,t)$) according to the Siegert relation (5.13).

$$g_2(q,t) = 1 + g_1(q,t)^2 \tag{5.13}$$

In a system of perfect monodisperse spheres, this fluctuation of the electric field autocorrelation function can be modelled as a monoexponential decay with relaxation time (τ) according to equation (5.14).

$$g_1(q,t) = e^{-\frac{t}{\tau}} \tag{5.14}$$

These electric field fluctuations are caused by Brownian motion of the scattering particles; diffusion due to thermal density fluctuations of the solvent. Polymeric nanoparticles are

not perfect monodisperse spheres, but are instead polydisperse. Furthermore, multimodal distributions of scattering particles are often observed. Therefore $g_1(q,t)$ is fit to a continuous distribution of relaxation times $A(\tau)$, each characterised by a polydispersity, using a fitting routine. A translational diffusion coefficient (D) is defined to characterise the Brownian particle motion, with the concentration dependant (apparent) value (D_{app}) dependent on the relaxation time (τ) and the scattering vector (q) according to equation (5.15).

$$\tau^{-1} = D_{app}q^2 \tag{5.15}$$

This angular independent D_{app} is therefore calculated as the average value of $\tau^{-1} \cdot q^{-2}$ over all angles of observation. This process eliminates the effect of intraparticle interactions, where scattering from different parts of the particle have a different path length at non-zero angles.

In the dilute concentration regime D_{app} has a linear dependence on concentration as shown in equation (5.16), where k_D is the dynamic second virial coefficient. The concentration independent diffusion coefficient (D) is found by extrapolation of D_{app} to $c = 0$.

$$D_{app} = D(1 + k_D c) \tag{5.16}$$

According to the Stokes-Einstein equation (5.17), D is related to the hydrodynamic radius of the particle (R_h), where k_B is the Boltzmann constant, T is the absolute temperature, and η is the viscosity of the solvent in which the particles are dispersed.

$$R_h = \frac{k_B T}{6\pi\eta D} \tag{5.17}$$

In static light scattering (SLS) the intensity of scattered light is averaged over a timescale much greater than τ (typically one thousand times longer) so that fluctuations in scattered light due to Brownian motion are lost. Instead, the intensity of scattered light (I) is related to particle size and mass according to the Zimm equation (5.18), where R_g is the radius of gyration, M_w is the weight average molecular weight, and A_2 is the second

virial coefficient (which represents the strength of interactions between pairs of particles – positive for repulsion and negative for attraction).

$$\frac{Kc}{R_\theta} = \frac{q^2 R_g^2}{3M_w} + \frac{1}{M_w} + 2A_2 c \tag{5.18}$$

The Zimm equation is valid in the regime $R_g \cdot q < 1$, which for a HeNe laser ($\lambda = 632.8$ nm) and maximum angle of observation $\theta = 150°$ corresponds to $R_g < 40$ nm. K is a collection of constants given by equation (5.19), where $n_{standard}$ is the refractive index of the standard (toluene), dn/dc is the refractive index increment of the sample solution (measured using a differential refractometer), and N_A is Avogadro's number.

$$K = \frac{4\pi^2 n_{standard}^2 \left(\frac{dn}{dc}\right)^2}{N_A \lambda^4} \tag{5.19}$$

The Rayleigh ratio (R_θ) contained in the Zimm equation corresponds to the contribution of the sample to the scattering intensity, and is given by equation (5.20), where I_{sample}, $I_{solvent}$, and $I_{standard}$ are scattering intensity of the sample, solvent and standard (toluene) respectively, and $R_{\theta,standard}$ the known Rayleigh ratio of the standard.

$$R_\theta = \frac{I_{sample} - I_{solvent}}{I_{standard}} R_{\theta,standard} \tag{5.20}$$

By measuring I_{sample} at a range of angles, a plot of Kc/R_θ *vs.* q^2 will give a straight line, with gradient dependant on R_g. The intercept gives a zero angle Rayleigh ratio ($Kc/R_{\theta,0}$). This process is repeated at a range of concentrations, so that concentration can be extrapolated to zero to remove the effect of non-ideal interactions between particle and solvent. This plot of $Kc/R_{\theta,0}$ *vs.* c will give a straight line with intercept $1/M_w$ and gradient $2A_2$.

5.3.2.2. Analysis of **5i-5iv** solutions by DLS/SLS

Self-assembled solutions of **5i-5iv** were analysed by multi-angle laser light scattering using a goniometer. Samples were analysed at multiple concentrations ($c = 1$, 0.8, 0.6, 0.4,

0.2 g/L) and multiple angles (θ = 70-150° in 10° steps) with the intensity of scattered light (I_{sample}) and the intensity autocorrelation function ($g_2(q,t)$) collected simultaneously. The REPES routine which directly fits $g_2(q,t)$ by an Inverse Laplace transformation,[18, 19] was used to obtain the distribution of relaxation times $A(\tau)$. In most cases $A(\tau)$ consisted of a single relaxation time, however for some measurements multiple τ were obtained, due to spurious 'slow modes' as the result of inter-particle aggregation or poorly defined aggregates. In this case the relaxation time for the fast mode (τ_{fast}, with corresponding amplitude A_{fast}) was used for further calculations. The advantage of the simultaneous DLS/SLS measurement is that a corrected Rayleigh ratio (R'_θ) can be calculated according to equation (5.21).[20]

$$R'_\theta = A_{fast} R_\theta \tag{5.21}$$

As scattering intensity is proportional to the molecular weight of the scattering species (and therefore to the third power of their radius), the concentration of the 'slow mode' scatterers can be assumed to be negligible.

An example of the data obtained by DLS for the ILMs (self-assembled **5i**) is shown in Figure 5.18. The $g_2(q,t)$ autocorrelation function, and distribution of relaxation times ($A(\tau)$) is shown for the solution at 0.6 g/L, measured at 80° and 90°. For the 80° sample, fitting with the REPES routine gave a slow mode and a fast mode, with corresponding amplitudes $A_{\text{slow}} = 0.065$, $A_{\text{fast}} = 0.935$ and relaxation times $\tau_{\text{slow}} = 4.44$ ms, $\tau_{\text{fast}} = 0.449$ ms. For the 90° sample fitting with the REPES routine gave a single relaxation time, $\tau = 0.455$ ms.

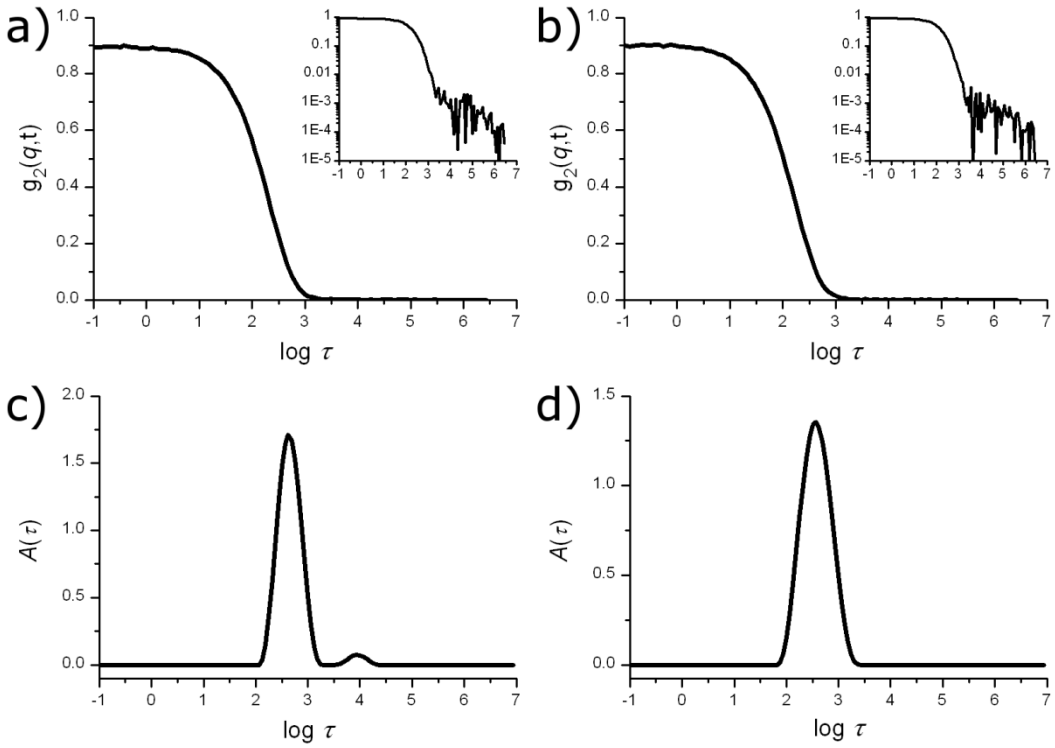

Figure 5.18. The intensity autocorrelation function $g_2(q,t)$ for ILMs (0.6 g/L) measured at a) 80° and b) 90°, with the corresponding distribution of relaxation times $A(\tau)$ for c) 80° and d) 90°.

The values of τ_{fast} and τ obtained for 80° and 90° respectively fit to the linear plot of τ^{-1} *vs.* q^2, confirming that these two relaxation times characterise the same species in solution. Furthermore, the linearity of the plot of τ^{-1} *vs.* q^2 indicates that this species has spherical morphology and diffuses under Brownian motion (Figure 5.19). D_{app} was calculated as the average value of $\tau^{-1} \cdot q^{-2}$ (Figure 5.19), and the plot of D_{app} *vs.* c for all concentrations of the ILM solutions gave D as the intercept, corresponding to $R_{\text{h}} = 24.7$ nm (Figure 5.20).

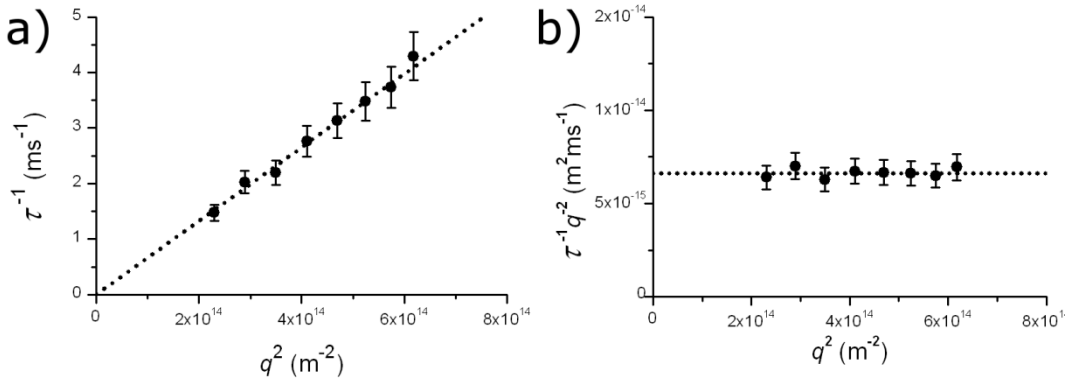

Figure 5.19. Plot of a) τ^{-1} *vs.* q^2 and b) $\tau^{-1} \cdot q^{-2}$ *vs.* q^2 for ILMs (0.6 g/L).

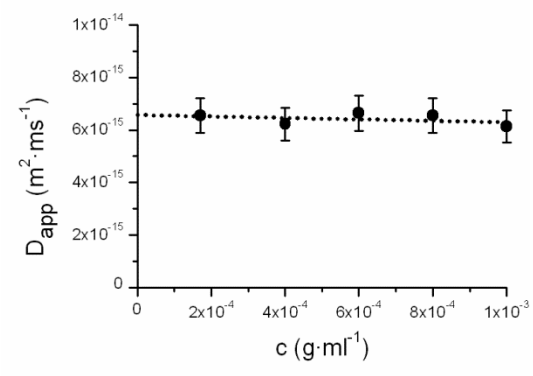

Figure 5.20. Plot to determine the diffusion coefficient (D) for ILMs.

The plot of Kc/R_θ *vs.* q^2 for each concentration of the ILMs showed that within the 10% error applied to laser light scattering measurements,[21] Kc/R_θ was independent of q^2 (Figure 5.21). This is because for spherical particles smaller than $\lambda/20$ (*ca.* 30 nm in this case) there is a negligible phase difference between light scattered by different scattering centres within the same particle, and therefore scattering intensity is independent of the angle of observation.[16] For this reason, a reliable gradient for Kc/R_θ *vs.* q^2 cannot be measured when $R_g \lesssim 20$ nm, and it is standard practise to take $Kc/R_{\theta,0}$ as the average Kc/R_θ over the measured q range. From the resultant plot of $Kc/R_{\theta,0}$ *vs.* c, the particle M_w was calculated to be 5.2 Mg·mol^{-1}, with a negative A_2 value of -3.6×10^{-5} mL·mol·g^{-2} (Figure 5.21).

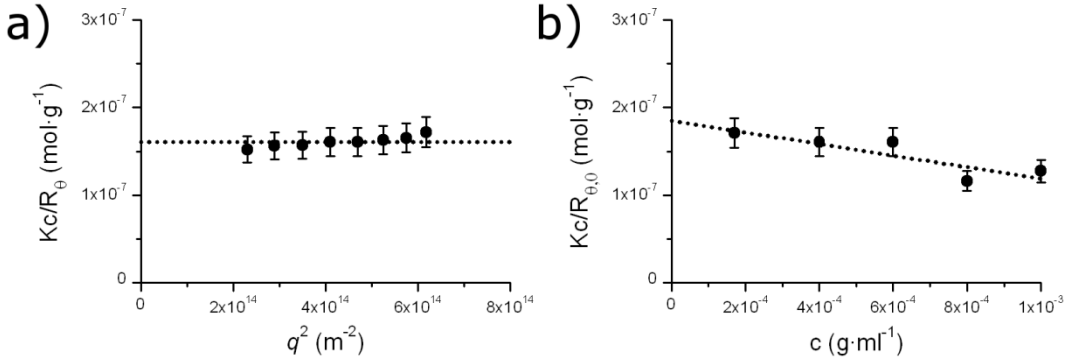

Figure 5.21. a) Plot of Kc/R_θ *vs.* q^2 to determine $Kc/R_{\theta,0}$ for ILMs at 0.6 g/L; b) Plot of $Kc/R_{\theta,0}$ *vs.* c to determine M_w and A_2 for ILMs.

An aggregation number (N_{agg}) for the micelles can be calculated according to equation (5.22), where $M_{w,polymer}$ can be approximated by the M_n calculated by NMR multiplied by $Đ_M$ calculated by SEC. For the ILMs, $N_{agg} = 111$.

$$N_{agg} = \frac{M_{w,particle}}{M_{w,polymer}} \tag{5.22}$$

Assuming that the micelle core is completely dehydrated, it is then possible to approximate the radius of the core (R_{core}) from N_{agg} according to equation (5.23).[21] This equation simply relates the volume of a sphere with radius R_{core} to the mass of the polymer core of the micelle ($M_{\text{w,core}} = M_{\text{n,core}}(\text{NMR}) \times Đ_{\text{M,core}}$ for **3xiv**), whose volume is approximated by the bulk density of the core-forming polymer ($\rho = 1.25 \times 10^6$ g·m^{-3} for PLA[22]).

$$\frac{4\pi\rho R_{core}^3}{3} = N_{agg}\frac{M_{w,core}}{N_A} \tag{5.23}$$

For the ILMs $R_{\text{core}} = 6.2$ nm, which gives a corresponding core volume (V_{core}) of 9.9×10^{-22} dm^{-3}. As the DTM fluorophore is situated at the core-shell interface, an approximate concentration of the fluorophore ([DTM]) can be calculated according to equation (5.24), assuming that the fluorophores occupy this core volume. For the ILMs [DTM] = 186 mM.

$$[DTM] = \frac{N_{agg}}{N_A V_{core}} \tag{5.24}$$

Knowledge of R_{core} and R_{h} allows the simple calculation of the radius of the micelle shell (R_{shell}) according to equation (5.25).

$$R_h = R_{core} + R_{shell} \tag{5.25}$$

In an analogous fashion the volume of the shell (V_{shell}) can also be calculated. For spherical micelles R_{shell} will depend on the degree to which the chains in the corona are stretched. A maximum chain length (L_{max}) for a linear polymer can be calculated according to equation (5.26), as its degree of polymerisation (DP) multiplied by the repeat unit length (L_{M}), which for the two C-C tetrahedral σ-bonds derived from a vinyl monomer is 0.25 nm.[21]

$$L_{max} = DP \times L_M \tag{5.26}$$

Comparison of L_{max} to R_{shell} therefore gives an indication of the degree of stretching (ω) of corona chains, which is calculated using equation (5.27).

$$\omega = \frac{R_{shell}}{L_{max}} \tag{5.27}$$

The value of ω gives a good indication of whether or not the measured particle radius is realistic, as a spherical micelle could not have $\omega > 1$. For the ILMs $\omega = 0.56$. A summary of all the data obtained by DLS/SLS for the ILMs is given in Table 5.2.

Table 5.2. DLS/SLS characterisation data for micelles obtained by the solution self-assembly of DTM-labelled BCPs.

	ILMs	**SLMs**	**CLMs**	**NLMs**
BCP	**5i**	**5ii**	**5iii**	**5iv**
f_C (%)	17	15	16	18
dn/dc	0.083	0.12	0.11	0.11
R_h (nm)	24.7	25.9	26.8	26.9
M_w (Mg·mol^{-1})	5.2	1.9	4.9	6.6
A_2 (mL·mol·g^{-2})	-3.6×10^{-5}	-1.4×10^{-4}	-2.2×10^{-5}	-9.8×10^{-6}
N_{agg}	111	37	106	152
R_{core} (nm)	6.2	4.6	6.3	7.3
R_{shell} (nm)	18.5	21.3	20.5	19.6
ω	0.56	0.59	0.64	0.62
V_{core} (dm^{-3})	9.9×10^{-22}	4.0×10^{-22}	1.1×10^{-21}	1.6×10^{-21}
V_{shell} (dm^{-3})	6.2×10^{-20}	7.2×10^{-20}	8.0×10^{-20}	8.0×10^{-20}
[DTM] (mM)	186	0.94	181	-

Similar DLS/SLS analysis was performed on the SLMs (from **5ii**), CLMs (**5iii**) and NLMs (**5iv**). The plots to determine R_h, M_w and A_2 are shown in Figure 5.22. In all cases Kc/R_θ was independent of q^2 and as a result it was not possible to calculate R_g. For R_{core} calculations the bulk density (ρ) was taken be that of P^{t}BA (1.00 g·m^{-3}),[23] with contribution from PDTMA units assumed to be negligible. Refractive index increments (dn/dc) of the samples prepared for light scattering were measured with a differential refractomer. Characterisation data is included in Table 5.2.

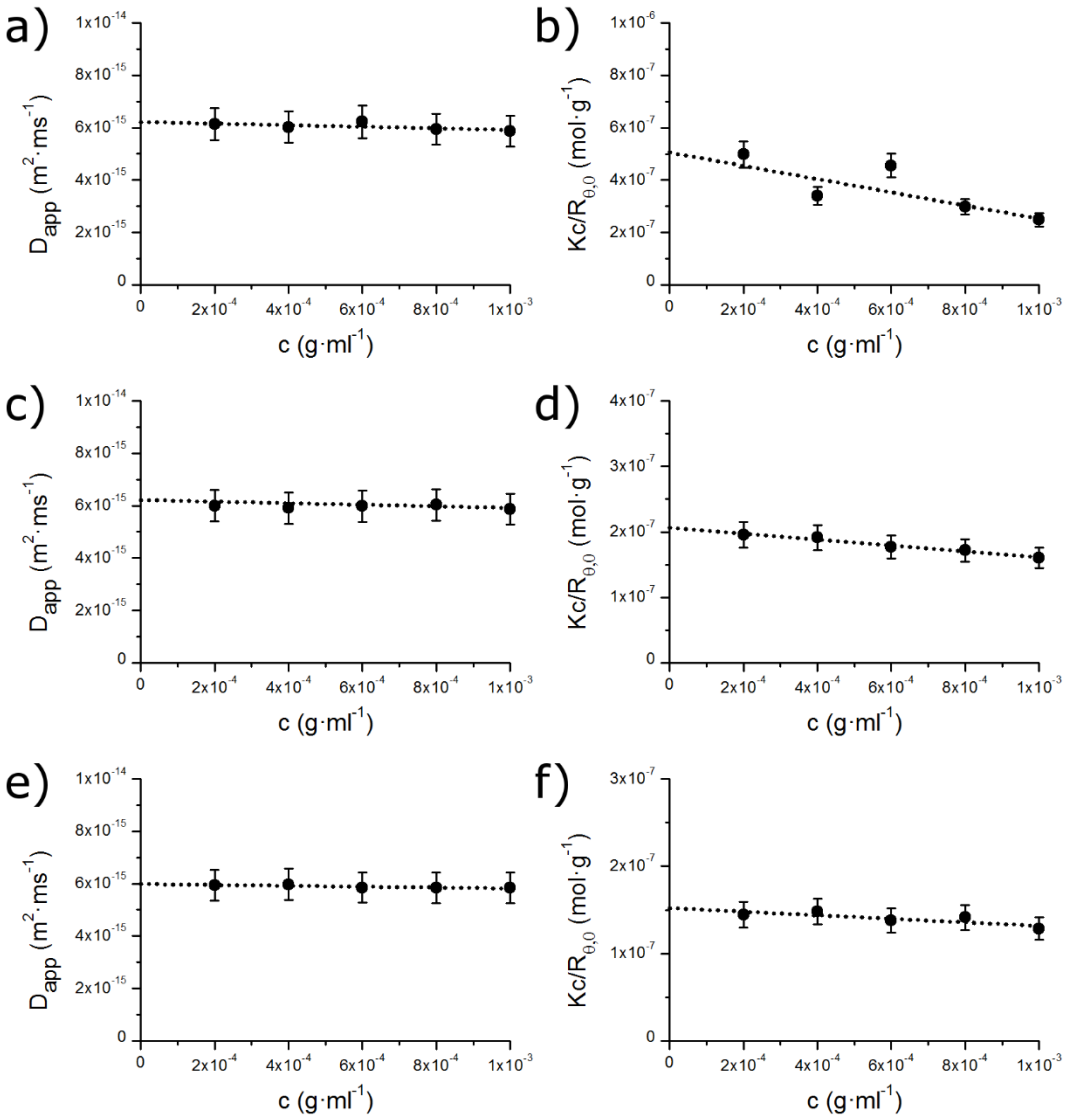

Figure 5.22. Plots to determine D (left hand side) and plots to determine M_w and A_2 (right hand side) for; a & b) SLMs; c & d) CLMs; e & f) NLMs.

In all cases the particle R_h was approximately equivalent (24.7-26.9 nm), and A_2 was negative indicating an attractive force between pairs of particles. In addition, the degree of stretching of corona chains (ω) was also broadly similar (0.54-0.64), which is not surprising as all four systems have the same hydrophilic block (PTEGA). Aggregation number (N_{agg}) was found to vary between the systems, with a trend of increasing N_{agg} with f_C for the micelles with P^{t}BA based cores (derived from **5ii-5iv**). For starlike spherical micelles the equilibrium morphology is independent of the coronal block length (and therefore independent of f_C).[13] However, BCP self-assemblies often form out of equilibrium ('frozen') structures, with N_{agg} dependent on the preparation pathway.[24] During assembly the particles nucleate, then grow by insertion of unimers, which

continues until the energy barrier for insertion becomes too high, at a value of N_{agg} below the equilibrium value. The energy barrier for insertion will be lower for BCPs with a higher f_C, as their greater hydrophobic character makes them less stable in aqueous solution. Therefore, in the case of **5ii-5iv** N_{agg} increases with f_C, as it approaches the equilibrium value. Despite this variation in N_{agg}, the structural similarity of the DTM-labelled micelles prepared from **5i-5iii** compared to the NLMs prepared from **5iv** indicates that incorporation of the DTM label has not had a detrimental effect on the BCP self-assembly.

Calculation of the local concentration of the fluorescent label ([DTM]) for the self-assembled aggregates reveals that despite using the same ratio of dye for labelling the BCPs **5i-5iii** (*ca.* 1 *eq.* per chain) two very different local environments can be created. A *ca.* 200 fold decrease in local concentration is obtained by locating the DTM in the shell (SLMs), compared to locating the DTM in the core (CLMs) or at the core-shell interface (ILMs). It will be important to consider [DTM] when comparing fluorescence emission from the different particles (see below).

5.3.2.3. Analysis of **5i-5iv** solutions by TEM

Micelle solutions were imaged by dry state transmission electron microscopy (TEM) using graphene oxide (GO) support TEM grids. These grids comprise lacey carbon covered with a few layers (often just one) of GO, to provide a nearly electron transparent support for high contrast imaging thereby eliminating the need for heavy metal staining for BCP self-assemblies.[25] Samples were prepared by addition of 10 μL of micelle solution to a GO TEM grid (purchased from Agar Scientific), with excess solution wicked off after 1 min. As shown in Figure 5.23, particles derived from both PTEGA-*b*-$(PLA)_2$ (ILMs) and PTEGA-*b*-P^{t}BA (SLMs) provided a circular projection when dried to a GO surface, suggesting they had a spherical morphology, in agreement with light scattering data. In line with previous observations,[25] only micelle cores (comprising PLA and P^{t}BA for ILMs and SLMs respectively) provided sufficient contrast to be visualised by TEM, with core diameters in reasonable agreement with those obtained by light scattering.

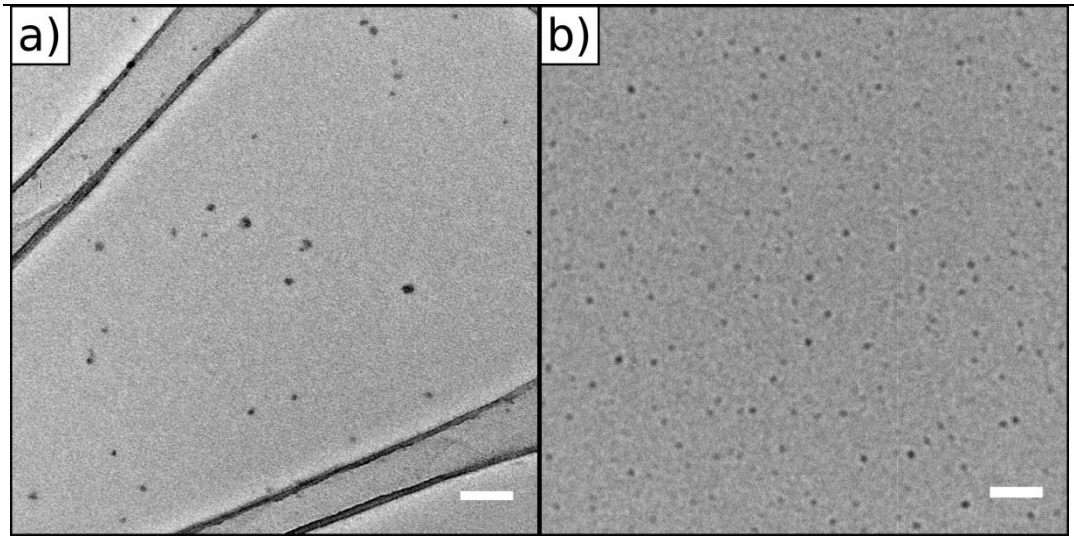

Figure 5.23. a) ILMs (prepared from **5i**) and b) SLMs (prepared from **5ii**) imaged by TEM on a GO support. Scale bars 100 nm.[vii]

5.3.3. Nanogel synthesis and characterisation

In addition to self-assembled BCP particles, aqueous solutions of DTM-labelled nanogels were also synthesised. Nanogel synthesis was performed by radical cross-linking emulsion polymerisation, following the procedure recently reported by our group for the synthesis of L-proline-functionalised nanogels.[26] The particles were formed from methyl methacrylate (MMA), with the degree of functionalisation (*DoF*) with DTM label controlled by copolymerisation of dithiomaleimide methacrylate (**4i**, DTMMA), and the crosslinking density (*CLD*) controlled by copolymerisation of ethyleneglycol dimethacrylate (EGDMA), according to Scheme 5.3.

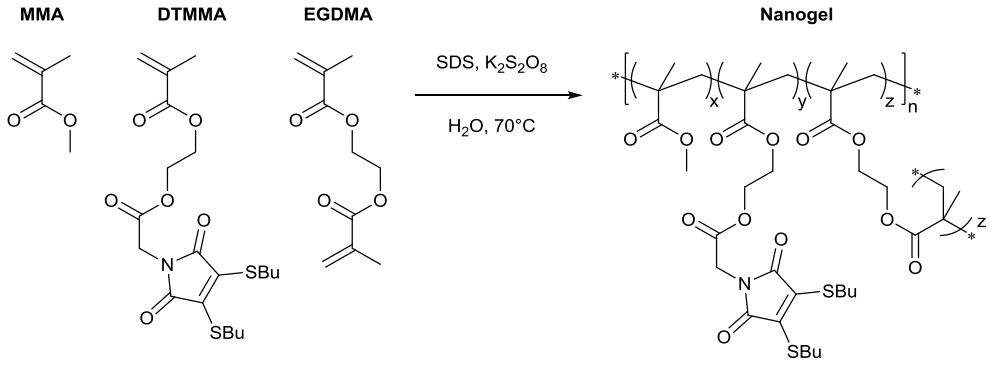

Scheme 5.3. Synthesis of DTM-labelled nanogels by radical cross-linking emulsion polymerisation

[vii] TEM images acquired by Anaïs Pitto-Barry and Yan Kang.

Potassium persulfate was used as the radical initiator, and the reaction performed at 70 °C for 14 h. The reaction solvent was water (18.2 MΩ·cm) with an MMA concentration of 10 g/L. A high concentration (2 g/L) of sodium dodecyl sulfate (SDS) was used as the surfactant to target nanogels with radii in the 10-25 nm size range.[26] To investigate the effect of changes in dye loading on fluorescence emission, *DoF* was varied (for a constant *CLD* of 0.5 wt%) from 0.3 mol% to 0.0003 mol%. The upper value in this range corresponds to 1 DTM group per 34 kg·mol^{-1} PMMA in the resultant nanogels, giving an approximately equivalent loading to BCPs **5i-5iii**, as explained in equation (5.28) where M_{MMA} is the molar mass of MMA.

$$DoF = \left(\frac{34\ kg \cdot mol^{-1}}{M_{MMA}}\right)^{-1} = 0.0030 = 0.3\ mol\% \qquad (5.28)$$

CLD was also varied (for a constant *DoF* of 0.03 mol%) as 0.5 wt%, 3 wt% and 10 wt% so that the effect of the core mobility on fluorescence emission could be investigated. These parameters are summarised in Table 5.3. The resultant nanogels were stabilised by SDS, with excess SDS and any unreacted monomer removed by exhaustive dialysis against water (18.2 MΩ·cm). This step resulted in small changes in sample volume, leading to a range of final concentrations as shown in Table 5.3

Table 5.3. Composition and characterisation of DTM-labelled nanogels (**NG1**-**NG6**)

	NG1	**NG2**	**NG3**	**NG4**	**NG5**	**NG6**
DoF (mol%)	0.3	0.03	0.03	0.03	0.003	0.0003
CLD (wt%)	0.5	0.5	3	10	0.5	0.5
c (g/L)	10.0	9.9	9.0	9.0	9.3	8.9
dn/dc	0.10	0.061	0.087	0.093	0.065	0.084
R_{h} (nm)	9.0	12.4	10.5	9.4	11.7	11.5
V_{NG} (10^{-21} dm^{-3})	3.1	8.0	4.9	3.5	6.8	6.4
M_{w} (Mg·mol^{-1})	2.4	11.6	4.8	4.0	9.7	7.8
DoF_{NG}	71	34	14	12	2.8	0.23
[DTM] (mmol)	38	7.1	4.8	5.5	0.70	0.059

Nanogel hydrodynamic radius (R_{h}) and molecular weight (M_{w}) were determined by DLS/SLS as described above. For each sample, measurements were made with c = 5, 4, 3,

2 & 1 g/L, at $\theta = 40°$-$150°$ (10° step), and the dn/dc was determined using the scattering samples with a differential refractometer. It was found that R_h was very similar for all samples, with values between 9.0 nm and 12.4 nm. Nanogel volume (V_{NG}) could be determined from R_h, and subsequently the average number of DTM units per nanogel (DoF_{NG}) could be calculated using equation (5.29), where DoF is expressed as a decimal, and where it was assumed that the final contribution of SDS to the particle mass was negligible.

$$DoF_{NG} = DoF \times \frac{M_w}{M_{MMA}} \tag{5.29}$$

Using DoF_{NG} and V_{NG}, the concentration of DTM confined in the nanogels could also be calculated, according to equation (5.30).

$$[DTM] = \frac{DoF_{NG}}{V_{NG} \times N_A} \tag{5.30}$$

Due to the similarity in size between **NG1**-**NG6** [DTM] varied over 3 orders of magnitude in accordance with the loading of DTMMA (DoF) used in the radical cross-linking polymerisation.

A dry state TEM image of **NG2** on a GO support is show in Figure 5.24. The particles showed a tendency to aggregate when dried to the GO surface (as seen in the top right corner of the image). However, individual particles were observed to possess a spherical morphology, in agreement with light scattering measurements.

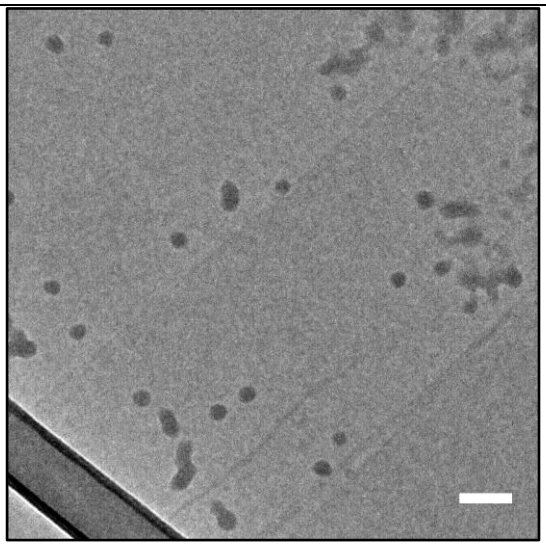

Figure 5.24. **NG2** imaged by TEM on a GO support. Scale bars 100 nm.[viii]

5.3.4. Steady state fluorescence

5.3.4.1. Excitation and emission spectra

The steady state emission and excitation spectra for solutions of labelled micelles and nanogels were found to be very similar to that of the analogous small molecule DTM (**3i**).

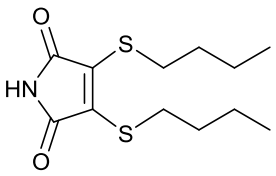

3i

2D excitation-emission spectra for a micelle sample (CLMs) and a nanogel sample (**NG1**) are shown in Figure 5.25. It can be seen from these spectra that in both systems the excitation maxima at *ca.* 260 nm and *ca.* 400 nm are observed, with the corresponding emission maximum at *ca.* 510 nm, in accordance with the spectra for **3i** (shown in Chapter 3).

[viii] TEM image acquired by Anaïs Pitto-Barry.

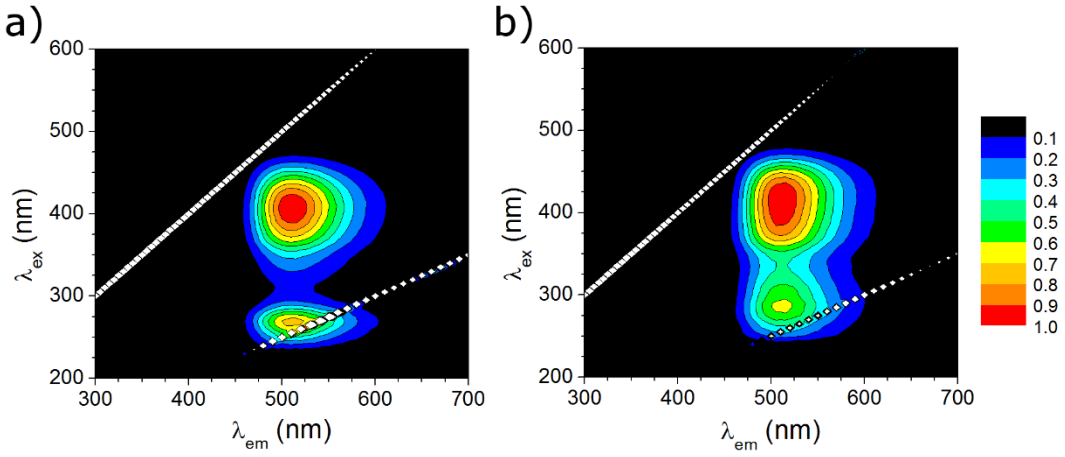

Figure 5.25. 2D excitation-emission spectra with a 5 nm step for aqueous solutions of a) CLMs and b) **NG1**.

5.3.4.2. Quantum yield

The quantum yield (Q) for **NG1** was calculated relative to the reference 5(6)-FAM (5-(6)-carboxyfluorescein) which has $Q = 0.92$.[27] Quantum yield can be described according to equation (5.31), where n is the refractive index of the solvent, $\bar{I}$ is the integrated emission over all wavelengths for excitation at λ, and Abs is absorption at λ.

$$Q = Gn^2 \frac{\bar{I}}{Abs} \tag{5.31}$$

The factor G encompasses the efficiency of emission detection for the apparatus being used and is essentially incalculable. However, if the emission and absorption spectra of a reference (ref) with known Q are collected under the same conditions as those of the sample, then Q for the sample can be calculated according to equation (5.32), where $G_{\text{sample}}/G_{\text{ref}} = 1$.

$$\frac{Q_{sample}}{Q_{ref}} = \frac{G_{sample}}{G_{ref}} \frac{n^2_{sample}}{n^2_{ref}} \frac{\bar{I}_{sample}}{\bar{I}_{ref}} \frac{Abs_{ref}}{Abs_{sample}} \tag{5.32}$$

$\bar{I}/Abs$ is best calculated by measuring the emission and excitation spectra for the reference and sample at a range of concentrations, and finding the gradient of a plot of $\bar{I}$ *vs.* Abs.[28] Because **NG1** is a colloidal solution, the measured absorption spectrum cannot be directly used for Q determination, as both scattering and absorption can contribute to a decrease

in light transmission.[29] Therefore it is necessary to subtract the contribution of light scattering from the absorption spectra of **NG1** at all concentrations. This was done by modelling the absorption spectra as the sum of three Gaussian functions (5.33) due the absorption maxima in the spectrum of **NG1**, a Rayleigh scattering term (5.34), and a background term (f_0), according to equation (5.35).

$$f_{1-3}(\lambda) = A_{1-3}e^{-\frac{(\lambda-\lambda_{max})^2}{2w^2}} \tag{5.33}$$

$$f_4(\lambda) = A_4\lambda^{-4} \tag{5.34}$$

$$Abs(\lambda) = \sum_{n=0}^{4} f_n(\lambda) \tag{5.35}$$

Peak fitting was performed using OriginPro 8.5 software, using the inbuilt GaussAmp peak function whose sample curve is shown in Figure 5.26. The GaussAmp parameters y_0, A, x_c and w represent the equation (5.33) parameters λ_0, A, λ_{max} and w respectively.

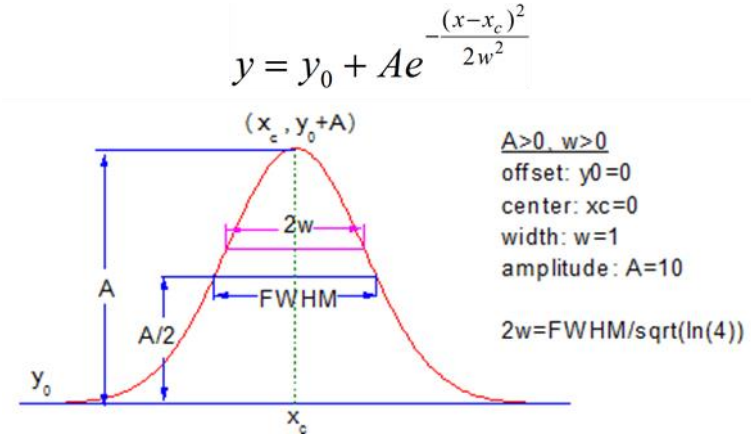

Figure 5.26. OriginPro 8.5 sample curve for the GaussAmp peak function.

An example of the result of this procedure for an absorption spectra of **NG1** is shown in Figure 5.27. For this concentration the peak fitting gave $A_4 = 3.87\times10^8$, allowing the effect of scattering $f_4(\lambda)$ to be subtracted from Abs.

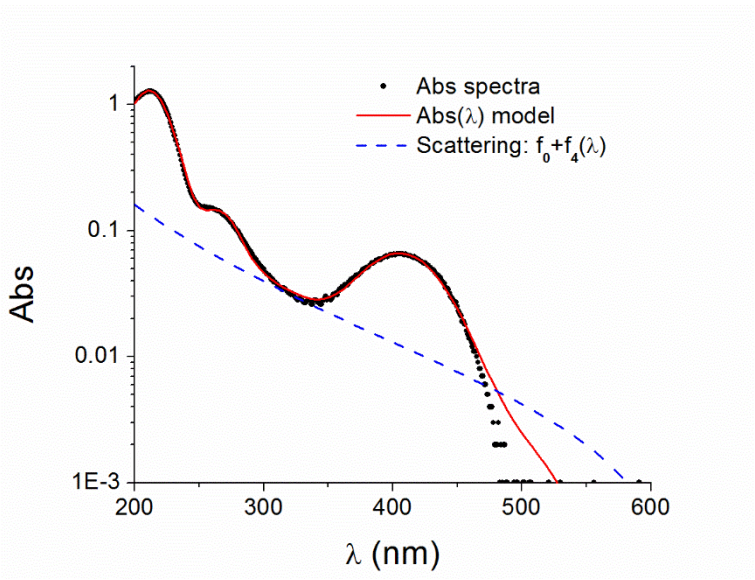

Figure 5.27. Absorption spectra of **NG1**, with the modelled function $Abs(\lambda)$, and the corresponding scattering and background component $f_0+f_4(\lambda)$. Data shown on a $\log(Abs)$ scale for clarity.

Emission spectra for 5(6)-FAM and **NG1** were recorded at $\lambda_{ex} = 445$ nm, the $\lambda_{ex,max}$ for 5(6)-FAM. Emission spectra were integrated using OriginPro 8.5, and $\bar{I}$ *vs.* Abs plotted for 5(6)-FAM and **NG1** (Figure 5.28). Using the ratio of the gradients of these plots and Q(5(6)-FAM) = 0.92 according to equation (5.32), Q(**NG1**) = 0.58.

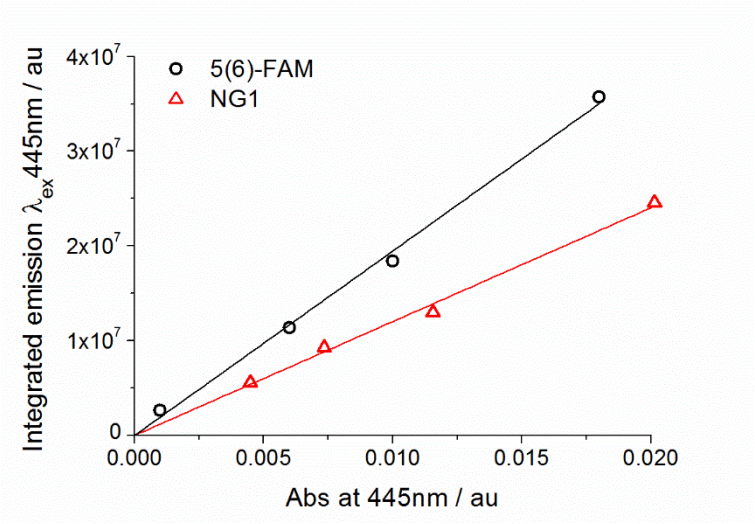

Figure 5.28. Plot of $\bar{I}$ *vs.* Abs to determine Q for **NG1**.

Unfortunately it was not possible to calculate Q for the other nanogel samples (**NG2**-**NG6**) or the BCP micelle samples because absorption was too low at 445 nm to obtain reliable results. This was due to the lower DoF for **NG1**-**NG6**, and the lower BCP micelle

concentrations (1 g/L) compared to **NG1** (10 g/L). However, it was possible to determine $Q = 0.34$ for a solution of **5i** in methanol using the method outlined above.[ix] In comparison, the analogous small molecule DTM **3i** has $Q = 0.011$ in methanol. This *ca.* 30-50 fold increase in emissivity for **5i** and **NG1** compared to **3i** is attributed to the protection of the DTM fluorophore from solvent/collisional quenching afforded by the polymer. It also appears that the polymeric support provides protection against DTM self-quenching, as [DTM] in **NG1** is relatively high (38 mM).

5.3.4.3. Molar emission and anisotropy[ix]

A dilution study was performed to investigate the effect of concentration on DTM emission. First, the integrated molar emission for aqueous solutions of polymer **5i** (which forms the ILMs) at a range of concentrations (1×10^{-3} M - 1×10^{-8} M) was measured, and compared with that of solutions (in methanol) of the small molecule DTM **3i** (Figure 5.29).

[ix] Quantum yield, molar emission, and molar anisotropy measurements for **3i** and **5i** were performed by Jeffery Raymond (Texas A&M University, USA).

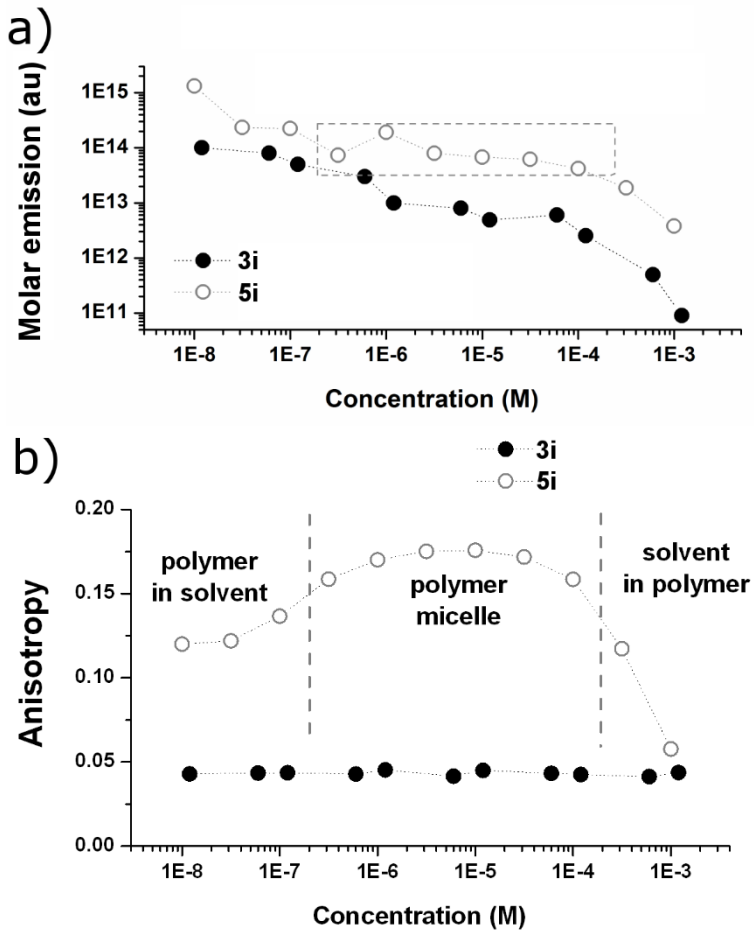

Figure 5.29. a) Concentration-based molar emissivity and b) Emission anisotropy for small-molecule **3i** and polymer **5i**.

Molar emission for **3i** scales with concentration, which is typical of self-quenching fluorophores.[1] On the contrary, molar emission of polymer **5i** in solution is relatively flat over 3 orders of magnitude in concentration (1×10^{-4} M – 1×10^{-7} M, corresponding to 3.6 g/L – 3.6 mg/L). In this concentration regime **5i** would be expected to exist as micelles (ILMs). Above 1×10^{-4} M, the system is best described as a solvent-in-polymer state, while below 1×10^{-7} M the system exists as solvated polymer unimers (polymer-in-solvent), as depicted in Figure 5.30. This latter state corresponds to micelles diluted below their critical micelle concentration (CMC), with BCP CMCs typically on the order of 1 mg/L.[30] In the solvent-in-polymer and polymer-in-solvent states emission increases upon dilution like **3i**, due to decrease in self-quenching. On the contrary in the micellar state the local concentration of DTM fluorophores would be expected to be constant for all micelle concentrations, resulting in no change in the extent of fluorophore self-quenching. An interesting point to note is that local fluorophore concentration in the ILMs is much

higher that the highest solvent-in-polymer state investigated (0.19 M as determined by light scattering). The protection from self-quenching (with resultant high molar emissivity) at this high local concentration is due to the ordered arrangement of fluorophores within the micellar structure.[31]

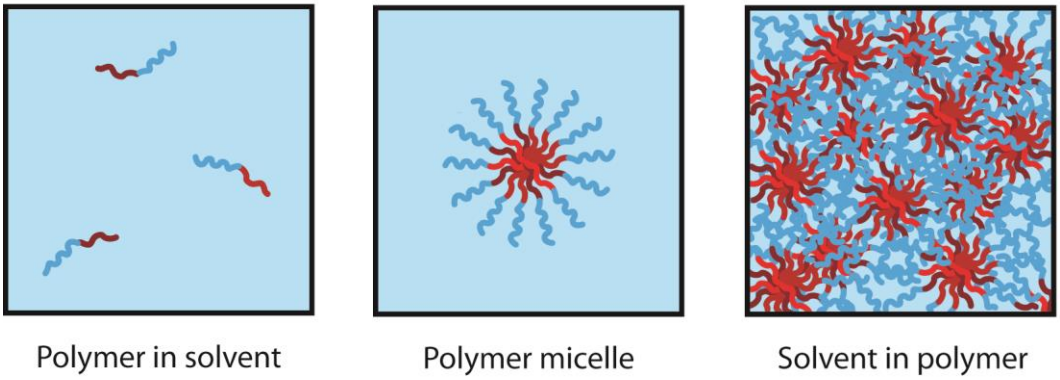

Figure 5.30. Schematic representation of the three states in which **5i** can exist in aqueous solution. Polymer concentration increases from left to right.

Further evidence that fluorescence emission is giving an indication of the supramolecular state of **5i** was provided by measuring the fluorescence emission anisotropy (Figure 5.29). For comparison, the emission anisotropy (r) of **3i** was measured over the entire concentration range, and found to be constant at $r = 0.043 \pm 0.001$. This low r is due to the freedom of rotation for the excited fluorophore in solution (high rotational diffusion coefficient), leading to depolarised emission. In contrast r varied significantly with concentration for **5i**. Anisotropy reaches a maximum for the micellar state (1×10^{-7} M $< c \leq 1\times10^{-4}$ M) due to two factors. Encapsulation in a micelle reduces both the rate of tumbling for the excited state fluorophores, and collisional quenching, both of which lead to a more polarised emission.[32] For the solvent-in-polymer state ($c \geq 5\times10^{-4}$ M) r decreases with increasing concentration, due to increasing energy transfer (ET) events leading to a less polarised emission. For the polymer-in-solvent state ($c \leq 1\times10^{-7}$ M) r decreases to *ca.* 0.12, as tumbling rate is increased compared to the micellar state due to disassembly of the micelles into unimers.

Molar emission and anisotropy were also measured over a range of concentrations for aqueous solutions of **5ii** and **5iii** (Figure 5.31). For both polymers a relatively flat molar emission over 3 orders of magnitude in concentration was observed, corresponding to the

micellar state (SLMs for **5ii** and CLMs for **5iii**). Concentrations above 1×10^{-4} M could not be measured, as homogeneous solutions of **5ii** and **5iii** could not be formed above this concentration. Deviation from this flat molar emission occurred at $c \leq 1\times10^{-7}$ M for **5ii** and $c \leq 5\times10^{-8}$ M for **5iii**, corresponding to CMCs of 3.8 mg/L and 1.7 mg/L for SLMs and CLMs respectively. A flat region for emission anisotropy was also observed within the micellar concentration range (Figure 5.31). Unfortunately it was not possible to measure r at $c \leq$ CMC for either **5ii** or **5iii**, due to the overlap of the Raman scattering peak of water with the emission of the DTM group at these low concentrations.

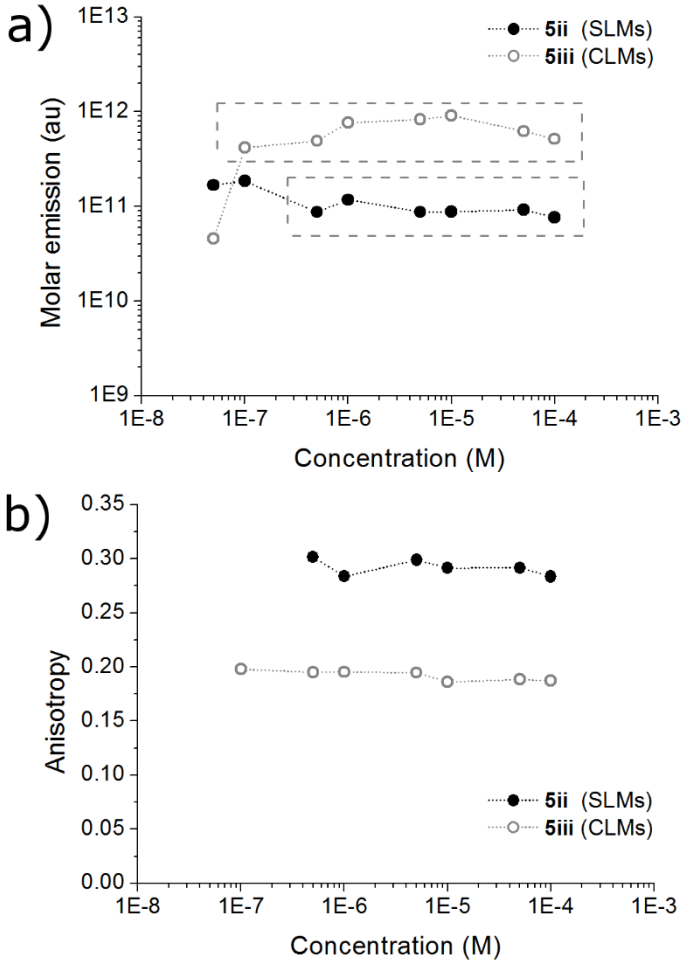

Figure 5.31. a) Concentration-based molar emissivity and b) Emission anisotropy for polymer 5ii and 5iii.

Anisotropy and relative molar emission (calculated as integrated emission/DoF) were also measured for the nanogel samples **NG1-NG6**, with results shown in Figure 5.32. Molar emission was found to increase with decreasing DoF for nanogels with $CLD = 0.5$ wt% (Figure 5.32 a). This was due to the decrease in nanogel [DTM] with decreasing DoF,

leading to decreased self-quenching of the DTM fluorophores. Varying the *CLD* from 10 wt% to 0.5 wt% for nanogels with $DoF = 0.03$ mol% was found to have little effect on molar emission (Figure 5.32 b), with values of $2.37\times10^{8} \pm 0.16\times10^{8}$. Anisotropy was high ($r > 0.2$) for all samples indicating that the DTM fluorophore was incorporated into a macromolecular structure. Again, due to overlap of the Raman scattering peak of water with the DTM emission it was not possible to measure r for $DoF = 0.0003$ mol% (**NG6**). With only three samples in each series it is difficult to identify a trend in r for variable *DoF* and *CLD*.

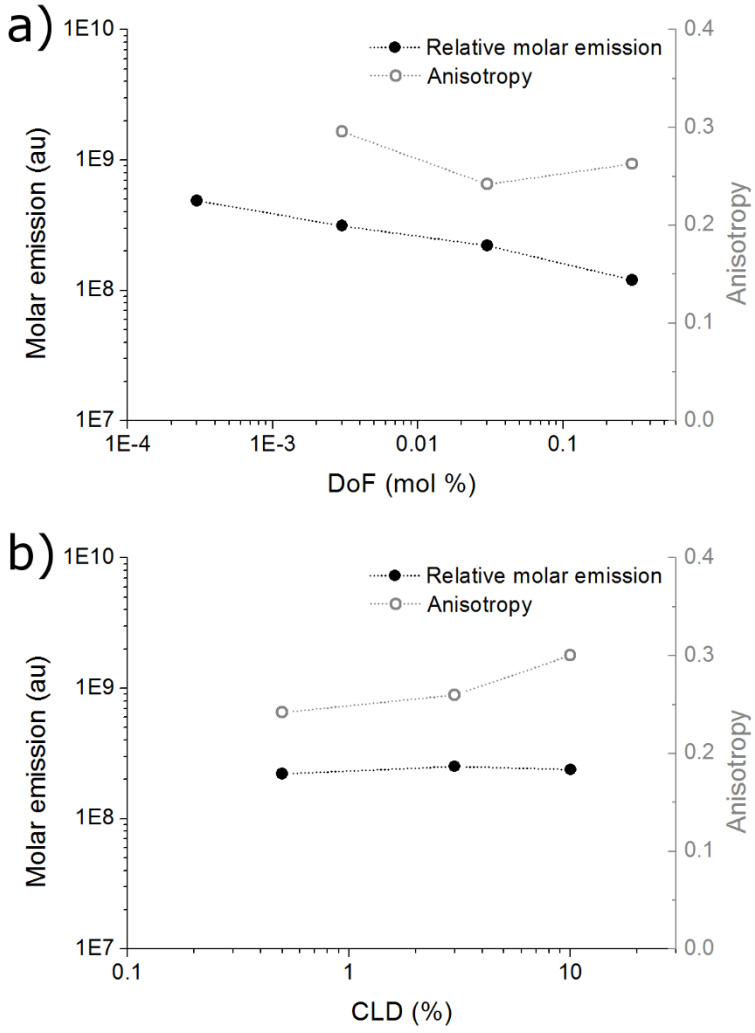

Figure 5.32. Molar emission and anisotropy for nanogels **NG1-NG6**. a) $CLD = 0.5$ wt% with variable *DoF*; b) $DoF = 0.03$ mol% with variable *CLD*.

As the emission spectra for both micelle and nanogel samples (with the exception of **5i** ILMs) were recorded at the same time using the same instrument set-up the spectra can be directly compared (Figure 5.33 a). Normalising the emission spectra of these particles

according to the particles' degree of DTM functionalisation gives molar emission spectra (Figure 5.33 b). These spectra show that **NG6** has the greatest molar emission, which is because it has the lowest local [DTM], and therefore the lowest degree of fluorophore self-quenching. Molar emission for the CLMs and **NG1** are very similar, suggesting that encapsulation within a micelle or nanogel core provides a similar degree of protection to the fluorophore excited state. In contrast, molar emission for SLMs is *ca.* 2 orders of magnitude lower, indicating that being located in the micelle shell provides a lesser degree of protection to the fluorophore excited state than being located in a micelle or nanogel core. As the local [DTM] is *ca.* 200× lower in the SLMs compared to the CLMs, this suggests that it is protection from solvent collisions which leads to the higher molar emission for CLMs.

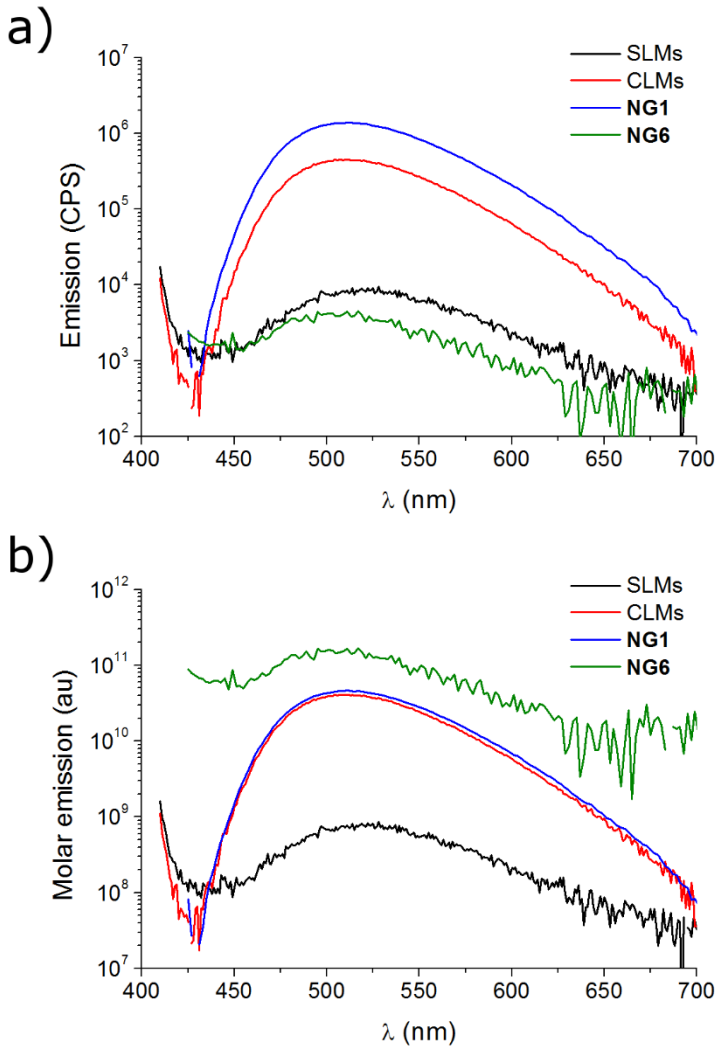

Figure 5.33. a) Emission spectra and b) Molar emission spectra for micelles and nanogels.

5.3.5. TCSPC and FLIM

Solution state fluorescence lifetime was measured for the micelle and nanogel samples, as well as the small molecule DTM **3i**, using time-correlated single photon counting (TCSPC). Samples were excited with a pulsed 405 nm diode laser (59 ps FWHM), and the resultant emission decay were modelled as a sum of exponential decays after deconvolution with the instrument response function (IRF) obtained using a dilute solution of Ludox (colloidal silica). Decay spectra for **3i**, and polymers **5i**, **5ii** and **5iii** are shown in Figure 5.34, with the average lifetimes and lifetime components listed in Table 5.4.[x]

The decay spectra (Figure 5.34 a) clearly shows that for the lone dye (**3i**) emission decays almost immediately. The intensity-averaged lifetime of the excited state ($\tau_{Av,I}$) is 1.0±0.1 ns, with the majority of the decay comprised of two near-ultrafast lifetimes ($\tau_1 = 0.31\pm0.01$ ns and $\tau_2 = 0.77\pm0.1$ ns), which are assigned to non-radiative annihilation of the excited state (due to nonemissive aggregation and solvent-collision effects).[33] The longer decay ($\tau_3 = 5.2\pm0.1$ ns) represents the intrinsic relaxation event for DTM dyes.

In contrast, it is obvious from Figure 5.34 (a) that **5i** in the form of ILMs displays a much higher $\tau_{Av,I}$ (19.8±0.2 ns). As well as displaying the intrinsic DTM relaxation ($\tau_1 = 5.1\pm0.2$ ns) the **5i** micelles also possess two longer lifetime components ($\tau_2 = 17.5\pm0.1$ ns and $\tau_3 = 39.4\pm0.5$ ns). This is the result of better fluorophore protection due to encapsulation within the supramolecular structure.[32] However, upon dissolution of **5i** to unimers, a reduction in $\tau_{Av,I}$ to 14.9±0.2 ns is observed, due to reduction in all three components of the decay (τ_1, τ_2, and τ_3). This is the result of better fluorophore protection in the micelles, compared to the polymer unimers. Importantly, this observation allows the micellar state of **5i** to be discriminated simply by comparison of the average lifetimes.

[x] TCPSC measurements and analysis for **3i** and **5i** were performed by Jeffery Raymond (Texas A&M University, USA).

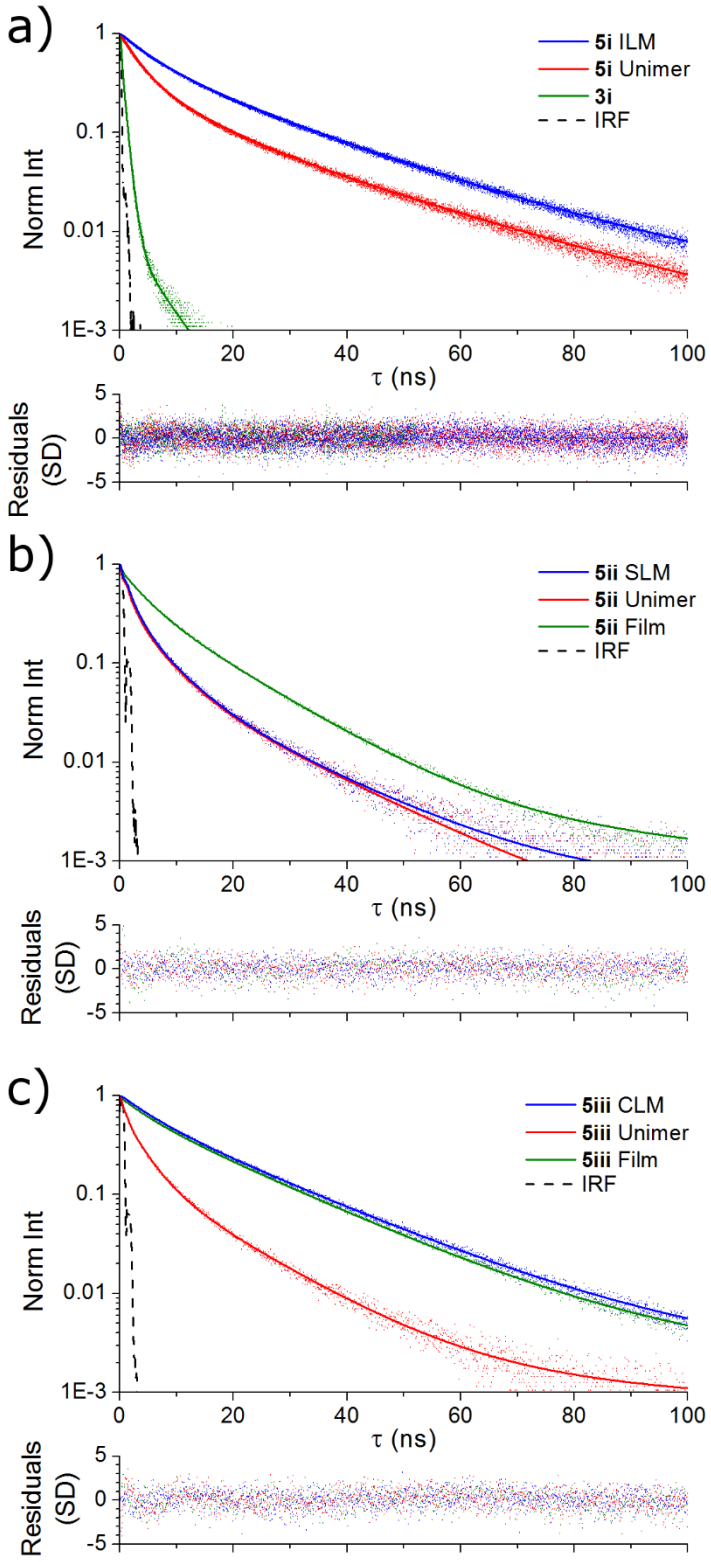

Figure 5.34. Fluorescence lifetime decay spectra (points) with fitting (line) and residuals (bottom) for a) **3i** and **5i**; b) **5ii**; c) **5iii**.

Table 5.4. Kinetic data for solution state fluorescence emission decay spectra.

	τ_1	A_1	τ_2	A_2	τ_3	A_3	τ_4	A_4	$\tau_{Av,I}$	$\tau_{Av,A}$
3i	0.31±0.01	0.68	0.77±0.1	0.31	5.2±0.1	0.01			1.0±0.1	0.50±0.07
5i Micelles	5.1±0.2	0.45	17.5±0.1	0.48	39.4±0.5	0.07			19.8±0.2	13.5±0.2
5i Unimers	3.0±0.1	0.66	9.1±0.2	0.29	25.2±0.2	0.15			14.9±0.2	7.6±0.2
5ii Micelles	0.40±0.03	0.70	1.8±0.1	0.01	5.4±0.1	0.23	15.9±0.3	0.05	7.0±0.1	2.2±0.3
5ii Unimers	0.32±0.02	0.71	1.5±0.1	0.01	5.0±0.1	0.22	15.5±0.2	0.05	7.0±0.1	2.0±0.3
5iii Micelles	5.5±0.2	0.02	17.5±0.1	0.96	73.7±2.7	0.02			18.8±0.3	13.5±0.4
5iii Unimers	0.56±0.04	0.60	3.4±0.1	0.31	12.5±0.2	0.09			9.2±0.2	2.6±0.4
NG1	5.8±0.4	0.24	23.2±0.1	0.73	65.5±1.5	0.03			26.0±0.3	20.3±0.5
NG2	5.9±0.4	0.26	21.5±0.1	0.71	58.7±1.2	0.04			24.4±0.3	18.8±0.5
NG3	5.8±0.4	0.27	22.2±0.2	0.69	57.6±1.2	0.04			25.1±0.3	19.2±0.5
NG4	5.6±0.4	0.27	22.7±0.2	0.68	57.6±1.1	0.04			25.8±0.3	19.5±0.5
NG5	5.1±0.4	0.27	22.7±0.2	0.69	58.6±1.2	0.04			26.1±0.3	19.6±0.6
NG6	5.9±.3	0.27	23.9±0.2	0.42	65.0±1.7	0.02	1.02±0.2	0.28	25.5±0.4	13.4±1.1

In the case of **5ii** (Figure 5.34 b) the average lifetime is much lower in the micellar state, than for **5i** ($\tau_{Av,I} = 7.0\pm0.1$ ns for **5ii** micelles). This is as a result of a near ultra-fast lifetime with significant amplitude ($\tau_1 = 0.40\pm0.03$ ns, $A_1 = 0.70$), which is assigned to excited state annihilation by solvent collision, in analogy to the small molecule **3i**. Upon dissolution to unimers there is almost no change in the emission decay (Figure 5.34 b), which is reflected in $\tau_{Av,I}$ which remains unchanged at 7.0±0.1 ns. This indicates that being located in the shell of the SLMs of **5ii** provides poor protection to the DTM fluorophore from solvent quenching. As a result it is not possible to discriminate between micelles and unimers for **5ii** by florescence lifetime. To demonstrate that these lower $\tau_{Av,I}$ values were the result of solvent, rather than a property of the polymer **5ii**, the fluorescence lifetime decay was also measured for a dehydrated sample. A solution of SLMs was dried to a glass slide as a thin film, and the sample analysed by fluorescence lifetime microscopy (FLIM). An emission decay is measured for each pixel, and average lifetimes for each pixel represented using a colour scale, as shown in Figure 5.35 a. The overall intensity decay was calculated by summation of the decays for each pixel in the image, to give the decay spectrum shown in Figure 5.34 b. An increase in $\tau_{Av,I}$ to 14.8±0.3 ns (compared to 7.0 ns for SLMs and unimers in solution), confirmed that it is poor protection from the surrounding solvent that results in the lower $\tau_{Av,I}$ for the SLMs and unimer solutions.

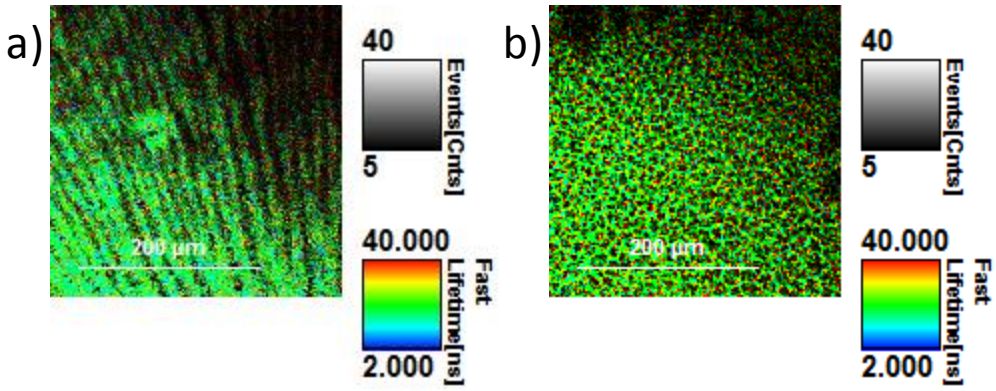

Figure 5.35. FLIM image of the thin film formed from a) **5ii** micelles (SLMs); b) **5iii** micelles (CLMs).

Fluorescence lifetime spectra for **5iii** gave very similar results to **5i** (Figure 5.34 c). A long lifetime was observed for **5iii** in the micellar state ($\tau_{Av,I} = 18.8\pm0.3$ ns), whereas the

unimer state showed a significant decrease to $\tau_{Av,I} = 9.2\pm0.2$ ns, due to an ultra-fast (solvent collision) component to the decay ($\tau_1 = 0.56\pm0.04$ ns). FLIM indicated that a dried film of micelles (Figure 5.35 b) had the same average lifetime as the micelle solution ($\tau_{Av,I} = 18.5\pm0.2$ ns). These results demonstrate that the CLMs provide good protection to the DTM fluorophore, and that fluorescence lifetime spectroscopy can be used to discriminate between micelles and unimers in solution for **5iii**.

The nanogel samples (**NG1**-**NG6**) were also analysed by fluorescence lifetime spectroscopy in the solution state (Figure 5.36 a). All samples showed very similar emission decay, with three components $\tau_1 \approx 5$ ns, $\tau_2 \approx 22$ ns, $\tau_3 \approx 60$ ns, and a long average lifetime $\tau_{Av,I} \approx 25$ ns. The only exception was **NG6**, which in addition showed a fast component to the lifetime ($\tau_4 = 1.02\pm0.2$ ns), however this did not have a significant effect on $\tau_{Av,I}$ which was 25.5 ± 0.4 ns. For all samples (**NG1**-**NG6**) the fluorescence lifetime of thin films prepared by drying the nanogel solutions to a glass slide were also investigated by FLIM. In all cases near identical fluorescence decay was observed to the nanogel solutions. As an example, a film of **NG1** (Figure 5.36 and Figure 5.37) had $\tau_{Av,I} = 23.4\pm0.2$ ns. These results suggest that as with the ILMs and CLMs, encapsulation within a nanogel provides excellent protection to the DTM fluorophore's excited state, leading to long lifetimes and exceptional molar emissivities. Furthermore, when considering the high concentrations of DTM in the particle cores (up to 0.19 M) the lack of self-quenching is quite remarkable, as most dye or dye/polymer blends would be 'off-switched' in the solid state at these concentrations.

5.3.6. *In vitro* FLIM

The potential use of the DTM-labelled nanoparticles as self-reporting contrast agents was investigated by our collaborators at Texas A&M University (USA) lead by Dr Jeffery Raymond. The aim was to test whether discrimination between micellar states was possible *in vitro*. In the test 0.1 mL of a 10 g/L solution of ILMs (polymer **5i**) in phosphate-buffered solution was applied to a cross-section of living rat hippocampal tissue for 1 h. The tissue was then fixed with ethanol, and imaged by FLIM (Figure 5.38).

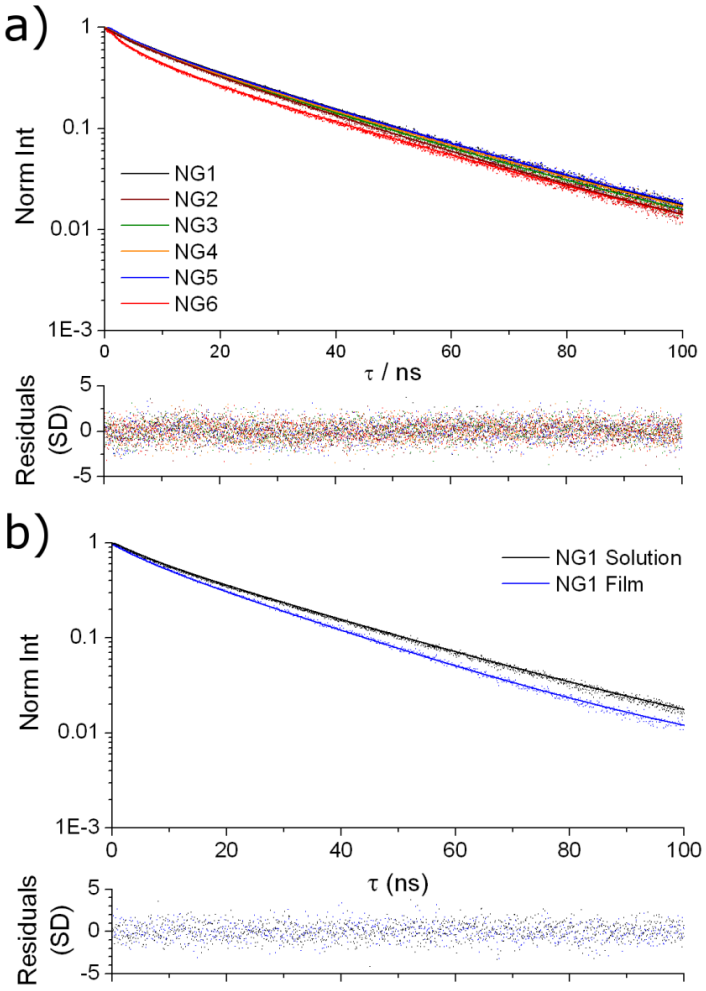

Figure 5.36. Fluorescence lifetime decay spectra (points) with fitting (line) and residuals (bottom) for a) **NG1**-**NG6** in solution; b) **NG1** in solution and dried to a film.

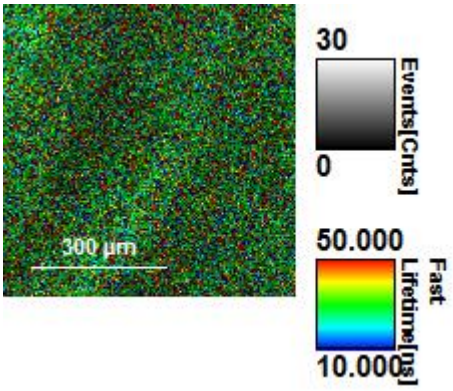

Figure 5.37. FLIM image of the thin film formed from **NG1**.

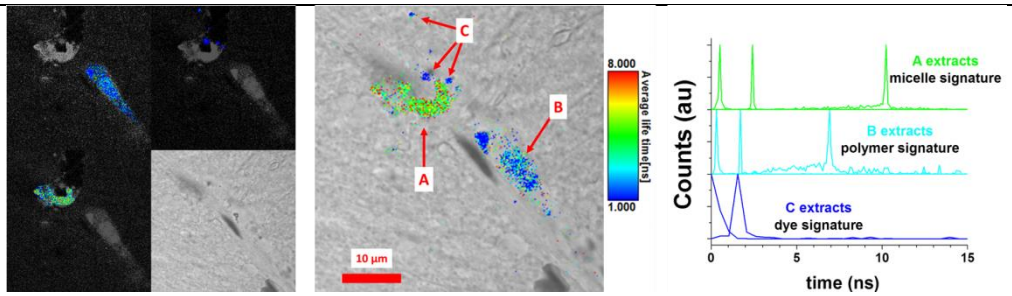

Figure 5.38. Left; FLIM images of rat hippocampal tissue subjected to ILMs solution, filtered by lifetime corresponding to (clockwise from bottom left) micelle, unimer, free dye, and a bright-field image. Middle; Overlay of FLIM and bright-field images. Right; Fast-FLIM emission lifetime extractions for the clotting region (A), vascular tissue (B), and leukocytes (C).[34]

The test showed that both the fast-FLIM signal and a fast-FLIM component signal of the decay allowed identification of **5i** in either micelle, unimer or degraded states. Micellar emission was observed in clotted regions (A), whereas non-micellar polymer (unimers) were observed on the vascular wall (B). Emission with very short lifetime was seen in the leukocytes (C), possessing an emission decay that overlays almost exactly with that of **3i** in solution (τ_{av} = 1.1 ns and 1.0 ns respectively) as shown in Figure 5.39. This suggested that polymer degradation, with release of small molecule dye had occurred, which is reasonable given the role of the leukocytes. Therefore, by taking a relatively simple and non-invasive measurement, the fate of the ILMs upon uptake into rat hippocampal tissue could be tracked.

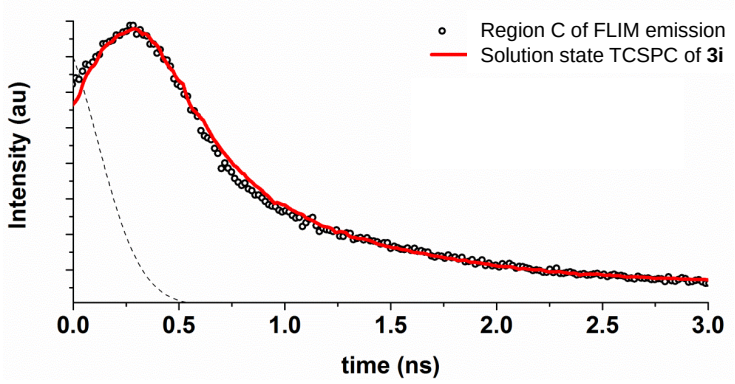

Figure 5.39. Comparison of raw spectral data from FLIM (region C) of rat hippocampal tissue with solution state TCSPC spectrum of **3i**.

5.4. Conclusions

The synthesis of a range of fluorescently-labelled nanoparticles has been presented. A DTM-functional ROP initiator/RAFT agent and acrylate monomer has been shown to be compatible with block copolymer synthesis. Self-assembly of the resultant amphiphilic polymers gives rise to spherical polymer micelles that contain the DTM dye in either the shell, core, or core-shell interface. DLS was used to analyse these micelles, showing them to have $R_h \approx 25$ nm in all cases. Additionally, the combination of DLS and SLS analysis allowed the local DTM concentration to be calculated, which was almost 200 mM for core and core-shell interface functionalisation, but < 1 mM for shell-labelled micelles with an equivalent degree of functionalisation.

It was demonstrated using steady-state and time-resolved fluorescence spectroscopy that location of the DTM group in the core, or at the core-shell interface provides good protection to the fluorophore excited state, leading to highly emissive particles with long fluorescence lifetimes ($\tau_{Av,A} \approx 20$ ns). Furthermore, the fluorescence was shown to self-report on the supramolecular state of these two systems, with micelles and non-assembled polymer unimers showing differences in molar emission, anisotropy and fluorescence lifetime. This self-reporting was exploited for *in vitro* FLIM, with polymer identified as being in either micelle, unimer, or degraded states in different components of rat hippocampal tissue. In contrast, incorporation of the DTM fluorophore into the micelle shell provided poorer protection for the excited state, with increased solvent collisions leading to a shorter fluorescence lifetime ($\tau_{Av,A} \approx 7$ ns) and lower molar emission than core and core-shell interface-labelled micelles.

DTM-functional nanogels synthesised by radical cross-linking emulsion polymerisation were shown to be a simpler (and potentially scalable) route to DTM-labelled particles. The effect of the cross-linking density ($CLD = 0.5$-10 wt%), and degree of DTM functionalisation ($DoF = 0.3$-0.0003 mol%) was investigated. DLS/SLS analysis of the nanogels showed that their size was minimally affected by either variable ($9.0 \leq R_h \leq 12.4$ nm), while the number of dye groups per particle could also be calculated, ranging from 70-0.2 depending on *DoF*. The desirable features of long fluorescence lifetimes ($\tau_{Av,A} \approx 25$ ns), and high quantum yield (0.58) were retained in these

nanogels. While *CLD* had little effect on the spectral properties of the nanogels, it was found that molar emission increased with decreasing *DoF*, due to the reduction in dye self-quenching.

5.5. Experimental

5.5.1. Materials and apparatus

5.5.1.1. General

Tert-butyl acrylate was vacuum distilled over CaH_2 prior to use, and stored at 4 °C. Methyl methacrylate (MMA) was passed through a column of neutral alumina (Al_2O_3) prior to use, and stored at 4 °C. 2,2'-azobis(2-methylpropionitrile) (AIBN) was recrystallized twice from methanol and stored at 4 °C in the dark. 1,4-Dioxane was passed through a basic alumina plug immediately before use. The RAFT agent cyanomethyl dodecyl trithiocarbonate (**4xx**) was purchased from Aldrich and used as received. All other chemicals and reagents were purchased from Aldrich and used as received. Solvents were purchased from Fisher Scientific and used as received.

^{1}H and ^{13}C NMR spectra were recorded on a Bruker DPX-300, DPX-400, DRX-500, AV-600 or AV-700 spectrometer in $CDCl_3$ unless otherwise stated. Chemical shifts are given in ppm downfield from the internal standard tetramethylsilane, and coupling constants (J) correspond to $^{3}J_{H\text{-}H}$ unless otherwise stated. Size exclusion chromatography (SEC) measurements were conducted using a Varian 390-LC-Multi detector suite fitted with differential refractive index (DRI), and UV-Vis or photodiode array (PDA) detectors. A guard column (Varian Polymer Laboratories PLGel 5 µm, 50 × 7.5 mm) and two mixed D columns (Varian Polymer Laboratories PLGel 5 µm, 300 × 7.5 mm) were used. The mobile phase was tetrahydrofuran with 2% triethylamine, or chloroform with 2% triethylamine, or dimethylformamide with NH_4BF_4 (5 mM) eluent at a flow rate of 1.0 mL/min. Data was analysed using Cirrus v3.3 with calibration curves produced using Varian Polymer laboratories Easi-Vials linear poly(styrene) standards (162 Da – 240 kDa) or linear poly(methyl methacrylet) standards (690 Da – 790 kDA). UV-Vis spectra were determined with the use of Shimadzu UV-2550 spectrophotometer. Transmission electron microscopy (TEM) imaging was performed on a Jeol 2011 200 kV LaB_6 instrument fitted with a Gatan UltraScan™ 1000 camera, using Agar Graphene Oxide Support Film grids.

5.5.1.2. Light scattering

Static light scattering (SLS) and dynamic light scattering (DLS) measurements were performed on a ALV CGS3 goniometer operating at $\lambda = 632.8$ nm. The temperature of the toluene bath was regulated using a Julabo F32-ME refrigerated and heating circulator set to 20 °C. Refractive index increment ($\mathrm{d}n/\mathrm{d}c$) was measured by injecting samples of a known concentration into a Shodex RI-101 refractive index detector. The response was calibrated using solutions of poly(styrene) in toluene. Intensity autocorrelation functions ($g_2\,(q,t)$) were fitted with the REPES routine using GENDIST software,[18, 19] which performs an Inverse Laplace transformation to produce a distribution of relaxation times $A(\tau)$.

$$g_2(q,t) - 1 = \beta \left[\int A(\tau) e^{-\frac{t}{\tau}} d\tau \right]^2$$

An error of $\pm$ 10% was applied to light scattering data, in accordance with previous reports.[21]

5.5.1.3. Fluorescence spectroscopy

All steady state emission, excitation and anisotropy spectra were obtained with a Horiba FluoroMax4 with automatic polarizers, and analyzed in FluoreEssence (Horiba) and Origin 8.6 Pro (Origin Labs). Time correlated single photon counting (TCSPC) was employed to obtain all fluorescence lifetime spectra. This was done with a Fluorotime 100 fluorometer and 405 nm solid state ps diode laser source (PicoQuant) in matched quartz 0.7 mL cells (Starna Cell). Instrument response functions (IRF) were determined from scatter signal solution of Ludox HS-40 colloidal silica (0.01% particles in water w/w). Analysis was performed on Fluorofit (PicoQuant). Fluorescence lifetime imaging was performed using a FLIM LSM upgrade kit for the FV1000 (PicoQuant) mounted on a FV1000 (Olympus) confocal microscope on a IX-81 inverted base (Olympus). A PlanApo N 60x oil lens (NA 1.42, Olympus) was used for all imaging. The FV1000 system was driven with the FV10-ASW v3.1a software platform (Olympus) with scan rates of 4 μs/pixel at 256×256 pixels. FLIM images and spectra were collected using bins of 16 ps with a 405 nm (LDH-P-C-405B, PicoQuant) driven at 2.5 MHz. FWHM for the 405 nm laser head was 59 ps and maximum power was 0.21 mW (attenuated by variable neutral

density filters to prevent count pile up and maintain counting rates below 1% bin occupancy). SymphoTime 64 (Picoquant) software was used for collection and analysis of FLIM images and spectra. All IRF deconvolved exponential fits were performed with the 3 or 4 exponents selected for completeness of fit as determined by boot-strap chi-squared analysis in Fluorofit.

5.5.1.4. Animal Tissue Studies.

All animal tissue studies were performed at the Department of Neuroscience and Experimental Therapeutics, College of Medicine, Texas A&M University System, Health Sciences Center, Bryan, TX, USA by Joanne Damborsky, Elizabeth Thom, and Ursula Winzer-Serhan.

Fresh 300 µm thick adult rat hippocampi slices maintained in artificial cerebrospinal fluid, as outlined in detail elsewhere,[35] were incubated with 0.1 mL of a 10 µM (PBS, Hyclone, Thermo Scientific) solution of **5i** immediately after dissection. The rat used was not killed for the purposes of this experiment and all tissues used were excess from an unrelated study. In brief, an adult female Sprague-Dawley rat was decapitated under isoflurane anesthesia, and its brain was quickly removed and submerged in an ice-cold cutting solution containing (in mM) 0.3 Kynurenic acid, 120 NaCl, 11 D-Glucose, 26 $NaHCO_3$, 6 $MgCl_2$, 3 KCl, 0.5 $CaCl_2$, and 5 HEPES. While still in the cutting solution, 300 µM coronal slices were taken through brain using a Vibratome 3000 Sectioning System. The hippocampi were dissected from the slices, and transferred to artificial cerebrospinal fluid containing (in mM) 124 NaCl, 3 KCl, 1.5 $MgSO_4.7H_2O$, 1.2 NaH_2PO_4, 2.4 $CaCl_2$, 26 $NaHCO_3$, and 10 D-Glucose bubbled with 95% O_2 / 5% CO_2. The solution of **5i** was directly applied to the surface of the slices and allowed to incubate for 1 hour, then fixed with ethanol and mounted before imaging.

5.5.2. Synthetic protocols

Triethylene glycol monomethylether methacrylate (TEGA) was synthesised as previously reported.[36]

The synthesis of 3,4-bis(butylsulfanyl)-2,5-dihydro-1H-pyrrole-2,5-dione (**3i**) was described in Chapter 3.

The synthesis of dithiomaleimide-labelled poly(D,L-lactide) (**3xiv**) was described in Chapter 3.

The synthesis of 2-([2-(3,4-bis[butylsulfanyl]-2,5-dioxo-2,5-dihydro-1H-pyrrol-1-yl)acetyl] oxy)ethyl 2-methylprop-2-enoate (**4i**) was described in Chapter 4.

The synthesis of 2-[(2-[3,4-bis(butylsulfanyl)-2,5-dioxo-2,5-dihydro-1H-pyrrol-1-yl]acetyl) oxy]ethyl prop-2-enoate (**4ii**) was described in Chapter 4.

3μ-[P(TEGA)]-*b*-[P(D,L-LA)]$_2$ star block copolymer (5i)

A solution of **3xiv** (100 mg, 15.0 μmol), TEGA (0.441 g, 2.02 mmol), and AIBN (0.30 mg, 1.8 μmol) in $CHCl_3$ (1.19 mL) was added to a polymerisation ampoule. The solution was degassed by three freeze-pump-thaw cycles and sealed under N_2. The reaction was stirred at 60 °C for 8 hours, then quenched by rapid cooling and exposure to air. The solvent was removed in vacuo, and the residue was purified by exhaustive dialysis (MWCO 6-8 kDa) against distilled water. The product was obtained as a fluorescent yellow waxy solid by lyophilisation.

^{1}H NMR spectra shown in Figure 5.8.

P(TEGA-*co*-DTMA)-*b*-P(^{t}BA) block copolymer (5ii)

A solution of **5v** (0.150 g, 25.2 μmol), TEGA (1.10 g, 5.03 mmol), **4ii** (16.2 mg, 37.7 μmol) and AIBN (0.41 mg, 2.5 μmol) in dioxane (2.96 mL) was added to a polymerisation ampoule. The solution was degassed by three freeze-pump-thaw cycles and sealed under N_2. The reaction was stirred at 65 °C for 5 hours, then quenched by rapid cooling and exposure to air. Dioxane (2 mL) was added, and the solution precipitated into ice cold hexane (200 mL × 2). The crude product was redissolved in dioxane/H_2O (1/2, *v/v*) and purified by exhaustive dialysis (MWCO 3.5 kDa) against distilled water. The product was obtained as a fluorescent yellow waxy solid by lyophilisation.

^{1}H NMR spectra shown in Figure 5.11.

P(TEGA)-*b*-P(^{t}BA-*co*-DTMA) block copolymer (5iii)

A solution of **5vi** (0.130 g, 24.3 μmol), TEGA (1.06 g, 4.86 mmol), 37.7 μmol) and AIBN (0.40 mg, 2.4 μmol) in dioxane (2.86 mL) was added to a polymerisation ampoule. The solution was degassed by three freeze-pump-thaw cycles and sealed under N_2. The reaction was stirred at 65 °C for 3.5 hours, then quenched by rapid cooling and exposure to air. H_2O (10 mL) was added, and the solution purified by exhaustive dialysis (MWCO 3.5 kDa) against distilled water. The product was obtained as a fluorescent yellow waxy solid by lyophilisation.

^{1}H NMR spectra shown in Figure 5.15.

P(TEGA)-*b*-P(^{t}BA) block copolymer (5iv)

A solution of **5v** (0.150 g, 25.2 μmol), TEGA (0.878 g, 4.02 mmol), and AIBN (0.41 mg, 2.5 μmol) in dioxane (2.37 mL) was added to a polymerisation ampoule. The solution was degassed by three freeze-pump-thaw cycles and sealed under N_2. The reaction was stirred at 65 °C for 4.5 hours, then quenched by rapid cooling and exposure to air. H_2O (10 mL) was added, and the solution purified by exhaustive dialysis (MWCO 3.5 kDa) against distilled water. The product was obtained as a yellow waxy solid by lyophilisation.

^{1}H NMR spectra shown in Figure 5.16.

P(^{t}BA) (5v)

A solution of **4xx** (0.282 g, 887 μmol), ^{t}BA (5.00 g, 39.0 mmol), and AIBN (14.6 mg, 88.7 μmol) in dioxane (5.66 mL) was added to a polymerisation ampoule. The solution was degassed by three freeze-pump-thaw cycles and sealed under N_2. The reaction was stirred at 65 °C for 2 hours, then quenched by rapid cooling and exposure to air. The product was purified by repeated precipitation into ice-cold methanol/H_2O (9/1, *v/v*) and isolated as a yellow glassy solid.

^{1}H NMR spectra shown in Figure 5.9.

P(^{t}BA-*co*-DTMA) (5vi)

A solution of **4xx** (40.0 mg, 126 μmol), ^{t}BA (0.807 g, 6.30 mmol), **4ii** (81.2 mg, 189 μmol) and AIBN (2.07 mg, 12.6 μmol) in dioxane (0.914 mL) was added to a polymerisation ampoule. The solution was degassed by three freeze-pump-thaw cycles and sealed under N_2. The reaction was stirred at 65 °C for 5 hours, then quenched by rapid cooling and exposure to air. The product was purified by repeated precipitation into ice-cold methanol/H_2O (9/1, *v/v*) and isolated as a fluorescent yellow glassy solid.

^{1}H NMR spectra shown in Figure 5.12.

Block copolymer self-assembly

Interface-labelled micelles (ILMs) were assembled by direct dissolution of **5i** in water (18.2 MΩ·cm) at a concentration of 1 g/L. In order to fully disperse the particles the solutions were sonicated until completely transparent.

Shell-labelled micelles (SLMs), core-labelled micelles (CLMs) and non-labelled micelles (NLMs) were assembled by direct dissolution of **5ii**, **5iii**, and **5iv** (respectively) in water (18.2 MΩ·cm) at a concentration of 1 g/L. In order to fully disperse the particles the solutions were stirred at 60 °C for 3 h, then sonicated until completely transparent.

P(MMA-*co*-EGDMA-*co*-DTMMA) nanogel solutions (NG1-NG6)

In a typical reaction; Sodium dodecyl sulfate (0.100 g) was added to water (50 mL, 18.2 MΩ·cm) in a 100 mL RBF. The RBF was sealed with a rubber septum, and the solution deoxygenated by bubbling with N_2. A mixture of MMA (0.500 g, 4.99 mmol), EGDMA, and **4i** was added to the solution *via* syringe under N_2 flow with constant stirring. Potassium persulfate (10 mg) was added, and reaction stirred (800 rpm) at 70 °C for 14 h. Polymerisation was terminated by allowing the reaction mixture to cool to room temperature while exposing to air. Excess surfactant was removed by exhaustive dialysis (MWCO 3.5 kDa) against water (18.2 MΩ·cm). Final concentration was determined by weighing the solution recovered after dialysis.

	EGDMA (wt%)[a]	**4i** (mol%)[a]
NG1	1.25 mg (0.25)	6.65 mg (0.3)
NG2	1.25 mg (0.25)	0.665 mg (0.03)
NG3	7.50 mg (1.5)	0.665 mg (0.03)
NG4	25.0 mg (5.0)	0.665 mg (0.03)
NG5	1.25 mg (0.25)	66.5 μg (0.003)
NG6	1.25 mg (0.25)	6.65 μg (0.0003)

[a] With respect to MMA.

5.6. References

1. J. R. Lakowicz, *Principles of Fluorescence Spectroscopy*, Springer, 2009.

2. A. Sillen and Y. Engelborghs, *Photochem. Photobiol.*, 1998, **67**, 475-486.

3. K. Suhling, P. M. W. French and D. Phillips, *Photochem. Photobiol. Sci.*, 2005, **4**, 13-22.

4. P. I. H. Bastiaens and A. Squire, *Trends Cell Biol.*, 1999, **9**, 48-52.

5. S. Seidenari, F. Arginelli, C. Dunsby, P. M. W. French, K. König, C. Magnoni, C. Talbot and G. Ponti, *PLOS ONE*, 2013, **8**, e70682.

6. M. J. Ruedas-Rama, J. D. Walters, A. Orte and E. A. H. Hall, *Anal. Chim. Acta*, 2012, **751**, 1-23.

7. J. S. Basuki, H. T. T. Duong, A. Macmillan, R. B. Erlich, L. Esser, M. C. Akerfeldt, R. M. Whan, M. Kavallaris, C. Boyer and T. P. Davis, *ACS Nano*, 2013, **7**, 10175-10189.

8. N. Petzetakis, A. P. Dove and R. K. O'Reilly, *Chem. Sci.*, 2011, **2**, 955-960.

9. N. Petzetakis, M. P. Robin, J. P. Patterson, E. G. Kelley, P. Cotanda, P. H. H. Bomans, N. A. J. M. Sommerdijk, A. P. Dove, T. H. Epps, III and R. K. O'Reilly, *ACS Nano*, 2013, **7**, 1120-1128.

10. J. R. Dorgan, J. Janzen, D. M. Knauss, S. B. Hait, B. R. Limoges and M. H. Hutchinson, *J. Polym. Sci., Part B: Polym. Phys.*, 2005, **43**, 3100-3111.

11. P. A. Clay and R. G. Gilbert, *Macromolecules*, 1995, **28**, 552-569.

12. R. C. Hayward and D. J. Pochan, *Macromolecules*, 2010, **43**, 3577-3584.

13. O. V. Borisov, E. B. Zhulina, F. A. M. Leermakers and A. H. E. Müller, in *Self Organized Nanostructures of Amphiphilic Block Copolymers I*, eds. A. H. E. Müller and O. V. Borisov, Springer Berlin Heidelberg, 2011, vol. 241, pp. 57-129.

14. D. E. Discher and A. Eisenberg, *Science*, 2002, **297**, 967-973.

15. D. E. Discher and F. Ahmed, *Annu. Rev. Biomed. Eng.*, 2006, **8**, 323-341.

16. W. Schärtl, *Light scattering from polymer solutions and nanoparticle dispersions*, Springer Berlin, 2007.

17. J. P. Patterson, M. P. Robin, C. Chassenieux, O. Colombani and R. K. O'Reilly, *Chem. Soc. Rev.*, 2014, **43**, 2412-2425.

18. J. Jakeš, Collect. *Czech. Chem. Commun.*, 1995, **60**, 1781-1797.

19. T. Nicolai, W. Brown, R. M. Johnsen and P. Stepanek, *Macromolecules*, 1990, **23**, 1165-1174.

20. J. P. Patterson, E. G. Kelley, R. P. Murphy, A. O. Moughton, M. P. Robin, A. Lu, O. Colombani, C. Chassenieux, D. Cheung, M. O. Sullivan, T. H. Epps, III and R. K. O'Reilly, *Macromolecules*, 2013, **46**, 6319-6325.

21. O. Colombani, M. Ruppel, M. Burkhardt, M. Drechsler, M. Schumacher, M. Gradzielski, R. Schweins and A. H. E. Müller, *Macromolecules*, 2007, **40**, 4351-4362.

22. P. T. DeLassus and N. F. Whiteman, in *Polymer Handbook*, eds. J. Brandrup, E. H. Immergut and E. A. Grulke, John Wiley & Sons, New York, Fourth edn., 1999, p. V/159.

23. A. R. Esker, C. Mengel and G. Wegner, *Science*, 1998, **280**, 892-895.

24. T. Nicolai, O. Colombani and C. Chassenieux, *Soft Matter*, 2010, **6**, 3111-3118.

25. J. P. Patterson, A. M. Sanchez, N. Petzetakis, T. P. Smart, T. H. Epps, III, I. Portman, N. R. Wilson and R. K. O'Reilly, *Soft Matter*, 2012, **8**, 3322-3328.

26. A. Lu, D. Moatsou, D. A. Longbottom and R. K. O'Reilly, *Chem. Sci.*, 2013, **4**, 965-969.

27. Spectra Database hosted at the University of Arizona. www.spectra.arizona.edu. Retrieved on 28/02/2014

28. A Guide to Recording Fluorescence Quantum Yields, Horiba Scientific.

29. C. Würth, M. Grabolle, J. Pauli, M. Spieles and U. Resch-Genger, *Nat. Protoc.*, 2013, **8**, 1535-1550.

30. M. Wilhelm, C. L. Zhao, Y. Wang, R. Xu, M. A. Winnik, J. L. Mura, G. Riess and M. D. Croucher, *Macromolecules*, 1991, **24**, 1033-1040.

31. A. Olaya-Castro and G. D. Scholes, *Int. Rev. Phys. Chem.*, 2011, **30**, 49-77.

32. M. Beija, A. Fedorov, M.-T. Charreyre and J. M. G. Martinho, *J. Phys. Chem. B*, 2010, **114**, 9977-9986.

33. Y. Hong, J. W. Y. Lam and B. Z. Tang, *Chem. Commun.*, 2009, 4332-4353.

34. M. P. Robin, A. B. Mabire, J. C. Damborsky, E. S. Thom, U. H. Winzer-Serhan, J. E. Raymond and R. K. O'Reilly, *J. Am. Chem. Soc.*, 2013, **135**, 9518-9524.

35. J. C. Damborsky and U. H. Winzer-Serhan, *Neuroscience*, 2012, **225**, 105-117.

36. F. Hua, X. Jiang, D. Li and B. Zhao, *J. Polym. Sci., Part A: Polym. Chem.*, 2006, **44**, 2454-2467.

6. Exploring the effect of bromo- and thio-maleimides on RAFT polymerisations

6.1. Abstract

In this Chapter, data from Chapter 2, 3, and 4 is discussed concerning the effect of monobromomaleimide (MBM), dibromomaleimide (DBM) and dithiomaleimide (DTM) on RAFT polymerisations. The reactivity of these three groups toward radicals is explored, and compared to the reactivity of maleimide (MI) in radical polymerisation. The external order of DBM and DTM is calculated in both methacrylate and acrylate RAFT polymerisations. An attempt is made to explain the differences in reactivity that are observed, in terms of the electronic structure of the different maleimide groups, with the effect of steric hindrance also considered. Finally, some model reactions are performed to test the resultant hypothesis.

6.2. Introduction

Throughout this thesis, the presence of the dibromomaleimide (DBM) and dithiomaleimide (DTM) functional groups has caused a deviation from ideal RAFT polymerisation behaviour. In this chapter, all the relevant data from previous chapters is brought together for comparison, and new experiments conducted to try and identify the cause of this effect.

6.2.1. Maleimides in radical polymerisation

The reactivity of maleimides under radical polymerisation conditions is well established.[1] Free radical homopolymerisation of *N*-alkyl maleimides using either 2,2′ -azobis(2-methylpropionitrile) (AIBN) or benzoyl peroxide (BPO) as radical initiator was first reported over 50 years ago.[2] In this same contribution copolymers of *N*-butyl maleimide with styrene were found to have a 'nearly alternating' structure. This has been explained using the *Q*-*e* scheme of Alfrey and Price,[3] where *Q* represents a vinyl monomers reactivity, and *e* represents the polarity its double bond. Maleimide monomers are electron accepting monomers having large positive e values, due to the low electron density of their C=C double bond, whereas styrene has a large negative e value due to its electron donating phenyl ring. Alternating copolymerisation of a pair of monomers is then favoured when e values are large and of opposite sign, due to the formation of charge transfer complexes during propagation.[4] Alternating copolymers of styrene and *N*-alkyl maleimides have been synthesised by reversible deactivation radical polymerisation (RDRP) techniques;[5] for example by nitroxide mediated polymerisation (NMP),[6] atom transfer radical polymerisation (ATRP),[7] and most recently by reversible addition-fragmentation chain transfer (RAFT) polymerisation.[8]

In addition to the polymerisations with an equimolar loading of styrene and *N*-maleimide that lead to alternating copolymers, the use of an excess of styrene can lead to more complex polymer structures. For example Deng and Chen showed that when a maleimide-functional ATRP initiator (BiBEMI) is used in the polymerisation of styrene (Sty) at a ratio of [BiBEMI]:[Sty] = 1:50 star polymers are formed (Figure 6.1).[9] The maleimide C=C double bond of the initiator (BiBEMI) is consumed by alternating copolymerisation

with Sty within the early stages of polymerisation to form the core, with subsequent arm growth by Sty homopolymerisation

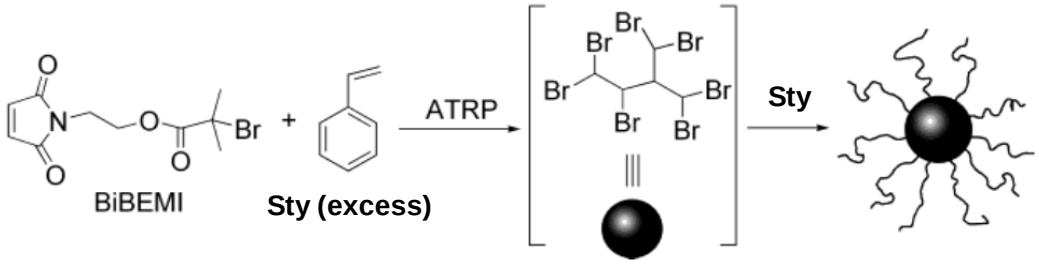

Figure 6.1. One-pot synthesis of poly(styrene) star polymers. Figure adapted from ref.[9]

The selective alternating copolymerisation of maleimide and styrene need not be confined to the start of the reaction. Lutz and co-workers have showed that addition of small equivalents of *N*-functional maleimide during a styrene polymerisation allows precise control of the location of the maleimide units within the polymer chains.[10, 11] This sequence control is achieved by adding the maleimide at different time-points, with complete maleimide incorporation occurring rapidly after addition. This system was optimised using single electron transfer living radical polymerisation (SET-LRP), whereby maleimides were added at high styrene conversions to maximise the tendency for alternating copolymerisation, and therefore precision of maleimide incorporation (Figure 6.2).[12]

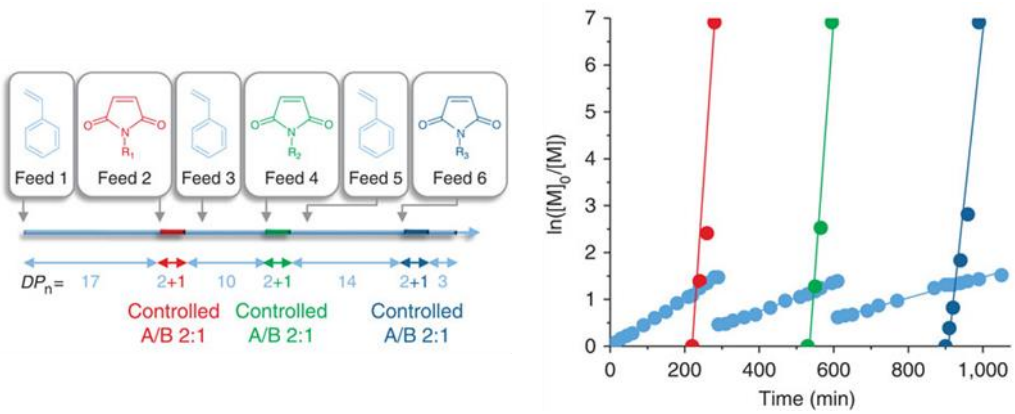

Figure 6.2. Probable microstructure of the polymer prepared *via* a six-step strategy for sequence control in styrene *N*-maleimide polymerisations (left) and the corresponding experimental first-order plots of monomer consumption (right). Figure adapted from ref.[12]

6.2.2. Dibromomaleimides and dithiomaleimides in ATRP

Just prior to the work in this thesis, Jones and Haddleton *et al.* had investigated ATRP of methacrylates and acrylates in the presence of the DBM group, with the aim of

synthesising DBM-terminated polymers by ATRP for disulfide bridging PEGylation. They first demonstrated that 2,3-DBM severely retarded ATRP of oligoethyleneglycol methacrylate (OEGMA), with ethyl 2-bromoisobutyrate as the initiator and Cu(I)Br/*N*-(ethyl)-2-pyridyl methanimide as the catalyst system. Monomer conversion was monitored in the presence and absence of 1 *eq.* of 2,3-DBM (relative to the initiator), with severe inhibition of conversion in the former case (Figure 6.3).[13]

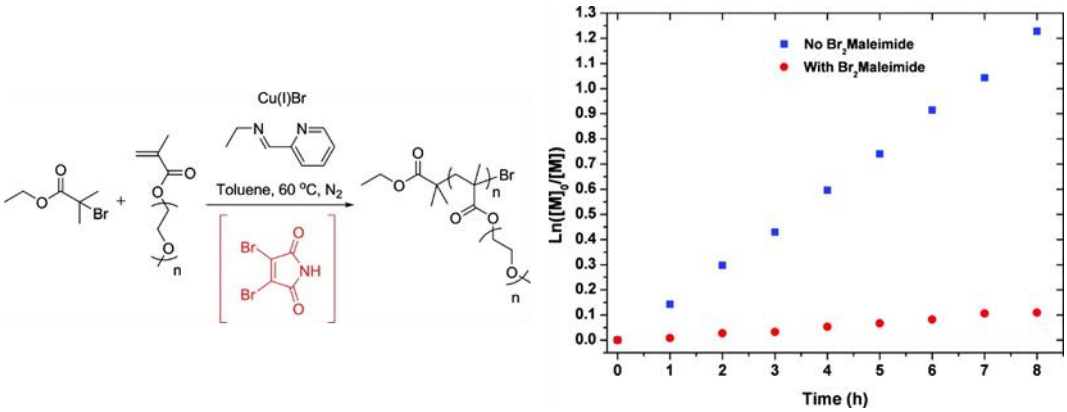

Figure 6.3. Reaction scheme (left) and first-order kinetic plot (right) for the polymerisations of OEGMA using [ethyl 2-bromoisobutyrate]:[Cu(I)Br]: [Lig.]:[OEGMA]= 1:1:3:40, toluene:OEGMA 2:1 (*v/w*), 60 °C in the absence (blue data) and presence of 1 *eq.* of 2,3-DBM (red data). Figure adapted from ref.[13]

This data dissuaded them from synthesising a DBM-functional ATRP initiator, and they instead followed a post-polymerisation functionalisation route. They also investigated a dithiophenolmaleimide-functional ATRP initiator (**6A**, Figure 6.4), as DTMs had shown advantages over DBMs for disulfide bridging PEGylation. Baker *et al.* had recently reported that dithiophenolmaleimide was less susceptible than 2,3-DBM to nucleophilic attack by tris(2-carboxyethyl)phosphine (TCEP), the reducing agent for the disulfide cleavage step of the polymer-protein conjugation.[14] In this case polymerisation of diethyleneglycol methacrylate (DEGMA) under the same conditions, using the DTM-functional initiator (**6A**) gave linear first-order monomer consumption and good control over molecular weight with a linear increase of M_n with conversion and low dispersities (Figure 6.4).[15]

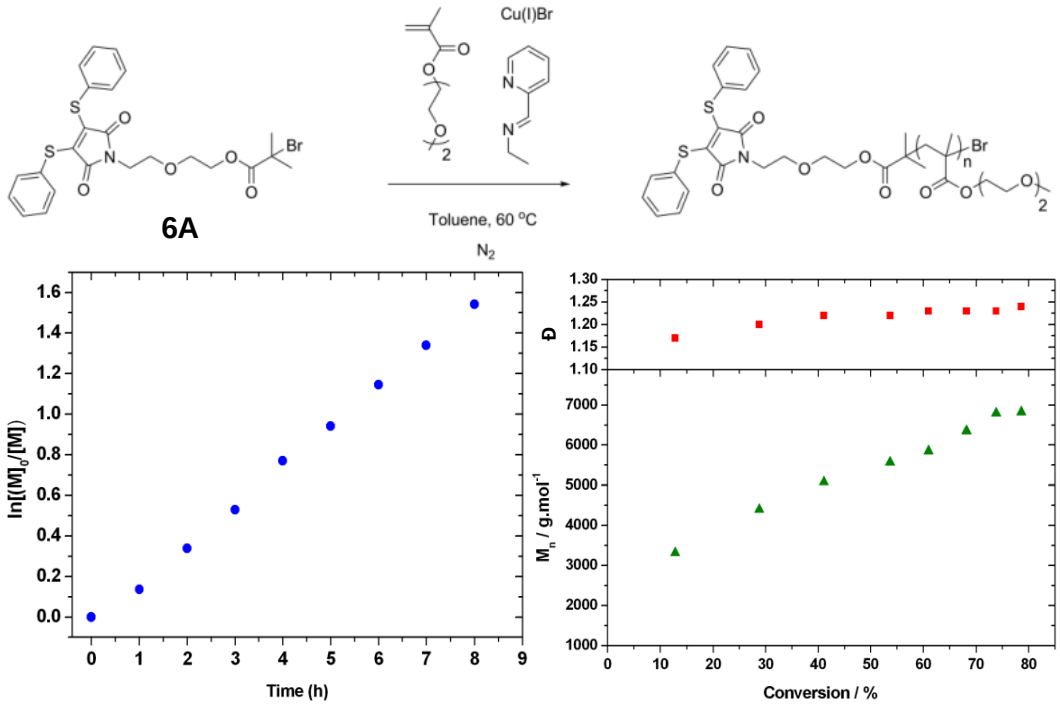

Figure 6.4. Reaction scheme (top), first-order kinetic plot (left), and evolution of M_n and $Đ_M$ (right), for the polymerisations of DEGMA using [ethyl 2-bromoisobutyrate]:[Cu(I)Br]:[Lig.]:[OEGMA]= 1:1:3:20, toluene:OEGMA 2:1 (*v*/*w*), 60 °C in the absence (blue data) and presence of 1 *eq.* of 2,3-DBM (red data). Figure adapted from ref.[15]

Subsequent to this work, collaboration with Jones and Haddleton prompted the investigation of DBM-functional initiators in the ATRP of acrylate monomers. Two initiators were synthesised (**6B** and **6C**, Figure 6.5) and tested in the ATRP of *tert*-butyl acrylate (^{t}BA) and methyl acrylate (MA), using standard conditions.

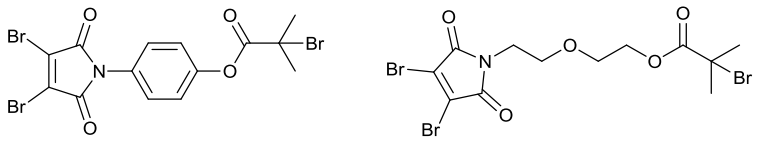

Figure 6.5. DBM-functional ATRP initiators **6B** and **6C**, used in the polymerisation of ^{t}BA and MA.

With both **6B** and **6C**, no inhibition was observed and polymerisations of ^{t}BA and MA proceeded with linear first order consumption of monomer. However, in all cases a loss of control over molecular weight was observed from the onset of polymerisation with molecular weight distributions showing low molecular weight tailing, and high molecular shoulders suggestive of polymer-polymer coupling. Unlike polymerisations with a

maleimide-functional ATRP initiator however, no evidence for branching was observed.(Figure 6.6).[16]

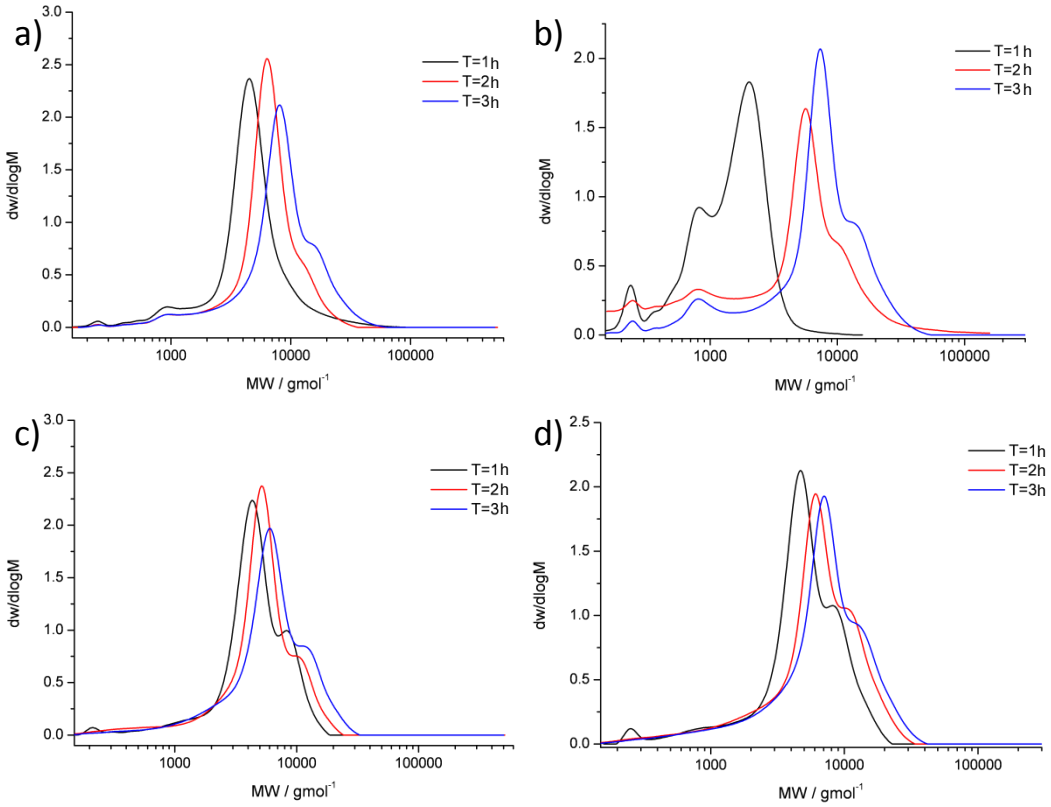

Figure 6.6. Molecular weight distributions at 1 h, 2 h and 3 h for the ATRP of a) ^{t}BA with **6B**; b) MA with **6B**; c) ^{t}BA with **6C**; d) MA with **6C**; using Cu(I)Br/Me_6TREN as the catalyst system, with 50 *eq.* monomer w.r.t. initiator. Figures reproduced from ref.[16]

6.3. Results and Discussion

6.3.1. Summary of the data

To begin, a summary of all the relevant data regarding polymerisations in the presence of maleimide derivatives (shown in Figure 6.7) is given. In each case, the class of maleimide derivative, the polymerisation method, details of the reaction, and the outcome are listed (Table 6.1).

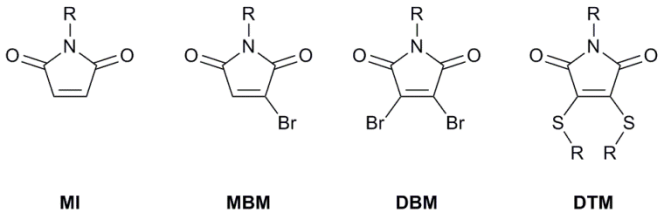

Figure 6.7. Maleimide (MI), monobromomaleimide (MBM), dibromomaleimide (DBM), and dithiomaleimide (DTM) groups.

Table 6.1. Summary of data for polymerisations in the presence of maleimide (MI), monobromomaleimide (MBM), dibromomaleimide (DBM), and dithiomaleimide (DTM) groups.

	Method [a]	Details	Outcome	Ref
MI	FRP	Homopolym. of *N*-alkyl MI using AIBN or BPO	Polym. of MI C=C double bond	[2]
	FRP	Copolym. of *N*-substituted MI with Sty, MMA and MA	Low reactivity ratio for MI and comonomers, leading to alternating copolymers	[17]
	ATRP/ RAFT	Copolym. of *N*-alkyl MI and Sty	Alternating copolymer with *MW* control	[7, 8]
	ATRP	Sty polym. using MI-functional initiator	Copolym. of Sty and MI C=C leading to star polymers	[9]
MBM	RAFT	Homopolym. of MBM-functional CTA	No reaction	Ch.2

	RAFT	Acrylate polym. with MBM-functional CTA	Copolym. of acrylates and MBM C=C leading to branched polymers	Ch.2
	RAFT	NIPAM and Sty polym. with MBM-functional CTA	Low conv. for NIPAM and Sty, with complete polym. of MBM C=C	Ch.2
DBM	RAFT	Homopolym. of DBM-functional CTA	No reaction	Ch.2
	ATRP	Methacrylate polym. in presence of 2,3-DBM	Complete polym. retardation	[13]
	RAFT	Copolym of methacrylates with DBM-methacrylate	Linear polym. with intact DBM groups.	Ch.4
	ATRP	Acrylate polym. with DBM-functional initiator	Loss of MW control	[16]
	RAFT	Acrylate polym. with DBM-functional CTA	Linear polym. with intact DBM end-groups. Retardation at high conv.	Ch.2
	RAFT	Copolym of acrylates with DBM-acrylate	Linear polym. with intact DBM groups. Retardation at moderate conv.	Ch.4
	RAFT	NIPAM and Sty polym with DBM-functional CTA	Complete retardation	Ch.2
	RAFT	Copolym of Sty with DBM-styrene	Complete retardation	Ch.4
DTM	ATRP	Methacrylate polym. with DTM-functional initiator	Linear polym. with intact DTM end-groups	[15]
	RAFT	Copolym of methacrylates with DTM-methacrylate	Linear polym. with intact DTM groups	Ch.4

	RAFT	Acrylate polym. with DTM-functional CTA	Linear polym. with intact DTM end-groups	Ch.3
	RAFT	Copolym of acrylates with DTM-acrylate	Linear polym. with intact DTM groups	Ch.4
	RAFT	NIPAM and Sty polym with DTM-functional CTA	Some retardation, worse for NIPAM	Ch.3
	RAFT	Copolym of Sty with DTM-sty	*ca.* 20% DTM C=C bonds polym. leading to branching	Ch.4

[a] FRP; Free radical polymerisation. ATRP; Atom transfer radical polymerisation. RAFT; Reversible addition-fragmentation chain transfer

6.3.2. Monobromomaleimide

In Chapter 2 an MBM-functional RAFT agent was synthesised, and polymerisations with acrylate, Sty and NIPAM monomers investigated. Initially, the MBM-functional RAFT agent and AIBN were heated in dioxane at 65 °C for 6 h. No polymer was formed, indicating that unlike MI, the MBM group will not homopolymerise in the presence of a radical initiator (Scheme 6.1).

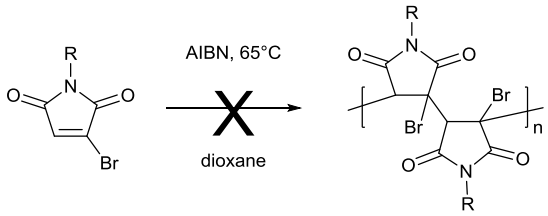

Scheme 6.1. Reaction of MBM in the presence of a radical initiator (AIBN).

It was observed that acrylate polymerisations mediated by the MBM-functional RAFT agent resulted in multimodal molecular weight distributions. Analysis by SEC with viscometry detection indicated the formation of branched polymers, with ^{1}H conversion NMR spectra showing rapid consumption of the MBM C=C double bond, and evidence for succinimide repeat units in the isolated product. It appears that in this case MBM is reacting as a comonomer with acrylates (Scheme 6.2), in an analogous fashion to MI.[18]

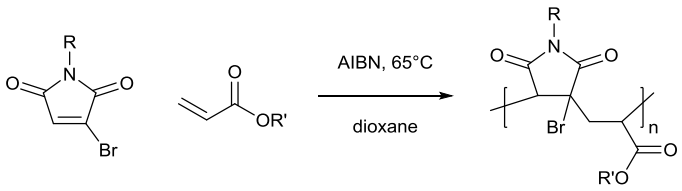

Scheme 6.2. Reaction of MBM in the presence of an acrylate, and a radical initiator (AIBN).

For bulk polymerisations of Sty (thermal initiation), complete consumption of the MBM C=C double bond with corresponding broad molecular weight distribution due to branching was also observed. However only 19% Sty conversion was obtained after 16 h, compared to 64% for an analogous polymerisation with non-MBM-functional RAFT agent. It appears that unlike Sty/MI copolymerisations where the alternating copolymerisation occurs at a greater rate than Sty homopolymerisation,[1] in the case of Sty/MBM the copolymerisation is slow leading to a reduced Sty conversion (Scheme 6.3). This may be caused by the asymmetry of MBM which results in a less electron-deficient C=C double bond (also observed with monobromo-monoamino-maleimides[19]) and as a result a weaker charge transfer complex with Sty during propagation. Steric hindrance can also lead to poor charge transfer complex formation,[4] which in this case could be the result of the Br atom of MBM.

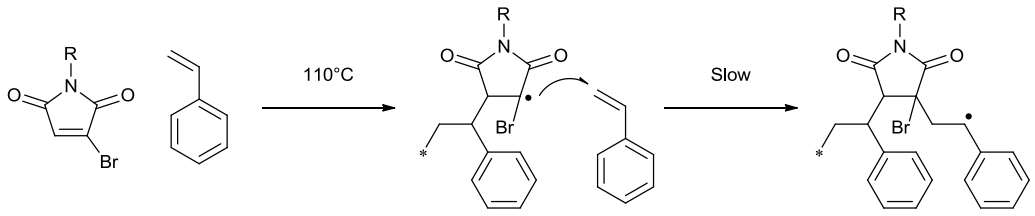

Scheme 6.3. Reaction of MBM in the presence styrene, under thermal initiation.

Polymerisation of NIPAM with the MBM RAFT agent was found to go to very low (3%) NIPAM conversion, while 89% consumption of the MBM double bond was observed. A broad molecular weight distribution resulted, suggesting branching due to polymerisation of MBM had occurred. In this case it appears that copolymerisation is occurring, but that reaction of the succinimide-based radicals with NIPAM is even slower than in the case of Sty. However, this cannot be rationalised in terms of charge transfer complex formation, as this does not take place in polar solvents such as dioxane,[4] and would not be expected for an acrylamide. It would appear that inhibition must be due to radicals forming on the bromosuccinimide carbon, which then have a low rate of propagation with NIPAM

(Scheme 6.4). Conversely, radicals formed on NIPAM would be free to react with NIPAM monomer, and this homopolymerisation would be expected to reach *ca.* 100% conversion under these conditions, as was observed when using a non-MBM-functional RAFT agent.

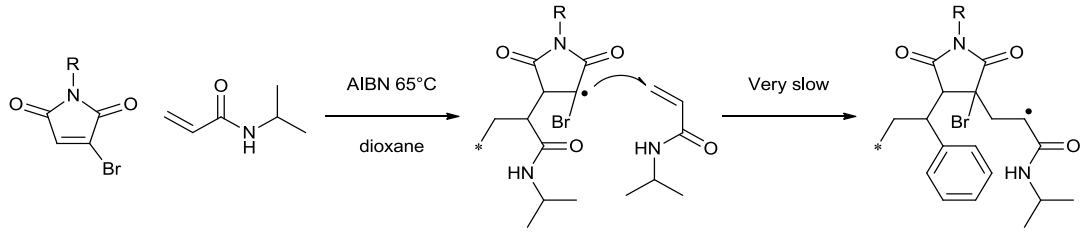

Scheme 6.4. Reaction of MBM in the presence of NIPAM, and a radical initiator (AIBN).

In conclusion, MBM is unable to self-propagate under radical polymerisation conditions. However, in the presence of a comonomer, donor-acceptor copolymerisation allows the MBM to be polymerised. It appears that the extent to which this copolymerisation can occur depends on the reactivity of the succinimide-based radicals towards the comonomer.

6.3.3. Dibromomaleimide

In this thesis RAFT polymerisation with both DBM-functional monomers (Chapter 4) and a DBM-functional CTA (Chapter 2) has been investigated. Initially, the DBM-functional RAFT agent and AIBN were heated in dioxane at 65 °C for 6 h (Scheme 6.5). No polymerisation occurred indicating that DBM (like MBM, but in contrast to MI) will not homopolymerise in the presence of a radical initiator.

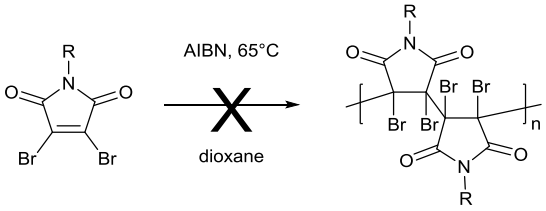

Scheme 6.5. Reaction of DBM in the presence of a radical initiator (AIBN).

RAFT copolymerisation of a DBM-functional methacrylate monomer with MMA was studied in Chapter 4. Again there was no evidence for reaction of the DBM C=C double bond, as linear polymers were produced. Retention of the DBM group in the polymer products was observed by ^{13}C NMR spectroscopy, and also inferred by the ability of the polymers to undergo post-polymerisation conjugation with thiols to form DTM-functional

products. It was therefore concluded that formation of a copolymer of DBM and MMA did not occur, in contrast to MI/MMA which does form a copolymer (Scheme 6.6).[20]

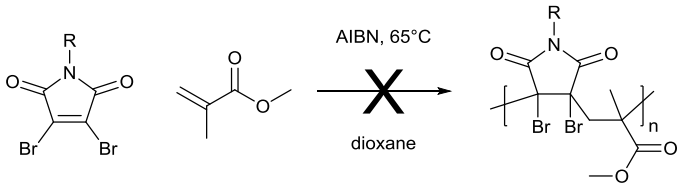

Scheme 6.6. Reaction of DBM in the presence of MMA and a radical initiator (AIBN).

RAFT polymerisation of acrylates with a DBM-functional CTA was performed in Chapter 2, and the copolymerisation of a DBM-functional acrylate monomer with acrylates studied in Chapter 4. In both cases polymerisation retardation was observed. Branching was not observed in either case, and intact DBM groups were observed by ^{13}C NMR spectroscopy, by MALDI-TOF MS, and inferred by the ability of the polymers to undergo post-polymerisation conjugation with thiols to form DTM-functional products. Therefore it was concluded that unlike MI and MBM, the DBM group will not copolymerise with acrylates (Scheme 6.7).

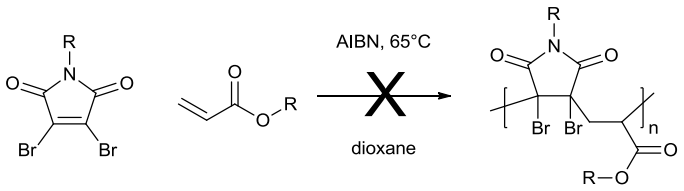

Scheme 6.7. Reaction of DBM in the presence of an acrylate and a radical initiator (AIBN).

However, it was clear that DBM was having a detrimental effect on the RAFT polymerisation. Following the method of Bell *et al.*,[21] the external order of reaction for 2,3-dibromo-*N*-methylmaleimide (DBMM) in the RAFT polymerisation of ^{t}BA was calculated. The initial rate of monomer consumption (k_{app}) with a range of DBMM concentrations was measured, and the reaction order calculated as the gradient of a plot of $\ln(k_p^{app})$ *vs.* $\ln([DBMM])$ (Figure 6.8). The reaction order was found to be -0.68 for DBMM, which is a clear indication that the DBM group has a retarding effect on the RAFT polymerisation of ^{t}BA.

In contrast, when the same experiment was repeated to determine the external order of DBMM in MMA RAFT polymerisation, an order of -0.14 was found (Figure 6.9). This

means that DBMM has a much weaker effect on RAFT polymerisations of MMA, which explains why no significant retardation was observed in the polymerisation of DBM-methacrylate.

RAFT polymerisation of Sty and NIPAM with a DBM-functional CTA was performed in Chapter 2, and the copolymerisation of a DBM-functional styrene monomer with styrene studied in Chapter 4. In all cases polymerisation retardation was even more severe than the corresponding acrylate polymerisations, with conversion $< 10\%$ in all cases.

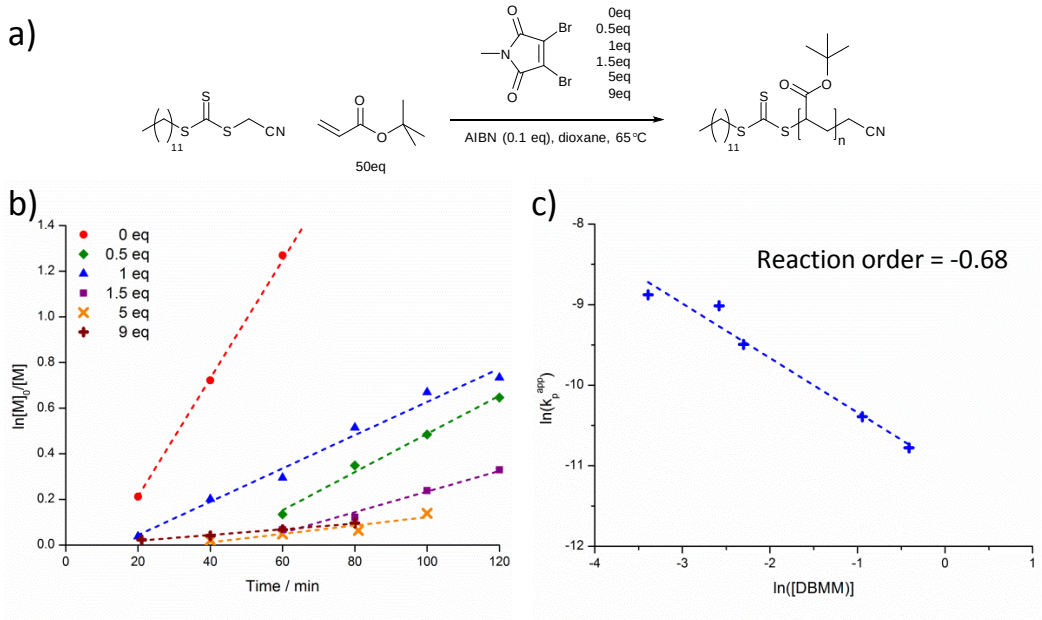

Figure 6.8 a) Determining the external order of reaction for DBMM in RAFT polymerisation of ^{t}BA; b) Initial rates of monomer consumption; c) Plot to determine reaction order.

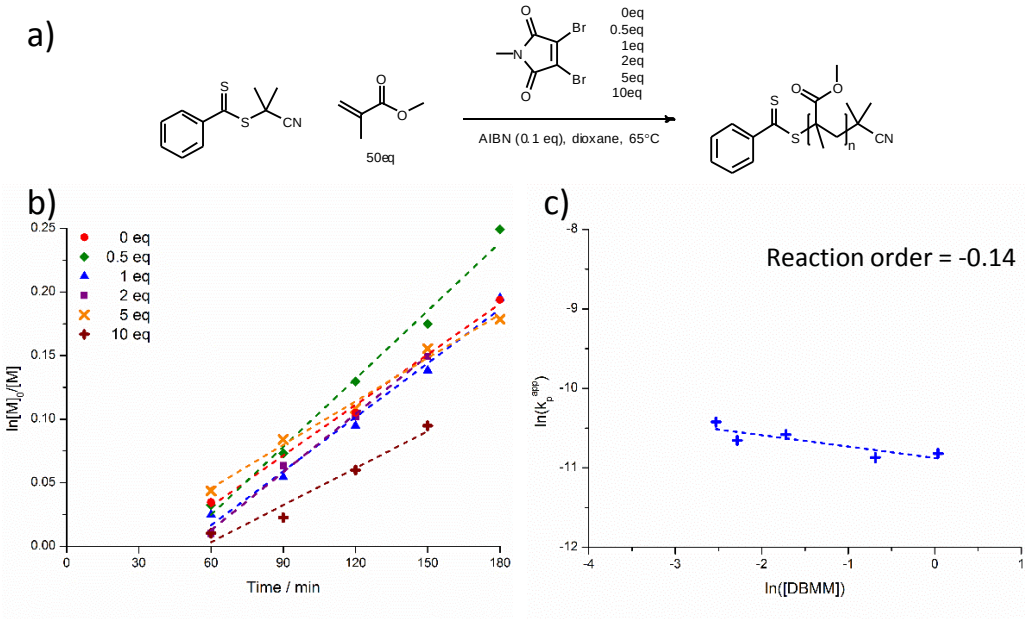

Figure 6.9 a) Determining the external order of reaction for DBMM in RAFT polymerisation of MMA; b) Initial rates of monomer consumption; c) Plot to determine reaction order.

Next, the possible cause of this retardation effect was investigated. Control reactions of DBMM with the individual components of a RAFT polymerisation of ^{t}BA – namely CTA, ^{t}BA and AIBN – were performed under polymerisation conditions and monitored by HPLC. In each case an equimolar ratio of DBMM and the second reagent were used. Toluene was chosen as the solvent to provide a UV active standard for HPLC, and also because the half-life of AIBN at 80 °C in toluene is known to be *ca.* 75 minutes.[22] As shown in Figure 6.10, no reaction was observed between DBMM and the CTA or ^{t}BA after 4 h, with HPLC spectra showing starting materials present at their initial concentrations relative to toluene (Figure 6.10 b and c). However, reaction of DBMM and AIBN (Figure 6.10 d) showed loss of 77% of DBMM, with the formation of a major product (red circle, RT= 10.15 min), as well as multiple additional impurities (green star, RT≈ 12 min).

Reaction of DBMM with AIBN does not fully explain the retardation observed in RAFT polymerisation. If AIBN radicals were simply consumed by reaction with DBM groups, DBM would be expected to affect RAFT polymerisations of all monomers to the same extent, as rate of polymerisation for a free radical process is proportional to the square root of initiator concentration.[23] However, this result does indicate the reactivity of DBM towards radicals. Reaction of DBM with the propagating radicals, rather than AIBN,

would explain the fact that DBM affects polymerisation of different monomers to different extents.

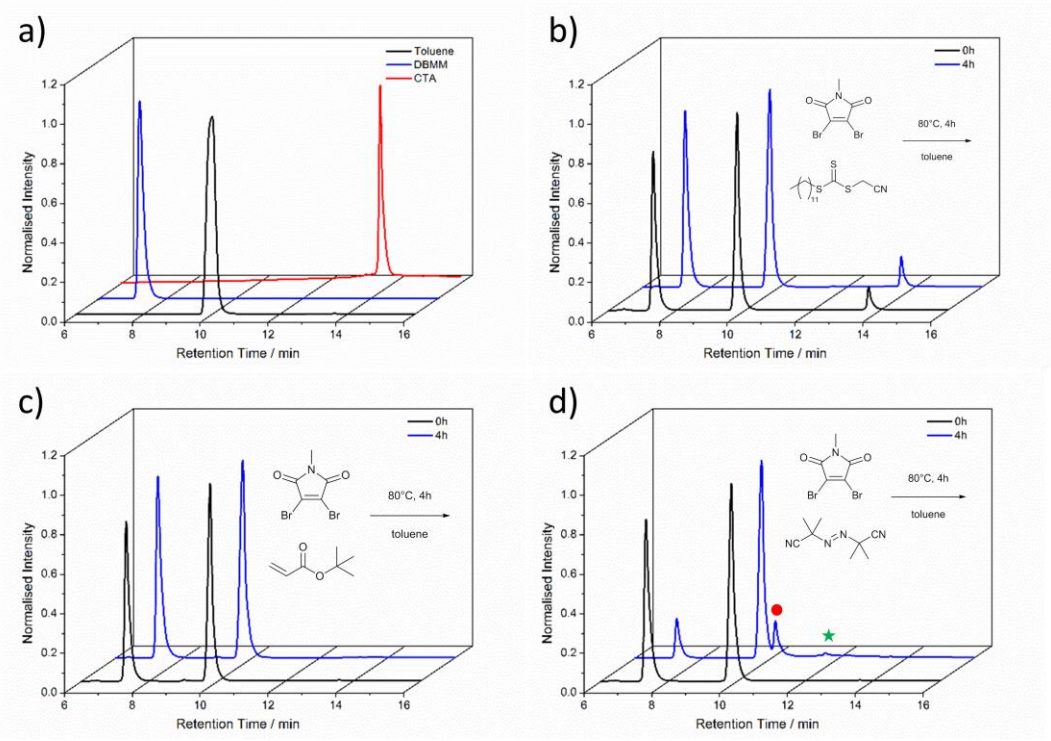

Figure 6.10. HPLC spectra with UV absorption (254 nm) detection of a) toluene, DBMM, and the CTA; and the reactions between b) DBMM and CTA; c) DBMM and ^{t}BA; d) DBMM and AIBN. Note that neither AIBN nor ^{t}BA absorb at 254 nm.

It seems unlikely that reactivity of DBM towards propagating radicals leads to formation of an irreversibly bound adduct. If an irreversible reaction were occurring, it would be expected to have a dramatic effect on the molecular weight distribution of the products (Scheme 6.8). In the case of the DBM-functional RAFT agent used in Chapter 2, irreversible reaction between DBM and propagating radicals would lead to oligomerisation of the RAFT polymers. The propagating radicals at the ω-chain end would be able to form an adduct with the DBM group at the α-chain end, leading to the formation of high molecular weight species. However, this was not observed in Chapter 2. Instead, linear increase of molecular weight with conversion, and narrow dispersities throughout the polymerisation were obtained, with high DBM end-group fidelity for the products.

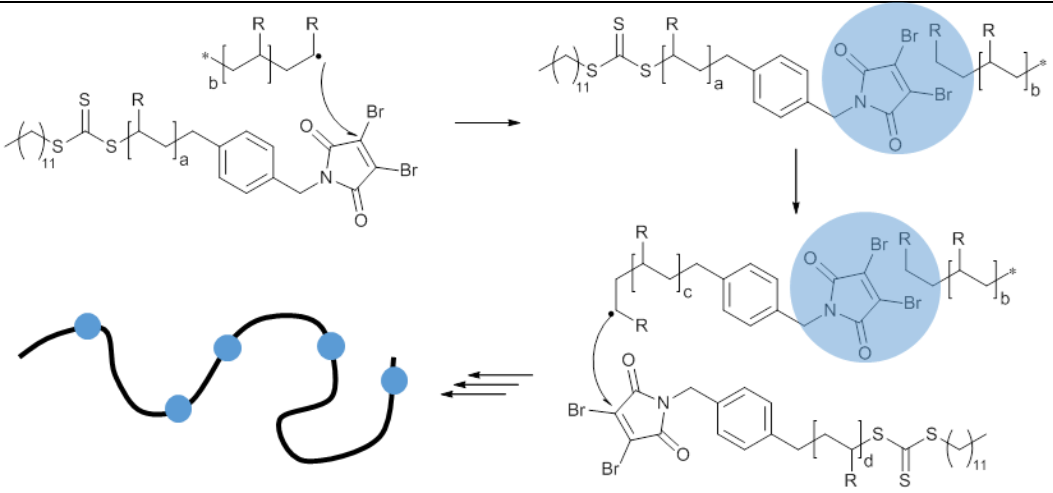

Scheme 6.8. Formation of high molecular weight species resulting from an irreversibly bound adduct between DBM and propagating radicals for the DBM-functional RAFT agent.

Further evidence against an irreversible reaction comes from RAFT polymerisation of ^{t}BA and TEGA with a non-DBM-functional CTA, instead having 1 *eq.* of 2,3-DBM as an additive ([CTA]:[^{t}BA]:[2,3-DBM]:[AIBN] = 1:100:1:0.1 and [CTA]:[TEGA]:[2,3-DBM]:[AIBN] = 1:50:1:0.1) as shown in Scheme 6.9.

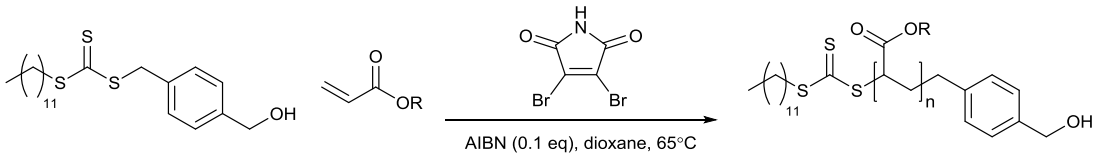

Scheme 6.9. RAFT polymerisation of acrylates in the presence of 2,3-DBM.

In this case irreversible reaction of propagating radicals with DBM would be expected to lead to accumulation of low molecular weight products and therefore complete loss of control over molecular weight. However, as shown in Figure 6.11, ^{t}BA polymerisation proceeded with excellent control over molecular weight, while PTEGA was shown by MALDI-TOF MS to comprise a single distribution corresponding to the CTA-derived end-groups.

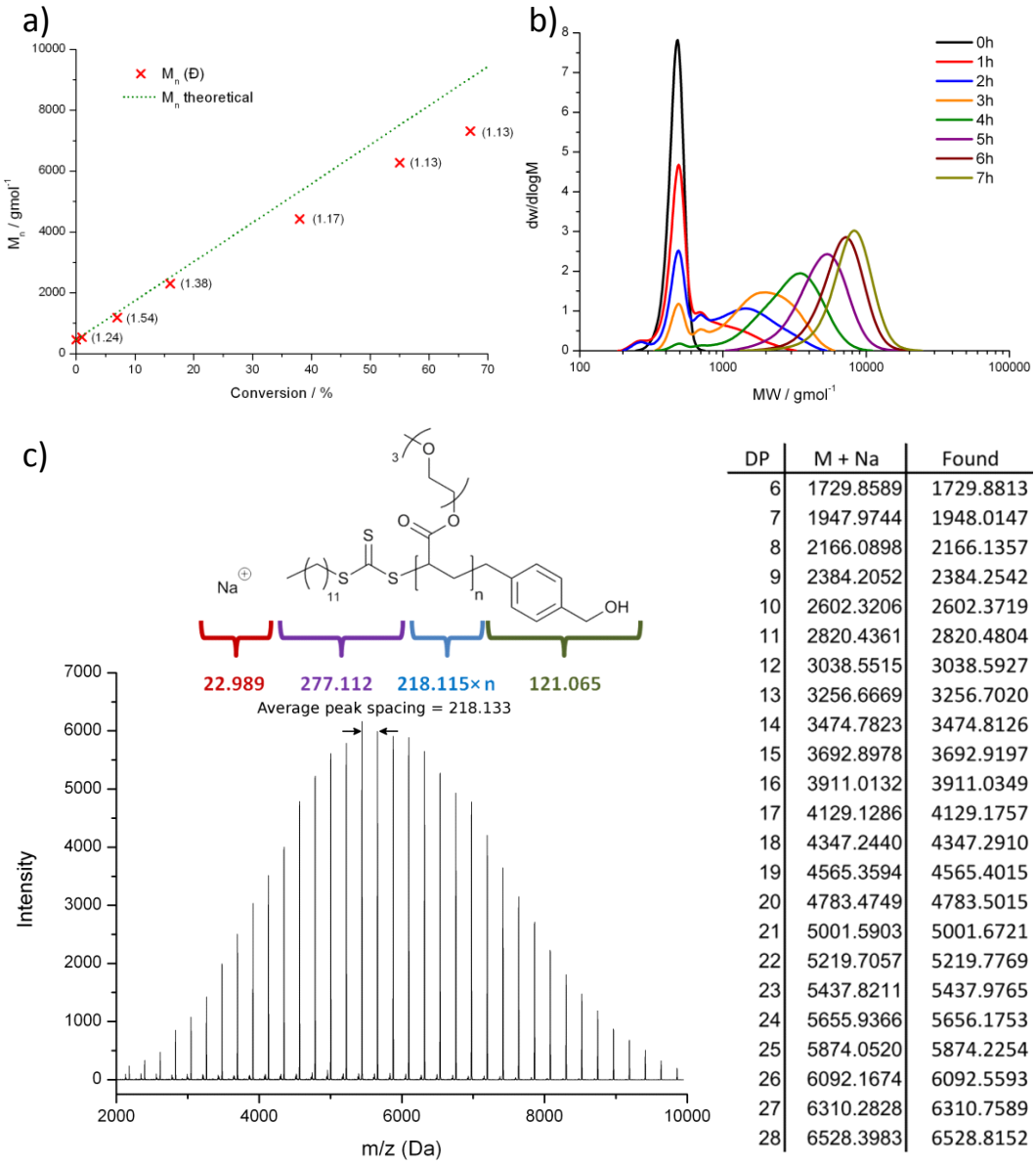

DP	M + Na	Found
6	1729.8589	1729.8813
7	1947.9744	1948.0147
8	2166.0898	2166.1357
9	2384.2052	2384.2542
10	2602.3206	2602.3719
11	2820.4361	2820.4804
12	3038.5515	3038.5927
13	3256.6669	3256.7020
14	3474.7823	3474.8126
15	3692.8978	3692.9197
16	3911.0132	3911.0349
17	4129.1286	4129.1757
18	4347.2440	4347.2910
19	4565.3594	4565.4015
20	4783.4749	4783.5015
21	5001.5903	5001.6721
22	5219.7057	5219.7769
23	5437.8211	5437.9765
24	5655.9366	5656.1753
25	5874.0520	5874.2254
26	6092.1674	6092.5593
27	6310.2828	6310.7589
28	6528.3983	6528.8152

Figure 6.11 a) M_n and $Đ_M$ (obtained by SEC) *vs.* conversion for polymerisation of ^{t}BA with theoretical values (line); b) *MW* distributions obtained by SEC for polymerisation of ^{t}BA; c) MALDI-TOF mass spectrum of PTEGA collected in linear mode, with high resolution masses obtained in reflector mode. Average difference between calculated and found $m/z = 0.1118$.

Results in Chapter 4 also suggest that reaction between DBM and propagating radicals is not irreversible. An irreversible reaction between DBM groups in the monomer side chains and propagating radicals would lead to the formation of brush polymers with very high molecular weight (Scheme 6.10), however this was not observed.

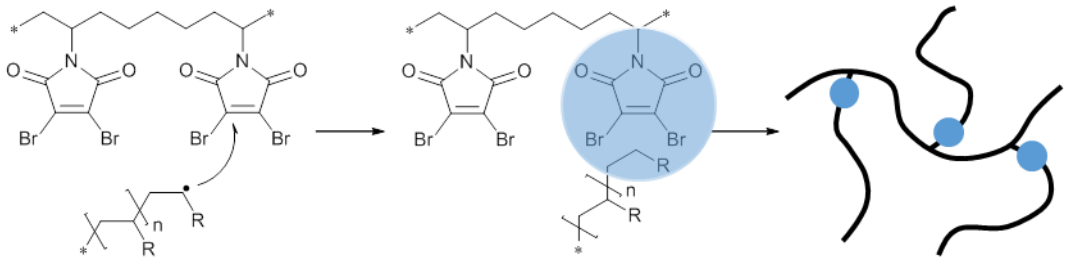

Scheme 6.10. Formation of high molecular weight 'brush' polymer resulting from an irreversibly bound adduct between DBM and propagating radicals for the DBM-functional monomer.

In conclusion, it is proposed that retardation of RAFT polymerisations by DBM is the result of a reversible reaction between propagating radicals and DBM. This would account for both the difference in the extent of retardation for different monomers, and the fact that no permanent adducts between propagating chains and DBM have been observed (Scheme 6.11).

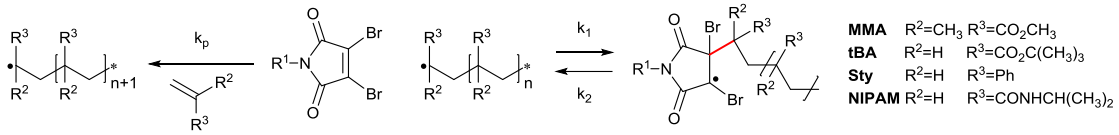

Scheme 6.11. Proposed scheme for the retardation of RAFT polymerisations caused by DBM.

In this case polymerisation retardation becomes dependant on competition between DBM and monomer for reaction with the propagating radical.

- Where k_p is high, as in the case of acrylates such as ^{t}BA, propagation will occur until high conversion (*i.e.* until monomer concentration is low). At this point reaction with DBM becomes significant leading to retardation.
- For MMA k_p is lower, however k_1 will be low (and k_2 high) due to increased steric crowding (as R^2=CH_3), which weakens the new (red) bond leading to a high energy transition state. As such there is little retardation.
- Sty also has a low k_p, however in this case the new (red) bond will be stronger due to minimal steric crowding with R^2=H, leading to a higher k_1 and lower k_2. The result is that retardation is more significant than for acrylates and methacrylates.
- NIPAM has a greater k_p than Sty, but also less steric crowding with R^3=$CONHCH(CH_3)_2$. The result is that retardation is also very significant

An attempt was made to try and trap an adduct of DBM with a non-propagating analogue of an acrylate radical (Scheme 6.12). These non-propagating radicals would be formed by the fragmentation of RAFT agent **6i**, upon addition of a radical initiator (I-I).

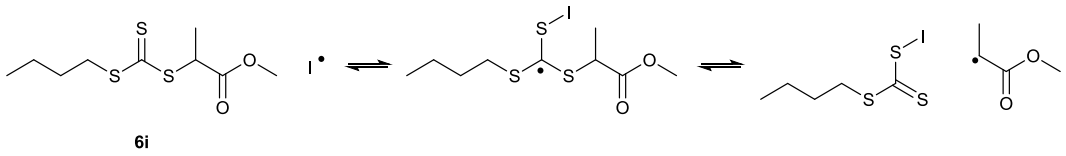

Scheme 6.12. Formation of non-propagating acrylate radicals from RAFT agent **6i**.

Unfortunately attempts to generate the acrylate radical were unsuccessful. When AIBN was chosen as the radical initiator (I-I), fragmentation of the intermediate radical towards reformation of **6i** was more favourable due to the greater stability of the tertiary AIBN-derived radical compared to the secondary acrylate radical. This same problem has been observed in radical-induced trithiocarbonate end-group removal from RAFT poly(acrylates) using AIBN.[24] In this case the solution was to use lauroyl peroxide (LPO) as the radical initiator to generate the primary *n*-undecyl radical. However, when LPO was used in place of AIBN for reaction with **6i** multiple products were formed, making this approach unsuitable for a subsequent control reaction with DBMM.

6.3.4. Dithiomaleimide

Polymerisations with a DTM-functional RAFT agent (Chapter 3) and DTM-functional acrylate, methacrylate and styrenic monomers (Chapter 4) have been performed. In contrast to DBM, no retardation of acrylate polymerisations in the presence of DTM was observed. The external order of reaction for an *N*-dithio-*N*-methylmaleimide (DTMM) was determined for RAFT polymerisation of ^{t}BA and MMA in an analogous fashion to reactions with DBMM (Figure 6.12 and Figure 6.13).

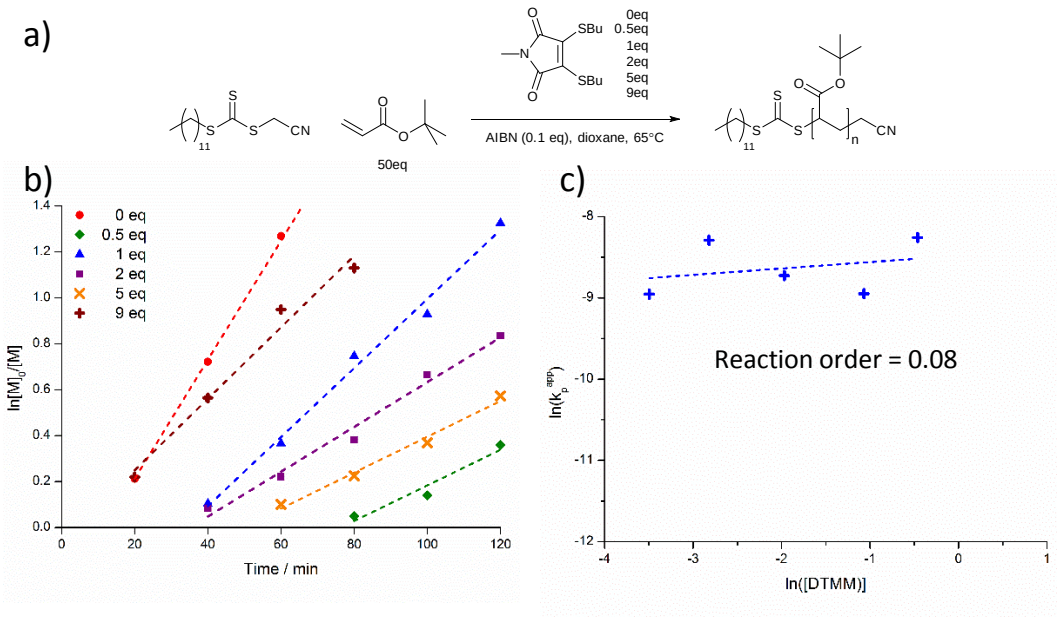

Figure 6.12 a) Determining the external order of reaction for DTMM in RAFT polymerisation of ^{t}BA; b) Initial rates of monomer consumption; c) Plot to determine reaction order.

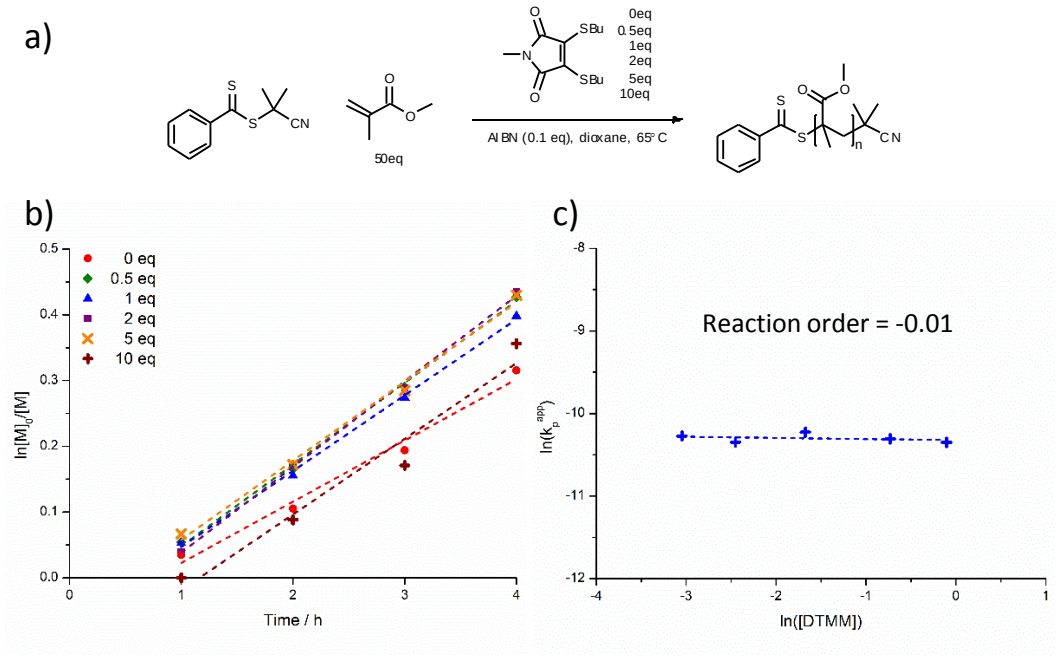

Figure 6.13 a) Determining the external order of reaction for DTMM in RAFT polymerisation of MMA; b) Initial rates of monomer consumption; c) Plot to determine reaction order.

The external order of reaction for DTMM was found to be near zero (0.08 and -0.01 in ^{t}BA and MMA polymerisations respectively), indicating that neither acrylate nor methacrylate polymerisations are retarded by DTM. This difference in reactivity between DBM and DTM may be explained using the mechanism shown below (Scheme 6.13).

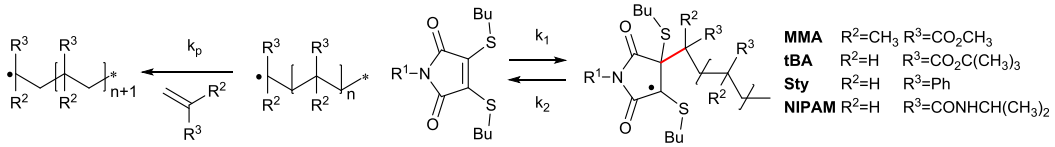

Scheme 6.13. Proposed scheme for the retardation of RAFT polymerisations caused by DTM.

With DTMM increased steric hindrance (compared to DBMM) as the result of the Bu groups further weakens the new (red) bond for acrylates, leading to a smaller k_1 and therefore no retardation. This also explains why polymerisations of NIPAM with the DTM-functional CTA (Chapter 3) were less retarded than those with the DBM-functional CTA (Chapter 2). Again, a reduction of k_1 in comparison to k_p leads to an increase in monomer propagation. Further proof that this new (red) bond is more hindered for DTM in comparison to DBM comes from the control reaction with AIBN. Unlike DBMM which underwent reaction with AIBN in toluene at 80 °C after 4 h, DTMM does not react with AIBN (Figure 6.14) due to the greater steric hindrance around the DTM C=C double bond.

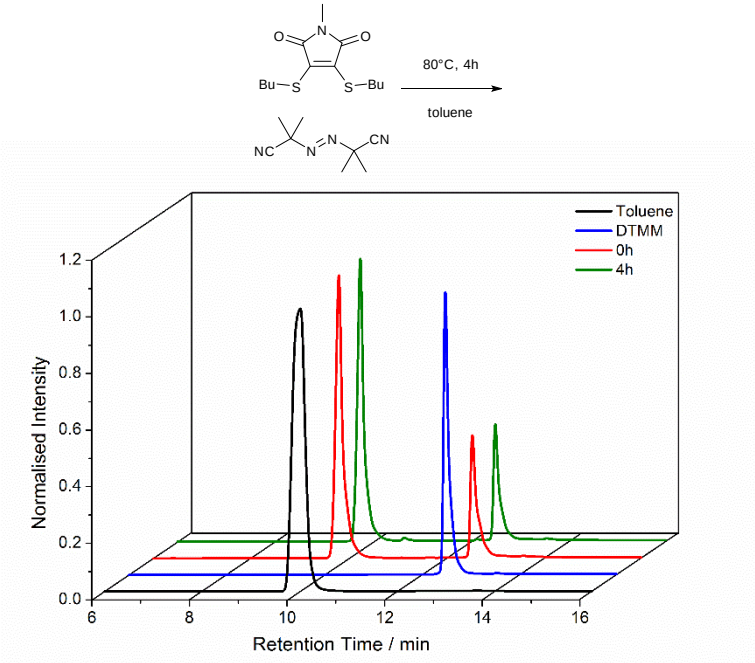

Figure 6.14. HPLC spectra with UV absorption (254 nm) detection of toluene, DTMM, and the reaction between DTMM and AIBN (0 h and 4 h). Note that AIBN does not absorb at 254 nm.

In Chapter 4 it was shown that polymerisation of a DTM-functional styrene monomer leads to the formation of branched polymers. It was calculated that 20% of these

monomers undergo polymerisation of the DTM C=C double bond. Of this 20%, approximately a third also polymerised through their vinyl C=C double bond resulting in 7% of the DTM-styrene monomers acting as cross-linkers. Polymerisations of Sty with the DTM-functional RAFT agent in Chapter 3 resulted in the formation of polymers with intact DTM groups (as observed by polymer fluorescence). This PSty had a unimodal molecular weight distribution, however dispersity was quite high ($Đ_M = 1.39$), so it is possible that there was also a small amount of branching in this reaction.

The reason for DTM propagation with Sty may be due to the expected weaker C=C double bond of DTM relative to DBM. Better orbital overlap between C and S (compared to C and Br) would lead to a more electron deficient C=C double bond, according to the resonance structures shown below (Scheme 6.14).

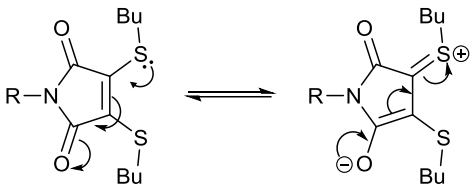

Scheme 6.14. Resonance structures for DTM.

A weaker C=C double bond would make polymerisation both kinetically and thermodynamically more favourable. As polymerisations were performed in bulk (Sty as solvent) charge transfer complex formation between DTM and Sty would have been possible. In this case a more electron deficient DTM C=C double bond would be expected to result in a stronger charge transfer complex and therefore a greater propensity for copolymerisation.

6.4. Conclusion

In this Chapter, the interaction of monobromomaleimide (MBM), dibromomaleimide (DBM) and dithiomaleimide (DTM) in RAFT polymerisations has been discussed. Data from Chapter 2, 3, and 4 has been considered, and comparison made with reactivity of maleimide (MI) in radical polymerisations as reported in the literature.

The trend in reactivity can be summarised as follows:

- MI will homopolymerise, and also copolymerise with most common monomers. These copolymers are often donor acceptor alternating copolymers (particularly with styrene) due to the electron deficient nature of the MI double bond.
- MBM is unable to self-propagate, however, in the presence of a comonomer, donor-acceptor copolymerisation allows the MBM to be polymerised. The extent to which this copolymerisation can occur depends on the reactivity of the succinimide-based radicals towards the comonomer.
- DBM is unable to self-propagate, and does not form copolymers. However it has a retarding effect on the RAFT polymerisation of acrylates, Sty, NIPAM, and to a small extent MMA. This effect is caused by the formation of reversible adducts of the propagating radicals with DBM.
- DTM does not self-propagate, and has a less retarding effect on RAFT polymerisations than DBM. DTM will copolymerise with Sty to a small extent.

These trends were explained by the nature of the different maleimides' electronics – symmetry and electron density – and by the steric crowding around the different maleimides' C=C double bond.

6.5. Experimental

6.5.1. Materials and apparatus

Tert-butyl acrylate (^{t}BA) was vacuum distilled over CaH_2 prior to use, and stored at 4 °C. Methyl methacrylate (MMA) was passed through a column of neutral alumina (Al_2O_3) prior to use, and stored at 4 °C. 2,2'-azobis(2-methylpropionitrile) (AIBN) and lauroyl peroxide (LPO) were recrystallised twice from methanol and stored at 4 °C in the dark. 1,4-Dioxane was passed through a basic alumina plug immediately before use. The RAFT agents 2-cyano-2-propyl benzodithioate (**4xiii**) and cyanomethyl dodecyl trithiocarbonate (**4xx**) were purchased from Aldrich and used as received. All other chemicals and reagents were purchased from Aldrich and used as received. Solvents were purchased from Fisher Scientific and used as received.

^{1}H and ^{13}C NMR spectra were recorded on a Bruker DPX-300, DPX-400, DRX-500, AV-600 or AV-700 spectrometer in $CDCl_3$ unless otherwise stated. Chemical shifts are given in ppm downfield from the internal standard tetramethylsilane, and coupling constants (J) correspond to $^{3}J_{H\text{-}H}$ unless otherwise stated. Size exclusion chromatography (SEC) measurements were conducted using a Varian 390-LC-Multi detector suite fitted with differential refractive index (DRI), and UV-Vis or photodiode array (PDA) detectors. A guard column (Varian Polymer Laboratories PLGel 5 µm, 50 × 7.5 mm) and two mixed D columns (Varian Polymer Laboratories PLGel 5 µm, 300 × 7.5 mm) were used. The mobile phase was tetrahydrofuran with 2% triethylamine, or chloroform with 2% triethylamine eluent at a flow rate of 1.0 mL/min. Data was analysed using Cirrus v3.3 with calibration curves produced using Varian Polymer laboratories Easi-Vials linear poly(styrene) standards (162 Da – 240 kDa). MALDI-TOF mass spectrometry was conducted using a Bruker Daltonics Ultraflex II MALDI-TOF mass spectrometer, equipped with a nitrogen laser delivering 2 ns laser pulses at 337 nm with positive ion TOF detection performed using an accelerating voltage of 25 kV. Solutions in tetrahydrofuran (50 µL) of trans-2-[3-(4-*tert*-butylphenyl)-2-methyl-2-propylidene] malonitrile (DCTB) as a matrix (40 g/L), sodium trifluoroacetate as cationisation agent (0.1 g/L) and sample (1.0 g/L) were mixed, and 0.5 µL of the mixture was applied to the target plate. Spectra were recorded in reflector mode calibrating with SpheriCal (1200-

8000 Da) standards, and linear mode calibrating with PEG-Me 2 kDa and 5 kDa standards. High pressure liquid chromatograms were recorded on a Varian 9250 HPLC, fitted with a Supelco Discovery C18 column and a PDA and fluorescence detector. The mobile phase was a gradient of water and methanol.

6.5.2. Synthetic protocols

Triethylene glycol monomethylether methacrylate (TEGA) was synthesised as previously reported.[25]

Methyl 2-([(butylsulfanyl)methanethioyl]sulfanyl)propanoate (**6i**) was synthesised as previously reported.[26]

The synthesis of (dodecylsulfanyl)([(4-[hydroxymethyl]phenyl)methyl]sulfanyl) methanethione (**2iii**) was reported in Chapter 2.

The synthesis of 3,4-bis(butylsulfanyl)-1-methyl-2,5-dihydro-1H-pyrrole-2,5-dione (DTMM) was reported in Chapter 5.

Reaction order determination

The external reaction order of DBMM and DTMM in ^{t}BA and MMA RAFT polymerisations were calculated according to the method of Bell *et al.*[21]

^{t}BA/DBMM

To a polymerisation ampoule was added a solution of **4xx** (26.3 mg, 82.7 μmol), ^{t}BA (0.530 g, 4.13 mmol), AIBN (1.36 mg, 8.27 μmol) and DBMM (11.1 mg – 223 mg) in dioxane (0.600 mL). The exact initial ratio of [^{t}BA]:[DBMM] was calculated by ^{1}H NMR spectroscopy. The solution was degassed by three freeze-pump-thaw cycles, the ampoule sealed under N_2 and the reaction stirred at the 65 °C. Periodically samples were taken for ^{1}H NMR spectroscopy analysis to calculate conversion. The apparent rate constants of propagation (k_p^{app}) was calculated as the gradient of $\ln([M]_0/[M])$ *vs.* time, and the reaction order calculated as the gradient of a plot of $\ln(k_p^{app})$ *vs.* $\ln([DBMM])$.

^{t}BA/DTMM

To a polymerisation ampoule was added a solution of **4xx** (12.0 mg, 37.8 μmol), ^{t}BA (0.242 g, 1.89 mmol), AIBN (0.62 mg, 3.78 μmol) and DTMM (5.43 mg – 109 mg) in dioxane (0.274 mL). The exact initial ratio of [^{t}BA]:[DTMM] was calculated by ^{1}H NMR spectroscopy. The solution was degassed by three freeze-pump-thaw cycles, the ampoule sealed under N_2 and the reaction stirred at the 65 °C. Periodically samples were taken for ^{1}H NMR spectroscopy analysis to calculate conversion. The apparent rate constants of propagation (k_p^{app}) was calculated as the gradient of $\ln([M]_0/[M])$ *vs.* time, and the reaction order calculated as the gradient of a plot of $\ln(k_p^{app})$ *vs.* ln([DTMM]).

MMA/DBMM

To a polymerisation ampoule was added a solution of **4xiii** (10.0 mg, 45.2 μmol), MMA (0.226 g, 2.26 mmol), AIBN (0.74 mg, 4.52 μmol) and DBMM (6.07 mg – 121 mg) in dioxane (0.242 mL). The exact initial ratio of [MMA]:[DBMM] was calculated by ^{1}H NMR spectroscopy. The solution was degassed by three freeze-pump-thaw cycles, the ampoule sealed under N_2 and the reaction stirred at the 65 °C. Periodically samples were taken for ^{1}H NMR spectroscopy analysis to calculate conversion. The apparent rate constants of propagation (k_p^{app}) was calculated as the gradient of $\ln([M]_0/[M])$ *vs.* time, and the reaction order calculated as the gradient of a plot of $\ln(k_p^{app})$ *vs.* ln([DBMM]).

MMA/DTMM

To a polymerisation ampoule was added a solution of **4xiii** (10.0 mg, 45.2 μmol), MMA (0.226 g, 2.26 mmol), AIBN (0.74 mg, 4.52 μmol) and DTMM (6.5 mg – 130 mg) in dioxane (0.242 mL). The exact initial ratio of [MMA]:[DTMM] was calculated by ^{1}H NMR spectroscopy. The solution was degassed by three freeze-pump-thaw cycles, the ampoule sealed under N_2 and the reaction stirred at the 65 °C. Periodically samples were taken for ^{1}H NMR spectroscopy analysis to calculate conversion. The apparent rate constants of propagation (k_p^{app}) was calculated as the gradient of $\ln([M]_0/[M])$ *vs.* time, and the reaction order calculated as the gradient of a plot of $\ln(k_p^{app})$ *vs.* ln([DBMM]).

Control reactions of DBMM and DTMM

DBMM and RAFT agent

4xx (29.5 mg, 93.0 μmol) and DBMM (25.0 mg, 93.0 μmol) were dissolved in toluene (0.93 mL) and added to an ampoule. The solution was degassed by three freeze-pump-thaw cycles, the ampoule sealed under N_2 and the reaction stirred at the 80 °C for 4 h. Samples of the reaction mixture at 0 h and 4 h were diluted with methanol, and analysed by HPLC. Spectra were normalised by the height of the toluene peak.

DBMM and ^{t}BA

^{t}BA (11.9 mg, 93.0 μmol) and DBMM (25.0 mg, 93.0 μmol) were dissolved in toluene (0.93 mL) and added to an ampoule. The solution was degassed by three freeze-pump-thaw cycles, the ampoule sealed under N_2 and the reaction stirred at the 80 °C for 4 h. Samples of the reaction mixture at 0 h and 4 h were diluted with methanol, and analysed by HPLC. Spectra were normalised by the height of the toluene peak.

DBMM and AIBN

AIBN (15.3 mg, 93.0 μmol) and DBMM (25.0 mg, 93.0 μmol) were dissolved in toluene (0.93 mL) and added to an ampoule. The solution was degassed by three freeze-pump-thaw cycles, the ampoule sealed under N_2 and the reaction stirred at the 80 °C for 4 h. Samples of the reaction mixture at 0 h and 4 h were diluted with methanol, and analysed by HPLC. Spectra were normalised by the height of the toluene peak.

DTMM and AIBN

AIBN (14.3 mg, 87.0 μmol) and DTMM (25.0 mg, 87.0 μmol) were dissolved in toluene (0.87 mL) and added to an ampoule. The solution was degassed by three freeze-pump-thaw cycles, the ampoule sealed under N_2 and the reaction stirred at the 80 °C for 4 h. Samples of the reaction mixture at 0 h and 4 h were diluted with methanol, and analysed by HPLC. Spectra were normalised by the height of the toluene peak.

^{t}BA polymerisation in the presence of 2,3-DBM

To a polymerisation ampoule was added a solution of **2iii** (25.0 mg, 62.7 μmol), ^{t}BA (0.804 g, 6.27 mmol), AIBN (1.03 mg, 6.27 μmol) and 2,3-DBM (16.0 mg, 62.7 μmol) in dioxane (0.910 mL). The solution was degassed by three freeze-pump-thaw cycles, the ampoule sealed under N_2 and the reaction stirred at the 65 °C. Periodically samples were taken for ^{1}H NMR spectroscopy and SEC analysis.

TEGA polymerisation in the presence of 2,3-DBM

To a polymerisation ampoule was added a solution of **2iii** (20.0 mg, 50.2 μmol), TEGA (0.548 g, 2.51 mmol), AIBN (0.82 mg, 5.02 μmol) and 2,3-DBM (12.8 mg, 50.2 μmol) in dioxane (1.10 mL). The solution was degassed by three freeze-pump-thaw cycles, the ampoule sealed under N_2 and the reaction stirred at the 65 °C for 16 h. The reaction was quenched by exposure to air followed by rapid cooling. Deionised water (2 mL) was added, and the mixture dialysed exhaustively against deionised water (MWCO = 3.5 kDa). The product was isolated by lyophilisation as a yellow oil.

Reversible addition-fragmentation reaction with 6i

6i (0.100 g, 0.396 mmol) and AIBN (65.1 mg, 0.396 mmol) or LPO (0.158 g, 0.396 mmol) were dissolved in toluene (3.96 mL) and added to an ampoule. The solution was degassed by three freeze-pump-thaw cycles, the ampoule sealed under N_2 and the reaction stirred at the 80 °C for 4 h. Samples of the reaction mixture at 0 h and 4 h were diluted with methanol, and analysed by HPLC. Spectra were normalised by the height of the toluene peak.

6.6. References

1. J.-F. Lutz, B. V. K. J. Schmidt and S. Pfeifer, *Macromol. Rapid Commun.*, 2011, **32**, 127-135.

2. L. E. Coleman and J. A. Conrady, *J. Polym. Sci.*, 1959, **38**, 241-245.

3. T. Alfrey and C. C. Price, *J. Polym. Sci.*, 1947, **2**, 101-106.

4. A. A. Mohamed, *Acta Polym.*, 1986, **37**, 514-517.

5. G. Moad, E. Rizzardo and S. H. Thang, *Acc. Chem. Res.*, 2008, **41**, 1133-1142.

6. J. Lokaj, P. Vlček and J. Kříž, *J. Appl. Polym. Sci.*, 1999, **74**, 2378-2385.

7. G.-Q. Chen, Z.-Q. Wu, J.-R. Wu, Z.-C. Li and F.-M. Li, *Macromolecules*, 2000, **33**, 232-234.

8. P. Yang, L. P. D. Ratcliffe and S. P. Armes, *Macromolecules*, 2013, **46**, 8545-8556.

9. G. Deng and Y. Chen, *Macromolecules*, 2004, **37**, 18-26.

10. S. Pfeifer and J.-F. Lutz, *J. Am. Chem. Soc.*, 2007, **129**, 9542-9543.

11. J.-F. Lutz, *Acc. Chem. Res.*, 2013, **46**, 2696-2705.

12. M. Zamfir and J.-F. Lutz, *Nat. Commun.*, 2012, 1138.

13. M. W. Jones, R. A. Strickland, F. F. Schumacher, S. Caddick, J. R. Baker, M. I. Gibson and D. M. Haddleton, *J. Am. Chem. Soc.*, 2012, **134**, 1847-1852.

14. F. F. Schumacher, M. Nobles, C. P. Ryan, M. E. B. Smith, A. Tinker, S. Caddick and J. R. Baker, *Bioconjugate Chem.*, 2011, **22**, 132-136.

15. M. W. Jones, R. A. Strickland, F. F. Schumacher, S. Caddick, J. R. Baker, M. I. Gibson and D. M. Haddleton, *Chem. Commun.*, 2012, **48**, 4064-4066.

16. M. P. Robin, M. W. Jones, D. M. Haddleton and R. K. O'Reilly, *ACS Macro Lett.*, 2012, **1**, 222-226.

17. R. Z. Greenley, in *Polymer Handbook*, eds. J. Brandrup, E. H. Immergut and E. A. Grulke, Jonh Wiley & Sons, New York, Fourth edn., 1999, p. II/181.

18. J. D. Patel and M. R. Patel, *J. Polym. Sci., Polym. Chem. Ed.*, 1983, **21**, 3027-3032.

19. E. Awuah and A. Capretta, *J. Org. Chem.*, 2011, **76**, 3122-3130.

20. T. Oishi and T. Kimura, *Kobunshi Ronbunshu*, 1976, **33**, 685-691.

21. C. A. Bell, Q. Sun, H. Zhang, S. C. Smith, P. V. Bernhardt and M. J. Monteiro, *Polym. Chem.*, 2010, **1**, 207-212.

22. K. W. Dixon, in *Polymer Handbook*, eds. J. Brandrup, E. H. Immergut and E. A. Grulke, John Wiley & Sons, New York, Fourth edn., 1999, p. II/1.

23. C. Barner-Kowollik, P. Vana and T. P. Davis, in *Handbook of Radical Polymerization*, eds. K. Matyjaszewski and T. P. Davis, John Wiley & Sons, Inc., 2002, pp. 187-261.

24. M. Chen, G. Moad and E. Rizzardo, *J. Polym. Sci., Part A: Polym. Chem.*, 2009, **47**, 6704-6714.

25. F. Hua, X. Jiang, D. Li and B. Zhao, *J. Polym. Sci., Part A: Polym. Chem.*, 2006, **44**, 2454-2467.

26. C. N. Urbani and M. J. Monteiro, *Macromolecules*, 2009, **42**, 3884-3886.

Conclusions and future work

In this thesis the dithiomaleimide (DTM) group has been presented as a novel fluorophore, and incorporation of this DTM fluorophore into polymers and polymer nanoparticles has been explored. DTM labelling has been achieved by pre-polymerisation functionalisation, using both a RAFT agent and vinyl monomers containing the DTM group. DTM labelling has also been achieved by post-polymerisation functionalisation through the highly efficient conjugate-addition of thiols to dibromomaleimide (DBM). DBM functional groups have been incorporated into both a RAFT agent and vinyl monomers, with the post-polymerisation functionalisation reaction demonstrated at polymer end-groups and along polymer backbones. These DBM-functional polymers can therefore be described as profluorescent, as this post-polymerisation functionalisation reaction leads to an OFF-to-ON switching of emission.

An application for the DTM fluorophore has been demonstrated, which exploits its desirable fluorescent properties of a large Stokes shift and long fluorescence lifetime. DTM-labelled polymer nanoparticles have been shown to act as contrast agents which can self-report on their supramolecular structure, with our collaborators utilising this for *in vitro* fluorescence lifetime imaging. Future work will aim to establish the full potential of the DTM-functional polymer nanoparticles fabricated in Chapter 5, for example by comparison with widely used alternative contrast agents.

We believe that the small size, high processability, and versatile chemistry of the DTM group could allow this fluorescent label to be widely utilised in polymer science. The DTM and DBM-functional RAFT agents and monomers could readily be applied to the synthesis of fluorescent or profluorescent polymers with a wide variety of architectures or additional functionality. Furthermore, the potential for DTM thiol exchange demonstrated by Baker and Caddick *et al.* could provide a mechanism for ON-to-OFF or OFF-to-ON switching of emission.

Several questions raised in this thesis remain to be answered. The origin of the DTM group's emissive behaviour needs to be better understood, in order for the full potential of this fluorophore to be realised. In addition, the rate retarding effect of the DBM group in

RAFT polymerisation (as considered in Chapter 6) currently limits its compatibility to acrylate and methacrylate polymers. A more complete understanding of the mechanistic cause of this retardation may allow it to be overcome.